UNIVERSITY OF SOUTHAMPTON

FACULTY OF ENGINEERING AND THE ENVIRONMENT

Institute of Sound and Vibration Research

Analytical Modelling of Sound Transmission in a Lined Duct

by

Nabilah binti Ramli

Thesis for the degree of Doctor of Philosophy

September 2013

UNIVERSITY OF SOUTHAMPTON

ABSTRACT

FACULTY OF ENGINEERING AND THE ENVIRONMENT

Institute of Sound and Vibration Research

Thesis for the degree of Doctor of Philosophy

ANALYTICAL MODELLING OF SOUND TRANSMISSION IN A LINED DUCT

Nabilah binti Ramli

The focus of this thesis is on the prediction of sound attenuation through a lined duct, based on a mathematical model. Ducts with a single section as well as multi-segmented sections are discussed. The duct of interest has a rectangular cross-section as normally used for ventilation purposes. The mean flow in a ventilation duct is very low and can be neglected. In this thesis, two-dimensional analytical models are developed for sound transmission in a series of different duct configurations. Two models of the lining behaviour are considered, either locally-reacting or bulk-reacting.

The models are used first to obtain the transverse and axial wavenumbers of various modes of the duct. The required finite numbers of wavenumbers are tracked using Müller's method. The wavenumbers are traced from a very low frequency to high frequency using small frequency steps. It is found that, for a duct with a bulk-reacting lining, the number of modes with a transverse wavenumber below a particular value may exceed the corresponding number of modes in a duct with a locally-reacting lining. These additional modes are termed lining modes. The number of lining modes depends on the lining thickness. Dispersion curves are presented for both types of lining.

The transmission of sound through the duct is then calculated using the mode-matching technique. The mode-matching model allows analysis of multi-modal wave propagation in the duct. The model is first developed for an infinitely long rigid duct with a finite length of lined insert. The estimation from the locally reacting model, that is widely available in the literature, is compared with the estimation from the newly developed bulk-reacting model. Although the locally reacting model often overestimates the performance of a bulk-reacting lining it is found that this is not always the case, especially for a small lining thickness and at lower frequencies where the locally reacting model may under-estimate the performance.

The analytical model is then extended to a multi-segmented lining where the lined section is uniformly segmented with rigid walled sections in a periodic manner. For a bulk-reacting lining, the segmented arrangement renders the lining more similar to the behaviour of a duct with a locally-reacting lining and improves the peak attenuation. Little improvement is found in the case of a multi-segmented locally-reacting lining. The effect of duct height, lining thickness and lining flow resistivity on sound attenuation is studied using the analytical model. Experiments are presented which validate the analytical model.

Contents

List of tables

List of figures

DECLARATION OF AUTHORSHIP

I, Nabilah binti Ramli

declare that the thesis entitled

Analytical Modelling of Sound Transmission in a Lined Duct

and the work presented in the thesis are both my own, and have been generated by me as the result of my own original research. I confirm that:

- this work was done wholly or mainly while in candidature for a research degree at this University;
- where any part of this thesis has previously been submitted for a degree or any other qualification at this University or any other institution, this has been clearly stated;
- where I have consulted the published work of others, this is always clearly attributed;
- where I have quoted from the work of others, the source is always given. With the exception of such quotations, this thesis is entirely my own work;
- I have acknowledged all main sources of help;
- where the thesis is based on work done by myself jointly with others, I have made clear exactly what was done by others and what I have contributed myself;
- parts of this work have been published as:

  N. Ramli, D. J. Thompson, T. P. Waters, "Analytical model of a finite length rectangular duct with bulk-reacting lining", presented at the 20th International Congress on Sound & Vibration, Bangkok, Thailand, 2013

Signed: NABILAH BINTI RAMLI

Date: 4th September 2013

Acknowledgements

In the name of God, most Gracious, most Compassionate.

All praise is due to Allah, for His blessings and His guidance, and for giving the strength and perseverance for me to pursue and to make this study possible.

This degree is never the work of anyone alone. The contributions of many people, in their different ways, have made this amazing journey possible. Foremost, I would like to express my sincere gratitude towards both my supervisors, Dr. Tim Waters and Prof. David Thompson, for their patient, motivation, immense knowledge and continuous support throughout my Ph.D years. I started with little knowledge on the topics and over time they help me to understand the subject and instil the research values in me and have always guided me in the right direction.

My thanks to the thesis examiners, Dr. Ray Kirby from Brunel University and Dr Alan McAlpine from ISVR, for the time they have willingly given up to appraise my work.

Special thanks to the technical staff, Mr. Phil Oxborrow and his team in helping me with the testing rig and duct constructions. Heartiest dedication to the Dynamics Group members, especially to Mr. Nuttarut Prananda and Ms. Nuthnapa Triepaischajonsak. The friendship and kindness everyone has shown make my stay in ISVR a memorable one.

Last but not the least, my greatest gratitude towards my family especially my parents, Mr. ramli Muda and Mrs. N. Shiham W. Mashhor, for their patience and motivation. Thank you for keeping me calm and driven to go through every obstacle in life. And thank you to all my friends for the support, emotionally and spiritually, during my stay in the United Kingdom.

To them, I am eternally grateful. Praise be to Allah.

List of symbols

A, B	Modal wave amplitudes
D	Level difference
L	Sound pressure level
L_h	Length of unlined section
L_s	Length of lined section
M	Order of mode
R	Real part of impedance
$\mathbf{R}_a$, $\mathbf{R}_b$, $\mathbf{R}_c$	Reflection matrix coefficients
T_{60}	Reverberation time
V	Room volume
X	Imaginary part of impedance
Z_c	Specific acoustic impedance
Z_c'	Non-dimensional specific acoustic impedance
Z_n	Surface normal wall impedance
Z_n'	Non-dimensional surface normal wall impedance
Z_{ir}	Ratio of real part to imaginary part of wall impedance
a, b, c,	Modal wave amplitudes
c_0	Speed of sound, 340.31 m/s
$c_{p,N}$	Wave amplitude from matching N modes
$c_{p,R}$	'True' amplitude
$\tilde{c}$	Speed of sound in absorptive material
d	Lining thickness
d_p	Penetration depth
f_s	Schroeder frequency
h	Duct height
h_1, h_2	Müller's algorithm parameters
i	$\sqrt{-1}$
k_x, k_y, k_z	Wavenumbers in airway
k_0	Wavenumber in air
$\tilde{k}$, $\tilde{k}_x$, $\tilde{k}_y$, $\tilde{k}_z$	Wavenumbers in absorptive material
l	Distance
m, n	Order of mode

List of symbols

p	Pressure
r	Flow resistivity
s	Tortuosity
t	Time
u_x, u_y	Particle velocity
x_0, x_1, x_2	Initial guesses for Müller's method
(x, y, z)	Cartesian coordinate system
Δ_1, Δ_2	Müller's algorithm parameters
Δc_p	Convergence of transmitted wave amplitude
Λ, Λ_m	Attenuation rate
Φ , $\tilde{\Phi}$	Mode shape
Ω	Non-dimensional frequency
α	Absorption coefficient
γ	Imaginary non-dimensional transverse wavenumber
ε	Porosity
ε_{ij}	Error function
λ	Wavelength
ρ	Material density
$\tilde{\rho}$	Complex acoustic density of absorptive material
ρ_0	Density of air, 1.225 kg/m^3
σ	Standard deviation
ϕ	Incident angle
ω	Angular frequency

Abbreviations

CI	Confidence interval
IL	Insertion loss
SPL	Sound pressure level
TL	Transmission loss

1. Introduction

1.1 Background

According to statistics published by the World Health Organization, 33 countries have 80% or more of their population living in urban areas [1] and for the first time in human history, in 2009, more than half of the world's population resides in urban areas. Urbanization has a dramatic effect on energy consumption. The rate of change in energy usage in urban areas is twice that of rural areas [2]. Urban buildings are the largest energy consumers in cities where a large amount of this energy is used for heating and air conditioning purposes. The awareness of energy consumption in buildings started after the oil crisis in 1973 when people became conscious of the limit of energy availability. New national regulations on buildings in the 1980s emphasized the need for large reductions in energy requirements for building heating and air conditioning [3]. Global energy consumption has reduced significantly since then but at the same time resulted in the emergence of sick building syndrome where the thermal comfort of building occupants was compromised and poor indoor air quality became commonplace due to a low air-change rate. Thus it is evident that energy conservation cannot be dissociated from the quality of the indoor and outdoor environment.

Natural ventilation emerged as a very attractive solution in the 1990s to reduce energy consumption while ensuring good indoor quality and acceptable comfort conditions [3]. A study conducted by Mendell *et al.* [4] shows that occupants reported fewer symptoms of sick building syndrome in naturally ventilated buildings compared to buildings with mechanical ventilation. Furthermore, 9 of the 10 buildings with the lowest CO_2 emissions were naturally ventilated [5]. Despite these promising results of natural ventilation, fluctuations in indoor temperature and air quality may be experienced and it is difficult to achieve efficient heat recovery [6]. This is because natural ventilation systems rely on small pressure differentials to move fresh air through doors, windows or other intentional openings in the building.

Design targets for natural ventilation may be based on air flow rates to control indoor air quality and prevent overheating. However, the small pressure differentials available require a system to have inherently low airflow resistance to achieve adequate ventilation rates [7]. Opening large areas of the building façade can help to achieve low airflow resistance but at the cost of compromising acoustical comfort of the building, one of many competing factors in design of a building. The task of designing a naturally ventilated building becomes more challenging in addressing the acoustic issues for example noise ingress to the space from outside, cross-talk between spaces, or noise egress from the space to the surroundings. Although noise caused by

ventilation systems is not controlled under the Building Regulations [8], such noise may be disturbing to the building occupants and it is recommended that measures be taken to minimise the passage of sound whilst allowing maximum flow of air into and through a building.

There are three fundamental approaches to natural ventilation: wind-driven cross ventilation, buoyancy-driven stack ventilation, and single-sided ventilation [9]. In a cross ventilation strategy where openings are placed between internal spaces to allow free air transfer, acoustic separation is important between noisy areas and noise-sensitive areas for example, between an open office and private meeting room, a school corridor and a quite classroom, or in hotels between corridors and guest rooms. Buoyancy-driven stack ventilation relies on density differences to draw cool, outdoor air in at low ventilation openings and release warm, indoor air at higher ventilation openings, while single-sided ventilation typically serves single rooms and provides a local ventilation solution. Acoustic separation can be achieved with the use of acoustic attenuators placed in the ventilation openings. The size of ventilation openings should be appropriate to cope with the increased pressure drop per square metre of aperture that is caused by the blockage drag from acoustic attenuators [10].

De Salis *et al*. [11] reviewed various noise control strategies for natural ventilation systems in buildings. One of the main control measures is to treat the ventilation duct with sound absorbing materials. The ability to predict quantitatively the acoustic performance of a lined duct at its design stage is highly desirable. The acoustic performance depends on duct geometry, lining arrangement and the acoustic properties of the lining material used. Ventilation ducts commonly have a rectangular cross-section and are lined with a bulk-reacting absorbing material.

One of the available ventilation ducts on the market is the SoundScoop by Passivent that is claimed to offer an open design with up to 90% increase in open area compared to other ventilation ducts available on the market [12]. This results in low airflow resistance due to the unimpeded path. The SoundScoop was designed to target the attenuation of noise from speech and footfall, the most common requirements of an internal acoustic duct. Figure 1.1 shows the performance of the SoundScoop acoustic air transfer unit compared to another “market leading” acoustic duct. It compares the SoundScoop with 45% open area to a 30% open design foam lined duct, both 1200 mm in length. The SoundScoop was designed to have optimum performance in the frequency range 500 Hz to 2 kHz where it is claimed to give a further 10 dB reduction in noise level compared to the other product.

The attractive feature of the SoundScoop is the periodic arrangement of the wall linings with strips of the sound absorbing material separated by ribs as shown in Figure 1.2. The patented internal arrangement features ribs at regular intervals giving resistive interference where the

sound is claimed to be partly reflected and partly absorbed at frequencies whose wavelengths relate to the period of the ribs. The discontinuities along the propagation path of the sound wave are claimed to scatter the travelling plane wave at low frequencies into non-plane waves of higher order wave modes. Thus the usually least attenuated plane wave in a uniformly lined duct is now disturbed by the ribs and is more readily attenuated.

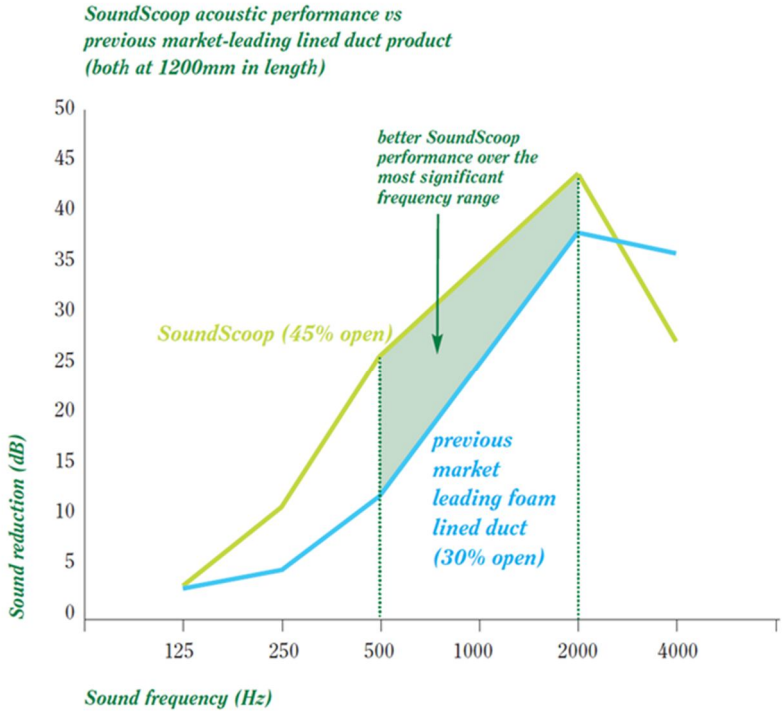

Figure 1.1: Performance of SoundScoop compared to the lined ventilation duct, obtained from SoundScoop brochure [12]

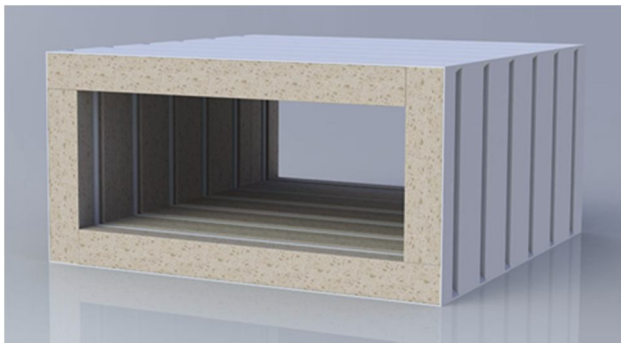

Figure 1.2: The SoundScoop, image from the Soundscoop brochure [12]

For ventilation duct purposes, the duct design process still relies heavily on finite element modelling and/ or an empirical approach. This is due to complications in determining the wave propagation parameters for complex arrangements of absorbing materials, for example the

honeycomb structure used in the NAT Vent Attenuator [13], and the extensive computation involved in modelling wave propagation through numerous discontinuities. To quantify the duct performance by laboratory testing according to the International standards [14] can be expensive and time consuming. Furthermore, a laboratory based standard relies on a number of assumptions which are not always applicable in real operating conditions [15].

The development of studies on sound transmission through lined ducts owes much to the studies of turbofan aero-engines and automotive exhaust systems. The acoustical theory in each of these fields is the same but the duct design and the main concern in each area differ. For ventilation systems, the mean flow is not of concern since the Mach number for a ventilation duct is well below 0.1 [16]. A mathematical model of sound propagation in a lined duct is a desirable tool that can provide a quick assessment on duct acoustic performance while serving as a platform to understand the physics behind sound attenuation in a lined duct.

In this thesis, the topic of duct acoustics is addressed. Duct acoustics is the branch of acoustics concerned with sound propagation in pipes and ducts. Sound propagation within ducts is of practical concern in many areas of acoustics and noise control. Apart from facilitating fluid flow, they are also a channel for unwanted noise. It is recommended to attenuate the sound travelling in the duct to reduce the problem of noise pollution. Knowledge of acoustics is important in creating an environment that can provide acoustical comfort where the spaces are reasonably free from harmful and/or intruding noise and vibration.

Lining materials have been used as sound absorbers for some time. Basically, lining materials can be divided into two types; locally reacting linings and bulk-reacting linings. Locally reacting linings are liners that permit propagation only in the direction normal to the duct wall. These type of linings usually consist of a perforated sheet or a thin layer of porous material followed by a honeycomb core and backed by the impervious wall of the duct [17]. Bulk-reacting linings are liners that permit propagation in more than one direction. These liners are more effective to attenuate broad-band and low frequency noise compared to locally reacting linings [18] and many applications can be found in air-conditioning and ventilation ducts. The liners used in aircraft engines are normally of locally reacting type due to structural design difficulties of using a bulk-reacting lining. Furthermore, a bulk-reacting lining cannot be used in the hot ducts, where combustible fluid retention is a fire hazard, because to its fibrous form [19].

The theoretical analysis of sound transmission in a simple duct has long been studied and has been well established since the late 1930s [20-23]. At this stage most of the works dealt with locally reacting linings. In general, the wall boundary condition can be described by the concept of acoustic impedance without directly considering the sound propagation inside the liners. This

approach has been applied extensively in the area of aero-engine and automotive exhaust systems where the complexity due to mean flow and added complications at high frequencies can be reduced to a great extent [24, 25].

Most of the available works focus on a locally reacting lining that represents the lining by a surface impedance; works involving bulk-reacting linings, i.e. including sound propagation within the absorption material itself, are scarce. Furthermore, literature for ducts with multiple inserts or with a periodic lining arrangement such as used in the SoundScoop is not that extensive. Thus, it is the aim of this research work to provide a framework of analytical modelling for an acoustic duct with periodic lining, using both a locally reacting lining model and a bulk-reacting lining model.

1.2 Literature review

1.2.1 Sound absorbing materials and impedance model

In air, sound travels with very little attenuation apart from the effect of geometric spreading in two or three dimensions. However when sound waves travel in the small spaces of the interconnected pores of a porous material, the energy is dissipated via friction with the pore walls, and also loss in momentum due to changes in flow as the sound moves through irregular pores. Significant absorption can be achieved if the porous material is placed where the particle velocity is high. Thus, for an absorptive material with a backing surface, the material close to the boundary does not give significant absorption. The thickness of the absorptive material should be at least a tenth of a wavelength to give significant absorption [26].

The study of sound dissipation in sound-absorbent materials was first conducted by Lord Rayleigh [27] using a capillary tube approach to predict the absorption coefficient. The approach was adopted by Scott [28] to characterize the absorbing material by two frequency dependent complex quantities: the propagation constant and the characteristic impedance. These are determined by introducing the flow resistivity of the material into the model. Flow resistivity is a measure of how much resistance a porous material applies to air entrance and the resistance to air flow within the material.

There are various types of porous material available for the purpose of acoustic absorption. Among them are mineral wool that is made from materials such as sand, basaltic rock and recycled glass, and open cell foam for example melamine, polyester, polyurethane and rubber foam. Acoustic absorption is determined from the properties of the porous material. However, modelling the propagation of sound within a porous material is difficult due to its complex

geometry and some factors related to the pore shapes are difficult to obtain except empirically. There are two main approaches found to be useful in modelling the sound propagation in a porous material. The first is a completely empirical approach and the second is the semi-analytical approach.

For the first approach, the most widely used empirical model is that of Delany and Bazley [29]. The empirical model was produced from measurements of the acoustical properties of a range of porous materials and the limits of flow resistivity, r, in the measurements were $1000 \le r \le 50000$ rayls/m. The measurements were carried out in an impedance tube and the results were normalised by plotting them against frequency divided by flow-resistance and represented in terms of power-law relations. This empirical relation requires only knowledge of the flow-resistance of the material and the empirical curves may be used with confidence within the interpolating range of $10 \le f/r \le 1000$. At low frequency the absorption is often very low so that the lack of accuracy in prediction is not important [30]. Mechel and Grundmann produced a more complex but improved empirical relationship [31]. However for many cases, the difference in the prediction quantity from both empirical models is relatively small.

Although empirical models are the simplest to apply to existing materials and can be most effective in certain cases, the relationships were derived based on normal incidence impedance tube measurements. Thus the model can be accurately used only in the case where the porous material is locally reacting where the impedance produced is independent of the incident wave type and angle of incidence. In this work, apart from locally reacting liners, bulk-reacting liners are considered as well. Another approach on modelling the wall impedance is required that can accurately give the impedance of a bulk-reacting material.

By using analytical approach, a simple impedance model can be setup by assuming that the absorptive material is rigid where the classical theories of sound propagation in small pores can be applied. However due to the complex geometry of vast majority of absorptive material, a mixture of experiment and theory is required to determine the key properties of the material. One such semi-analytical model available was derived from a modified plane wave equation for sound propagation in gases contained within rigid porous materials [32]. The linearized equations of conservation of mass and momentum was modified to include the effects of flow resistivity, r, porosity, ε, and tortuosity, s. The specific acoustic impedance and the complex wavenumbers can be directly calculated from those three parameters.

Flow resistivity is a measure of the resistance that air flow meets through a structure; a low flow resistivity implies that air can readily enter a porous material. When a steady airflow travels through a layer of porous material, the viscous resistance gives rise to a static pressure gradient.

The flow resistivity is defined as the ratio of the pressure gradient to the mean flow velocity or effectively the resistance per unit material thickness. The unit of flow resistance in MKS units is $Nm^{-3}s$, or rayl. Flow resistivity thus has units of rayl/m. This is the parameter that varies most between common porous materials and hence it is the most important parameter to determine.

Good sound absorbers tend to have high porosity. Porosity, ε, is a non-dimensional quantity that gives the fractional amount of air volume within the absorber. The value is often between 0.9 and 0.95, which means 90 - 95% of the material is air. The orientation of the pores relative to the incident sound field also affects the sound propagation in a porous absorber. The more complex the propagation path through the material, the higher is the absorption and the complexity is partly represented by the tortuosity. The vibrating fluid is forced to undergo accelerations in various directions by the tortuous and irregular forms of the pores.

Tortuosity, s, is a non-dimensional quantity that expresses the influence of the geometric form of the structure on the effective density of the fluid. The quantity generally cannot be estimated theoretically and often is found through empirical means.

A more complicated impedance models are also available such as the phenomenological model [33-35] and relaxation model [36], that require additional information, apart from the three material properties, such as characteristic length (weighted ratio of the volume to surface area of the pores) [30], specific heat capacity, the thickness of viscous and thermal boundary layer, and the characteristic time for viscous relaxation process for the latter model. These two models assume a rigid frame absorptive material as well.

1.2.2 Wave propagation in a lined duct

Studies of noise propagation through rectangular or circular ducts lined with absorbing material started in the late 1930's. There are three approaches in solving such problems: empirical, theoretical and computational methods. Before the theoretical approach was well established, an empirical approach was favoured to produce a simple yet reasonably accurate mathematical relationship, that relates the attenuation of sound in a lined duct to duct design parameters, to the frequency of the sound and to the absorptive properties of the lining [22, 37]. This requires a setup of an actual duct system under as close conformity as possible to the actual practice while permitting accurate control of the variables under investigation. It is time consuming and costly to build various duct designs to establish a reliable empirical relationship and there are inconsistencies among the few proposed empirical rules.

The theoretical approach started at around the same period as empirical studies were taking place. The fundamental work on the theoretical approach was provided for example by Sivian [20], Morse [21], Scott [38] and Rogers [23]. These analytical methods are the most rigorous compared to the empirical or computational methods, providing exact solutions. Furthermore, the analytical model gives more insight into the physical behaviour of wave acoustics in a lined duct and the physical factors controlling the ducting system. The limiting behaviour can be obtained in understanding the underlying physics. However analytical methods are limited to simple duct geometry problems such as circular or rectangular ducts, and become more complicated when involving mean flow, especially when involving a bulk-reacting liner.

Apart from the difficulty in modelling a complex geometry and duct design, the analytical approach also suffers from the difficulties in finding the solutions to the governing eigenvalue problem. This results in many authors resorting to a computational approach using numerical tools such as the boundary element method (BEM) [39, 40] and finite element method (FEM) [41-43]. BEM solves the acoustic quantities on the boundary and the solution within the acoustic domain is then computed based on the solution on the boundary, while FEM solves for the response in the acoustic domain itself by computing the mass and stiffness of the acoustic domain [44]. The accuracy of these two methods depends on having a sufficient number of nodes in the model. However a large number of nodes can results in a longer computation time and a large memory is required. These two requirements typically restrict their use to the final design stage and to low or mid frequency application.

Kirby [45] compares the accuracy of predicted results, and the computational expenses between analytical and numerical methods. The comparison was made between an analytical mode matching approach and two modified finite element approaches. The predicted transmission loss from the three methods is in excellent agreement and the numerical methods were found to provide shorter computation time compared to the analytical method. This is said to be due to the iterative algorithm required to find the roots to the lined duct eigenequation in the analytical method. However the speed of finding the roots depends on the algorithm used and how fast the roots converge.

The numerical methods can handle complicated geometries and complex problems as found in practice, and give the solution directly. However, analytical solutions can give insights to physical understanding of the nature of the results. Moreover, analytical methods are easier to use for setting up the model and to code without the need of complicated and expensive software. In many of reported works it is claimed that analytical models require less time to implement and run [6, 46, 47].

In the early works, the absorbing material was assumed to be locally reacting, where the sound propagation in the lining material parallel to the duct axis is prohibited. Thus the motion at the surface depends only on the acoustic impedance and on the local acoustic pressure and not on the acoustic pressure elsewhere.

Morse applied theory of room acoustics [48] to solve the sound attenuation in a duct and the theory was validated by Beranek's experimental work. The absorbing qualities of the lining material were represented by its normal acoustic impedance. Only the simplest wave type was considered and theoretical analysis was provided based on this fundamental mode. It is generally agreed that this assumption is valid for frequencies where the wavelength is longer than twice the longest transverse dimension [37], above which the higher order modes will be excited. At these high frequencies, the sound energy will be propagated along the duct by these higher order modes in addition to the energy carried by the fundamental mode. However the attenuation of higher order modes is in general much greater than that of the fundamental wave and was often neglected in the early analysis.

The determination of roots of transcendental equations is a problem that manifests itself in duct acoustics and only rarely are the roots readily available. For example for a duct with a locally reacting lining, the wavenumbers at a given frequency with known normal wall impedance can be readily obtained from so-called Morse charts [21, 49] that relates the wavenumbers to the wall impedance without solving the characteristic equation explicitly, as introduced by Morse [21]. The transverse wavenumbers for a rectangular lined duct are mapped over the complex plane of the lining impedance. The equivalent chart for wavenumbers in a circular lined duct was produced by Molloy and Honigman [50] but all these charts were produced only for the fundamental mode.

Extensive work by Morse produced two plots of Riemann surfaces for the two lowest order duct modes that can be used to calculate the attenuation of sound in a long rectangular duct. The first plot relates the known acoustic impedance at a frequency of interest and the duct dimension, to the transverse wave propagation constant. From these known values, the attenuation constant can be obtained from the second Riemann surface plot. Based on the Morse charts, Cremer's rule [51] was introduced where the optimum impedance to give the maximum possible attenuation can be found at the branch point between the first two modes.

These two plots are applicable to a wide range of typical values of acoustic impedance except for certain values of complex impedance where there are a few curves missing from the plot. This occurs in the case where the reactance part of the complex wall impedance is negative i.e. the impedance has a stiffness reactance part. These missing curves correspond to the surface

wave solution which was addressed by Mechel [49] in his work in reproducing a more complete Morse chart. They are named surface waves because their field is only significant close to the wall as it decays exponentially away from the wall. These surface waves were studied in detail by Rienstra [52] where the waves are not classified as duct modes but only coupled to the impedance wall. The surface waves occur at high frequencies and for a duct with zero mean flow, two surface waves can exist that depend on the wall impedance [53].

The assumption by Morse of locally reacting linings is valid under certain circumstances, particularly when the attenuation in the duct is small and where the lining consists of a densely packed collection of fibres [38]. For narrow ducts and at high frequencies in the range where the attenuation is higher, Morse's theory gives attenuations of much higher magnitude than found in practice [37]. However, the locally reacting assumption is still widely adopted because it results in a great simplification in the analysis. In practice, sound propagation in the lining parallel to the surface can be restricted in some way by placing solid partitions in the liner to prevent axial wave propagation in the lining. These may be thin impervious metal or wooden strips or sudden density changes in the liner [54].

If the sound propagation in the liner parallel to the surface is not prevented, the locally reacting assumption should be replaced with an alternative assumption that the liner is bulk-reacting. For a bulk-reacting material, acoustic waves can propagate in the liner in the axial direction as an attenuated wave. Scott [28] demonstrated that part of the initial energy of a wave which travels along a duct lined with sound absorbing material is transmitted through the lining itself. The oscillatory velocity at the surface of the lining depends on the effects of wave disturbances inside and outside the lining and cannot be described merely in terms of the acoustic impedance and the oscillatory pressure at the surface of the lining. The axial wave propagation in the lining was taken into account and a complete theory of wave propagation through a duct lined with sound absorbing material was presented by Scott [38]. This leads to a complete solution of wavenumber equations that could be solved numerically.

There are several numerical techniques available to solve the resulting governing eigenvalue equation for the wavenumbers. Often, these numerical techniques suffer from the problem of missing roots. There are few reliable techniques by which to determine whether all the roots in a certain range have been found. One such rigorous technique is the Argument Principle [55] where the winding number integral, being a contour integral around a closed path in the complex plane, determines the presence of zeros and poles in the enclosed area. This technique has been used with great effect by Doolittle *et al*. [56] to ensure that certain areas of the complex plane are free of roots in finding creeping ray solutions to acoustic scattering from cylinders.

To locate these roots in a complex plane is not a trivial task and most of the techniques require an initial approximation for the eigenvalue in order to start the algorithm. The most adopted approach is to use the asymptotic approximations that are close to the actual value and then track the roots in the complex plane with respect to some parameter which is either frequency [57], the Mach number of the gas flow [58] or the admittance for the case of a locally reacting liner. Eversman [58, 59] developed an integration scheme that employed a fourth-order Runge-Kutta integration to solve the eigenvalue problem. Another two widely used numerical techniques are the Newton-Raphson method [60, 61] and Müller's method [49, 57, 62].

For ducts containing finite segments of lining, it is common practice to formulate the physical problem of interest as a boundary value problem where analytical solution methods such as the Wiener-Hopf technique [63-65] or the mode-matching technique [62, 66, 67] can be applied. Of these two methods, the mode-matching technique is more widely used for formulating boundary-value problems in waveguide theory [68]. In the field of duct acoustics, it was used by Lansing and Zorumski [25] in their early study of the effects of changes in duct wall acoustic properties on the transmission of sound through ducts. The mode-matching technique is more flexible than the Wiener-Hopf technique since it is relatively more straightforward to extend the model to include a duct with variable duct geometries [69, 70].

However, some authors use other approaches as demonstrated in [71, 72] to avoid the process of root finding but these methods are not easily generalized [55]. A point collocation method is a numerical mode-matching technique that avoids the root finding process and has been used to model relatively small dissipative silencers [43]. This method has been used extensively by Kirby [15, 73, 74] in studying the attenuation of a large ventilation duct lined with a bulk-reacting lining. Although the reported works show promising results in a study of conventional lined ducts as well as ducts with parallel splitters, the method has yet to be demonstrated in a case of a multi-segmented lined duct.

In modelling a three-dimensional duct, the corner condition is important to be included in the analysis. At the corners, the so-called edge condition [75, 76], the energy integral of the field in a neighbourhood of an edge must be finite. This condition is necessary when dealing with corners/ edges because the edge conditions in three-dimensions conflict with one another at the corners, in which in two-dimensions the edge conditions can be satisfied. The analytical and semi-analytical methods in duct acoustics which are based on the expansion of the sound field in terms of modes lead to the possible reduction of a three-dimensional problem into a two-dimensional one [15, 62, 67]. This reduces the complexity in formulating the problem especially with the four corners of a fully lined rectangular duct.

The wave fields in a duct of arbitrary cross-section can be expanded in terms of eigenvectors defined over a two-dimensional duct cross-section. By matching expansions of this type at the interface between different uniform duct segments, the effect of impedance mismatch can be modelled with far fewer parameters than would be required for a three-dimensional analysis. However, when flow is present, this approach can only be applied to ducts whose cross-sectional geometry is uniform in axial direction [66].

The effect of changes in wall admittance on the acoustic wave propagation has been studied earlier by Lansing and Zorumski [25]. From a multimode analysis of the reflection and transmission of a plane wave at the junction of a hard-walled and lined rectangular duct, it was found that dissipative liners and reactive liners with positive imaginary wall impedance reflect substantial acoustic energy only at low frequencies and for large modulus of the impedance. A multi-segmented duct liner was also studied by Unruh [77] and Tsai [78]. The method of solution requires the continuity of mass and momentum at the discontinuity to be satisfied by matching acoustic pressure and axial particle velocity. A vanishingly small resistive impedance can give a highly reflective design for a segmented liner [77] and hence can increase the performance of the silencer. Apart from reflecting most of the incident wave, an impedance mismatch can give a favourable scattering effect by transferring the energies of lower order modes into higher ones which have a greater attenuation. This can be achieved if the first lining in a multi-segmented liner is a nearly reactive one [78].

More recent studies on multi-segmented liners have focused on the application to turbofan aero-engines at high frequency for high supersonic fan speeds. An attempt at an optimization study for a higher number of segmented liners was presented by Lafronza et al. [79] but a further study is still required to understand fully the potential benefit of a multi-segmented axial liner. McAlpine et al. [80] presented an analytical approach for designing a duct lined with two segments. This work demonstrated that two lined segments could be designed to give improved attenuation of a duct where only two radial modes are cut-on. A higher number of liner segments can cause the energy in higher order modes to be scattered into the lower order modes hence giving an adverse effect on the silencer performance [78]. However Law et al. [81] suggested that broadband noise does not appear to be adversely affected by the presence of scattering at a segment interface and there is potential for improving the silencer broadband performance with segmented liners.

1.3 Motivation and research aims

The research work presented in this thesis primarily covers the subject of analytical modelling of sound propagation in a rectangular duct lined with a bulk-reacting lining for zero mean flow. The particular application of interest is a duct typical of those used in a ventilation system.

Theoretical analysis of sound propagation in a lined duct for automotive dissipative silencers and turbofan aero-engines is now well established where the majority of studies involve fluid flow but are based on the assumption of a locally reacting lining [58, 79, 80, 82]. A duct in a ventilation system is usually lined with a bulk-reacting lining material and is of a larger size compared to the automotive silencer. The assumption of a locally reacting lining reduces the applicability of the available techniques since in practice it requires the lining to be relatively thin compared to the overall duct dimensions, or the absorbent material to have a very high flow resistivity, which is unlikely to be found in the ventilation system.

Although numerical methods offer the benefits of avoiding the root search [41, 74, 83], through an analytical approach useful and intuitive design relations between the characteristics of the lined duct and its acoustic attenuation behaviour can be established more easily compared to the numerical approach. Most applications of the finite element approach address the three-dimensional duct acoustic problems [41, 66]. However, for the sake of simplicity in this analytical approach, a two-dimensional duct acoustic is considered.

The analytical modelling of sound propagation in a lined duct typically involves finding roots of the governing wavenumber equations and the corresponding wave mode shapes and then using these to determine the acoustic pressure and velocity fields at the inlet and outlet junctions of a finite length lined duct in terms of the modal amplitudes. The mode-matching technique requires a complete set of wavenumbers in order to achieve a converged solution for the problem. The eigenvalue solutions for the wavenumbers of a locally reacting lined duct are well researched [21, 49] and for example the Morse charts are available to provide the relationship between the wavenumbers and a single quantity that represents the wall lining, i.e. the surface normal wall impedance.

However for a bulk-reacting lining, the specific wall impedance cannot be represented by a single quantity and thus the modal structure with a bulk-reacting lining is far more difficult to determine than with a locally reacting lining. Furthermore the problem of locating a complete set of roots is yet to be solved, not only in the case of a bulk-reacting lining but also for a locally reacting lining [74]. This has been the main drawback in developing the analytical approach to model sound propagation in a finite length lined duct with a bulk-reacting lining. The use of a

numerical approach such as the finite element method or the boundary element method is limited to low frequencies and/or small ducts since the number of degrees of freedom in the problem grows rapidly with increasing duct dimension and excitation frequency.

Recent developments in the acoustic treatment for turbofan aero-engines have seen the use of multi-segmented liner design to broaden the effective frequency band [25, 84]. This is achieved by redistributing modal energy from the least attenuated mode into other more readily attenuated modes. The benefits of this scattering effect are claimed [12]to work also in a ventilation duct where lined and unlined segments of ducts are used to disturb the plane wave motion at low frequency and excites non-plane wave motion. Furthermore, by preventing axial wave motion in the lining the absorbing material is effectively forced to behave in a locally reacting way.

Most of the modelling work on multi-segmented liners is attributed to turbofan aero-engine applications and is based on the assumption of a locally reacting lining. Therefore the benefit of wave energy scattering on duct attenuation has been discussed in the literature mainly for locally reacting linings. To the author's knowledge, no analytical work on sound propagation in a multi-segmented lined duct with a bulk-reacting lining has been published to date. Hence an analytical study is required to analyse the effect of a multi-segmented lining on a duct lined with a bulk-reacting material, particularly for a periodically lined duct.

The key aim of this work is to provide a complete analytical model of wave propagation in a lined duct with a bulk-reacting lining, for a continuously lined duct as well as a periodically lined duct. The mode matching technique is preferred since the technique allows for a modal solution and hence the scattering effects over the inlet and outlet planes can be quantified. Apart from the analytical model, a method to track all the required wavenumbers in a duct with a bulk-reacting lining is proposed where the wavenumbers are tracked from very low frequency up to high frequency with small frequency intervals. A general guideline is identified so that no solution should be missed at any frequency steps.

1.4 Research contributions

The following are identified as the main research contributions:

1. The dispersion curves for a large number of wave modes in a duct with a bulk-reacting lining are derived. As well as conventional airway modes an additional set of modes associated with the lining is identified. At low frequencies these modes have significant

amplitudes not only in the lining but in the airway as well and so they cannot be neglected in the analysis.

2. An analytical model of wave propagation in a lined duct with multiple lined segments is developed for both a locally reacting lining and a bulk-reacting lining. The model is derived using the well-known mode matching technique but includes additional modes for the case of a bulk-reacting lining, requiring additional constraint equations in the lining.
3. By using the established mode-matching technique for the bulk-reacting lining, the limitations and accuracy of the locally reacting approximation are identified and highlighted.
4. It is established that the attenuation of a section of duct lined with a bulk-reacting material above the cut-on frequency of higher order modes should be determined by taking into account these higher order modes, not just the least attenuated mode. The number of modes to be included has been identified.
5. The effect of periodicity on the performance of a lined duct with both types of lining is established.
6. Experiments have been designed and carried out to measure duct insertion loss with different wall lining configurations, and the measured data have been used to validate the theoretical predictions.

1.5 Thesis layout

This thesis consists of 7 chapters written in a sequence that leads to the final development and validation of an analytical model of sound propagation in a duct lined with periodic sound absorbing material. To reduce the complexity of the problem addressed, the duct is assumed throughout to be two-dimensional although the methods developed can readily be extended to three dimensions. The background and literature review have been laid out in Chapter 1. The problem of finding the wave propagation constants in a duct lined with a locally reacting material is addressed in Chapter 2. The duct is assumed to have a rectangular cross-section with zero mean flow, which is typical for a ventilation duct. For simplicity, the surface normal wall impedance is first treated as a constant independent of frequency to give insight into the nature of the solution. The algorithm used to find the wavenumbers, Müller's method, is developed in this chapter. The nature of the wavenumber solutions is discussed for three different cases of wall impedance: real, imaginary and complex.

In Chapter 3, the acoustic properties of the absorbent material are modelled using a semi-analytical model. The theory for wave propagation in a duct lined with a bulk-reacting lining is

presented leading to the governing dispersion relation. Using Müller's method, as developed in Chapter 2, the transverse wavenumbers in a duct with a bulk-reacting lining as well as a locally reacting lining are found. The dispersion curves for both cases are compared and the duct attenuations are predicted based on the least attenuated mode approach and on the assumption of equal energy density in all incident waves.

Analytical models of sound propagation in a finite length duct are presented in Chapter 4. The mode-matching technique is applied to match the pressure field and axial particle velocity at the inlet and outlet junctions of the lined section of duct. The models are developed both for ducts with a locally reacting and a bulk-reacting lining. The optimum number of modes to be included in the model is investigated and the effect of design parameters on duct attenuation is studied. The mode-matching models are then extended to a periodically/ multi-segmented lined duct in Chapter 5. The potential of having a periodic lining to improve duct attenuation is explored.

The theoretical work is validated with experimental work in Chapter 6. Measurements of duct insertion loss are presented. These were carried out between two adjacent small reverberation rooms with a small aperture connecting them. Various lining arrangements were tested and the results are compared with the theoretical predictions. Finally, conclusions drawn from the results obtained in this thesis are presented in Chapter 7 and potential areas for future research work are suggested.

2. Waves in a duct with a locally reacting lining

A two-dimensional rectangular duct with locally reacting linings on both sides is a classical model for acoustical studies of a lined duct. Sound transmission through a lined duct may be described by a sum of modes if geometry, lining and mean flow are independent of the axial coordinate. The expansion of a sound field in terms of modes forms the basis for many analytical and semi-analytical methods in duct acoustics. Many papers can be found in the literature addressing this topic. However there still exist some problems associated with this model which are yet to be solved and one of them is the numerical computation of the modal propagation constants.

Determination of the lined duct wavenumbers is not a simple task due to the topography of the corresponding eigenvalue problem and the complex arithmetic involved. These eigenvalues are the wavenumber solutions of the characteristic equation of the duct configuration and depend on the boundary conditions. The characteristic equation has an infinite number of solutions and various techniques have been proposed to solve this transcendental equation. For locally reacting linings, the wall properties can be represented in terms of the surface normal impedance and the wavenumber can be determined in terms of this quantity.

One approach is to use the Morse chart [21] that relates the wavenumbers to the wall impedance without having to solve the characteristic equation explicitly. Based on Morse charts, Cremer's rule can be applied to find the optimum impedance for maximum attenuation for a given frequency and duct geometry. However Cremer's rule is only valid for an infinitely long lined duct where the duct attenuation can be approximated from the least attenuated mode. For a finite length lined duct, a complete solution of wavenumbers is required and a technique to solve the characteristic equation directly is desired. The multi-modal solutions to the eigenvalue problem can be obtained by using a numerical approach, for example Müller's method [57, 62]. This iterative procedure starts at sufficiently low frequency where the lining is almost rigid for which the modal solutions are known [82]. For multi-modal solutions, no solution should be attributed to more than one mode and no important solution should be missed. Thus, it is important to identify the modes in order to ensure that the mode order is clear.

This chapter starts with the analysis of an unlined rectangular duct and the fundamental theoretical model is presented. Having identified the order of the modes in the rigid walled duct, the theoretical analysis is extended to the lined duct with a locally reacting lining. Müller's method is applied to solve the eigenvalue problem and the sound waves are studied for three

different wall impedance types: damping-controlled impedance, mass-controlled impedance and stiffness-controlled impedance.

2.1 Sound waves in a rectangular rigid walled duct

The sound propagation in a rectangular duct is governed by the standard wave equation and the special characteristics of the sound field in a duct arise principally from the boundary conditions. The boundary conditions in a duct are governed by the relationship between the acoustic pressure *p*, and particle velocity *u* that is defined by a wall impedance. A surface normal wall impedance is a quantity that relates the sound field at the interface between two media, in this case the airway and the sound-absorbent material. It is defined as the ratio of complex amplitudes of the sound pressure to the component of particle velocity that is normal to the interface. The simplest example of such a boundary condition is that of a sound wave reflecting off a hard surface [85]. Therefore the theory of sound propagation in a rigid walled duct is first presented here for clarity and serves as the basis for the theory of sound propagation in a lined duct.

Consider a rectangular duct as shown in Figure 2.1 with width *b* in the *z* direction and height *h* in the *y* direction. For an inviscid stationary medium, from the basic linearized equations for mass continuity and dynamical equilibrium, the three dimensional wave equation is given by:

$$\left[\frac{\partial^2}{\partial t^2} - c_0^2\nabla^2\right]p = 0 \tag{2.1}$$

where ∇^2 is the Laplacian operator, $\nabla^2 = \frac{\partial^2}{\partial x^2} + \frac{\partial^2}{\partial y^2} + \frac{\partial^2}{\partial z^2}$. c_0 is the speed of sound and p is pressure. For harmonic motion at frequency ω, the general solution of equation (2.1) can be given by [85]:

$$p(x,y,z,t) = (a^+e^{-ik_x x} + a^-e^{ik_x x})(A_1e^{-ik_y y} + A_2e^{ik_y y})(A_3e^{-ik_z z} + A_4e^{ik_z z})e^{i\omega t} \tag{2.2}$$

where a^+, a^- and A_i are arbitrary constants. The time factor of $e^{i\omega t}$ is supressed from this point on.

Following from equations (2.1) and (2.2), the acoustic wavenumbers, *k*, in *x*, *y* and *z* directions are related by:

$$k_x^2 + k_y^2 + k_z^2 = k_0^2 \tag{2.3}$$

where $k_0 = \omega/c_0$ is the acoustic wavenumber in the medium at frequency ω.

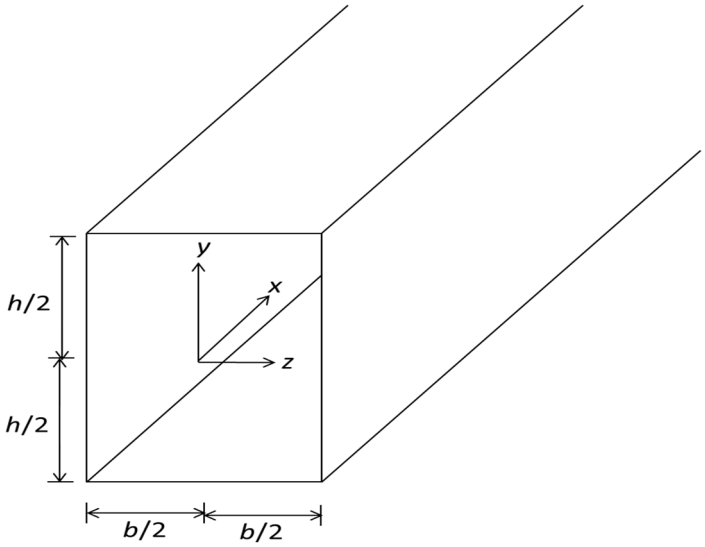

Figure 2.1: An infinitely long rectangular duct

The three dimensional wave problem can be reduced to a two dimensional one if the wavelength in the lateral (z) direction is always greater than twice the duct width, b. This assumption is also used to simplify further the analytical problem at hand even where $2b$ is not longer than the wavelength. In the following analysis, it is assumed that $k_z = 0$.

The axial wavenumber k_x can be found by first solving for the wavenumber k_y in the transverse y direction. Considering only the x-y plane, equation (2.3) can be rearranged into:

$$k_x = \pm\left[k_0^2 - k_y^2\right]^{1/2} \tag{2.4}$$

There are an infinite number of solutions to equation (2.4), corresponding to different modes m. Modes are made up of elementary functions which are solutions to the wave equation in the relevant co-ordinate system of the duct, and which satisfy the boundary conditions. Any wave modes can propagate unattenuated along the x-axis if k_x is real and non-zero. If the transverse wavenumber k_y is purely real or purely imaginary, any particular mode m would propagate unattenuated if

$$k_0^2 - k_y^2 \geq 0 \tag{2.5}$$

If the above inequality is not satisfied, then k_x is purely imaginary and the mode is cut-off and exists as a nearfield wave. It is highly attenuated in space and does not carry energy.

Waves in a duct with a locally reacting lining

To find the allowable values of k_y it is necessary to apply the boundary conditions at the duct wall. From equation (2.2) the pressure distribution across the duct height can be described by:

$$p(y,t) = A_1 e^{-ik_y y} + A_2 e^{ik_y y} \tag{2.6}$$

where A_1 and A_2 are the amplitudes of two acoustic waves travelling in opposite directions from each other along the y axis. From the dynamical equilibrium [85], the transverse particle velocity, u_y is related to the pressure p as:

$$u_y = \frac{-\partial p/\partial y}{i\omega\rho_0} = \frac{1}{\rho_0 c_0}\frac{k_y}{k_0}\left(A_1 e^{-ik_y y} - A_2 e^{ik_y y}\right) \tag{2.7}$$

where ρ_0 is the air density. The reference axis $y = 0$ is defined at the centre of the duct. Since the wall is rigid, the transverse particle velocity at $|y| = h/2$ is zero. Therefore from equation (2.7), we have:

$$A_2 = A_1 e^{-ik_y h} \tag{2.8}$$

Since $y = 0$ is at the centre of the duct and the duct has a symmetric geometry, the solutions to equations (2.6) and (2.7) will consist of symmetrical fields and anti-symmetrical fields. For a symmetrical pressure distribution the pressure gradient at the centre of the duct is zero. Thus, from equation (2.6) we have $A_1 = A_2$, and the solution to equation (2.8) for symmetrical wave modes yields:

$$k_y = m\pi/h, \quad m = 0,\ 2,\ 4,\ldots \tag{2.9}$$

where m refers to the mode index and the even values of m represent even duct modes.

For an anti-symmetrical pressure distribution, the pressure field at the centre of the duct is zero. Therefore equation (2.6) then gives $A_1 = -A_2$. This in turn yields, from (2.8):

$$k_y = m\pi/h, \quad m = 1,\ 3,\ 5,\ldots \tag{2.10}$$

where odd values of m refer to odd duct modes.

We can rewrite equation (2.6) as a cosine or sine function to describe the pressure distribution or the mode shape of each mode:

$$\Phi(y) = \frac{2\cos(k_y y)}{\left|2\cos\left(\frac{k_y h}{2}\right)\right|} = \cos(k_y y) \tag{2.11}$$

for even modes, and:

$$\Phi(y) = \frac{2\sin(k_y y)}{\left|2\sin\left(\frac{k_y h}{2}\right)\right|} = \sin(k_y y) \tag{2.12}$$

for odd modes. The mode shape is normalized with respect to the pressure magnitude at the duct wall, $y = h/2$ to give a maximum pressure amplitude of 1. Figure 2.2 shows the mode shapes of the first six lower order modes in a rigid walled two-dimensional rectangular duct. The fundamental mode, $m = 0$, has wave fronts normal to the axis of the duct and the sound field is in phase at all points across the duct. It is called the plane wave or zero-order mode. The left-hand plots are even modes while the right-hand plots are odd modes.

Figure 2.3 shows the plot of corresponding axial wavenumbers, k_x for the first six lower order modes. The plane wave propagates unattenuated at all frequencies since $k_x = k$ and is always larger than zero. Higher order modes start to propagate once the inequality in equation (2.5) is satisfied, i.e. $k_y < k_0 = \frac{\omega}{c_0}$. The cut-on frequencies are well defined in the absence of dissipation and are given by $k_0 h = m\pi$. Below the cut-on frequency, higher order modes exist as nearfield waves with large imaginary k_x and once they cut-on, they propagate unattenuated with purely real k_x which approaches k_0 at high frequency.

The task of finding the mode solutions are the same regardless of whether the duct is two-dimensional or three-dimensional. For the latter case, the same procedure has to be followed twice. As well as k_y this yields $k_z = n\pi/h$ for integer values n. The wave modes are then defined by (m,n) which cut-on at $\sqrt{k_y^2 + k_z^2} = \frac{\omega}{c_0}$.

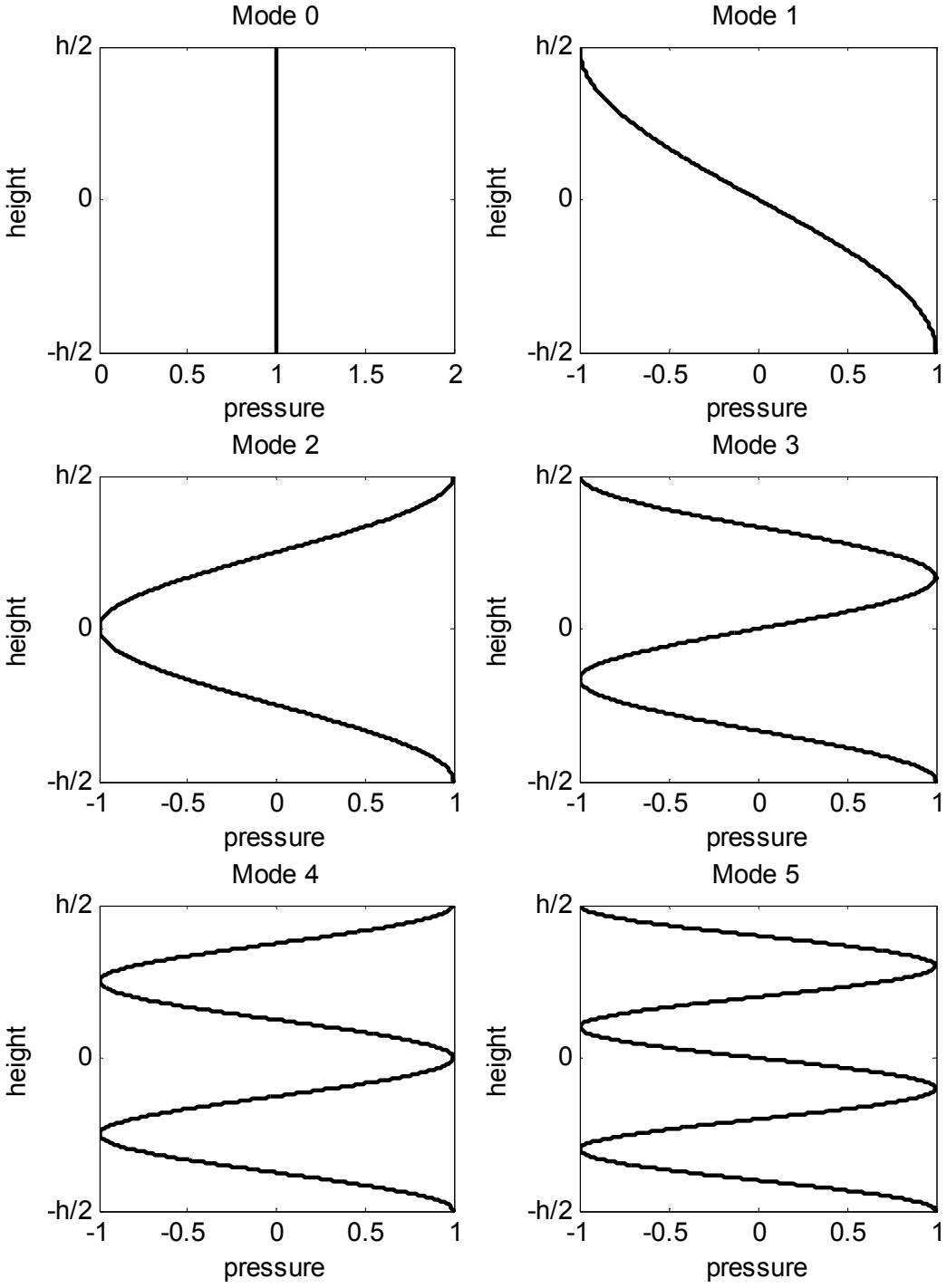

Figure 2.2: The mode shapes of the first six modes in a rigid walled rectangular duct

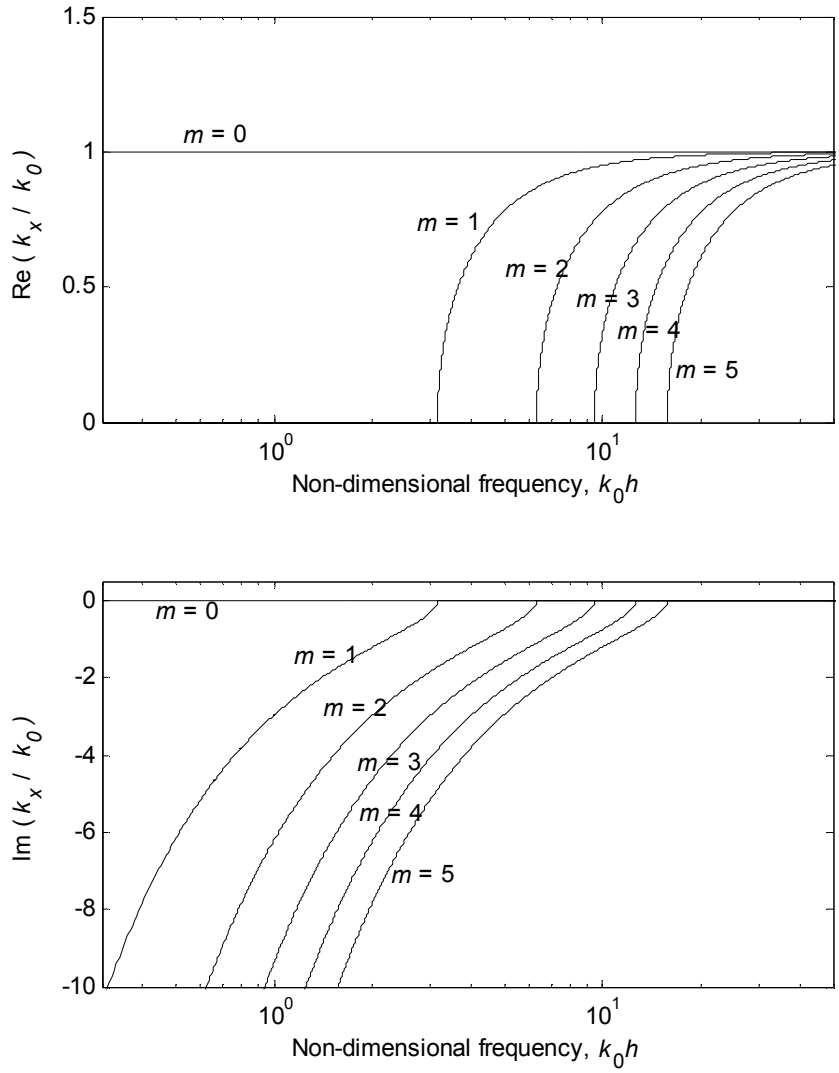

Figure 2.3: Axial wavenumbers k_x for the first six wave modes in a rigid walled duct

2.2 Sound waves in a duct with a locally reacting lining

When the walls of the duct are lined with absorptive material, the normal particle velocity at the boundary can be non-zero. The boundary condition is now changed and the modes may have complex valued axial wavenumbers and hence be attenuated along the duct. If the axial wave propagation in the wall lining is neglected, the normal particle velocity generated by incident sound at any point on the surface depends only on the local pressure and is independent of the incident angle. The material is said to be locally-reacting and the material surface can be characterized uniquely in terms of its surface normal wall impedance.

For a complex valued impedance, the real part of the impedance is called the resistance, *R*, with dissipative effects and the imaginary part is called the reactance, *X*, with reactive effects. Energy dissipation along the duct can only be achieved if the wall impedance contains resistive components. A reactive component alters the spatial form and propagation speed of the sound field, but dissipates no energy. The imaginary part of impedance can be positive (mass-controlled) or negative (stiffness-controlled) and these two cases have different effects on the acoustic modes of the duct.

In practice the wall impedance is frequency dependent and depends on the material characteristics and thickness of the lining. However, in this chapter, the wall impedance is treated as a constant value that does not vary with frequency. This is to reduce the complexity of problem at hand and to understand better the nature of the solution to the eigenvalue problem. It is convenient to non-dimensionalise the surface normal wall impedance by the acoustic impedance, $Z_n' = Z_n / \rho_0 c_0$.

Assuming a locally reacting lining, the transverse particle velocity at the surface depends only on the acoustic impedance and on the local pressure. Therefore at the boundary, the surface normal wall impedance can be represented by:

$$Z_n' = \frac{p\left(h/2\right)}{\rho_0 c_0 u_y\left(h/2\right)} = \frac{\left(A_1 e^{-ik_y h/2} + A_2 e^{ik_y h/2}\right)}{\frac{k_y}{k_0}\left(A_1 e^{-ik_y h/2} - A_2 e^{ik_y h/2}\right)} \tag{2.13}$$

Assuming a symmetrical arrangement, the duct modes will again be symmetric or anti-symmetric. For even duct modes, it was found earlier that $A_1 = A_2$. Then equation (2.13) can be rearranged into a more familiar form of characteristic equation for the wavenumber as found in the literature [85],

$$-iZ_n' \frac{k_y}{k_0} = \cot\left(\frac{k_y h}{2}\right) \tag{2.14}$$

For odd duct modes, $A_1 = -A_2$, which in turn yields

$$iZ_n' \frac{k_y}{k_0} = \tan\left(\frac{k_y h}{2}\right) \tag{2.15}$$

Both types of solution are possible and are orthogonal to each other in ducts with a symmetrical lining. There are an infinite number of solutions to the two wavenumber equations due to the

periodicity of the tan and cot functions. An index m is attributed to the solutions starting from $m = 0$. But the solutions for k_y are no longer correspond to the simple formulae (2.9) and (2.10). For a set of solutions, $m = 0,\ 1,\ 2,\ldots,\ M$, it is important to ensure that each mode is attributed to a unique value of m.

The transcendental equations (2.14) and (2.15) can be solved numerically. Among the widely used methods found in the literature are the Newton-Raphson method [49, 61, 80] and Müller's method [57, 62]. The Newton-Raphson method uses a starting value to search for a solution to an equation along the direction of the derivative of the function in the equation. Müller's method, on the other hand, requires three initial values to start the iteration, but it does not need the derivative of the function. Furthermore, the direction in which Müller's method searches for a solution can be adjusted through the selection of the initial values [57]. Müller's method is based on the secant method and uses a quadratic polynomial to fit an approximate function to the actual curve in the neighbourhood of the root [86] and is a more commonly used iteration method suited to complex roots [62]. The latter method is selected as the numerical tool for finding the wavenumber solutions in this work.

It is common to encounter numerical problems when solving equations (2.14) and (2.15) because the numerical methods may jump in an uncontrolled fashion from one solution to another due to the infinite number of possible of the solutions. It is proposed in the literature that the wavenumbers are tracked from low frequency to high frequency with sufficiently small frequency step [57]. At very low frequency, the acoustic wavelength is very long such that the acoustic wavenumber k_0 approaches zero. This yields $-i\infty$ and $i\infty$ for the left-hand side of equation (2.14) and (2.15) respectively which in turn gives solutions of $k_y h = m\pi$, where $m = 0,\ 1,\ 2,\ldots$, which are equivalent to the solutions for a rigid duct.

At very high frequency, the acoustic wavenumber $k_0 \to \infty$ resulting in the left-hand side of both equations (2.14) and (2.15) becoming equal to zero. This corresponds to the condition in a duct with a pressure release boundary where the wall impedance Z_n is zero due to the zero pressure at the wall. The pressure distributions, or mode shapes, for the first six lower order modes in a duct with a pressure release boundary are shown in Figure 2.4. The wavenumber solution is then given by $k_y h = (m \pm 1)\pi$. Therefore it is expected that the real part of the wavenumber k_y for mode m will start at $m\pi$ at low frequency and tend to $(m \pm 1)\pi$ at high frequency, while the imaginary part starts and ends at zero.

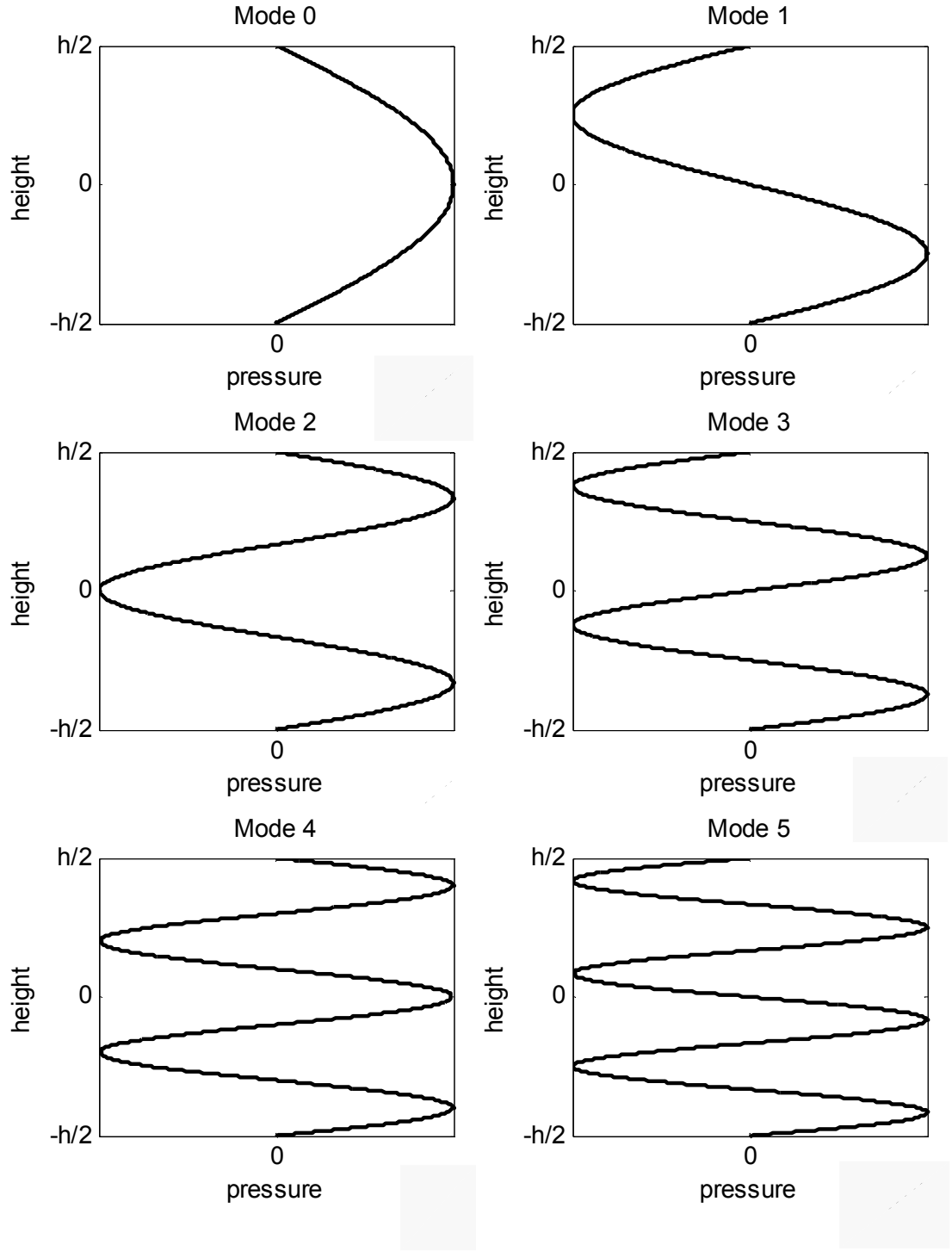

Figure 2.4: The mode shapes of the first six lower order modes in a rectangular duct with pressure release boundary

2.3 Use of Müller's method for solving wavenumber equation

Müller's method is an iterative method for solving an equation $f(x)=0$ that requires three initial guesses, x_0, x_1, and x_2 near a root. A second-degree polynomial is used to fit the three points. Using a modified quadratic formula, the zero of the polynomial is found and used as an improved estimate of the root. One of the new estimated roots replaces one of the initial guesses and the iteration continues until the solution converges [87].

From a numerical point of view, as it is numerically easier to find a zero than a pole [88], the reciprocals of the wavenumber equations (2.14) and (2.15) are taken to form the objective functions for use in Müller's method. Therefore the routine is used to find the zeros of the following functions of non-dimensional wavenumber for even modes:

$$f(k_y h)=\tan\left(\frac{k_y h}{2}\right)-i\frac{k_0 h}{k_y h Z_n'} \tag{2.16}$$

and for odd modes:

$$f(k_y h)=\cot\left(\frac{k_y h}{2}\right)+i\frac{k_0 h}{k_y h Z_n'} \tag{2.17}$$

where the non-dimensional variable $x=k_y h$ is used for the search. The iteration procedure in this method is as follows [89]:

1. Find three initial guesses, x_0, x_1 and x_2. The wavenumber for the hard-walled duct is used as the third guess, x_2 at the starting frequency. This is given by $k_y h=m\pi$, where m is the index of mode; $m=0,\ 1,\ 2,\ldots$. The other two guesses are slight changes to this value given by $x_0=x_2-0.01$ and $x_1=x_2+0.01$.
2. Evaluate $f_0=f(x_0)$, $f_1=f(x_1)$ and $f_2=f(x_2)$.
3. Follow Müller's algorithm:
   i. $h_1=x_1-x_0$ and $h_2=x_2-x_1$
   ii. $\Delta_1=(f_1-f_0)/h_1$ and $\Delta_2=(f_2-f_1)/h_2$
   iii. $a=(\Delta_2-\Delta_1)/(h_2+h_1)$, $b=\Delta_2+a\times h_2$ and $c=f_2$
4. The new root is given by the following quadratic formula:

$$x_3 = x_2 - \frac{2c}{b \pm \sqrt{b^2 - 4ac}} \tag{2.18}$$

There are two possible roots but the one of interest is the one that is closer to x_2. Thus, the sign of the square root is chosen such that it gives the maximum denominator value. However, since the roots may be complex, the solution is not so straight forward. Let $b = b_r + ib_i$ and the square root of the discriminant be represented by $d = d_r + id_i$. To maximize the denominator, whichever sign makes $b_r d_r + b_i d_i$ positive is chosen. In the case where this term is zero, then either the newly found x_3 is a root or one of b and d is real and the other is imaginary. In the latter case, the sign is chosen which makes d negative.

5. The new root, x_3, replaces x_2, and x_1 and x_0 take the previous values of x_2 and x_1 respectively. The iteration process stops when:
   i. The function evaluated at the point x_{n+1} is sufficiently small, $\left|f\left(x_{n+1}\right)\right| < tol$ where *tol* is a stopping condition set to 10^{-8}

   or

   ii. A maximum number of iterations, N, has been reached.
6. Having found the wavenumbers at one frequency these are used as the initial guess x_2 at the next frequency. The frequency step used is 1 Hz.

2.4 Wavenumbers for a duct with resistive or reactive wall impedance

By using Müller's method, the transverse wavenumbers of the acoustic waves in a duct with a locally reacting lining can be found. In practice, the impedance of the absorptive material is a function of frequency. However, in this chapter, for simplicity and to give insight into the nature of the solutions, constant values of the surface normal wall impedance are used. The variation of the wavenumbers with frequency alone can be studied and a simple visual check can be made of whether 'mode jumping' occurs with the method. The impedance is assumed to be resistive (impedance is real, $Z_n' = R$), reactive (impedance is imaginary, positive or negative, $Z_n' = \pm iX$), or it may consist of both resistive and reactive parts (complex impedance, $Z_n' = R \pm iX$). In the following examples, to calculate the wavenumbers for up to a total of 100 modes from 1 Hz to 10000 Hz with a frequency step of 1 Hz, the computation took less than a minute. The required wavenumbers can be found in a short time and this does not involve expensive computational cost.

2.4.1 Real impedance

A real impedance contains only a resistive component and from the wavenumber equation, for example equation (2.14), the resulting transverse wavenumbers, k_y are complex. This gives a complex axial wavenumber that leads to attenuation along the duct.

The transverse wavenumbers for the first six modes are found using Müller's method and are plotted in Figure 2.5 for a value of non-dimensional impedance $Z_n' = 2$. This shows the real and imaginary parts of $k_y h$ as a function of non-dimensional frequency $k_0 h$ as contained in equation (2.16) and (2.17). The transverse wavenumbers in a rigid duct were used as one of the initial guesses, $x_2 = m\pi$. The other two guesses were set as a slight variation to x_2 where $x_0 = x_2 - 0.01$ and $x_1 = x_2 + 0.01$. The real parts of the transverse wavenumber start at $m\pi$ at low frequency and end at $(m+1)\pi$ at high frequency and this is shown in the plot of $\mathrm{Re}(k_y h)$ in Figure 2.5. If any of the modes $(m+1)\pi$ is missing at high frequency or if any are duplicated, this would suggest that 'mode jumping' has occurred in Müller's algorithm and can be corrected by adjusting the values of x_0 and x_1, or by reducing the frequency step size.

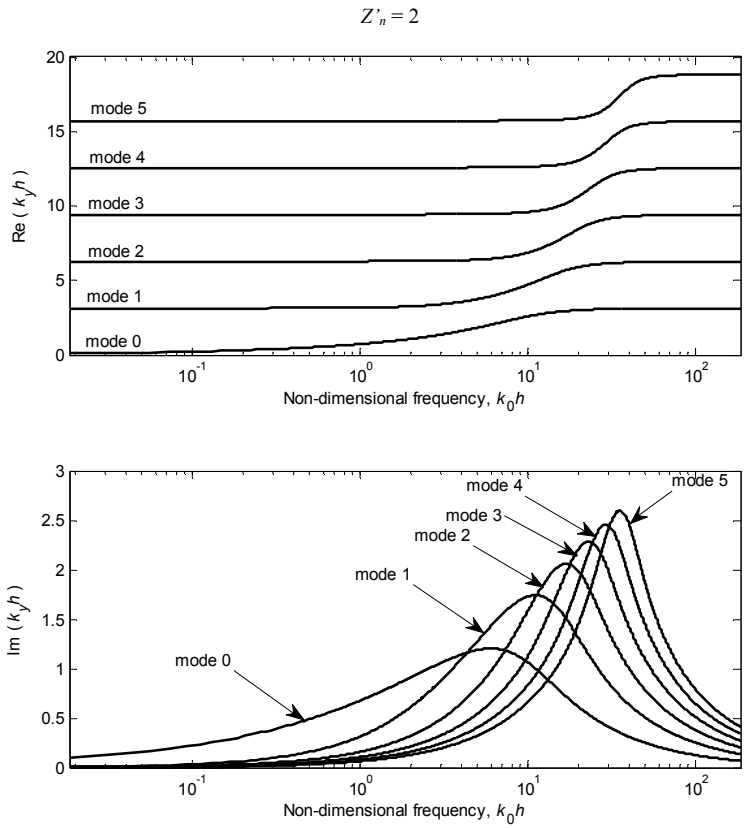

Figure 2.5: Wavenumber plot for a duct lining with real surface normal impedance

Figure 2.5 shows that, at low and high frequency, the imaginary part of the transverse wavenumbers approaches zero as noted previously. The effect of the non-dimensional impedance value on the transverse wavenumber is shown in Figure 2.6. From equation (2.16) and (2.17) it can be seen that Z_n' occurs in the ratio of Z_n'/k_0h. Therefore an increase in impedance corresponds to a decrease in frequency as shown in the figure.

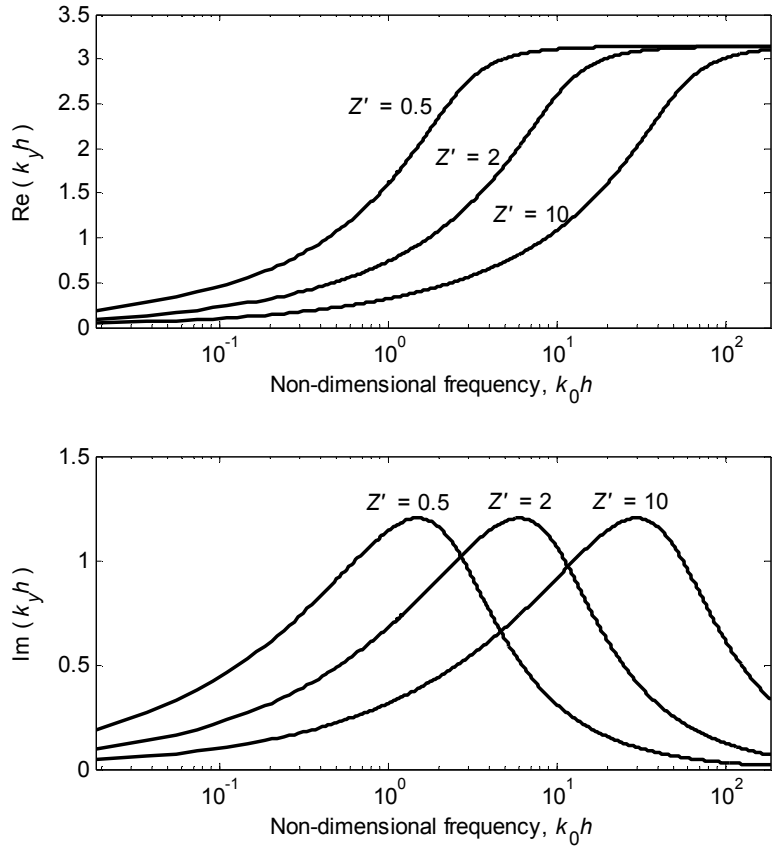

Figure 2.6: Transverse wavenumbers for mode 0 for various real values of impedance

The axial wavenumber can be calculated from the wavenumber relation $k_x = \sqrt{k_0^2 - k_y^2}$. The real part of the axial wavenumbers are shown in Figure 2.7 (a) where the wavenumber is normalized with respect to the acoustic wavenumber k_0. For a dissipative wall, the wavenumbers do not have a clear cut-on frequency. In a rigid duct, the transverse wavenumber k_y is always real which results in either real or imaginary axial wavenumber k_x; each mode starts to propagate at a well-defined cut-on frequency once the inequality in equation (2.5) is satisfied (a frequency point where the axial wavenumber changes from imaginary to real). In a lined duct with resistive wall impedance, the transverse wavenumbers are complex, resulting in complex axial

wavenumbers. Therefore, even at low frequency the axial wavenumbers k_x have non-zero real parts but with large imaginary parts.

At very low frequency, the imaginary part of the transverse wavenumber, k_y is close to zero. Writing $k_y = k_{yr} + ik_{yi}$ and expanding k_x/k_0 at low frequency gives

$$\frac{k_x}{k_0} \simeq \left(-\frac{k_{yr}^2}{k_0^2} - i\frac{2k_{yr}k_{yi}}{k_0^2} \right)^{1/2} \tag{2.19}$$

where for a complex number $y = a + ib$, the real part of $\sqrt{y}$ is given by

$$\mathrm{Re}\left(\sqrt{y}\right) = \sqrt{\frac{|y| + a}{2}} \tag{2.20}$$

Therefore, the real part of equation (2.19) can approximately be given by

$$\mathrm{Re}\left(\frac{k_x}{k_0}\right) \simeq \frac{k_{yi}}{k_0} \tag{2.21}$$

At high frequency, $\mathrm{Re}\left(k_x/k_0\right)$ approaches a value of 1 while the wave modes have small attenuation at high frequency.

For an infinitely long lined duct, the least attenuated mode is usually the fundamental mode [21]. Therefore the transmission loss for the duct can be estimated from the imaginary part of this axial wavenumber. The transmission loss for each mode over a distance l can be calculated by taking the ratio of the pressure at an initial point, $x = 0$, to the pressure at some distance, l away, in dB:

$$TL = 20\log_{10}\left|\frac{p(0)}{p(l)}\right| \tag{2.22}$$

The pressure at any point along an infinitely long duct is given by $p(x) = A^+ e^{-ik_x x}$. Since transmission loss is associated with the imaginary parts of the axial wavenumber, the transmission loss can be written as

$$\begin{aligned} TL &= 20\log_{10} e^{\mathrm{Im}(k_x)l} \\ &= 8.686\,\mathrm{Im}\left(k_x\right)l \end{aligned} \tag{2.23}$$

and can be expressed in general form as a transmission loss per standard length where here the standard length is chosen as the duct width [54]:

$$TL(h) = 8.686\,\mathrm{Im}\left(k_x h\right) \tag{2.24}$$

The fundamental mode propagates at all frequencies but with non-zero attenuation, while for higher order modes the wavenumbers at low frequency have non-zero real part and the imaginary part is very large. From the transmission loss plot in Figure 2.7 (b), it can be seen that the fundamental mode is the least attenuated mode at all frequencies.

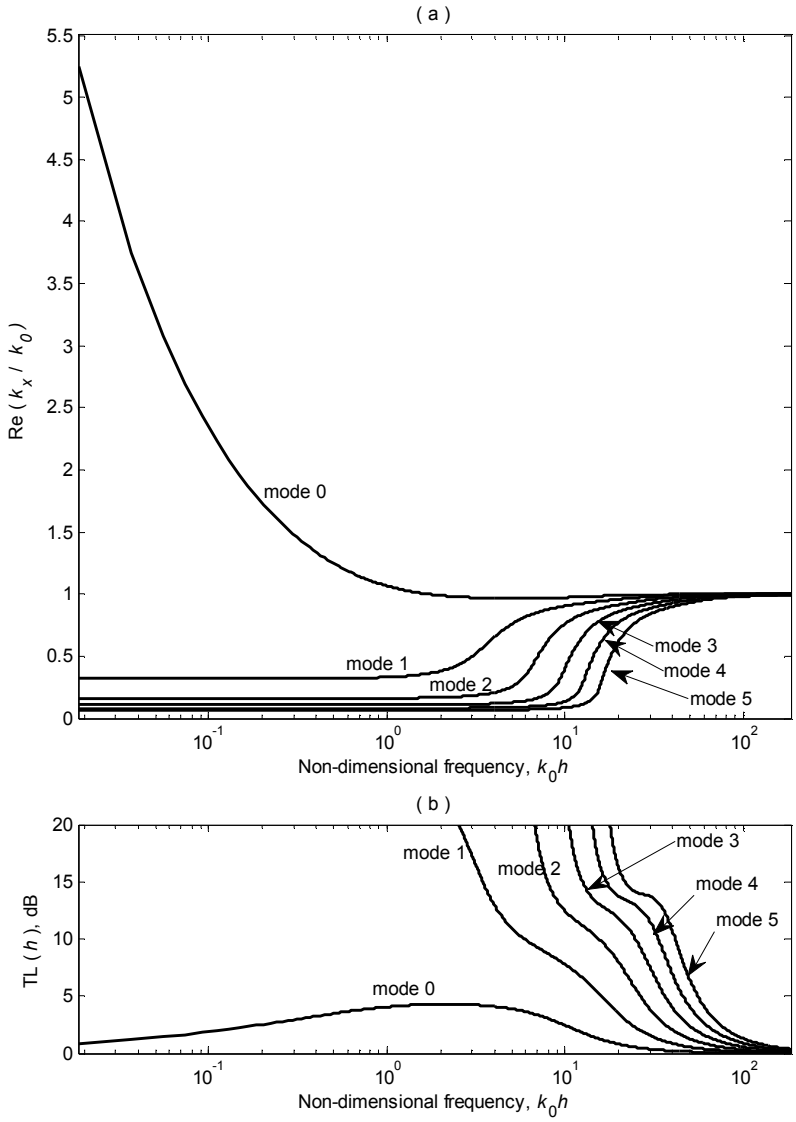

Figure 2.7: (a) Real part of the axial wavenumber normalized by the acoustic wavenumber, k_0 and (b) the transmission loss over a length h calculated from equation (2.24) for $Z_n' = 2$

2.4.2 Positive imaginary impedance

A wall lining with positive purely imaginary impedance is reactive and mass controlled. The wall lining does not dissipate sound energy and from the wavenumber equation in (2.14) and (2.15), a positive imaginary impedance results in a real $k_y h$. The wall lining only causes duct attenuation if the inequality in equation (2.5) is not satisfied, i.e. the mode is cut-off and exists as a nearfield wave.

Figure 2.8 shows the transverse wavenumbers for the first six modes obtained from Müller's method for an impedance of $Z_n' = 2i$. The same initial guesses are used as in the previous case. The same trend is observed in the plot of $\mathrm{Re}\left(k_y h\right)$ where at low frequency it starts at the value of $m\pi$ and ends at $(m+1)\pi$ at high frequency. The dashed line is added to indicate the non-dimensional acoustic wavenumber. The frequency at which the acoustic wavenumber curve crosses the transverse wavenumber curve i.e $k_y = k_0$, is the cut-on frequency of the respective wave mode.

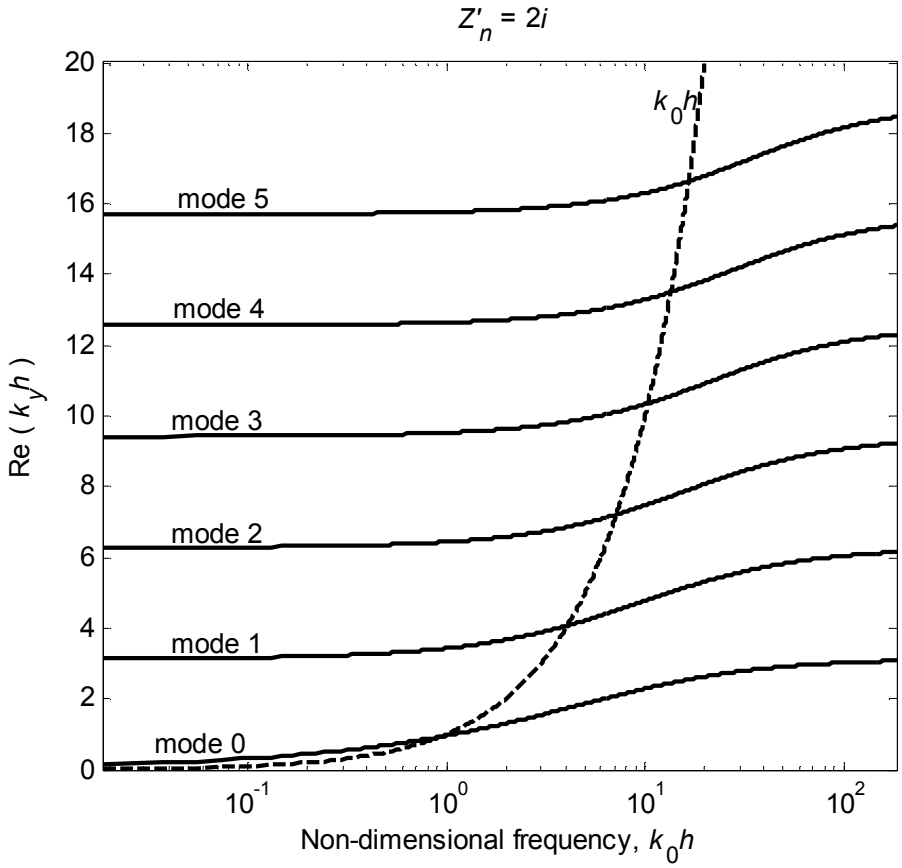

Figure 2.8: Real part of transverse wavenumbers in a lined duct with a positive imaginary surface normal impedance, $Z_n' = 2i$

Since the transverse wavenumber is real, the wave modes have a clear cut-on frequency as shown in the axial wavenumber plot in Figure 2.9. At very low frequency where $k_y > k_0$ for all modes, no waves propagate in the lined duct, not even the fundamental mode. The fundamental mode only exists as a nearfield wave at low frequency and does not carry energy. Once the modes cut-on, they propagate unattenuated and the only means of attenuation would be through reflection at the duct inlet and outlet. Reducing the impedance value shifts the mode's cut-on frequency to a higher frequency. The cut-on frequency can also be increased by reducing the duct height, h.

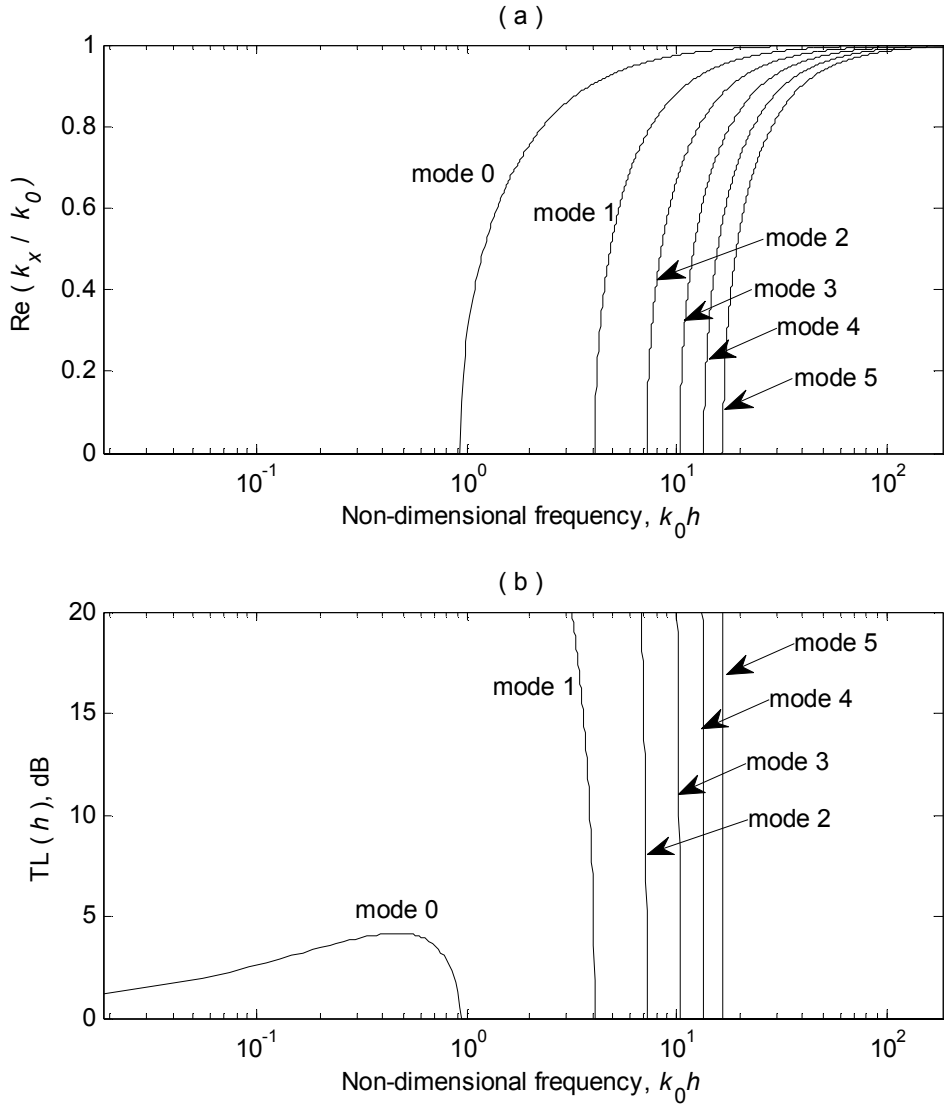

Figure 2.9: (a) Real part of the axial wavenumber normalized by the acoustic wavenumber, k_0 and (b) the transmission loss per unit length for a lined duct with a positive imaginary surface normal impedance, $Z_n' = 2i$

2.4.3 Negative imaginary impedance

A negative imaginary impedance is stiffness controlled. Using Müller's method and the same initial guesses as in previous cases, the transverse wavenumbers are obtained and plotted in Figure 2.10. From the even and odd wavenumber equations, a negative imaginary impedance results in real transverse wavenumbers, similar to the mass controlled impedance. At low frequency, $\cot\left(k_y h/2\right) \to -\infty$ and $\tan\left(k_y h/2\right) \to \infty$. The cotangent and tangent functions are plotted in Figure 2.11. According to this it can be expected that the wavenumbers start at $m\pi$ at low frequency and end at $(m-1)\pi$ at high frequency, where m starts at 1 (an odd mode). The first even mode is $m = 2$. This is seen in the results shown in Figure 2.10.

For other higher order modes, the transverse wavenumbers are real with zero imaginary parts. The transverse wavenumbers start at $m\pi$ at very low frequency but end at $(m-1)\pi$ at high frequency, unlike the other two previous cases. This is because the cotangent function approaches zero from $-\infty$ (and the tangent function approaches zero from ∞) so that its argument $k_y h$ decreases from $m\pi$ to $(m-1)\pi$. This is shown in the cotangent and tangent plot in Figure 2.11. For real or positive imaginary impedance, the cotangent function approaches zero from ∞ (and the tangent function approaches zero from -∞) corresponding to increasing $k_y h$ from $m\pi$ to $(m+1)\pi$. Therefore the surface normal wall impedance determines the direction of $\mathrm{Re}\left(k_y h\right)$ as frequency increases. The asymptotes for the lower and upper frequency limits for each mode can serve as a guide in tracking the wavenumbers to avoid any missed solution during the iteration process.

The fundamental mode $m = 0$ is missing in the plot of real transverse wavenumbers. In fact the corresponding transverse wavenumber is purely imaginary. This can be shown by taking an imaginary value for $k_{y,0} h = i\gamma$. Then from equation (2.14) for the negative imaginary impedance, $Z_n' = -iX$:

$$X \frac{\gamma_0}{k_0} = \coth\left(\frac{\gamma_0 h}{2}\right) \tag{2.25}$$

At high frequency as $\gamma_0 h$ increases, i.e. $\gamma_0 \to \infty$, and the value of coth approaches 1. For the first odd mode, $m = 1$, the transverse wavenumber $k_{y,1} h$ starts at π at low frequency and the real part goes to zero and it becomes imaginary at a particular frequency. For imaginary $k_{y,1} h = i\gamma_1$ with negative imaginary impedance, equation (2.15) now becomes:

$$X\frac{\gamma_1}{k_0}=\tanh\left(\frac{\gamma_1 h}{2}\right) \tag{2.26}$$

At the particular frequency when $\mathrm{Re}\left(k_y h\right)=0$, the value of γ is small such that $\tanh\left(\gamma_1 h/2\right)\simeq\gamma_1 h/2$ and consequently $k_0 h=2X$ as shown in Figure 2.10. As frequency increases, γ continues to increase with frequency. As $\gamma_1\to\infty$, the value of tanh approaches the limiting value of 1. In both of these modes the sound pressure decays away from the wall lining and the mode becomes localized at the wall. This type of wave is called a surface wave [49, 53].

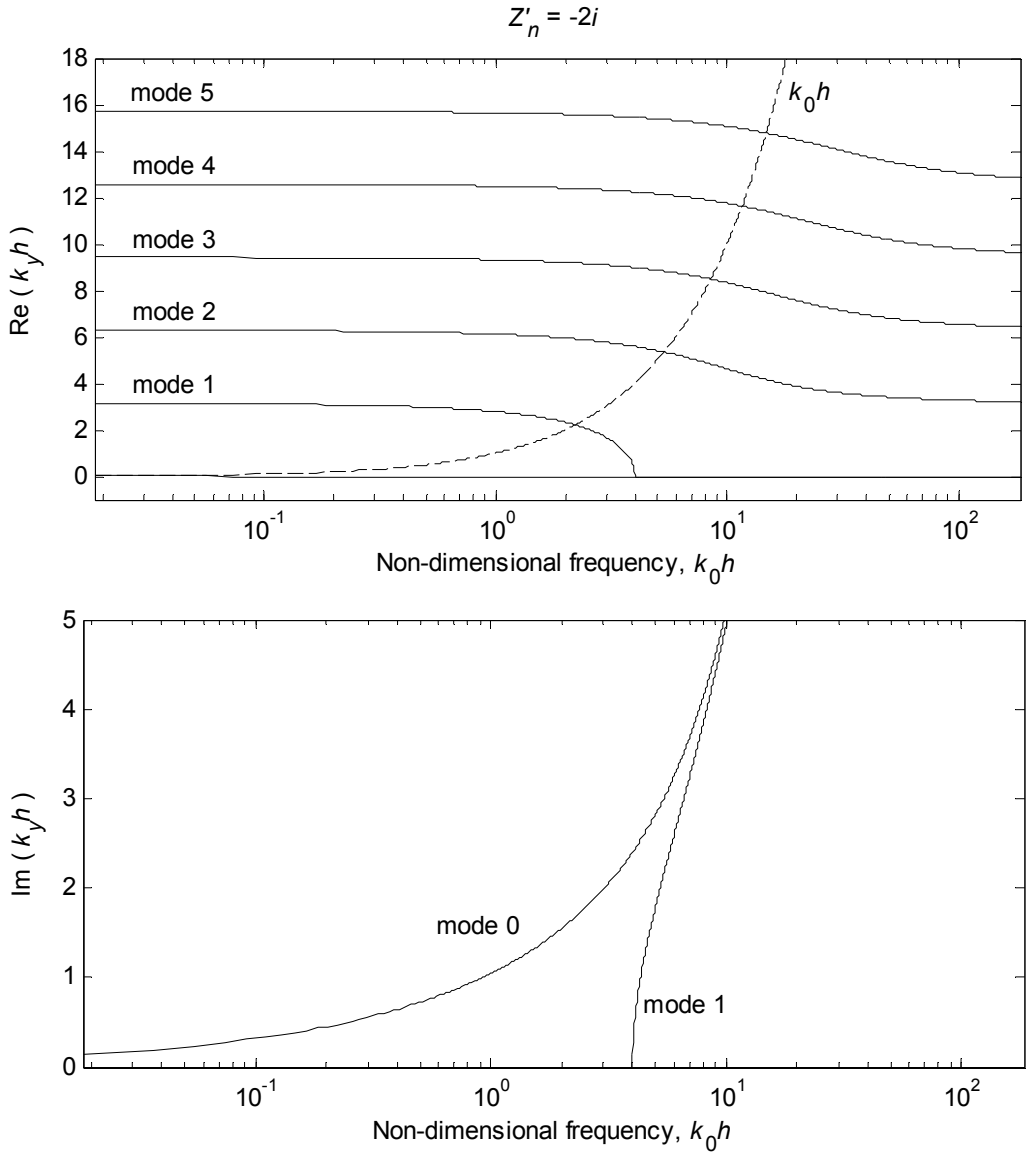

Figure 2.10: Transverse wavenumbers for a lined duct with negative imaginary surface normal impedance, $Z_n'=-2i$

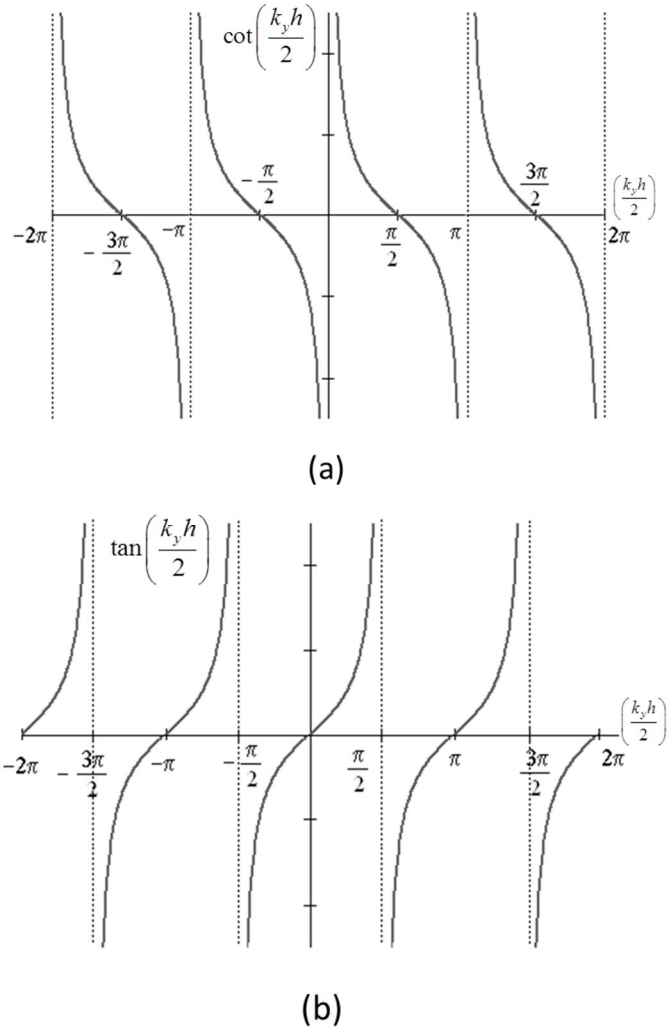

Figure 2.11: Plot of cotangent and tangent functions

Figure 2.12 shows the pressure distribution of mode 0 and mode 1 at three different frequencies; $k_0 h = 0.1$, $k_0 h = 10$ and $k_0 h = 100$. At low frequency represented by $k_0 h = 0.1$, the mode shapes are almost the same as the mode shapes in a duct with rigid walls. At mid frequency, $k_0 h = 10$, the imaginary parts of the transverse wavenumbers become larger and the sound pressure starts to decay away from the walls. At high frequency, $k_0 h = 100$, the imaginary parts of the wavenumbers become very large; the sound pressure is localized at the wall and is zero elsewhere. Since there is only a single positive solution to each of equations (2.25) and (2.26), for a lined duct with a negative imaginary surface normal impedance, two surface waves exist at high frequency. One is an even mode and the other is an odd mode. Since each even and odd mode has a pair of positive and negative going waves, a rectangular duct lined on two opposite

walls can have in total four surface waves at high frequency. This is double the number of surface waves found by Rienstra [53] in his analysis on a circular duct with zero mean flow.

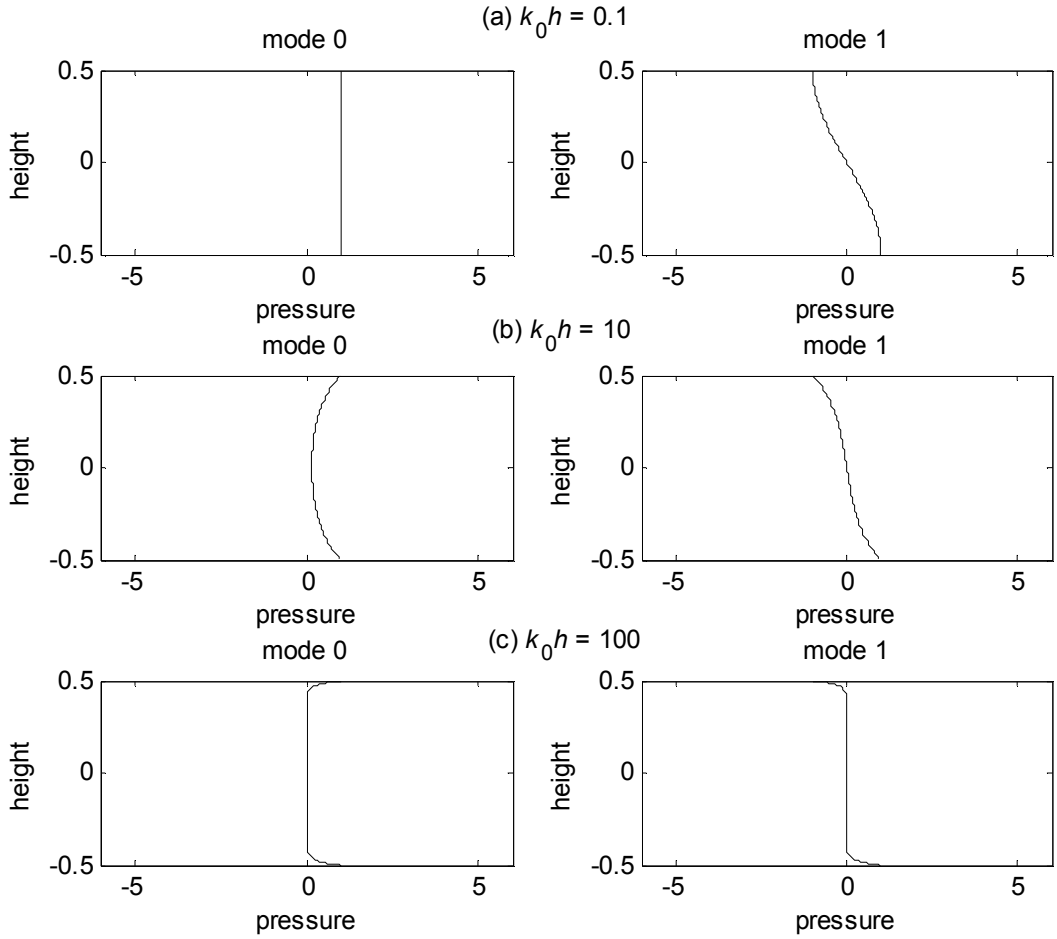

Figure 2.12: Mode shape of the two surface waves at three different frequencies for a lined duct with a negative imaginary surface normal impedance, $Z_n' = -2i$

The resulting axial wavenumbers corresponding to the transverse wavenumbers in Figure 2.10 are shown in Figure 2.13. The fundamental mode propagates unattenuated at all frequencies and other higher order modes propagate unattenuated once they are cut-on. For mode 0 and mode 1, that exist as surface waves at high frequency, they propagate at a slower speed than c_0 $\left(k_x > k_0\right)$ while for other modes, the axial wavenumber approaches k_0 at high frequency. This can be approximated as $k_x = \sqrt{k_0^2 + \dfrac{k_0^2}{X^2}} = k_0\sqrt{1+X^{-2}} \simeq 1.12k_0$ for $X = 2$.

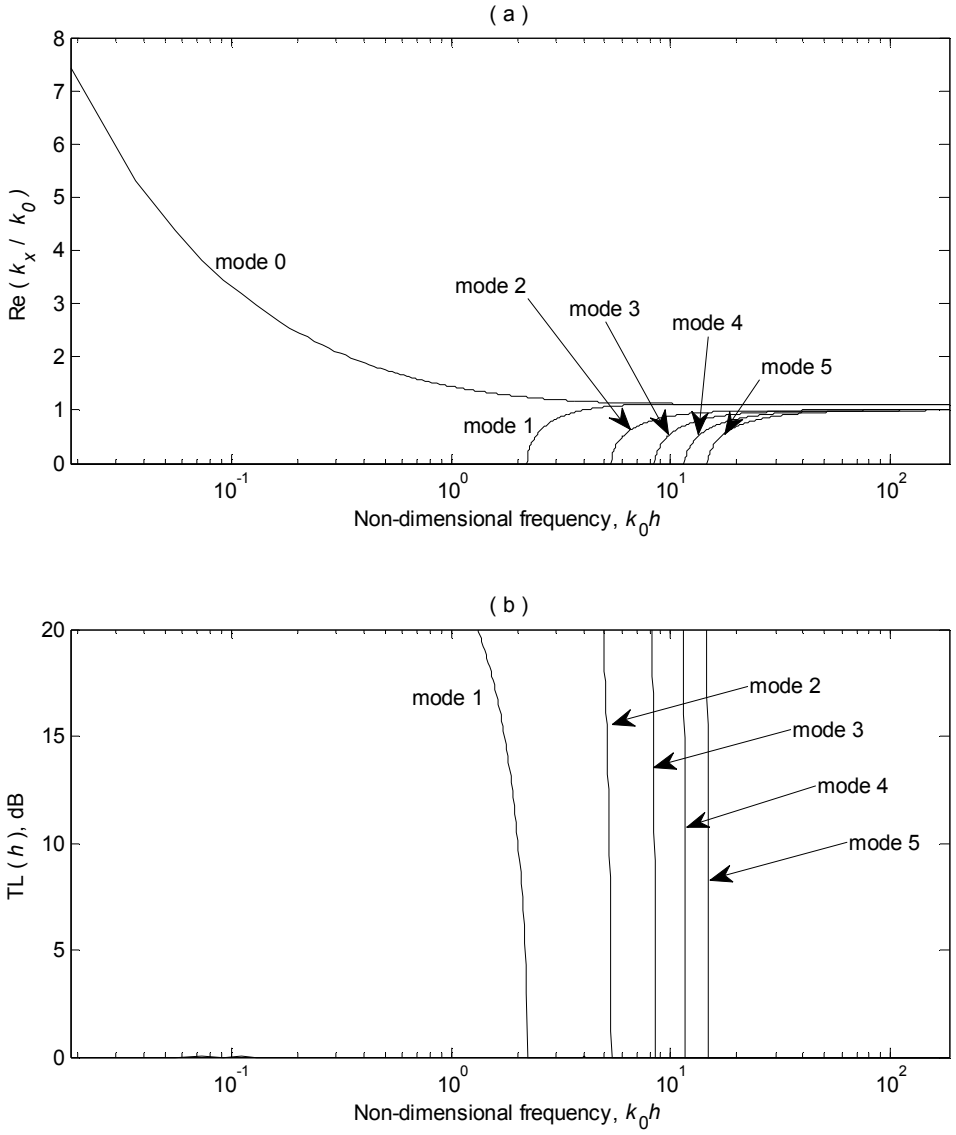

Figure 2.13: (a) Real part of the axial wavenumber normalized by the acoustic wavenumber, k_0 and (b) the transmission loss per length h for a lined duct with a negative imaginary surface normal impedance

2.5 Wavenumbers in a duct with complex wall impedance

The wall impedance in practice is complex and depending on frequency, the impedance can have a negative imaginary part. It has been shown in the previous section, by using a constant value of impedance, that when the impedance is purely imaginary and negative, two surface waves exist at high frequency. This is also the case when the impedance is complex with a negative imaginary part [49, 52].

In the case of purely negative imaginary impedance, the surface waves at high frequency correspond to mode 0 and mode 1 at low frequency and the transverse wavenumbers are purely imaginary. However when the wall impedance is complex, the transverse wavenumbers are found to be complex and increase with frequency. Let the complex impedance be written as $Z_n' = Z_r\left(1 + iZ_{ir}\right)$ where Z_{ir} is the ratio of the imaginary part to the real part, and Z_r is an arbitrary value.

The corresponding mode for surface waves is found to depend on the ratio Z_{ir} . A simulation study was carried out where Z_{ir} was varied from -2 to 2 and the value of $Z_r = 1$ was chosen. For $-2 \le Z_{ir} < -0.8$ the surface waves correspond to mode 0 and mode 1 as for the purely imaginary case. Figure 2.14 shows the transverse wavenumbers for $Z_n' = 1 - 0.8i$. Here the surface waves correspond to mode 1 and mode 2 at low frequency. At $Z_{ir} = -0.5$, the surface waves change to correspond to modes 2 and 3 as shown in Figure 2.15. The next four changing points are Z_{ir} = -0.38, -0.31, -0.26 and -0.23 where the surface waves correspond to modes 3 and 4, modes 4 and 5, modes 5 and 6, and modes 6 and 7, respectively. The simulation was repeated for $Z_r = 0.2$ with similar results; the corresponding results are shown in Figure 2.16. The "changing points" for the surface waves are the same with $Z_r = 1$.

From this simulation study, for a complex wall impedance with negative imaginary part, at high frequency surface waves exist but which low frequency modes they correspond to depends on the ratio of the imaginary part to the real part of the wall impedance. The transverse wavenumbers of the surface waves are complex and increase unboundedly with frequency. However for other wave modes the real part of the transverse wavenumbers starts at a low frequency asymptote, $m\pi$, and ends at a high frequency asymptote, $(m \pm 1)\pi$ where the $\pm$ depends on the order of the surface waves.

The axial wavenumbers corresponding to the transverse wavenumbers shown in Figure 2.14 and Figure 2.15 are plotted in Figure 2.17. At high frequency, the real part of k_x for the surface waves is smaller than k_0 but it is highly attenuated. For an infinitely long duct, these surface waves may not be significant due to their high attenuation, but for a finite length lined duct, they have to be included in the finite set of wavenumbers to define the pressure distribution completely across the duct height, especially at a region close to an impedance discontinuity. They are therefore important for the mode matching technique that will be considered in Chapter 4.

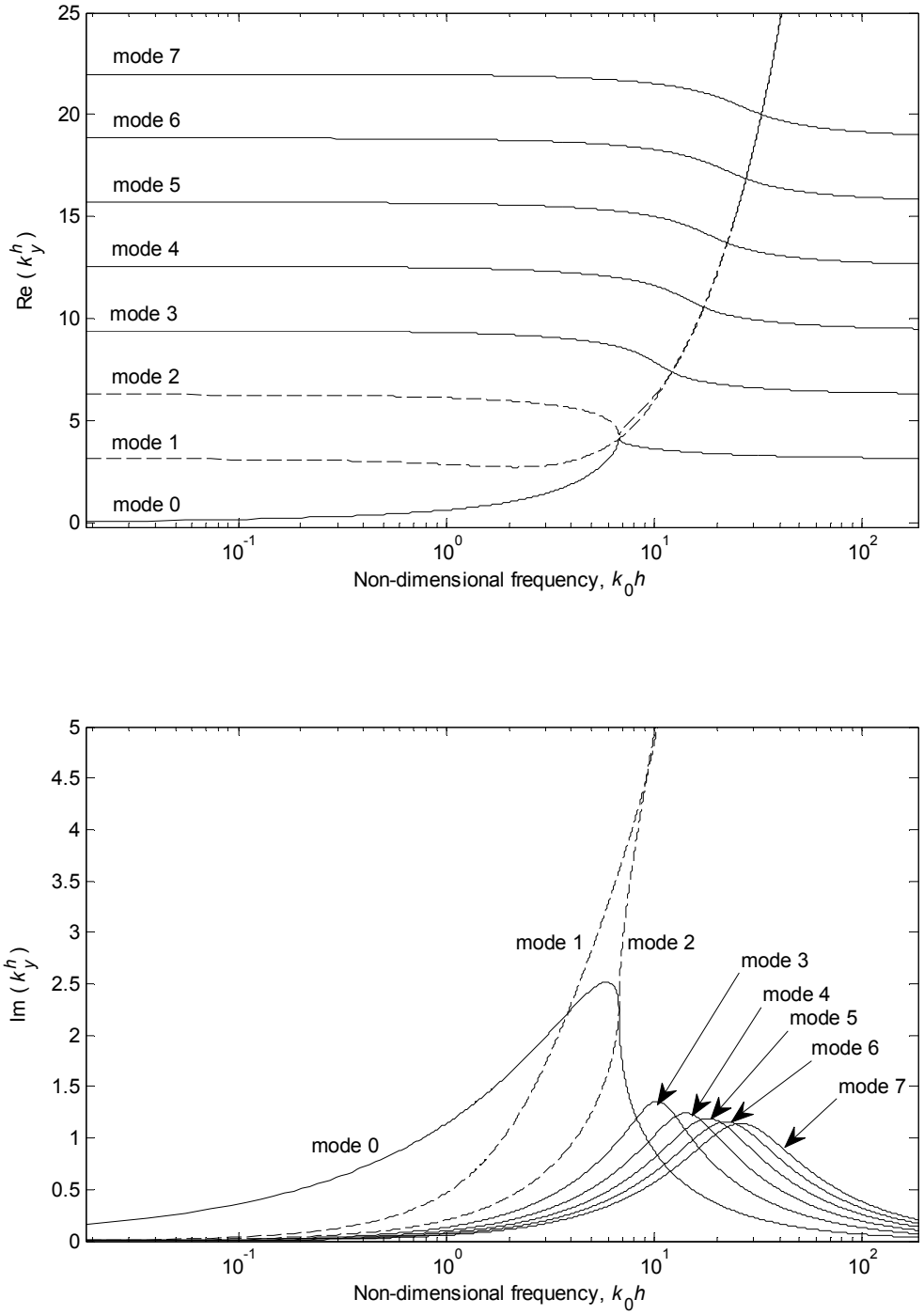

Figure 2.14: Transverse wavenumbers for a duct lined with a complex wall impedance $Z_n' = 1 - 0.8i$ where the surface waves (dashed) line correspond to mode 1 and mode 2

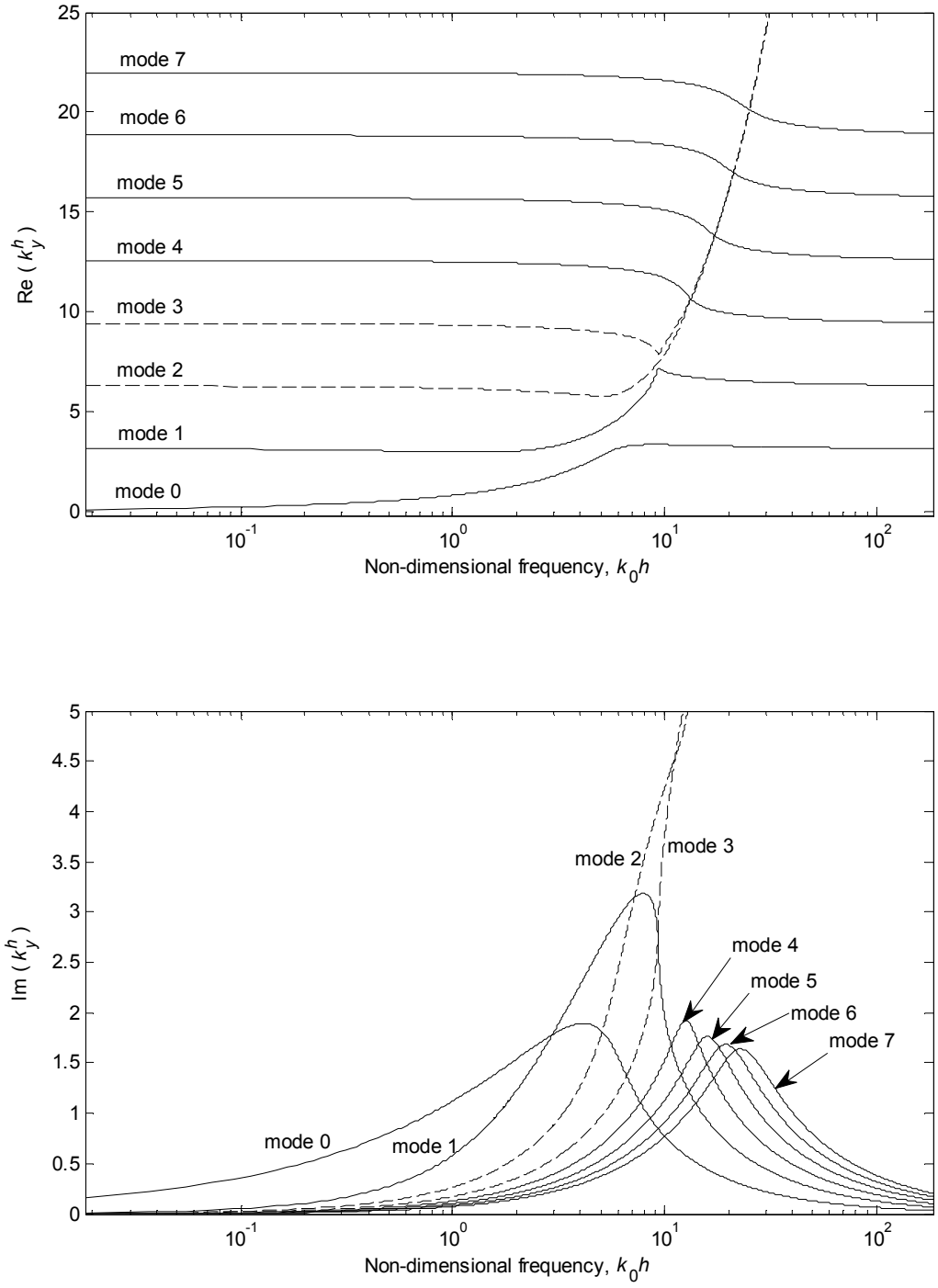

Figure 2.15: Transverse wavenumbers for a duct lined with a complex wall impedance $Z_n' = 1 - 0.5i$ where the surface waves (dashed line) correspond to mode 2 and mode 3

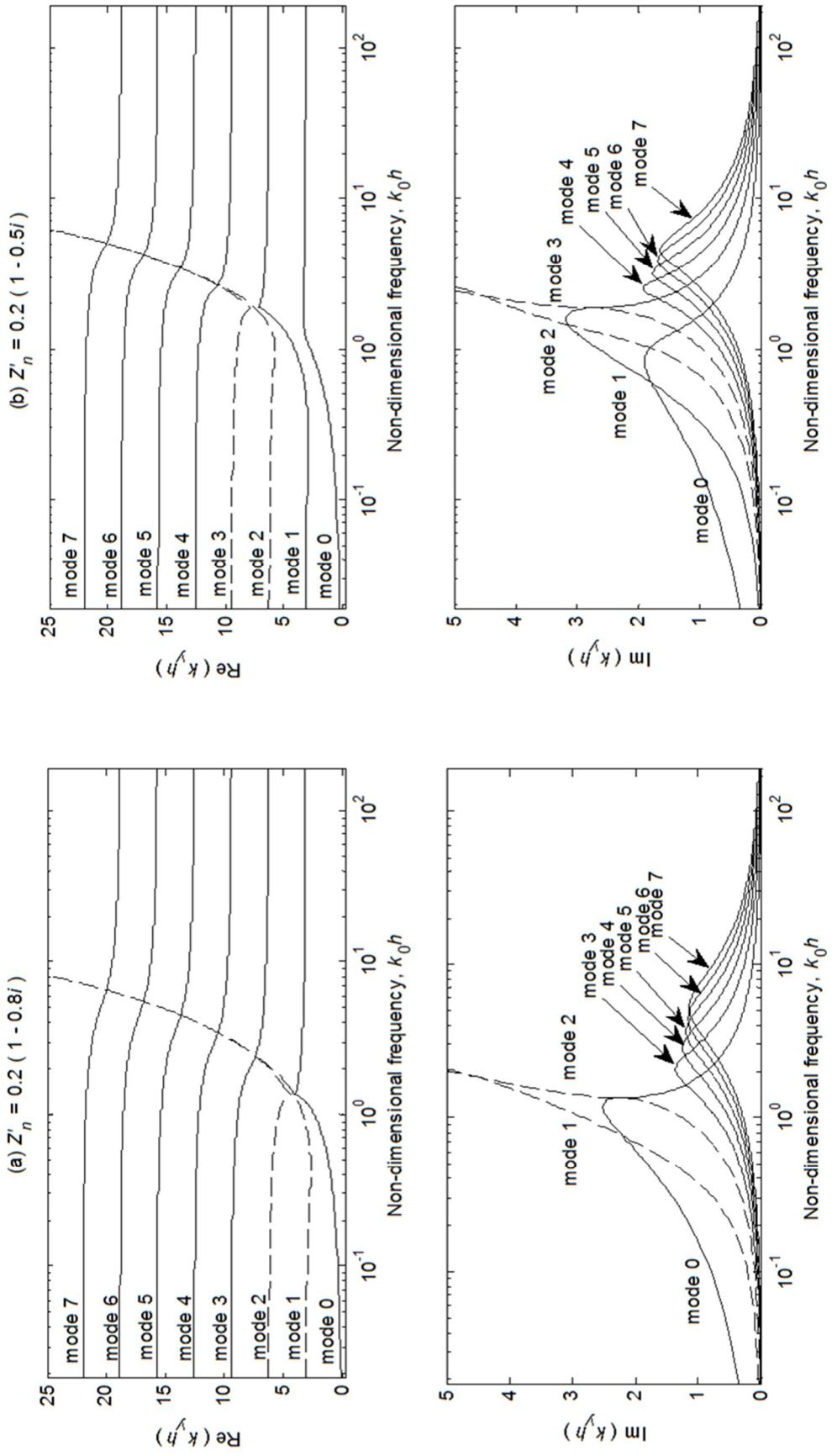

Figure 2.16: Transverse wavenumbers for a duct lined with a complex wall impedance with $Z_r = 2$ and (a) $Z_{ir} = -0.8i$ and (b) $Z_{ir} = -0.5i$

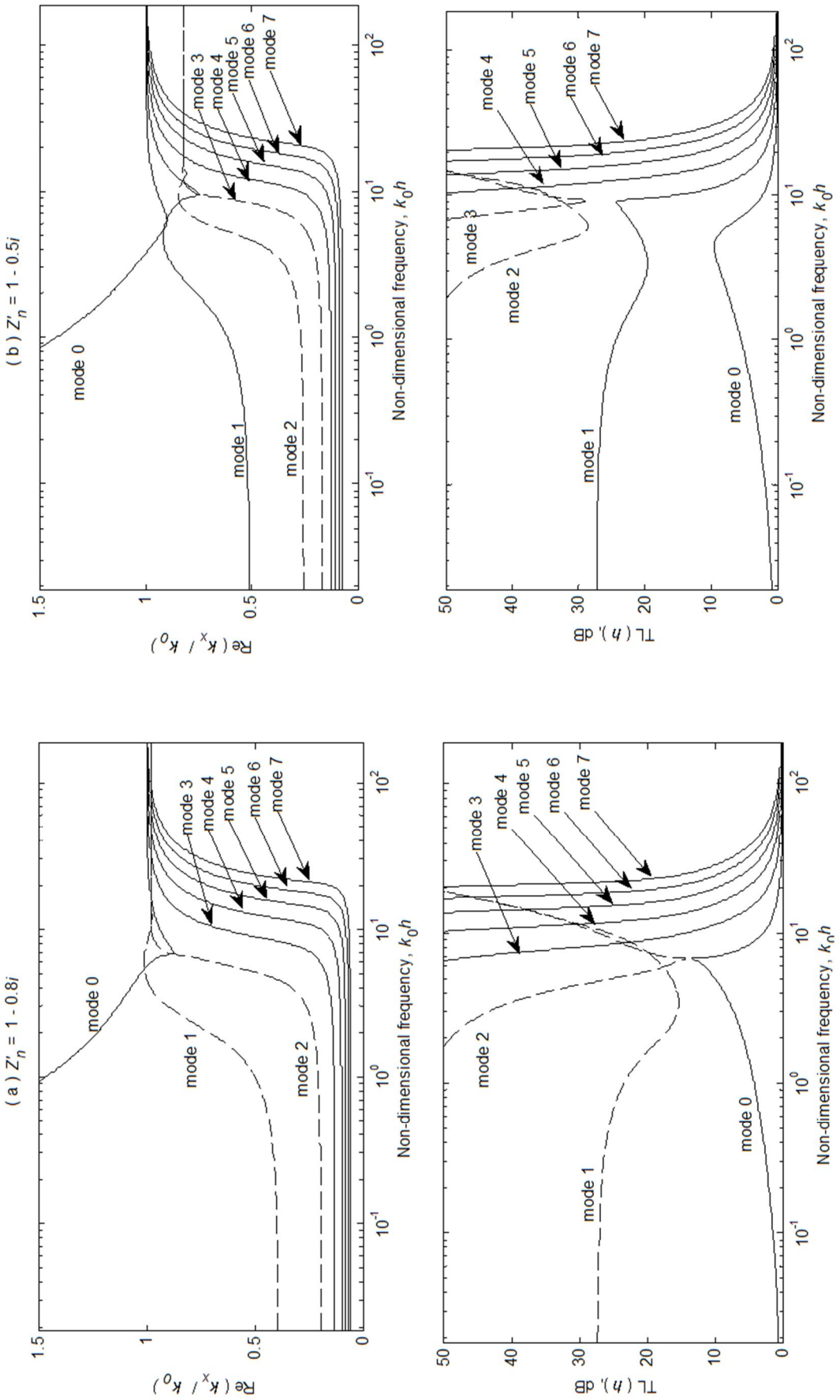

Figure 2.17: Axial wavenumbers for the transverse wavenumbers in Figure 2.14 and Figure 2.15

2.6 Conclusions

In this chapter, the fundamental theory of wave propagation in a lined duct has been presented and Müller's method has been implemented to solve the transcendental wavenumber equations. The wavenumbers are tracked from low to high frequency. To make the mode order unambiguous, the modes are numbered according to the mode order in a rigid duct. The low frequency and high frequency asymptotes for the real parts of transverse wavenumber for each wave mode have been identified and this serves as a check to ensure that all the required mode wavenumbers are found and no 'mode jumping' has occurred in the numerical method.

In a duct with a reactive lining (imaginary surface normal wall impedance) there is no dissipation of sound energy. The higher order modes have clear cut-on frequencies above which they propagate unattenuated. For a mass-controlled impedance, at low enough frequency no waves can propagate and the fundamental mode exists as a nearfield wave. For a stiffness controlled impedance, two surface waves exist at high frequency, one even mode and one odd mode. The surface waves propagate unattenuated in the axial direction but are localised at the wall in the transverse direction.

Surface waves are also found when the wall impedance is complex with negative imaginary part. However in this case, these surface waves are highly attenuated in the axial direction and for the case of an infinitely long duct, these waves may not be of significance. The corresponding low frequency modes for the surface waves differ depending on the ratio of the imaginary part to the real part of the complex wall impedance.

So far, the case studied has been kept simple where the wall lining is locally reacting and the wall impedance is kept constant with frequency. Using Müller's algorithm, a more realistic case will be studied in the next chapter, where the wall impedance is dependent on frequency and it is treated as bulk-reacting, a typical lining behaviour used in a lined ventilation duct.

3. Waves in a duct with a bulk-reacting lining

In the previous chapter the wall lining was treated as a "black box" in which it was represented by a constant surface normal wall impedance. The wall lining typically has a fibrous structure, for example glass wool, or an open cell structure such as melamine foam. It is difficult to generate a general model to predict the behaviour of most sound-absorbent materials entirely on the basis of theoretical models due to their geometrical and structural complexity. Three parameters have been identified that principally control their sound absorption characteristic, namely flow resistivity, porosity and tortuosity. Through introducing these three parameters into a modified equation for plane wave sound propagation in gases contained within a rigid porous material, a semi-analytical sound propagation model in an absorptive material can be obtained [32] and is presented in Appendix 1 for reference.

For a general case of sound absorbing material, the surface normal impedance depends on the angle of the incident wave because the normal component of the particle velocity at any point of the interface is influenced not only by the local sound pressure, but also by the sound pressure at all other points of the excited medium. The material with this extended property is termed a bulk-reacting material. In a bulk-reacting material, it is not possible to specify a unique boundary impedance independent of the incident wave profile over the interface. Since the specific wall impedance cannot be identified uniquely, the modal structure in a duct with a bulk-reacting lining is far more difficult to determine than with a locally reacting lining. A reference plot such as a Morse chart cannot be drawn for a bulk-reacting lining due to the many parameters involved.

Earlier work on bulk-reacting linings can be found in [90, 91] where the only feasible approach to solve for the eigenvalues is by a numerical approach as has also been used extensively for locally reacting linings. The method developed in Chapter 2 based on Müller's method is used here to solve for the wavenumbers in a duct with a bulk-reacting lining. The resulting wavenumbers are compared with the wavenumbers in a duct with a locally reacting lining based on the model in Chapter 2. From the two sets of results, the duct attenuation based on the least attenuated mode is determined and compared with published results [16, 54].

3.1 Eigensolution, boundary conditions and wavenumber equations for bulk-reacting lining

Consider an infinitely long two dimensional rectangular duct with height h as shown in Figure 3.1. The axial direction is represented by the x-axis and the distance from the centreline of the

duct is *y*. The top and bottom walls are lined with a porous material with a thickness of *d*. The liners used are assumed to consist of an isotropic and homogeneous sound absorbing material. For a bulk-reacting material, the sound wave in the duct travels in the axial direction in both the airway and the porous material. Region I is defined as the airway passage that extends from $-\frac{h}{2} \le y \le \frac{h}{2}$ and region II (and III) is the lining section with $\left(\frac{h}{2}\right) \le |y| \le \left(\frac{h}{2} + d\right)$. In the airway passage, sound waves propagate at a speed of c_0 and the wavenumber is given by $k_0 = \omega / c_0$. The wavenumber in the porous material is complex and is given by $\tilde{k}$; the wave propagates at a complex speed of $\tilde{c}$. $\tilde{\rho}$ is the complex acoustic density of the porous material. For both the airway passage and the absorbent material, the axial wavenumber for a given mode *m*, $k_{x,m}$, is the same but the transverse wavenumber is different. It is given by $k_{y,m}$ for the airway and $\tilde{k}_{y,m}$ for the lining material. These wavenumbers must satisfy

$$\begin{aligned} k_0^2 &= k_{x,m}^2 + k_{y,m}^2 \\ \tilde{k}^2 &= k_{x,m}^2 + \tilde{k}_{y,m}^2 \end{aligned} \tag{3.1}$$

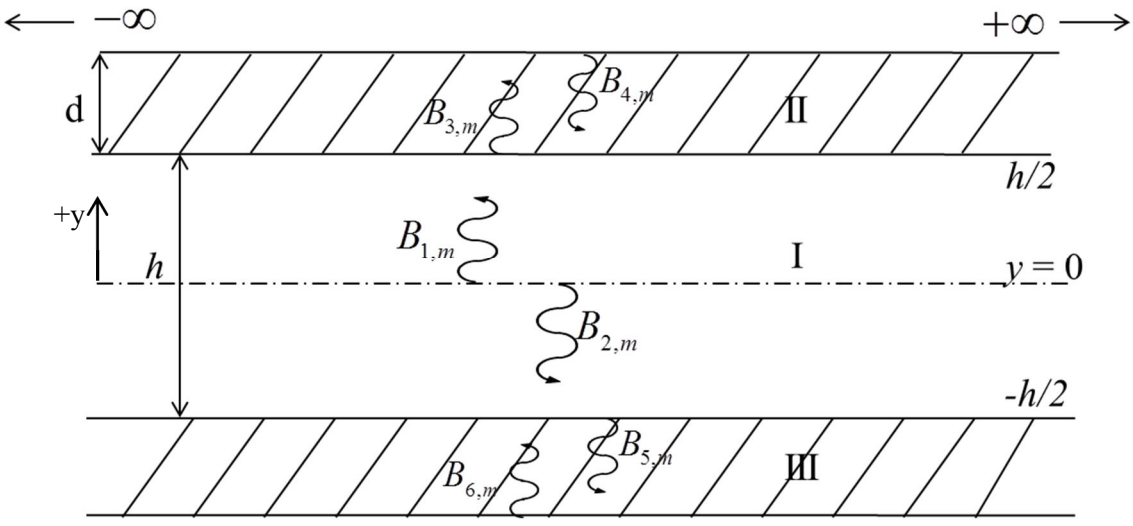

Figure 3.1: An infinitely long rectangular duct with porous material lining on top and bottom wall

The pressure field at any point in the duct is given by:

$$p(x,y) = \sum_{m=0}^{M} \left(A_m^+ e^{-ik_{x,m}x} + A_m^- e^{ik_{x,m}x} \right) \Phi_m(y) \tag{3.2}$$

where the mode shape across the height is given by:

$$\Phi_m(y)=\begin{cases}\Phi_{m,\mathrm{I}}(y)=B_{1,m}e^{-ik_{y,m}y}+B_{2,m}e^{ik_{y,m}y}, & -h/2\le y\le h/2\\ \Phi_{m,\mathrm{II}}(y)=B_{3,m}e^{-i\tilde{k}_{y,m}\left(y-h/2\right)}+B_{4,m}e^{i\tilde{k}_{y,m}(y-D)}, & h/2\le y\le D\\ \Phi_{m,\mathrm{III}}(y)=B_{5,m}e^{i\tilde{k}_{y,m}\left(y+h/2\right)}+B_{6,m}e^{-i\tilde{k}_{y,m}(y+D)}, & -D\le y\le -h/2\end{cases} \tag{3.3}$$

where $D=h/2+d$. A_m^+ and A_m^- are the axial wave amplitudes of the positive going and negative going wanes, and $B_{i,m}$ is the transverse wave amplitude in the airway or lining as shown in Figure 3.1. The coefficients B_1, B_2, B_3, B_4, B_5 and B_6 can be found by solving the following six boundary conditions: the transverse particle velocity is zero at the outer wall, $y=D$ and $y=-D$, the pressure and transverse particle velocity are continuous at the lining interface, $y=h/2$ and $y=-h/2$. As the problem is symmetric about $y=0$, wave modes are either symmetric (even modes) or anti-symmetric (odd modes). Therefore not all boundary conditions are required. Instead use is made of the condition that the pressure (for odd modes, for even modes it is the transverse particle velocity) is zero at the centre of the airway, $y=0$.

At the outer wall, $y=D$, the particle velocity in the y direction is zero which yields:

$$\begin{aligned}u_y(D)&=\frac{\tilde{k}_{y,m}}{\omega\tilde{\rho}}\left(B_{3,m}e^{-i\tilde{k}_{y,m}d}-B_{4,m}\right)=0\\ \therefore B_{4,m}&=B_{3,m}e^{-i\tilde{k}_{y,m}d}\end{aligned} \tag{3.4}$$

At the interface $y=h/2$, the continuity of pressure and transverse particle velocity yields

$$\begin{aligned}\Phi_{m,\mathrm{I}}\left(\frac{h}{2}\right)&=\Phi_{m,\mathrm{II}}\left(\frac{h}{2}\right)\\ B_{1,m}e^{-ik_{y,m}h/2}+B_{2,m}e^{ik_{y,m}h/2}&=B_{3,m}+B_{4,m}e^{-i\tilde{k}_{y,m}d}\end{aligned} \tag{3.5}$$

and

$$\begin{aligned}u_{y,\mathrm{I}}\left(\frac{h}{2}\right)&=u_{y,\mathrm{II}}\left(\frac{h}{2}\right)\\ \frac{k_{y,m}}{\rho_0}\left(B_{1,m}e^{-ik_{y,m}h/2}-B_{2,m}e^{ik_{y,m}h/2}\right)&=\frac{\tilde{k}_{y,m}}{\tilde{\rho}}\left(B_{3,m}-B_{4,m}e^{-i\tilde{k}_{y,m}d}\right)\end{aligned} \tag{3.6}$$

For even modes, by symmetry the pressure gradient at the duct centre is zero:

$$\frac{\partial p}{\partial y} = ik_{y,m}\left(B_{1,m} - B_{2,m}\right) = 0$$
$$\therefore B_{1,m} = B_{2,m} \tag{3.7}$$

Substituting equations (3.4) and (3.7) into equation (3.5), the wave amplitude in the upper lining can be related to the wave amplitude in the airway by:

$$B_{3,m} = \frac{B_{1,m}\left(e^{ik_{y,m}h/2} + e^{-ik_{y,m}h/2}\right)}{\left(1 + e^{-2i\tilde{k}_{y,m}d}\right)} \tag{3.8}$$

For the lower lining, by symmetry:

$$B_{5,m} = B_{3,m}$$
and (3.9)
$$B_{6,m} = B_{4,m}$$

Similarly, solving for the odd modes, at the duct centre the pressure is zero. Hence:

$$B_{1,m} + B_{2,m} = 0$$
$$\therefore B_{1,m} = -B_{2,m} \tag{3.10}$$

Then substituting equations (3.4) and (3.10) into equation (3.5) gives:

$$B_{3,m} = \frac{-B_{1,m}\left(e^{ik_{y,m}h/2} - e^{-ik_{y,m}h/2}\right)}{\left(1 + e^{-2i\tilde{k}_{y,m}d}\right)} \tag{3.11}$$

and by antisymmetry:

$$B_{5,m} = -B_{3,m}$$
and (3.12)
$$B_{6,m} = -B_{4,m}$$

The wavenumber equations can be obtained by dividing equation (3.5) by equation (3.6). Substituting the wave amplitude solutions for B_2, B_3 and B_4 the following relationship is obtained for even modes:

$$-\frac{\rho_0\left(e^{ik_{y,m}h/2} + e^{-ik_{y,m}h/2}\right)}{k_{y,m}\left(e^{ik_{y,m}h/2} - e^{-ik_{y,m}h/2}\right)} = \frac{\tilde{\rho}\left(1 + e^{-i2\tilde{k}_{y,m}d}\right)}{\tilde{k}_{y,m}\left(1 - e^{-i2\tilde{k}_{y,m}d}\right)} \tag{3.13}$$

and for odd modes:

$$-\frac{\rho_0\left(e^{ik_{y,m}h/2}-e^{-ik_{y,m}h/2}\right)}{k_{y,m}\left(e^{ik_{y,m}h/2}+e^{-ik_{y,m}h/2}\right)}=\frac{\tilde{\rho}\left(1+e^{-i2\tilde{k}_{y,m}d}\right)}{\tilde{k}_{y,m}\left(1-e^{-i2\tilde{k}_{y,m}d}\right)} \tag{3.14}$$

The exponential functions in these two equations can be replaced by trigonometric functions, and the wavenumber equation can be rewritten as:

$$\frac{\rho_0}{k_{y,m}}\cot\left(\frac{k_{y,m}h}{2}\right)=-\frac{\tilde{\rho}}{\tilde{k}_{y,m}}\cot\left(\tilde{k}_{y,m}d\right) \tag{3.15}$$

for even modes, and:

$$\frac{\rho_0}{k_{y,m}}\tan\left(\frac{k_{y,m}h}{2}\right)=\frac{\tilde{\rho}}{\tilde{k}_{y,m}}\cot\left(\tilde{k}_{y,m}d\right) \tag{3.16}$$

for odd modes. Since the axial wavenumber in the airway and wall lining is the same, using the wavenumber relation in (3.1), one can write (3.15) and (3.16) as [28]:

$$\frac{\rho_0}{k_{y,m}}\cot\left(\frac{k_{y,m}h}{2}\right)=-\frac{\tilde{\rho}}{\sqrt{\tilde{k}^2-k_0^2+k_{y,m}^2}}\cot\left(\sqrt{\tilde{k}^2-k_0^2+k_{y,m}^2}\;d\right) \tag{3.17}$$

and

$$\frac{\rho_0}{k_{y,m}}\tan\left(\frac{k_{y,m}h}{2}\right)=\frac{\tilde{\rho}}{\sqrt{\tilde{k}^2-k_0^2+k_{y,m}^2}}\cot\left(\sqrt{\tilde{k}^2-k_0^2+k_{y,m}^2}\;d\right) \tag{3.18}$$

For the case of a bulk-reacting lining, the transverse wavenumbers in the airway $k_{y,m}$ are found by solving equations (3.17) and (3.18) using the known bulk properties of the absorbent material, $\tilde{\rho}$ and $\tilde{k}$. These two properties can be obtained from any impedance model commonly used in literature. In principle, any model for the material can be used as long as it gives these two properties. While there are complete formulations that include all the parameters affecting material's sound absorption [93, 94], a semi-analytical model derived from a modified linearized wave equation that takes into account the effects of porosity, tortuosity and flow resistivity can accurately estimate acoustic parameters of a lining material. This theoretical model is used to obtain the acoustic parameters of sound absorbing material [32, 95]as described in Appendix 1. Another impedance model that is widely used in literature is the

empirical model of Delany and Bazley. The model is a function of the ratio between frequency and flow resistivity [29]; this has been used extensively in some duct acoustics work [73, 83, 92]. This empirical model was developed after numerous measurements using an impedance tube for materials of varying resistivity over a specific frequency range. Although such empirical models are simple to apply to existing materials and can be very effective in certain cases, the relationships were derived based on normal incidence impedance tube measurements. In a bulk-reacting lining, the impedance is dependent on the incident wave type and angle of incidence [30].

To illustrate some results in later sections, a set of example parameters are used and listed in Table 3.1. These values are of typical melamine foam usually used as a sound absorbing material.

Table 3.1: Material properties for melamine foam

Porosity, ε	0.993
Tortuosity, s	1.0056
Flow resistivity, r	18000 rayls/m

3.2 Numerical solution for the wavenumber

The solutions to both equations (3.17) and (3.18) can be obtained numerically by using Müller's method [62]. As mentioned in section 2.3, it is numerically easier to find zeros than poles of a function. Therefore the reciprocals to the wavenumber equations (3.17) and (3.18) are used to form the objective function for use in Müller's method. The solutions for the transverse wavenumbers are sought iteratively for even and odd modes respectively as the minima of the following functions:

$$f\left(k_{y,m}h\right)=\frac{k_{y,m}}{\rho_0}\tan\left(\frac{k_{y,m}h}{2}\right)+\frac{\sqrt{\tilde{k}^2-k_0^2+k_{y,m}^2}}{\tilde{\rho}}\tan\left(\sqrt{\tilde{k}^2-k_0^2+k_{y,m}^2}\,d\right) \tag{3.19}$$

and

$$f\left(k_{y,m}h\right)=\frac{k_{y,m}}{\rho_0}\cot\left(\frac{k_{y,m}h}{2}\right)-\frac{\sqrt{\tilde{k}^2-k_0^2+k_{y,m}^2}}{\tilde{\rho}}\tan\left(\sqrt{\tilde{k}^2-k_0^2+k_{y,m}^2}\,d\right) \tag{3.20}$$

The wavenumbers are sought from low frequency to high frequency at a fixed frequency step. The solution is first found for the wavenumber at the lowest frequency. Then that wavenumber

is used as the initial guess for the next frequency step and the process continues for the whole frequency range.

3.2.1 Initial guesses for wavenumbers

The initial guess of $k_{y,m}h$ at the lowest frequency for each mode is found from the low frequency approximation to equations (3.19) and (3.20). At low frequency, $\tilde{k} \to k_0$ and $\tilde{\rho}$ in equation tends to $-i\infty$. Thus (3.19) and (3.20) can be reduced to:

$$\frac{\cot\left(k_{y,m}d\right)}{\cot\left(\frac{1}{2}k_{y,m}h\right)} \simeq -\frac{\rho_0}{\tilde{\rho}} \tag{3.21}$$

and

$$\frac{\cot\left(k_{y,m}d\right)}{\tan\left(\frac{1}{2}k_{y,m}h\right)} \simeq \frac{\rho_0}{\tilde{\rho}} \tag{3.22}$$

The right hand side of both equations approaches zero at low frequency. This can be satisfied either when the denominator tends to infinity, or when the numerator tends to zero. The solution to $\cot\left(k_{y,m}h/2\right) \to \infty$ in equation (3.21) and $\tan\left(k_{y,m}h/2\right) \to \infty$ in equation (3.22) gives $k_{y,m}h = m\pi$ where $m = 0,\ 1,\ 2,\ldots$. These values are equivalent to the wavenumbers in the hard-walled duct and will be referred to as airway modes. In addition to these modes, $\cot\left(k_{y,m}d\right) = 0$ gives $k_{y,m}h = \frac{M\pi}{2}\frac{h}{d}$ where $M = 1,\ 3,\ 5,\ldots$. These additional modes do not appear for locally reacting liners. It was first suspected by Mechel [57], although it was not proven, that there are modal solutions that do not exist in ducts with locally reacting linings but are found in ducts with bulk-reacting linings (provided that the lining has a rigid backing) and this has not been found mentioned elsewhere.

The additional modes are referred to here as lining modes and are ordered according to the value of *M*. For the airway modes, the numbering of modes in a lined duct is derived from the corresponding mode order in a hard-walled duct. This labelling and numbering is used to keep the mode number unambiguous and make them easier to track from low to high frequency. However, as shown in later results, these waves may change in nature as frequency varies.

For the airway modes, the hard-walled wavenumbers are sufficient to form the initial guess in Müller's method. However, for the lining modes if $M\pi h/2d$ is used as the initial guess the method does not converge to the correct solution. To overcome this, initial solutions can be found by using the argument principle method. Details of argument principle method are given in Appendix 2. At low frequency, the solution $k_y h$ for the lining modes is close to $M\pi h/2d$ with a small imaginary part.

With the material properties value listed in Table 3.1, Figure 3.2 and Figure 3.3 show examples of the zeros and poles of equation (3.19) and (3.20)found from the argument principle method for M = 1, 3, 5 and 7 for even and odd modes respectively. From the two figures, it can be seen that for zeros at wavenumbers with positive real part, they can sometimes have a positive imaginary part and sometimes a negative imaginary part. In the locally reacting case considered in Chapter 2, the imaginary parts of the transverse wavenumbers were always positive.

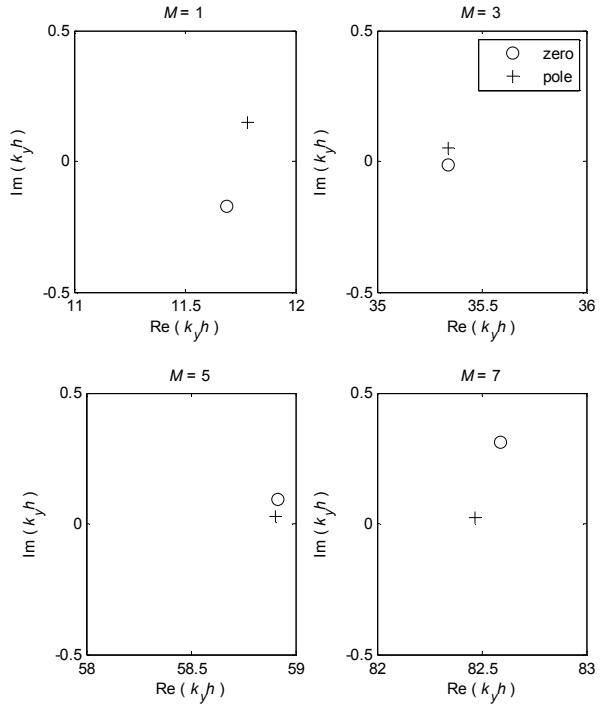

Figure 3.2: The zero and pole found at frequency 50 Hz for the first four even lining modes. The lining thickness is set to 40 mm.

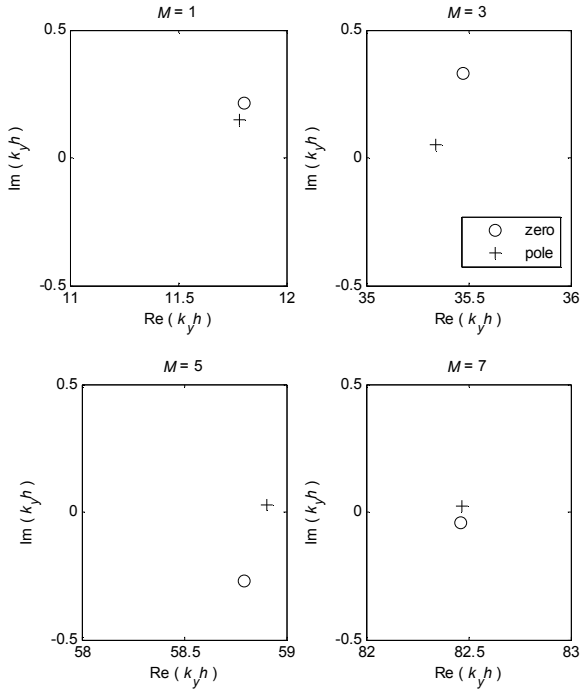

Figure 3.3: The zero and pole found at frequency 50 Hz for the first four odd lining modes. The lining thickness is set to 40 mm

Furthermore, the zero and pole for a particular value of M can sometimes be very close together. Therefore it is important to have the first estimated solution as close as possible to the true value since, for these modes, the zero and pole of the objective functions in equations (3.19) and (3.20) lie close to each other. Otherwise during the iteration process it is possible for Müller's method to reach a pole location instead of a zero and this would drive the solution away from the required mode wavenumbers to other neighbouring mode wavenumbers. For the airway modes, however, the poles are always located on the imaginary axis (refer to equation (3.17) and (3.18)) and the distance between poles and zeros are relatively large. Hence the hard-walled wavenumbers are sufficient to form the initial guess in Müller's method.

These wavenumbers (zeros) were found at a low frequency 50 Hz and are used as the initial guess x_2. As with the airway modes, the other two guesses for the lining mode are taken as slight variations to x_2 where $x_0 = x_2 - 0.01$ and $x_1 = x_2 + 0.01$. There are certain values of lining thickness that are particularly problematic and should be avoided if possible. These are when the value of d could result in $M\pi h/2d = m\pi$, or $m2d = Mh$ for any value of m and M. For these values of d it is difficult to identify the location of zeros for the lining mode at low frequency since it lies close to the solution for the airway mode. To deal with such a situation it

would be necessary to use a method such as the argument principle rather than Müller's method. However this is more time consuming so is avoided in the present study.

3.3 Dispersion curves and modal pressure distribution in a duct with bulk-reacting lining

Having found all the required initial guesses to start Müller's method, the wavenumbers are then tracked from low frequency up to high frequency. Similarly to the approach used for locally reacting lining in Chapter 2, the high frequency asymptote needs to be identified so that the set of modes can be checked for completeness.

At high frequency, the square root term in equations (3.17) and (3.18) is very large compared to $\tilde{\rho}$. This results in

$$i\frac{\rho_0}{k_{y,m}}\cot\left(\frac{k_{y,m}h}{2}\right)\simeq 0 \tag{3.23}$$

for even modes, and

$$i\frac{\rho_0}{k_{y,m}}\tan\left(\frac{k_{y,m}h}{2}\right)\simeq 0 \tag{3.24}$$

for odd modes. Consequently this gives the roots of $k_y h = m\pi$ where $m = 1,\ 3,\ 5,\ldots$ for even modes and $m = 2,\ 4,\ 6,\ldots$ for odd modes, equivalent to the wavenumbers found in a duct with a pressure release boundary, and similar to that found in the locally reacting case.

For comparison, the wavenumbers of the first twelve airway modes in a duct with a locally reacting lining are obtained and shown in Figure 3.4. The same duct geometry and material properties as the example case considered above are used. The impedance of the locally reacting lining is determined using equation . Figure 3.5 shows a plot of the real and imaginary parts of the transverse wavenumbers for a duct with a bulk-reacting lining where only the first four lining modes, the initial values for which are shown in Figure 3.2 and Figure 3.3, are included and are represented by the dashed lines.

Only few authors [96] presented the dispersion curves of the acoustic waves in lined ducts, hence it is difficult to make comparisons with published results. Therefore, for benchmarking purpose, and to ensure that no mode is missed in the process, a counter check using the argument principle method was carried out and the results are presented in Appendix 2. The

wavenumbers obtained from Müller's method and from the argument principle method at different frequencies are found to be the same and the argument principle method confirmed that no mode is missing in the results obtained by Müller's method. However the argument principle method is much more time consuming than Müller's method.

For the bulk-reacting case, in mid frequency region some of the wave modes have negative imaginary k_y. For these modes, the transverse waves travel from the central duct axis at $y = 0$ towards the duct wall with decreasing amplitude. For other wave modes with positive imaginary k_y, the transverse waves travel with increasing magnitude from the duct centre towards duct wall. Comparing Figure 3.4 and Figure 3.5, the real part of the transverse wavenumbers in both cases tend to the expected low and high frequency asymptotes. For a duct with a locally reacting lining, as discussed in section 2.4.3, at high frequency only two surface waves can exist, one even mode and one odd mode. This is shown in Figure 3.4 where at high frequency, there are at most two waves whose transverse wavenumbers have large imaginary parts. The surface waves are easily identified by their unbounded transverse wavenumbers and large imaginary parts.

In the case of the bulk-reacting lining, at high frequencies there are several waves in Figure 3.5 with similar behaviour (unbounded real and imaginary parts). Figure 3.6 shows the pressure distribution at 500 Hz of the first two airway modes, $m = 0$ and $m = 1$, and the first two even and odd lining modes, corresponding to $M = 1$. All these four modes have significant pressure amplitude in the wall lining as well as across the airway. At high frequency, for example at 10 kHz, the pressure distributions of the same wave modes are shown in Figure 3.7. Note that, for the modes corresponding to low frequency mode order $m = 0$ and $m = 1$, the pressure across the airway is close to zero especially in the central part of the duct and becomes significant at the wall surface and inside the lining. However, in the context of a bulk-reacting lining, the term surface wave may not be quite appropriate to describe these modes since they are distributed across the lining thickness and propagate in the axial direction; hence they are not localised to the wall surface only although they decay away from the surface in the airway region. In contrast to the two modes corresponding to lining modes $M = 1$ tend to $k_y h = 3\pi$ and 4π at high frequency and form part of the set corresponding to a pressure release boundary.

Selamet [92] used a secant method for tracking the wavenumbers in a bulk-reacting case but did not mention the additional wave modes nor provide any dispersion curves for the successfully tracked wave modes. He started his search at very high frequency and progressed towards low frequency and it is possible that the surface modes are missed at high frequency since the values are very large.

In this presented example, only modes corresponding to airway modes at low frequency become localized in the wall lining at high frequency while the lining modes at low frequency tend to airway modes at high frequency. However for other parameter values, modes corresponding to lining modes can become localized in the wall lining at high frequency as well, as presented in section 3.5. At low frequency there are $m + M$ modes that are typical of acoustic duct modes and at high frequency, only m of these remain as typical acoustic duct modes while the other M modes become localized in the wall lining. At a frequency at which the lining mode gets close to an airway mode, they are likely to exhibit veering [97, 98], i.e. the modes change nature when they get close.

It can be used to rearrange the propagating wave modes according to their contribution to the acoustic power in the duct. Here, an approach from [66] is adopted whereby modes are ordered on the basis of their cut-on ratio given by:

$$\eta = \left| \sqrt{1 - \left(k_{x,m} / k_0 \right)^2} \right| \tag{3.25}$$

In a hard-walled duct, a value of $\eta = 1$ corresponds to the transition from an evanescent mode to a propagating mode, values greater than 1 correspond to cut-off modes with imaginary $k_{x,m}$ and values less than 1 correspond to cut-on modes with $\mathrm{Re}\left(k_{x,m} \right) \leq k_0$. Since there is no sudden transition in a lined duct, the cut-on ratio is still a strong indicator of whether a mode contributes significantly to the acoustic power in the duct [66]. At high frequency, the airway modes have small attenuation as the pressure at the boundary is close to zero while the lining modes which are localized inside the lining are well attenuated. Hence these lining modes have a larger value of η compared to the airway modes. The airway modes and lining modes are then sorted according to their value of η.

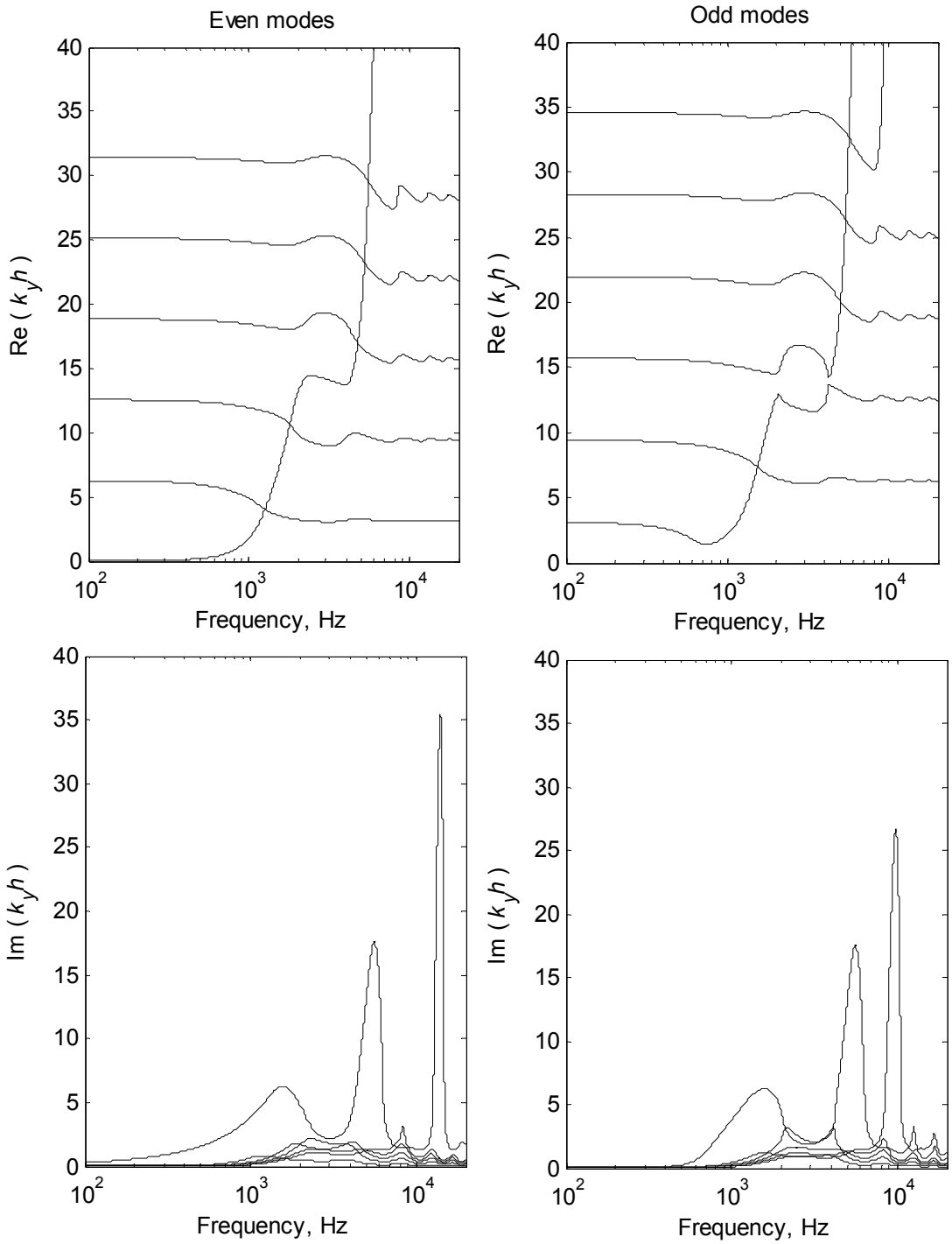

Figure 3.4: Transverse wavenumbers in a duct with a locally-reacting lining, h = 0.3 m, d = 0.04 m, r = 18000 rayls/m

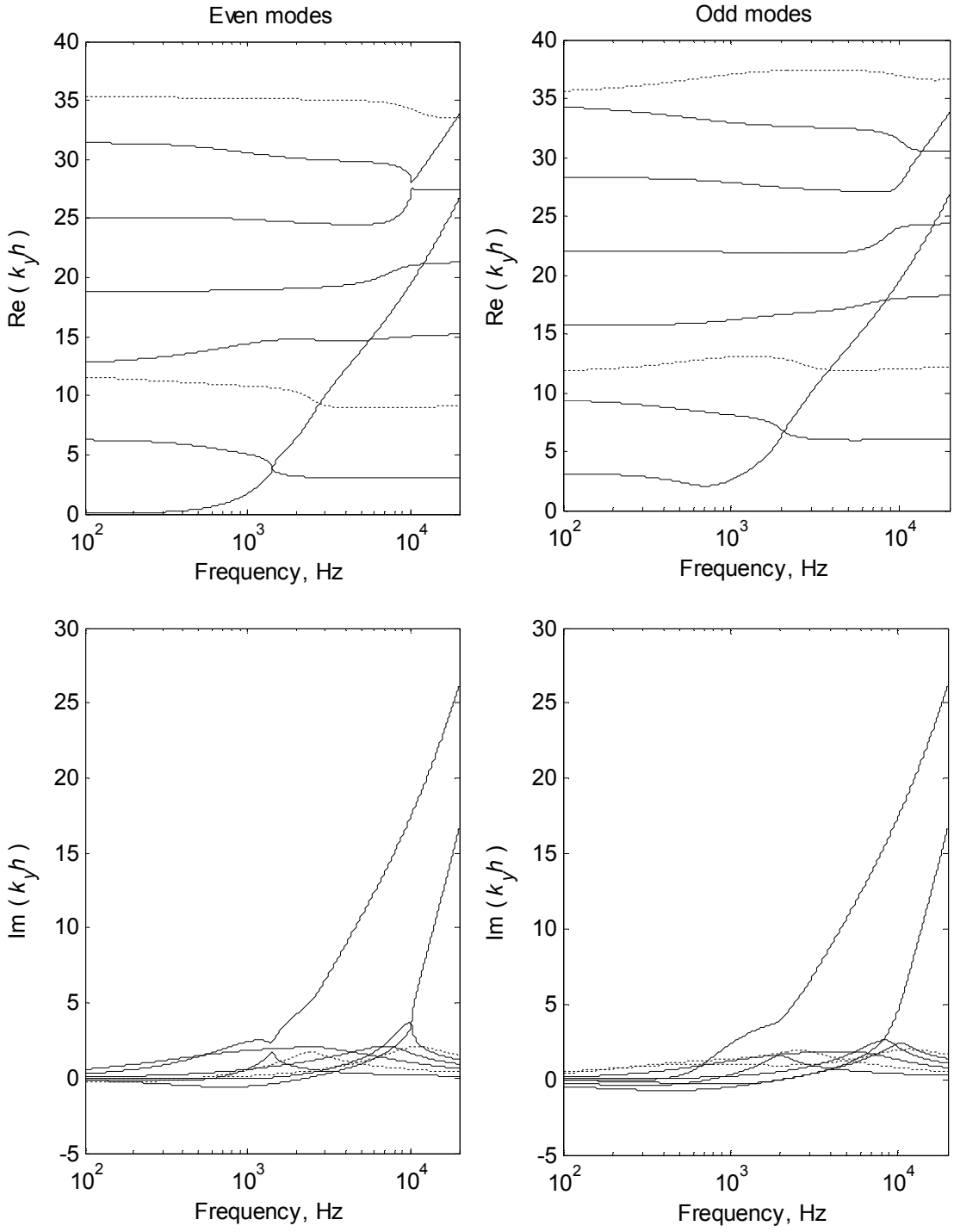

Figure 3.5: Transverse wavenumbers in a duct with a bulk-reacting lining, h = 0.3 m, d = 0.04 m, r = 18000 rayls/m

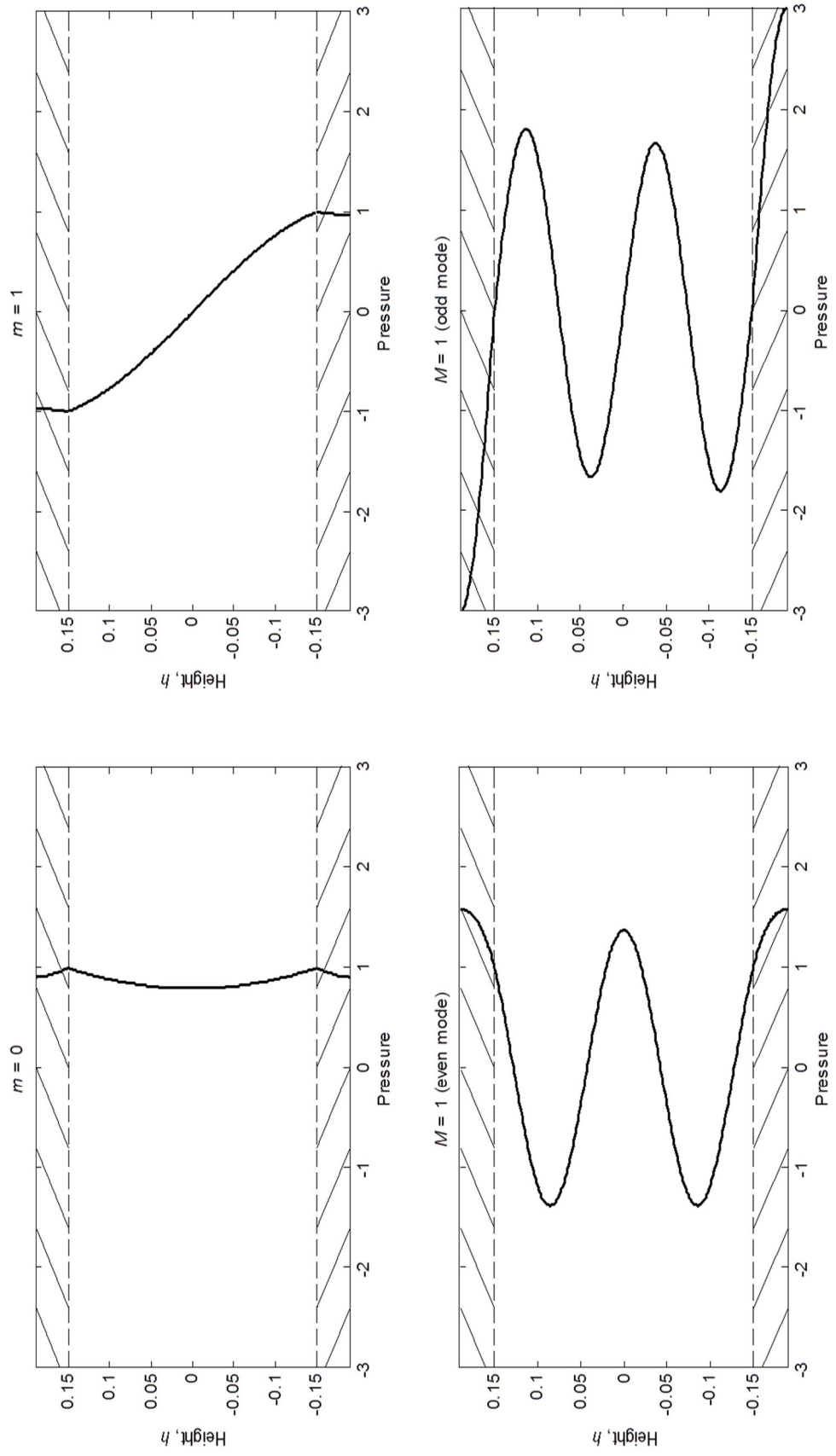

Figure 3.6: Pressure distribution across the duct height for the first two airway modes and lining modes: $m = 0$, $m = 1$, and $M =$ 1of even and odd lining mode at 500 Hz

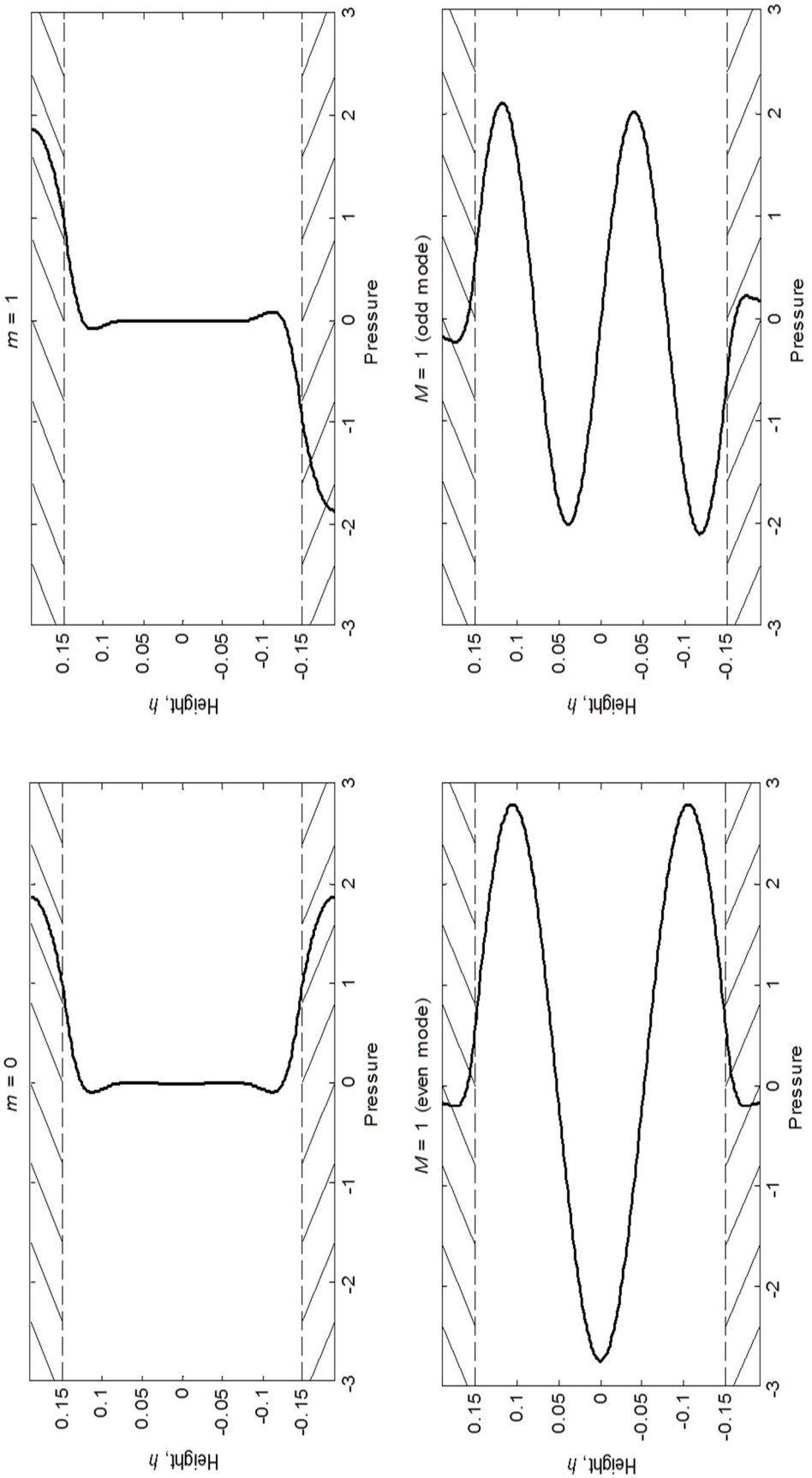

Figure 3.7: Pressure distribution across the duct height for the first two airway modes and lining modes: $m = 0$, $m = 1$ and $M = 1$ of even and odd lining mode at 10 kHz

3.4 Predicted duct attenuation based on the least attenuated mode

A classical way of predicting duct transmission loss is based on the least attenuated mode. An early approach was based on Cremer's rule [51] from which the optimized impedance value for a given frequency can be obtained to achieve maximum attenuation. The rule is based on the Morse chart [48] and is only valid for a duct with a locally reacting lining. With the advancement in computational capabilities, a complete solution of wavenumbers can be obtained for a given frequency range, for both locally reacting and bulk-reacting linings.

A general design chart has been provided by Bies and Hansen [54] that can be used to estimate the attenuation of the least attenuated propagating mode in lined ducts of both rectangular and circular cross-section. The charts are available for both locally reacting and bulk-reacting linings. The predicted attenuations are based on a rectangular duct lined on two opposite sides and can be read directly from the charts. The Delany and Bazley [29] empirical impedance model is used and the attenuation is predicted in overlapping octave bands to give a smoother plot and a reduction in peak values compared with single frequency predictions.

The lining flow resistivity is usually represented by a non-dimensional flow resistivity which is normalized with respect to the lining thickness and acoustic impedance, and is given by [51]:

$$R = \frac{rd}{\rho_0 c_0} \tag{3.26}$$

In general, a good absorption can be achieved by keeping the non-dimensional flow resistivity $R \approx 3$, although the performance is limited for a liner with a small thickness at low frequency for any flow resistivity [30]. The normalized flow resistivity can be seen as the total resistance of a lining of thickness *d* normalized with respect to the acoustic impedance.

A similar plot to those given by Bies and Hansen [54] is reproduced from the results found in this work and the consistency of the predicted attenuation (expressed in dB over a duct length *h*) can be checked against the published design charts. The attenuation is predicted for both locally reacting and bulk-reacting lining and is presented in Figure 3.8 and Figure 3.9 respectively. The frequency axis is plotted as h/λ for consistency with the published results. Five different curves are presented for different ratios of lining thickness to half of the duct airway height as listed in Table 3.2.

Table 3.2: Different ratios of lining thickness to half of the duct airway height for the curves in Figure 3.8 and Figure 3.9

Curve no.	$\frac{d}{h/2}$
1	0.25
2	0.5
3	1
4	2
5	4

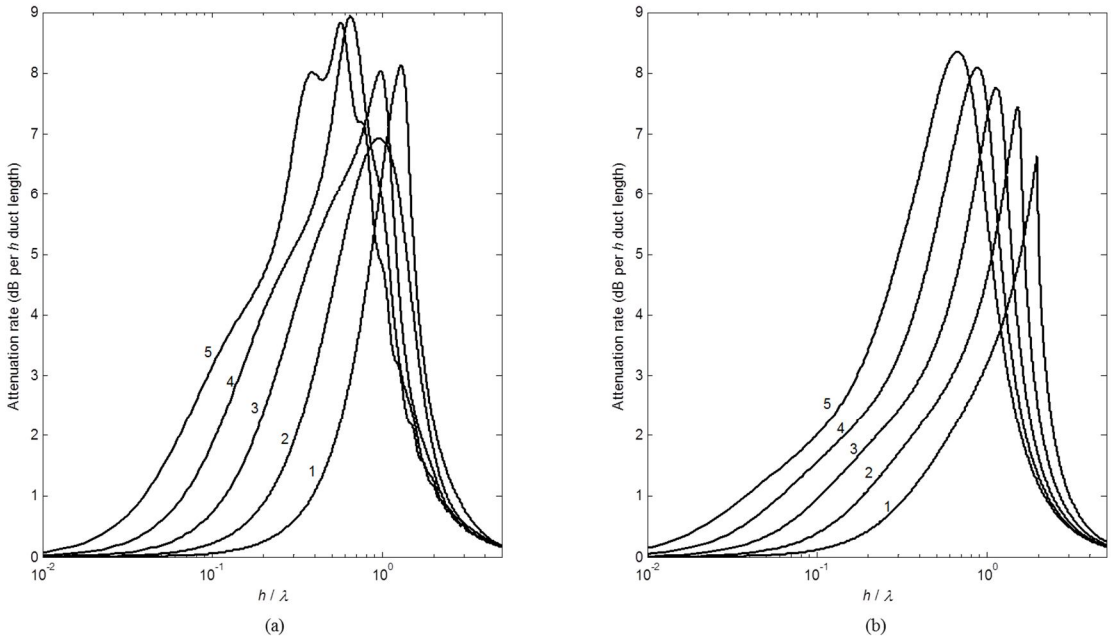

Figure 3.8: Predicted attenuations for a rectangular duct lined on two opposite sides based on the least attenuated mode. The duct is lined with a locally reacting lining with (a) $R = 4$ and (b) $R = 8$. Different curve number correspond to different ratio of lining thickness to half of the duct airway height as listed in Table 3.2

Comparing the attenuation plot for locally reacting and bulk-reacting linings, in all cases the locally reacting assumptions give higher attenuation than the bulk-reacting assumptions. The plot in Figure 3.9 starts at a much higher frequency compared to the locally reacting lining results in Figure 3.8. The corresponding frequency starts at 100 Hz which is the lowest frequency for which the initial guess for the lining mode can be found by the argument principle algorithm. This is because below 100 Hz the locations of poles and zeros are very close due to the chosen ratio of d/h and they can only be found if a very fine search grid is used that would

be very time consuming (refer to Appendix 1). At 100 Hz the location of poles and zeros are far enough apart. Nevertheless a considerable amount of computational time was spent to find these initial guesses.

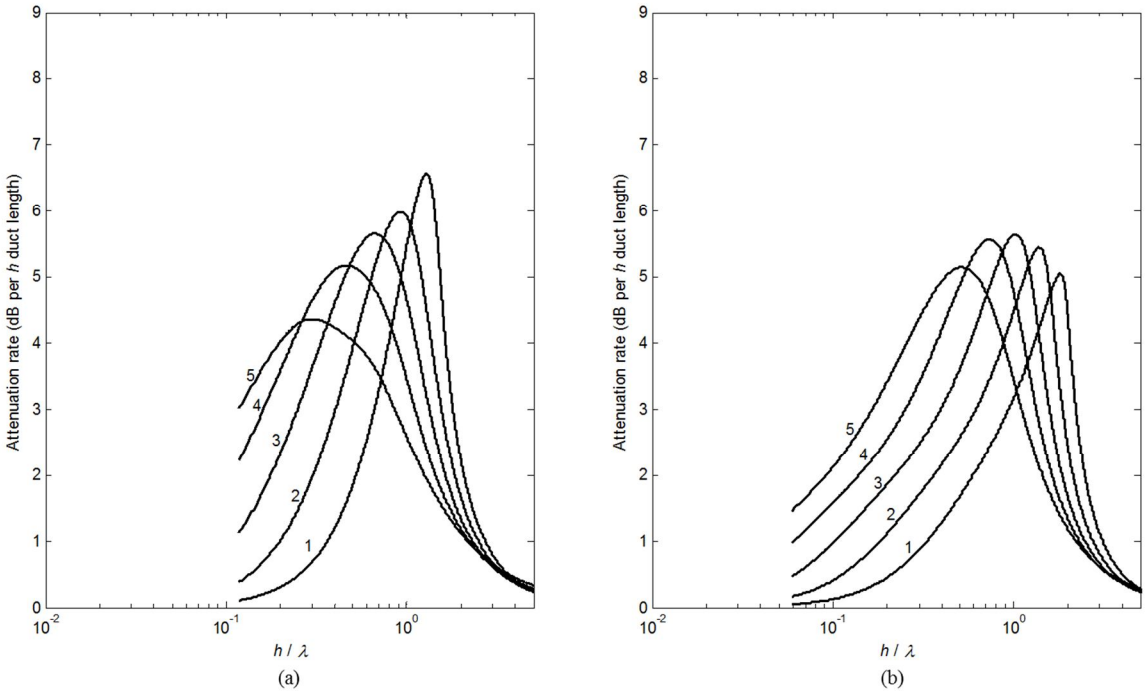

Figure 3.9: Predicted attenuations for a rectangular duct lined on two opposite sides based on the least attenuated mode. The duct is lined with a bulk-reacting lining with (a) $R = 4$ and (b) $R = 8$. Different curve number correspond to different ratio of lining thickness to half of the duct airway height as listed in Table 3.2

Comparing the results in Figure 3.8 and Figure 3.9 with the published result in [54], with the same ratio of lining thickness to half of the duct airway height, a similar trend in attenuation rate with increasing ratio $\frac{d}{h/2}$ is shown. However the published results are plotted in overlapping octave bands and hence the plots are smoother compared to the results presented here. Although there are some differences in the peak value which may be due to the different impedance model used in [54], this comparison is useful as an initial check to the wavenumbers obtained in this work. Furthermore the low frequency and high frequency attenuation as well as the peak attenuation match well with the published results.

3.5 Predicted duct attenuation with the assumption of equal energy distribution in incident waves

The assumption used previously that the duct attenuation can be estimated based on the least attenuated mode is not valid at higher frequency or for a larger duct height [62] where higher order modes cut-on. To accommodate the attenuation of higher order modes in the calculation of duct transmission loss, without calculating the modal amplitudes, Ramakrishnan and Watson [16] assumed that all the propagating waves have equal energy distribution. This assumption was made to correspond to the sound that is generated and propagates in a conventional ventilation system which is broadband in character without any strong tonal components. The overall attenuation rate i.e. attenuation per unit length, due to the sound absorbing material was estimated by Ramakrishnan as:

$$\Lambda = \Lambda_0 + 10\log\left(N\right) - 10\log\left[\sum_{m=1}^{N} 10^{\left(\Lambda_0 - \Lambda_m\right)/10}\right] \text{dB} \tag{3.27}$$

The number of modes included is N and Λ_0 is some large reference value set to 100 dB. Λ_m is the attenuation rate of the lined duct due to mode m, and is given by:

$$\Lambda_m = 8.686\,\text{Im}\left(k_{x,m}\right), \text{dB/m} \tag{3.28}$$

Only those modes with low attenuation rate, i.e. $\Lambda_m < 20$ dB/m, are included in estimating the overall attenuation. This summation procedure is in accordance with ASTM E477 [99] and is applied when one has to combine noise attenuation values for different modes.

Figure 3.10 and Figure 3.11 show the predicted attenuation rate for three different ratios of lining thickness to duct height, for a locally reacting lining and a bulk-reacting lining respectively. In general, by comparing the two figures with the previous Figure 3.8 and Figure 3.9, the least attenuated mode approach underestimates the duct attenuation when higher order modes start to cut on. This is to be expected since in this approach the attenuation rate calculation includes all possible modes. The curves plotted in this section are not smooth due to the effect of higher order modes. However the assumption of equal energy distribution among all modes does not ensure accuracy of prediction since in practice, the amplitude in each mode depends on the boundary conditions at the entrance and exit to the lined duct.

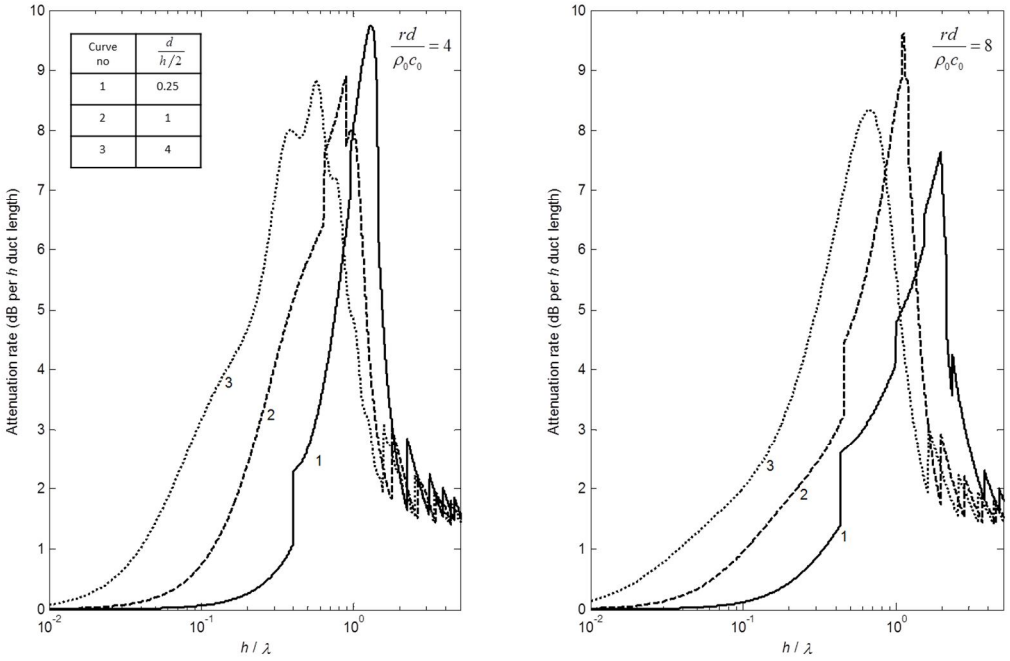

Figure 3.10: Predicted attenuation rate based on the assumption of same energy density in the incident wave. The duct is lined with a locally reacting lining.

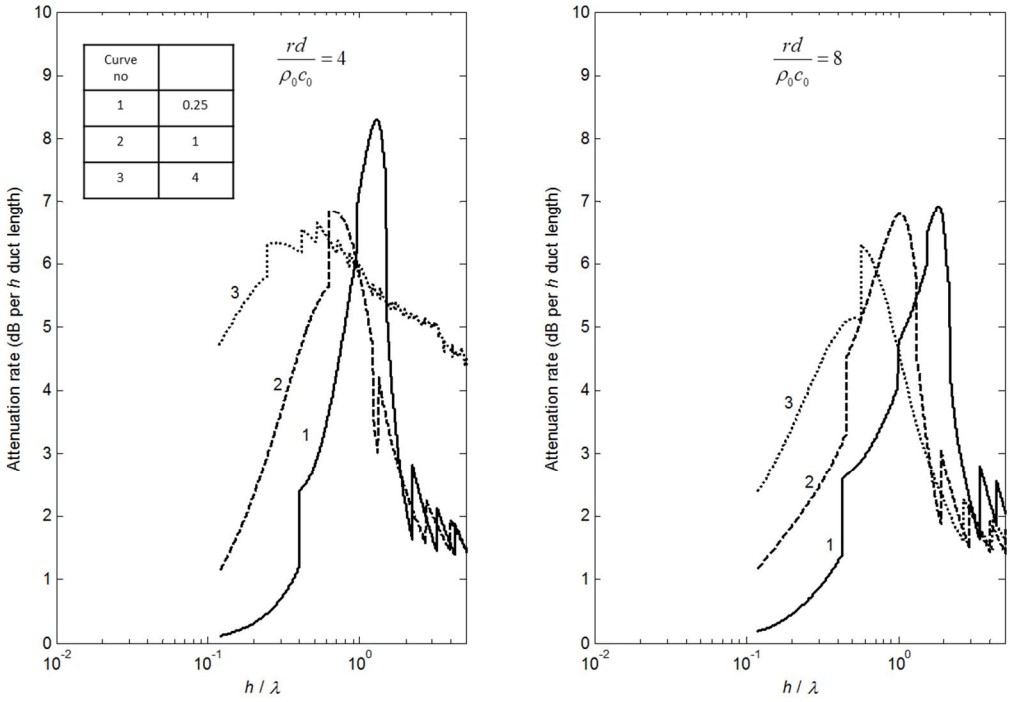

Figure 3.11: Predicted attenuation rate based on the assumption of same energy density in the incident wave. The duct is lined with a bulk-reacting lining.

Furthermore, the current estimation method may need to be modified for the case of a bulk-reacting lining. For a duct with a bulk-reacting lining, above the fundamental mode region, more propagating modes exist compared to the equivalent rigid duct. The predicted curves for the bulk-reacting lining have a lot of discontinuities due to the lining modes especially for a thicker lining.

Figure 3.12 shows the plot of real part of transverse wavenumbers for a duct with the same airway height and lining material properties, but with different lining thickness. The thicker the lining is the more lining modes exist. These lining modes can have a relatively low but significant attenuation rate at high frequency hence contributing to a much higher predicted attenuation rate which is obvious in curve number 3 for $R = 4$.

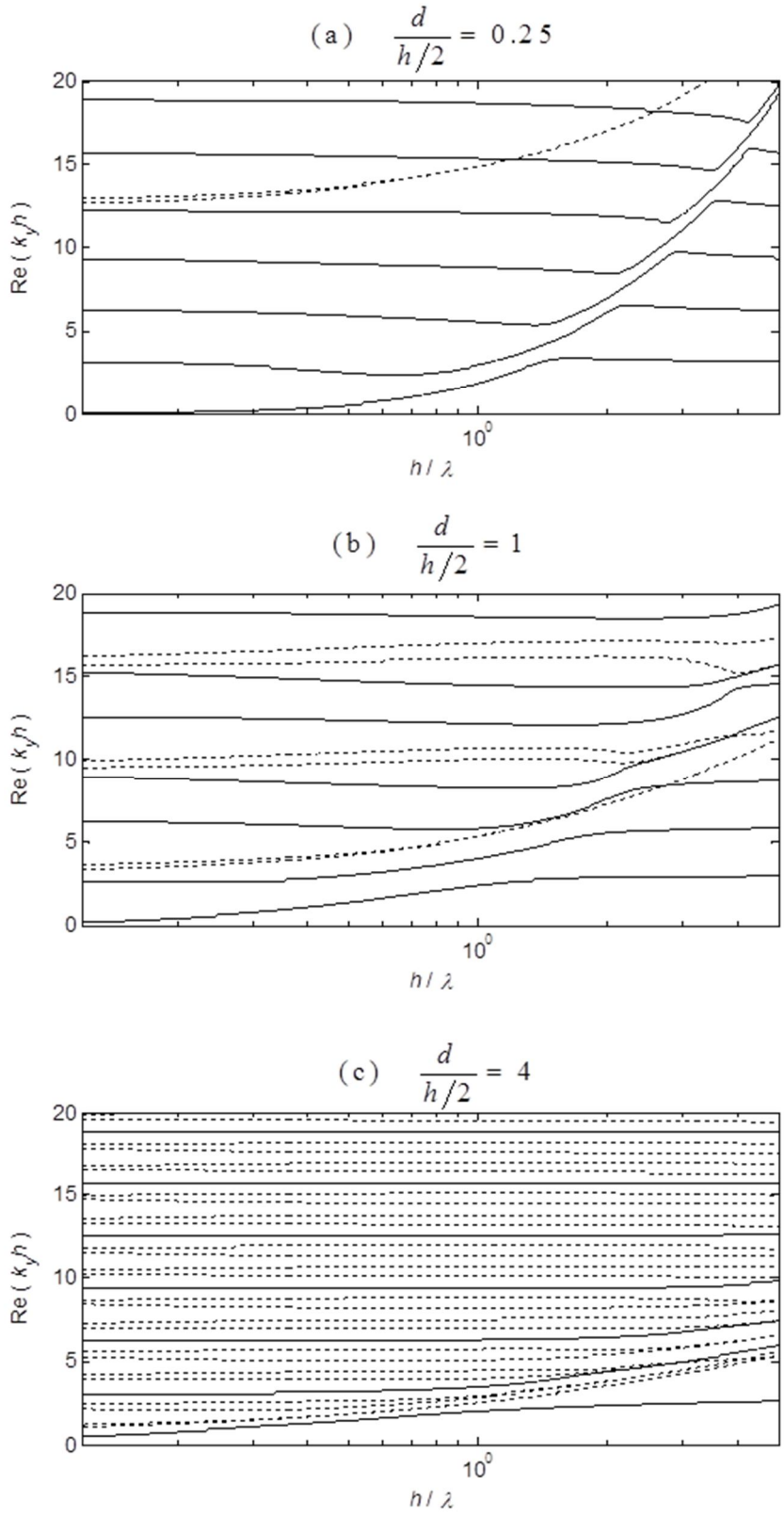

Figure 3.12: The real part of the transverse wavenumbers for the three different lining thicknesses where the solid lines represent airway modes and the dashed lines represent lining modes

3.6 Conclusions

In this chapter the theoretical framework for wave propagation in a duct with a bulk-reacting lining has been presented. The solution to the wavenumber equations was obtained using Müller's method. A semi-analytical model is used to obtain the acoustical properties of the bulk-reacting material which are required to solve the wavenumber equations.

For a duct with a bulk-reacting lining, there exist two types of wave modes, the airway modes, which depend on the value of h, and the lining modes, which depend on the lining thickness d. The wavenumbers in a hard-walled duct are used as the initial guesses for the airway modes, while the initial guesses for the lining modes were found using the argument principle method. These lining modes are not found in a duct with a locally reacting lining or in an unlined duct. For a duct with a locally reacting lining, there exist at most two surface waves at high frequency. However for a duct with a bulk-reacting lining, all the lining modes become localized in the lining at high frequency and their number at a given frequency depends on the lining thickness.

The attenuation rate of an infinite lined duct can be estimated by (i) the least attenuated mode and (ii) assuming equal energy distribution. Based on these two methods, it was found that the duct attenuation based on the locally reacting assumption is higher than the estimation for a bulk-reacting lining. The estimation based on the least attenuated mode can be used for small duct size since higher order modes cut on at a relatively high frequency.

In most cases the least attenuated mode is the fundamental mode and it is quite simple and straightforward to solve the problem. The second approach, where the same energy distribution is assumed, the predicted attenuation for the case of a bulk-reacting lining was found to be very high especially for a thicker lining, which is unlikely to be achieved in practice. The coupling between wave modes at the inlet and outlet junctions of a lined section of duct is an important factor which is not taken into account when the prediction of duct attenuation is based only on the least attenuated mode, or with the equal energy assumption. In the following chapter this factor will be taken into account by investigating an infinite duct with a finite length lined section. The technique for finding the required wavenumbers presented in this chapter will be applied in Chapter 4 where a closed-form solution for modal wave amplitudes is derived.

4. Wave propagation through a finite length lined duct

In this chapter, the problem of determining the sound field in a two-dimensional, finite lined duct is discussed. The lined section is located between two semi-infinite hard-walled ducts with the same airway height. The expansion of the sound field in terms of modes can simplify the problem. The two-dimensional acoustic field is decomposed into modal solutions of a one-dimensional eigenvalue problem, which has been addressed in the previous two chapters. These wave fields are expanded in terms of eigenvectors defined over the duct cross-section. The same approach could be used for a three-dimensional duct. However, for simplicity the analysis here is limited to a two-dimensional duct.

To formulate the analytical model, the duct system is treated as a boundary value problem and solved with the mode-matching technique. The mode-matching technique is a straight forward method that is based on matching the sound field at the interface between two duct segments at which the duct cross-section or acoustic impedance changes. Cummings and Chang [100] matched axial acoustic particle velocity and acoustic pressure across the lined duct discontinuity while Peat [101] developed a transfer matrix formulation by matching the average acoustic pressure and volume velocity across the discontinuity. The method of Peat that lacks accuracy above the cut-on frequency was improved by Kirby [102] where extra terms are included in the series expansion of the Bessel function. This successfully avoids the need for an iterative algorithm to find the required roots of eigenfunctions in performing the mode-matching. However, due to inherent limitation of expansions with a finite number of terms, this approach still remains confined to relatively low frequencies [92].

This mode-matching method is a very popular analytical tool and has been successfully applied in many fields when sudden transitions are present in the waveguide. The pressure and axial particle velocity should be continuous between duct sections at all positions across this cross-section. By expressing the pressure and axial particle velocity at either side of the junction as a sum over wave modes, analytical solutions can be obtained from which the wave mode amplitudes can be obtained. Then the acoustic field in each duct section is known and the corresponding transmission loss can be calculated.

The analytical study of sound transmission in a duct with a locally reacting lining is very well established and has wide applications for example to the area of turbo-fan aero engines [65, 77, 80, 82, 96]. However the case of a bulk-reacting lining has seen much less work. The main interest has been for silencers in automotive exhaust systems that involve perforated sheets and

mean flow [73, 92, 103]. In extending the method developed for automotive exhaust systems to a larger duct as used in ventilation systems, problems arise due to difficulties in finding all the required wavenumbers to carry out the mode-matching procedure. Some authors use an alternative technique whereby the root-finding process can be avoided [55, 71, 74].

In this chapter, with the aid of Müller's method for the root-finding process as discussed in the previous chapters, the mode-matching technique is applied to a duct that is continuously lined with either a locally reacting lining or a bulk-reacting lining. The number of modes to be included in the process is also investigated for both types of lining. The transmission loss is then calculated from the resulting modal wave amplitudes and this is compared with results reported in the literature. The duct attenuation predicted with the bulk-reacting model is compared with that from the locally reacting model. Some parametric studies are also performed to analyse the effect of duct geometry and lining material properties on duct attenuation.

4.1 Mode matching model

Consider, as shown in Figure 4.1, a lined section of duct with a finite length L_s (region *B*) connected to rigid walled semi-infinite ducts at its inlet and outlet (regions *A* and *C* respectively). The duct termination at either end is assumed to be anechoic; hence there are no returning negative going waves in region *C* and the reflected wave in A does not influence the incident field. The soft-wall duct in region B is lined at the upper (II) and lower (III) walls. The cross-sectional area of the airway (I) in the lined section is assumed to be the same as in the hard-walled duct [67]. For a duct with a changed airway height, additional boundary conditions are required to give a complete model. The incident wave a_m^+ travels from a source at $-\infty$. The impedance discontinuity introduced at $x = 0$ causes the incident wave to be reflected back as a_m^- and transmitted forward as b_m^+. At the second junction where $x = L_s$, the propagating wave b_m^+ is transmitted and reflected into c_m^+ and b_m^- respectively. Subscript *m* indicates the mode order for each wave amplitude. At each junction energy will also be scattered from one mode order to another. For convenience the local coordinate $v = x - L_s$ is used to describe the second junction.

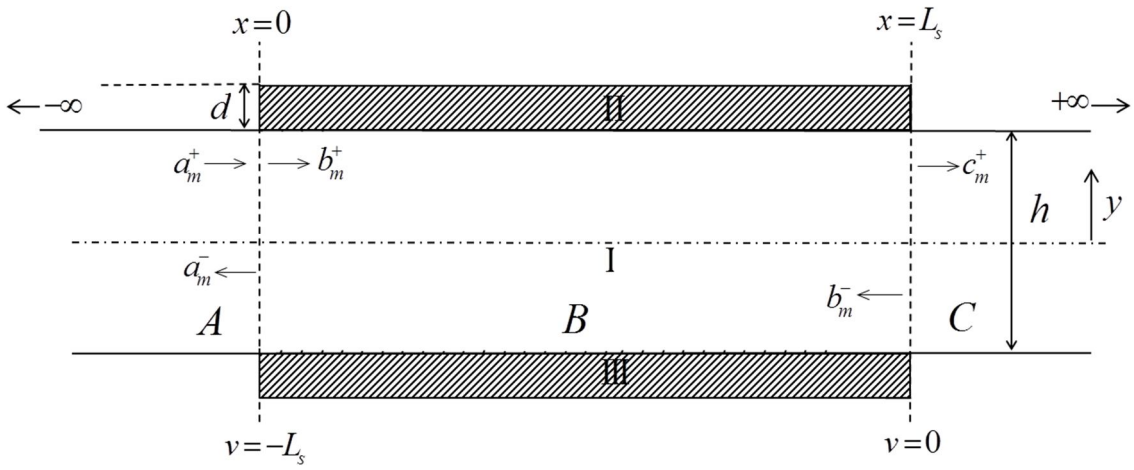

Figure 4.1: Finite length lined duct with rigid walled inlet and outlet sections

The mode matching technique used here is quite similar to the work by Cummings [67, 100] where a least squares method is used to minimize the error function. Least squares method uses derivatives of the error itself as weighting functions and requiring the square error to be a minimum. Another method commonly used by other authors [66, 80] is the Galerkin method where the weighting functions are chosen to be identical to the base functions.

In Cummings's technique, a few iterations are required to obtain converged wave amplitudes in all three regions, but here another approach is used so that the wave amplitudes can be evaluated in a direct manner. Both locally reacting and bulk-reacting linings are considered in the following analysis. Example results are given for both cases based on the same material properties as used in Chapter 3. The specific acoustic impedance of the lining material and the surface normal wall impedance are obtained from the semi-analytical material model (see Appendix 1). The locally reacting lining case is presented first followed by the bulk-reacting lining case.

4.1.1 Mode matching model for locally reacting lining

The sound pressure and axial particle velocity in regions *A*, *B* and *C* are written as:

$$\begin{aligned} p^a(x,y) &= \sum_{m=0}^{M} \Phi_m^a(y)\left(a_m^+ e^{-ik_{x,m}^a x} + a_m^- e^{ik_{x,m}^a x}\right) \\ u^a(x,y) &= \frac{1}{\omega\rho_0}\sum_{m=0}^{M} \Phi_m^a(y) k_{x,m}^a \left(a_m^+ e^{-ik_{x,m}^a x} - a_m^- e^{ik_{x,m}^a x}\right) \end{aligned} \tag{4.1}$$

$$
\begin{aligned}
p^b(x,y) &= \sum_{m=0}^{M} \Phi_m^b(y)\left(b_m^+ e^{-ik_{x,m}^b x} + b_m^- e^{ik_{x,m}^b v}\right) \\
u^b(x,y) &= \frac{1}{\omega\rho_0}\sum_{m=0}^{M} \Phi_m^b(y) k_{x,m}^b \left(b_m^+ e^{-ik_{x,m}^b x} - b_m^- e^{ik_{x,m}^b v}\right)
\end{aligned}
\tag{4.2}
$$

and

$$
\begin{aligned}
p^c(x,y) &= \sum_{m=0}^{M} \Phi_m^c(y) c_m^+ e^{-ik_{x,m}^c v} \\
u^c(x,y) &= \frac{1}{\omega\rho_0}\sum_{m=0}^{M} \Phi_m^c(y) k_{x,m}^c c_m^+ e^{-ik_{x,m}^c v}
\end{aligned}
\tag{4.3}
$$

where Φ is the normalized mode shape and the number of modes included, *M*, is taken to be the same for all three regions. The superscripts *a*, *b* and *c* refer to regions *A*, *B* and *C* respectively. The reference coordinate for the axial axis for waves a_m^+, a_m^-, and b_m^+ is *x* while for c_m^+ and b_m^- it is *v*. The mode shape is normalized by its magnitude at the wall surface $h/2$. This is to avoid numerical ill-conditioning when one of the wave modes considered in the calculation is a surface wave. For symmetrical modes, the normalized mode shape is given by:

$$
\Phi_m^R = \frac{\cos\left(k_{y,m}^R y\right)}{\left|\cos\left(k_{y,m}^R h/2\right)\right|} \tag{4.4}
$$

where the superscript *R* refers to region *A*, *B* or *C* and $k_{y,m}^R$ is the transverse wavenumber for mode *m* in the respective region *R*. Similarly for the anti-symmetrical mode, the normalized mode shape is given by:

$$
\Phi_m^R = \frac{-i\sin\left(k_{y,m}^R y\right)}{\left|\sin\left(k_{y,m}^R h/2\right)\right|} \tag{4.5}
$$

By forcing continuity conditions at the two (inlet and outlet) junctions, the required set of solutions that relates the four sets of unknown wave amplitudes a_m^-, b_m^+, b_m^- and c_m^+ can be obtained. The sound pressure difference and the axial particle velocity difference at both junctions are integrated across the duct height and then minimized with respect to the transmitted wave amplitude, b_n^+ for the first junction and with respect to b_n^- for the second junction for each *n*. The four error functions used are $\varepsilon_{1,1} = p^b(0) - p^a(0)$ and $\varepsilon_{2,1} = u^b(0) - u^a(0)$, at the first junction $x = 0$, and $\varepsilon_{1,2} = p^c(L_s) - p^b(L_s)$ and $\varepsilon_{2,2} = u^c(L_s) - u^b(L_s)$, at the second junction $x = L_s$ (or $v = 0$).

In the literature [67] the function to be minimized is the squared error. However, this is numerically incorrect since the error functions are based on the pressure and axial particle velocity difference which are complex in nature. Therefore, a correction has been made in this work where instead of the squared error function, the squared absolute error function, which is the product of the error function and its conjugate, is minimized. This introduces the product of $\Phi_m \Phi_n^*$ for which in the lined region, Φ_m and Φ_n^* are not orthogonal. Thus the orthogonality relation cannot be of benefit in reducing the size of equation matrices. However, this approach may have its advantage. The problem of singular matrices is not encountered when a large number of cut-off modes are included in the matching process which is carried out in the later part of this chapter.

In addition to the lack of orthogonality relation, the conjugate of the required wave amplitudes appears in the simultaneous equations, and cannot be solved directly. To address this issue, the real and imaginary parts of the complex variables are solved separately. This is done by minimizing for example, at the first junction, the integration of the squared absolute error across the duct height, with respect to the real and imaginary parts of the transmitted wave amplitudes, b_n^{+r} and b_n^{+i} respectively:

$$\begin{aligned} D_1 &= \int_{-h/2}^{h/2} \varepsilon_{k,1} \cdot \varepsilon_{k,1}^* dy \\ \frac{\partial D_1}{\partial b_n^{+r}} &= \int_{-h/2}^{h/2} \left(\varepsilon_{k,1} \frac{\partial \varepsilon_{k,1}^*}{\partial b_n^{+r}} + \varepsilon_{k,1}^* \frac{\partial \varepsilon_{k,1}}{\partial b_n^{+r}} \right) dy \\ \frac{\partial D_1}{\partial b_n^{+i}} &= \int_{-h/2}^{h/2} \left(\varepsilon_{k,1} \frac{\partial \varepsilon_{k,1}^*}{\partial b_n^{+i}} + \varepsilon_k^{1*} \frac{\partial \varepsilon_{k,1}}{\partial b_n^{+i}} \right) dy \end{aligned} \tag{4.6}$$

where * indicates complex conjugate. The superscript *r* indicates the real part and superscript *i* indicates the imaginary part.

For the sound pressure difference at the first junction, minimizing the error functions according to equation (4.6) yields:

$$\begin{aligned} &\left[\Lambda_{mn}^{bb*}\right]\left\{b_m^+\right\} + \left[\Lambda_{mn}^{bb*}T_s\right]\left\{b_m^-\right\} + \left[\Lambda_{mn}^{b*b}\right]\left\{b_m^{+*}\right\} + \left[\Lambda_{mn}^{b*b}T_s^*\right]\left\{b_m^{-*}\right\} \\ &\quad - \left[\Lambda_{mn}^{ab*}\right]\left\{a_m^+\right\} - \left[\Lambda_{mn}^{ab*}\right]\left\{a_m^-\right\} - \left[\Lambda_{mn}^{ab}\right]\left\{a_m^{+*}\right\} - \left[\Lambda_{mn}^{ab}\right]\left\{a_m^{-*}\right\} = 0 \end{aligned} \tag{4.7}$$

$$\begin{aligned} &-\left[\Lambda_{mn}^{bb*}\right]\left\{b_m^+\right\} - \left[\Lambda_{mn}^{bb*}T_s\right]\left\{b_m^-\right\} + \left[\Lambda_{mn}^{b*b}\right]\left\{b_m^{+*}\right\} + \left[\Lambda_{mn}^{b*b}T_s^*\right]\left\{b_m^{-*}\right\} \\ &\quad + \left[\Lambda_{mn}^{ab*}\right]\left\{a_m^+\right\} + \left[\Lambda_{mn}^{ab*}\right]\left\{a_m^-\right\} - \left[\Lambda_{mn}^{ab}\right]\left\{a_m^{+*}\right\} - \left[\Lambda_{mn}^{ab}\right]\left\{a_m^{-*}\right\} = 0 \end{aligned} \tag{4.8}$$

Wave propagation through a finite length lined duct

The superscripts *a* and *b* correspond to regions *A* and *B* respectively while *m* and *n* are the mode orders. $T_s = e^{-ik^b_{x,m}L_s}$ is the propagation term of wave amplitudes in the lined section, and

$$\Lambda^{ab*}_{mn} = \int_{-h/2}^{h/2} \Phi^a_m \Phi^{b*}_n dy \qquad \Lambda^{ab}_{mn} = \int_{-h/2}^{h/2} \Phi^a_m \Phi^b_n dy$$
$$\Lambda^{bb*}_{mn} = \int_{-h/2}^{h/2} \Phi^b_m \Phi^{b*}_n dy \qquad \Lambda^{b*b}_{mn} = \int_{-h/2}^{h/2} \Phi^{b*}_m \Phi^b_n dy \tag{4.9}$$

These are terms from within the matrices. Separating the real and imaginary parts and rearranging the solutions, equation (4.7) and (4.8) can be rewritten in the following form:

$$\begin{bmatrix} \Lambda^{bb*r}_{mn} & -\Lambda^{bb*i}_{mn} \\ \Lambda^{bb*i}_{mn} & \Lambda^{bb*r}_{mn} \end{bmatrix} \begin{Bmatrix} b^{+r}_m \\ b^{+i}_m \end{Bmatrix} + \begin{bmatrix} \Lambda^{bb*}_{mn} T_s{}^r & -\Lambda^{bb*}_{mn} T_s{}^i \\ \Lambda^{bb*}_{mn} T_s{}^i & \Lambda^{bb*}_{mn} T_s{}^r \end{bmatrix} \begin{Bmatrix} b^{-r}_m \\ b^{-i}_m \end{Bmatrix} =$$
$$\begin{bmatrix} \Lambda^{ab*r}_{mn} & -\Lambda^{ab*i}_{mn} \\ \Lambda^{ab*i}_{mn} & \Lambda^{ab*r}_{mn} \end{bmatrix} \begin{Bmatrix} a^{+r}_m \\ a^{+i}_m \end{Bmatrix} + \begin{bmatrix} \Lambda^{ab*r}_{mn} & -\Lambda^{ab*i}_{mn} \\ \Lambda^{ab*i}_{mn} & \Lambda^{ab*r}_{mn} \end{bmatrix} \begin{Bmatrix} a^{-r}_m \\ a^{-i}_m \end{Bmatrix} \tag{4.10}$$

Minimizing the error functions for the axial particle velocity at junction 1 according to equation (4.6) yields:

$$\left[\mathrm{K}^{bb*}_{mn}\Lambda^{bb*}_{mn}\right]\left\{b^+_m\right\} - \left[\mathrm{K}^{bb*}_{mn}\Lambda^{bb*}_{mn}T_s\right]\left\{b^-_m\right\} + \left[\mathrm{K}^{b*b}_{mn}\Lambda^{b*b}_{mn}\right]\left\{b^{+*}_m\right\} - \left[\mathrm{K}^{b*b}_{mn}\Lambda^{b*b}_{mn}T^*_s\right]\left\{b^{-*}_m\right\}$$
$$-\left[\mathrm{K}^{ab*}_{mn}\Lambda^{ab*}_{mn}\right]\left\{a^+_m\right\} + \left[\mathrm{K}^{ab*}_{mn}\Lambda^{ab*}_{mn}\right]\left\{a^-_m\right\} - \left[\mathrm{K}^{a*b}_{mn}\Lambda^{ab}_{mn}\right]\left\{a^{+*}_m\right\} + \left[\mathrm{K}^{a*b}_{mn}\Lambda^{ab}_{mn}\right]\left\{a^{-*}_m\right\} = 0 \tag{4.11}$$

$$-\left[\mathrm{K}^{bb*}_{mn}\Lambda^{bb*}_{mn}\right]\left\{b^+_m\right\} + \left[\mathrm{K}^{bb*}_{mn}\Lambda^{bb*}_{mn}T_s\right]\left\{b^-_m\right\} + \left[\mathrm{K}^{b*b}_{mn}\Lambda^{b*b}_{mn}\right]\left\{b^{+*}_m\right\} - \left[\mathrm{K}^{b*b}_{mn}\Lambda^{b*b}_{mn}T^*_s\right]\left\{b^{-*}_m\right\}$$
$$+\left[\mathrm{K}^{ab*}_{mn}\Lambda^{ab*}_{mn}\right]\left\{a^+_m\right\} - \left[\mathrm{K}^{ab*}_{mn}\Lambda^{ab*}_{mn}\right]\left\{a^-_m\right\} - \left[\mathrm{K}^{a*b}_{mn}\Lambda^{ab}_{mn}\right]\left\{a^{+*}_m\right\} + \left[\mathrm{K}^{a*b}_{mn}\Lambda^{ab}_{mn}\right]\left\{a^{-*}_m\right\} = 0 \tag{4.12}$$

where $\mathrm{K}^{ab*}_{mn} = k^a_{x,m}k^{b\ *}_{x,n}$, $\mathrm{K}^{a*b}_{mn} = k^{a*}_{x,m}k^b_{x,n}$, $\mathrm{K}^{bb*}_{mn} = k^b_{x,m}k^{b\ *}_{x,n}$ and $\mathrm{K}^{b*b}_{mn} = k^{b*}_{x,m}k^b_{x,n}$. By separating the real and imaginary parts, and rearranging, equations (4.11) and (4.12) can be written as:

$$\begin{bmatrix} \mathrm{K}^{bb*}_{mn}\Lambda^{bb*r}_{mn} & -\mathrm{K}^{bb*}_{mn}\Lambda^{bb*i}_{mn} \\ \mathrm{K}^{bb*}_{mn}\Lambda^{bb*i}_{mn} & \mathrm{K}^{bb*}_{mn}\Lambda^{bb*r}_{mn} \end{bmatrix} \begin{Bmatrix} b^{+r}_m \\ b^{+i}_m \end{Bmatrix} + \begin{bmatrix} \mathrm{K}^{bb*}_{mn}\Lambda^{bb*}_{mn}T_s{}^r & -\mathrm{K}^{bb*}_{mn}\Lambda^{bb*}_{mn}T_s{}^i \\ \mathrm{K}^{bb*}_{mn}\Lambda^{bb*}_{mn}T_s{}^i & \mathrm{K}^{bb*}_{mn}\Lambda^{bb*}_{mn}T_s{}^r \end{bmatrix} \begin{Bmatrix} b^{-r}_m \\ b^{-i}_m \end{Bmatrix} =$$
$$\begin{bmatrix} \mathrm{K}^{ab*}_{mn}\Lambda^{ab*r}_{mn} & -\mathrm{K}^{ab*}_{mn}\Lambda^{ab*i}_{mn} \\ \mathrm{K}^{ab*}_{mn}\Lambda^{ab*i}_{mn} & \mathrm{K}^{ab*}_{mn}\Lambda^{ab*r}_{mn} \end{bmatrix} \begin{Bmatrix} a^{+r}_m \\ a^{+i}_m \end{Bmatrix} + \begin{bmatrix} \mathrm{K}^{ab*}_{mn}\Lambda^{ab*r}_{mn} & -\mathrm{K}^{ab*}_{mn}\Lambda^{ab*i}_{mn} \\ \mathrm{K}^{ab*}_{mn}\Lambda^{ab*i}_{mn} & \mathrm{K}^{ab*}_{mn}\Lambda^{ab*r}_{mn} \end{bmatrix} \begin{Bmatrix} a^{-r}_m \\ a^{-i}_m \end{Bmatrix} \tag{4.13}$$

Similarly, the error functions at the second junction are integrated across the duct height and minimized with respect to the real and imaginary parts of the reflected wave amplitudes, b^{-r}_n and b^{-i}_n respectively:

$$
\begin{aligned}
D_2 &= \int_{-h/2}^{h/2} \varepsilon_{k,2} \cdot \varepsilon_{k,2}^{*} dy \\
\frac{\partial D_2}{\partial b_n^{-r}} &= \int_{-h/2}^{h/2} \left(\varepsilon_{k,2} \frac{\partial \varepsilon_{k,2}^{*}}{\partial b_n^{-r}} + \varepsilon_{k,2}^{*} \frac{\partial \varepsilon_{k,2}}{\partial b_n^{-r}} \right) dy \\
\frac{\partial D_2}{\partial b_n^{-i}} &= \int_{-h/2}^{h/2} \left(\varepsilon_{k,2} \frac{\partial \varepsilon_{k,2}^{*}}{\partial b_n^{-i}} + \varepsilon_{k,2}^{*} \frac{\partial \varepsilon_{k,2}}{\partial b_n^{-i}} \right) dy
\end{aligned}
\tag{4.14}
$$

Combining the equations from both junctions yields $8\times(M+1)$ equations that can be written in matrix form as:

$$
\mathbf{A}_{11} \begin{Bmatrix} b_m^{+r} \\ b_m^{+i} \end{Bmatrix} + \mathbf{B}_{11} \begin{Bmatrix} b_m^{-r} \\ b_m^{-i} \end{Bmatrix} = \mathbf{E}_{11} \begin{Bmatrix} a_m^{+r} \\ a_m^{+i} \end{Bmatrix} + \mathbf{F}_{11} \begin{Bmatrix} a_m^{-r} \\ a_m^{-i} \end{Bmatrix} \tag{4.15}
$$

$$
\mathbf{A}_{21} \begin{Bmatrix} b_m^{+r} \\ b_m^{+i} \end{Bmatrix} - \mathbf{B}_{21} \begin{Bmatrix} b_m^{-r} \\ b_m^{-i} \end{Bmatrix} = \mathbf{E}_{21} \begin{Bmatrix} a_m^{+r} \\ a_m^{+i} \end{Bmatrix} - \mathbf{F}_{21} \begin{Bmatrix} a_m^{-r} \\ a_m^{-i} \end{Bmatrix} \tag{4.16}
$$

$$
\mathbf{A}_{12} \begin{Bmatrix} b_m^{+r} \\ b_m^{+i} \end{Bmatrix} + \mathbf{B}_{12} \begin{Bmatrix} b_m^{-r} \\ b_m^{-i} \end{Bmatrix} = \mathbf{E}_{12} \begin{Bmatrix} c_m^{+r} \\ c_m^{+i} \end{Bmatrix} \tag{4.17}
$$

$$
\mathbf{A}_{22} \begin{Bmatrix} b_m^{+r} \\ b_m^{+i} \end{Bmatrix} - \mathbf{B}_{22} \begin{Bmatrix} b_m^{-r} \\ b_m^{-i} \end{Bmatrix} = \mathbf{E}_{22} \begin{Bmatrix} c_m^{+r} \\ c_m^{+i} \end{Bmatrix} \tag{4.18}
$$

where

$$
\begin{aligned}
\mathbf{A}_{11} &= \begin{bmatrix} \Lambda_{mn}^{bb*r} & -\Lambda_{mn}^{bb*i} \\ \Lambda_{mn}^{bb*i} & \Lambda_{mn}^{bb*r} \end{bmatrix} & \mathbf{A}_{21} &= \begin{bmatrix} \mathrm{K}_{mn}^{bb*} \Lambda_{mn}^{bb*r} & -\mathrm{K}_{mn}^{bb*} \Lambda_{mn}^{bb*i} \\ \mathrm{K}_{mn}^{bb*} \Lambda_{mn}^{bb*i} & \mathrm{K}_{mn}^{bb*} \Lambda_{mn}^{bb*r} \end{bmatrix} \\
\mathbf{B}_{11} &= \begin{bmatrix} \Lambda_{mn}^{bb*} T_s^{\,r} & -\Lambda_{mn}^{bb*} T_s^{\,i} \\ \Lambda_{mn}^{bb*} T_s^{\,i} & \Lambda_{mn}^{bb*} T_s^{\,r} \end{bmatrix} & \mathbf{B}_{21} &= \begin{bmatrix} \mathrm{K}_{mn}^{bb*} \Lambda_{mn}^{bb*} T_s^{\,r} & -\mathrm{K}_{mn}^{bb*} \Lambda_{mn}^{bb*} T_s^{\,i} \\ \mathrm{K}_{mn}^{bb*} \Lambda_{mn}^{bb*} T_s^{\,i} & \mathrm{K}_{mn}^{bb*} \Lambda_{mn}^{bb*} T_s^{\,r} \end{bmatrix} \\
\mathbf{E}_{11} &= \begin{bmatrix} \Lambda_{mn}^{ab*r} & -\Lambda_{mn}^{ab*i} \\ \Lambda_{mn}^{ab*i} & \Lambda_{mn}^{ab*r} \end{bmatrix} & \mathbf{E}_{21} &= \begin{bmatrix} \mathrm{K}_{mn}^{ab*} \Lambda_{mn}^{ab*r} & -\mathrm{K}_{mn}^{ab*} \Lambda_{mn}^{ab*i} \\ \mathrm{K}_{mn}^{ab*} \Lambda_{mn}^{ab*i} & \mathrm{K}_{mn}^{ab*} \Lambda_{mn}^{ab*r} \end{bmatrix} \\
\mathbf{F}_{11} &= \begin{bmatrix} \Lambda_{mn}^{ab*r} & -\Lambda_{mn}^{ab*i} \\ \Lambda_{mn}^{ab*i} & \Lambda_{mn}^{ab*r} \end{bmatrix} & \mathbf{F}_{21} &= \begin{bmatrix} \mathrm{K}_{mn}^{ab*} \Lambda_{mn}^{ab*r} & -\mathrm{K}_{mn}^{ab*} \Lambda_{mn}^{ab*i} \\ \mathrm{K}_{mn}^{ab*} \Lambda_{mn}^{ab*i} & \mathrm{K}_{mn}^{ab*} \Lambda_{mn}^{ab*r} \end{bmatrix} \\
\mathbf{A}_{12} &= \begin{bmatrix} \Lambda_{mn}^{bb*} T_s^{\,r} & -\Lambda_{mn}^{bb*} T_s^{\,i} \\ \Lambda_{mn}^{bb*} T_s^{\,i} & \Lambda_{mn}^{bb*} T_s^{\,r} \end{bmatrix} & \mathbf{A}_{22} &= \begin{bmatrix} \mathrm{K}_{mn}^{bb*} \Lambda_{mn}^{bb*} T_s^{\,r} & -\mathrm{K}_{mn}^{bb*} \Lambda_{mn}^{bb*} T_s^{\,i} \\ \mathrm{K}_{mn}^{bb*} \Lambda_{mn}^{bb*} T_s^{\,i} & \mathrm{K}_{mn}^{bb*} \Lambda_{mn}^{bb*} T_s^{\,r} \end{bmatrix} \\
\mathbf{B}_{12} &= \begin{bmatrix} \Lambda_{mn}^{bb*r} & -\Lambda_{mn}^{bb*i} \\ \Lambda_{mn}^{bb*i} & \Lambda_{mn}^{bb*r} \end{bmatrix} & \mathbf{B}_{22} &= \begin{bmatrix} \mathrm{K}_{mn}^{bb*} \Lambda_{mn}^{bb*r} & -\mathrm{K}_{mn}^{bb*} \Lambda_{mn}^{bb*i} \\ \mathrm{K}_{mn}^{bb*} \Lambda_{mn\ s}^{bb*\ i} & \mathrm{K}_{mn}^{bb*} \Lambda_{mn}^{bb*r} \end{bmatrix} \\
\mathbf{E}_{12} &= \begin{bmatrix} \Lambda_{mn}^{cb*r} & -\Lambda_{mn}^{cb*i} \\ \Lambda_{mn}^{cb*i} & \Lambda_{mn}^{cb*r} \end{bmatrix} & \mathbf{E}_{22} &= \begin{bmatrix} \mathrm{K}_{mn}^{cb*} \Lambda_{mn}^{cb*r} & -\mathrm{K}_{mn}^{cb*} \Lambda_{mn}^{cb*i} \\ \mathrm{K}_{mn}^{cb*} \Lambda_{mn}^{cb*i} & \mathrm{K}_{mn}^{cb*} \Lambda_{mn}^{cb*r} \end{bmatrix}
\end{aligned}
\tag{4.19}
$$

From equations (4.15) - (4.18), the unknown wave amplitudes are given by:

$$\begin{Bmatrix} b_m^+ \\ a_m^- \end{Bmatrix} = \begin{bmatrix} \mathbf{A}_{11} + \mathbf{B}_{11}\mathbf{R}_b & -\mathbf{F}_{11} \\ \mathbf{A}_{21} - \mathbf{B}_{21}\mathbf{R}_b & \mathbf{F}_{21} \end{bmatrix}^{-1} \begin{bmatrix} \mathbf{E}_{11} \\ \mathbf{E}_{21} \end{bmatrix} \left\{ a_m^+ \right\} \tag{4.20}$$

$$\left\{ c_m^+ \right\} = \left(\mathbf{E}_{12} \right)^{-1} \left(\mathbf{A}_{12} + \mathbf{B}_{12}\mathbf{R}_b \right) \left\{ b_m^+ \right\} \tag{4.21}$$

and

$$\left\{ b_m^- \right\} = \mathbf{R}_b \left\{ b_m^+ \right\} \tag{4.22}$$

where

$$\mathbf{R}_b = \left(-\left(\mathbf{E}_{22} \right)^{-1} \mathbf{B}_{22} - \left(\mathbf{E}_{12} \right)^{-1} \mathbf{B}_{12} \right)^{-1} \left(\left(\mathbf{E}_{12} \right)^{-1} \mathbf{A}_{12} - \left(\mathbf{E}_{22} \right)^{-1} \mathbf{A}_{22} \right) \tag{4.23}$$

Hence the wave amplitude coefficients in all three regions *A*, *B* and *C* are obtained in terms of the incident amplitudes $\left\{ a_m^+ \right\}$. From the wave amplitude coefficients, the transmission loss across the lined duct is then calculated. The transmission loss, *TL,* is defined as the ratio of the transmitted power in region *C* to the incident power. Expressing *TL* in dB**:**

$$\begin{aligned} TL &= 10\log_{10}\left(\frac{P_{a^+}}{P_{c^+}} \right) \text{ dB} \\ &= 10\log_{10}\left(\frac{\mathrm{Re}\left(\sum_{m=0}^{M} \int_{-h/2}^{h/2} p^a u^{a^*} dy \right)}{\mathrm{Re}\left(\sum_{m=0}^{M} \int_{-h/2}^{h/2} p^c u^{c^*} dy \right)} \right) \\ &= 10\log_{10}\left(\frac{\mathrm{Re}\left(\sum_{m=0}^{M} \left| a_m^+ \right|^2 k_{x,m}^{a^*} \int_{-h/2}^{h/2} \left| \Phi_m^a \right|^2 dy \right)}{\mathrm{Re}\left(\sum_{m=0}^{M} \left| c_m^+ \right|^2 k_{x,m}^{c^*} \int_{-h/2}^{h/2} \left| \Phi_m^c \right|^2 dy \right)} \right) \end{aligned} \tag{4.24}$$

where $k_{x,m}^{a^*}$ and $k_{x,m}^{c^*}$ are the conjugates of the axial wavenumbers in regions *A* and *C* respectively.

4.1.2 Mode matching model for bulk-reacting lining

For a bulk-reacting lining, it has been shown in the previous chapter that two types of wave mode exist in the soft-wall region: the airway modes, and the lining modes which are associated

with the liner thickness. Thus, at any given frequency, the number of cut-on modes in the soft-wall region may exceed the number of cut-on modes in the hard-walled region. For the mode-matching technique to be applied, extra equations are required to accommodate the additional lining modes. These can be obtained by introducing additional boundary conditions in the lining sections.

For the hard-walled regions (*A* and *C*), the sound pressure and axial particle velocity is the same as given in (4.1) and (4.3). As for the soft-wall region, the sound pressure and axial particle velocity in the duct are given by:

$$
\begin{aligned}
p^b &= \begin{cases}
\sum_{m=0}^{M} \Phi_m^b \left(b_m^+ e^{-ik_{x,m}^b x} + b_m^- e^{ik_{x,m}^b x} \right) + \\
\qquad \sum_{m_e=1}^{M_e} \Phi_{m_e}^b \left(b_{m_e}^+ e^{-ik_{x,m_e}^b x} + b_{m_e}^- e^{ik_{x,m_e}^b x} \right), & -h/2 \le y \le h/2 \\
\sum_{m=0}^{M} \tilde{\Phi}_m^b \left(b_m^+ e^{-ik_{x,m}^b x} + b_m^- e^{ik_{x,m}^b x} \right) + \\
\qquad \sum_{m_e=1}^{M_e} \tilde{\Phi}_{m_e}^b \left(b_{m_e}^+ e^{-ik_{x,m_e}^b x} + b_{m_e}^- e^{ik_{x,m_e}^b x} \right), & h/2 \le |y| \le D
\end{cases} \\
u_x^b &= \begin{cases}
\dfrac{1}{\omega \rho_0} \left[\begin{array}{l} \sum_{m=0}^{M} \Phi_m^b k_{x,m}^b \left(b_m^+ e^{-ik_{x,m}^b x} - b_m^- e^{ik_{x,m}^b x} \right) + \\ \qquad \sum_{m_e=1}^{M_e} \Phi_{m_e}^b k_{x,m_e}^b \left(b_{m_e}^+ e^{-ik_{x,m_e}^b x} - b_{m_e}^- e^{ik_{x,m_e}^b x} \right) \end{array} \right], & -h/2 \le y \le h/2 \\
\dfrac{1}{\omega \tilde{\rho}} \left[\begin{array}{l} \sum_{m=0}^{M} \tilde{\Phi}_m^b k_{x,m}^b \left(b_m^+ e^{-ik_{x,m}^b x} - b_m^- e^{ik_{x,m}^b x} \right) + \\ \qquad \sum_{m_e=1}^{M_e} \tilde{\Phi}_{m_e}^b k_{x,m_e}^b \left(b_{m_e}^+ e^{-ik_{x,m_e}^b x} - b_{m_e}^- e^{ik_{x,m_e}^b x} \right) \end{array} \right], & h/2 \le |y| \le D
\end{cases}
\end{aligned}
\tag{4.25}
$$

where the mode shape is defined by:

$$
\begin{aligned}
\Phi_m^b(y) &= \frac{\cos\left(k_{y,m}^b y\right)}{\left|\cos\left(k_{y,m}^b h/2\right)\right|}, && -h/2 \le y \le h/2 \\
\tilde{\Phi}_m^b(y) &= \frac{B_{3,m}\left(e^{-i\tilde{k}_{y,m}^b\left(y-h/2\right)} + e^{-i\tilde{k}_{y,m}^b d} e^{i\tilde{k}_{y,m}^b (y-D)} \right)}{\left|2\cos\left(k_{y,m}^b h/2\right)\right|}, && h/2 \le y \le D \\
\tilde{\Phi}_m^b(y) &= \frac{B_{5,m}\left(e^{i\tilde{k}_{y,m}^b\left(y+h/2\right)} + e^{-i\tilde{k}_{y,m}^b d} e^{-i\tilde{k}_{y,m}^b (y+D)} \right)}{\left|2\cos\left(k_{y,m}^b h/2\right)\right|}, && -D \le y \le -h/2
\end{aligned}
\tag{4.26}
$$

for even modes. The mode shapes for odd modes are given by:

$$\Phi_m^b(y) = \frac{-i\sin\left(k_{y,m}^b y\right)}{\left|\sin\left(k_{y,m}^b h/2\right)\right|}, \qquad -h/2 \le y \le h/2$$

$$\tilde{\Phi}_m^b(y) = \frac{B_{3,m}\left(e^{-i\tilde{k}_{y,m}^b\left(y-h/2\right)} + e^{-i\tilde{k}_{y,m}^b d} e^{i\tilde{k}_{y,m}^b (y-D)}\right)}{\left|2\sin\left(k_{y,m}^b h/2\right)\right|}, \qquad h/2 \le y \le D \tag{4.27}$$

$$\tilde{\Phi}_m^b(y) = \frac{B_{5,m}\left(e^{i\tilde{k}_{y,m}^b\left(y+h/2\right)} + e^{-i\tilde{k}_{y,m}^b d} e^{-i\tilde{k}_{y,m}^b (y+D)}\right)}{\left|2\sin\left(k_{y,m}^b h/2\right)\right|}, \qquad -D \le y \le -h/2$$

The tilde on $\tilde{\Phi}_m^b$ and $\tilde{k}_{y,m}^b$ is used to distinguish the mode shapes and transverse wavenumbers between those in the lining and those in the airway. M is the finite number of the airway modes included, and M_e is the number of lining modes included. The wave amplitude coefficients $B_{3,m}$ and $B_{5,m}$ are obtained by solving the boundary condition at $y = \pm h/2$ as shown in section 3.1 where for even modes, the wave amplitude coefficients are given by:

$$B_{3,m} = B_{5,m} = \frac{\left(2\cos\left(k_{y,m}^b \frac{h}{2}\right)\right)}{\left(1 + e^{-2i\tilde{k}_{y,m}^b d}\right)} \tag{4.28}$$

and for odd modes:

$$B_{3,m} = -B_{5,m} = \frac{\left(-2i\sin\left(k_{y,m}^b \frac{h}{2}\right)\right)}{\left(1 + e^{-2i\tilde{k}_{y,m}^b d}\right)} \tag{4.29}$$

With the same error functions as defined for the locally reacting case, and following the same procedure as in equations (4.6) and (4.14), four sets of simultaneous equations are obtained relating the unknown wave amplitudes. With the additional lining modes in the soft-wall region, two extra sets of equations are needed. Assuming the lining to be enclosed with a rigid backing, the axial particle velocity in lining sections II and III at the two junctions, $x = 0$ and $x = L_s$ is zero. Thus, defining two additional error functions as $\varepsilon_{31} = \tilde{u}_b(0)$ and $\varepsilon_{32} = \tilde{u}_b(L_s)$, these are integrated across the lining depth and minimized with respect to the real and imaginary part of the extra wave modes $b_{n_e}^+$ and $b_{n_e}^-$. This yields the additional equations. The full set of equations is given below:

$$\mathbf{A}_{11}\begin{Bmatrix} b_m^{+r} \\ b_m^{+i} \end{Bmatrix} + \mathbf{B}_{11}\begin{Bmatrix} b_m^{-r} \\ b_m^{-i} \end{Bmatrix} + \mathbf{C}_{11}\begin{Bmatrix} b_{m_e}^{+r} \\ b_{m_e}^{+i} \end{Bmatrix} + \mathbf{D}_{11}\begin{Bmatrix} b_{m_e}^{-r} \\ b_{m_e}^{-i} \end{Bmatrix} = \mathbf{E}_{11}\begin{Bmatrix} a_m^{+r} \\ a_m^{+i} \end{Bmatrix} + \mathbf{F}_{11}\begin{Bmatrix} a_m^{-r} \\ a_m^{-i} \end{Bmatrix} \tag{4.30}$$

$$\mathbf{A}_{21}\begin{Bmatrix} b_m^{+r} \\ b_m^{+i} \end{Bmatrix} - \mathbf{B}_{21}\begin{Bmatrix} b_m^{-r} \\ b_m^{-i} \end{Bmatrix} + \mathbf{C}_{21}\begin{Bmatrix} b_{m_e}^{+r} \\ b_{m_e}^{+i} \end{Bmatrix} - \mathbf{D}_{21}\begin{Bmatrix} b_{m_e}^{-r} \\ b_{m_e}^{-i} \end{Bmatrix} = \mathbf{E}_{21}\begin{Bmatrix} a_m^{+r} \\ a_m^{+i} \end{Bmatrix} - \mathbf{F}_{21}\begin{Bmatrix} a_m^{-r} \\ a_m^{-i} \end{Bmatrix} \tag{4.31}$$

$$\mathbf{A}_{12}\begin{Bmatrix} b_m^{+r} \\ b_m^{+i} \end{Bmatrix} + \mathbf{B}_{12}\begin{Bmatrix} b_m^{-r} \\ b_m^{-i} \end{Bmatrix} + \mathbf{C}_{12}\begin{Bmatrix} b_{m_e}^{+r} \\ b_{m_e}^{+i} \end{Bmatrix} + \mathbf{D}_{12}\begin{Bmatrix} b_{m_e}^{-r} \\ b_{m_e}^{-i} \end{Bmatrix} = \mathbf{E}_{12}\begin{Bmatrix} c_m^{+r} \\ c_m^{+i} \end{Bmatrix} \tag{4.32}$$

$$\mathbf{A}_{22}\begin{Bmatrix} b_m^{+r} \\ b_m^{+i} \end{Bmatrix} - \mathbf{B}_{22}\begin{Bmatrix} b_m^{-r} \\ b_m^{-i} \end{Bmatrix} + \mathbf{C}_{22}\begin{Bmatrix} b_{m_e}^{+r} \\ b_{m_e}^{+i} \end{Bmatrix} - \mathbf{D}_{22}\begin{Bmatrix} b_{m_e}^{-r} \\ b_{m_e}^{-i} \end{Bmatrix} = \mathbf{E}_{22}\begin{Bmatrix} c_m^{+r} \\ c_m^{+i} \end{Bmatrix} \tag{4.33}$$

$$\mathbf{A}_{31}\begin{Bmatrix} b_m^{+r} \\ b_m^{+i} \end{Bmatrix} - \mathbf{B}_{31}\begin{Bmatrix} b_m^{-r} \\ b_m^{-i} \end{Bmatrix} + \mathbf{C}_{31}\begin{Bmatrix} b_{m_e}^{+r} \\ b_{m_e}^{+i} \end{Bmatrix} - \mathbf{D}_{31}\begin{Bmatrix} b_{m_e}^{-r} \\ b_{m_e}^{-i} \end{Bmatrix} = 0 \tag{4.34}$$

$$\mathbf{A}_{32}\begin{Bmatrix} b_m^{+r} \\ b_m^{+i} \end{Bmatrix} - \mathbf{B}_{32}\begin{Bmatrix} b_m^{-r} \\ b_m^{-i} \end{Bmatrix} + \mathbf{C}_{32}\begin{Bmatrix} b_{m_e}^{+r} \\ b_{m_e}^{+i} \end{Bmatrix} - \mathbf{D}_{32}\begin{Bmatrix} b_{m_e}^{-r} \\ b_{m_e}^{-i} \end{Bmatrix} = 0 \tag{4.35}$$

where

$$\mathbf{A}_{31} = \begin{bmatrix} \mathrm{K}_{mn}^{bb_e*}\tilde{\Lambda}_{mn}^{bb_e*r} & -\mathrm{K}_{mn}^{bb_e*}\tilde{\Lambda}_{mn}^{bb_e*i} \\ \mathrm{K}_{mn}^{bb_e*}\tilde{\Lambda}_{mn}^{bb_e*i} & \mathrm{K}_{mn}^{bb_e*}\tilde{\Lambda}_{mn}^{bb_e*r} \end{bmatrix} \qquad \mathbf{A}_{32} = \begin{bmatrix} \mathrm{K}_{mn}^{bb_e*}\tilde{\Lambda}_{mn}^{bb_e*}T_s^{\,r} & -\mathrm{K}_{mn}^{bb_e*}\tilde{\Lambda}_{mn}^{bb_e*}T_s^{\,i} \\ \mathrm{K}_{mn}^{bb_e*}\tilde{\Lambda}_{mn}^{bb_e*}T_s^{\,i} & \mathrm{K}_{mn}^{bb_e*}\tilde{\Lambda}_{mn}^{bb_e*}T_s^{\,r} \end{bmatrix}$$

$$\mathbf{B}_{31} = \begin{bmatrix} \mathrm{K}_{mn}^{bb_e*}\tilde{\Lambda}_{mn}^{bb_e*}T_s^{\,r} & -\mathrm{K}_{mn}^{bb_e*}\tilde{\Lambda}_{mn}^{bb_e*}T_s^{\,i} \\ \mathrm{K}_{mn}^{bb_e*}\tilde{\Lambda}_{mn}^{bb_e*}T_s^{\,i} & \mathrm{K}_{mn}^{bb_e*}\tilde{\Lambda}_{mn}^{bb_e*}T_s^{\,r} \end{bmatrix} \qquad \mathbf{B}_{32} = \begin{bmatrix} -\mathrm{K}_{mn}^{bb_e*}\tilde{\Lambda}_{mn}^{bb_e*r} & \mathrm{K}_{mn}^{bb_e*}\tilde{\Lambda}_{mn}^{bb_e*i} \\ \mathrm{K}_{mn}^{bb_e*}\tilde{\Lambda}_{mn}^{bb_e*i} & \mathrm{K}_{mn}^{bb_e*}\tilde{\Lambda}_{mn}^{bb_e*r} \end{bmatrix}$$

$$\mathbf{C}_{11} = \begin{bmatrix} \Lambda_{m_en}^{b_eb*r} & -\Lambda_{m_en}^{b_eb*i} \\ \Lambda_{m_en}^{b_eb*i} & \Lambda_{m_en}^{b_eb*r} \end{bmatrix} \qquad \mathbf{C}_{21} = \begin{bmatrix} \mathrm{K}_{m_en}^{b_eb*}\Lambda_{m_en}^{b_eb*r} & -\mathrm{K}_{m_en}^{b_eb*}\Lambda_{m_en}^{b_eb*i} \\ \mathrm{K}_{m_en}^{b_eb*}\Lambda_{m_en}^{b_eb*i} & \mathrm{K}_{m_en}^{b_eb*}\Lambda_{m_en}^{b_eb*r} \end{bmatrix}$$

$$\mathbf{C}_{12} = \begin{bmatrix} \Lambda_{m_en}^{b_eb*}T_s^{\,r} & -\Lambda_{m_en}^{b_eb*}T_s^{\,i} \\ \Lambda_{m_en}^{b_eb*}T_s^{\,i} & \Lambda_{m_en}^{b_eb*}T_s^{\,r} \end{bmatrix} \qquad \mathbf{C}_{22} = \begin{bmatrix} \Lambda_{m_en}^{b_eb*r} & -\Lambda_{m_en}^{b_eb*i} \\ \Lambda_{m_en}^{b_eb*i} & \Lambda_{m_en}^{b_eb*r} \end{bmatrix}$$

$$\mathbf{C}_{31} = \begin{bmatrix} \mathrm{K}_{m_en}^{b_eb_e*}\tilde{\Lambda}_{m_en}^{b_eb_e*r} & -\mathrm{K}_{m_en}^{b_eb_e*}\tilde{\Lambda}_{m_en}^{b_eb_e*i} \\ \mathrm{K}_{m_en}^{bb_e*}\tilde{\Lambda}_{m_en}^{b_eb_e*i} & \mathrm{K}_{m_en}^{b_eb_e*}\tilde{\Lambda}_{m_en}^{b_eb_e*r} \end{bmatrix} \qquad \mathbf{C}_{32} = \begin{bmatrix} \mathrm{K}_{m_en}^{b_eb_e*}\tilde{\Lambda}_{m_en}^{b_eb_e*}T_s^{\,r} & -\mathrm{K}_{m_en}^{b_eb_e*}\tilde{\Lambda}_{m_en}^{b_eb_e*}T_s^{\,i} \\ \mathrm{K}_{m_en}^{b_eb_e*}\tilde{\Lambda}_{m_en}^{b_eb_e*}T_s^{\,i} & \mathrm{K}_{m_en}^{b_eb_e*}\tilde{\Lambda}_{m_en}^{b_eb_e*}T_s^{\,r} \end{bmatrix}$$

$$\mathbf{D}_{11} = \begin{bmatrix} \Lambda_{m_en}^{b_eb*}T_s^{\,r} & -\Lambda_{m_en}^{b_eb*}T_s^{\,i} \\ \Lambda_{m_en}^{b_eb*}T_s^{\,i} & \Lambda_{m_en}^{bb*}T_s^{\,r} \end{bmatrix} \qquad \mathbf{D}_{21} = \begin{bmatrix} \mathrm{K}_{m_en}^{b_eb*}\Lambda_{m_en}^{b_eb*}T_s^{\,r} & -\mathrm{K}_{m_en}^{b_eb*}\Lambda_{m_en}^{b_eb*}T_s^{\,i} \\ \mathrm{K}_{m_en}^{b_eb*}\Lambda_{m_en}^{b_eb*}T_s^{\,i} & \mathrm{K}_{m_en}^{b_eb*}\Lambda_{m_en}^{b_eb*}T_s^{\,r} \end{bmatrix}$$

$$\mathbf{D}_{12} = \begin{bmatrix} \mathrm{K}_{m_en}^{b_eb*}\Lambda_{m_en}^{b_eb*}T_s^{\,r} & -\mathrm{K}_{m_en}^{b_eb*}\Lambda_{m_en}^{b_eb*}T_s^{\,i} \\ \mathrm{K}_{m_en}^{b_eb*}\Lambda_{m_en}^{b_eb*}T_s^{\,i} & \mathrm{K}_{m_en}^{b_eb*}\Lambda_{m_en}^{b_eb*}T_s^{\,r} \end{bmatrix} \qquad \mathbf{D}_{22} = \begin{bmatrix} \mathrm{K}_{m_en}^{b_eb*}\Lambda_{m_en}^{b_eb*r} & -\mathrm{K}_{m_en}^{b_eb*}\Lambda_{m_en}^{b_eb*i} \\ \mathrm{K}_{m_en}^{b_eb*}\Lambda_{m_en}^{b_eb*i} & \mathrm{K}_{m_en}^{b_eb*}\Lambda_{m_en}^{b_eb*r} \end{bmatrix}$$

$$\mathbf{D}_{31} = \begin{bmatrix} \mathrm{K}_{m_en}^{b_eb_e*}\tilde{\Lambda}_{m_en}^{b_eb_e*}T_s^{\,r} & -\mathrm{K}_{m_en}^{b_eb_e*}\tilde{\Lambda}_{m_en}^{b_eb_e*}T_s^{\,i} \\ \mathrm{K}_{m_en}^{b_eb_e*}\tilde{\Lambda}_{m_en}^{b_eb_e*}T_s^{\,i} & \mathrm{K}_{m_en}^{b_eb_e*}\tilde{\Lambda}_{m_en}^{b_eb_e*}T_s^{\,r} \end{bmatrix} \qquad \mathbf{D}_{32} = \begin{bmatrix} \mathrm{K}_{m_en}^{b_eb_e*}\tilde{\Lambda}_{m_en}^{b_eb_e*r} & -\mathrm{K}_{m_en}^{b_eb_e*}\tilde{\Lambda}_{m_en}^{b_eb_e*i} \\ \mathrm{K}_{m_en}^{b_eb_e*}\tilde{\Lambda}_{m_en}^{b_eb_e*i} & \mathrm{K}_{m_en}^{b_eb_e*}\tilde{\Lambda}_{m_en}^{b_eb_e*r} \end{bmatrix} \tag{4.36}$$

and other matrices are as previously defined. The superscript b_e and subscript m_e refer to the lining modes. The expressions for the matrix components are given by:

$$\begin{aligned}
\mathrm{K}_{m_e n}^{b_e b_e^*} &= k_{x,m_e}^{b_e} k_{x,n}^{b_e^*} \\
\mathrm{K}_{m_e n}^{b_e b^*} &= k_{x,m_e}^{b_e} k_{x,n}^{b^*} \\
\mathrm{K}_{mn}^{b b_e^*} &= k_{x,m}^{b} k_{x,n}^{b_e^*} \\
\tilde{\Lambda}_{m_e n}^{b_e b_e^*} &= \int_{h/2}^{D} \tilde{\Phi}_{m_e}^{b_e} \tilde{\Phi}_n^{b_e^*} dy + \int_{-D}^{-h/2} \tilde{\Phi}_{m_e}^{b_e} \tilde{\Phi}_n^{b_e^*} dy \\
\tilde{\Lambda}_{m_e n}^{b_e b^*} &= \int_{h/2}^{D} \tilde{\Phi}_{m_e}^{b_e} \tilde{\Phi}_n^{b^*} dy + \int_{-D}^{-h/2} \tilde{\Phi}_{m_e}^{b_e} \tilde{\Phi}_n^{b^*} dy
\end{aligned} \tag{4.37}$$

From (4.34) and (4.35), the amplitudes of the M_e lining modes can be written in terms of the M airway modes:

$$\begin{Bmatrix} b_{m_e}^{+r} \\ b_{m_e}^{+i} \\ b_{m_e}^{-r} \\ b_{m_e}^{-i} \end{Bmatrix} = \boldsymbol{\beta} \begin{Bmatrix} b_m^{+r} \\ b_m^{+i} \\ b_m^{-r} \\ b_m^{-i} \end{Bmatrix} \tag{4.38}$$

where

$$\begin{aligned}
\boldsymbol{\beta} &= \begin{bmatrix} \beta_1 & \beta_2 \\ \beta_3 & \beta_4 \end{bmatrix} \\
&= \begin{bmatrix} -\mathbf{C}_{31} & \mathbf{D}_{31} \\ -\mathbf{C}_{32} & \mathbf{D}_{32} \end{bmatrix}^{-1} \begin{bmatrix} \mathbf{A}_{31} & -\mathbf{B}_{31} \\ \mathbf{A}_{32} & -\mathbf{B}_{32} \end{bmatrix}
\end{aligned} \tag{4.39}$$

The lining mode wave amplitudes $b_{m_e}^+$ and $b_{m_e}^-$ in equations (4.30)-(4.33) can be replaced using equation (4.38). Solving the simultaneous equations gives:

$$\begin{Bmatrix} b_m^+ \\ a_m^- \end{Bmatrix} = \begin{bmatrix} \mathbf{J}_{11} + \mathbf{K}_{11}\mathbf{R}_b & -\mathbf{F}_{11} \\ \mathbf{J}_{21} - \mathbf{K}_{21}\mathbf{R}_b & \mathbf{F}_{21} \end{bmatrix}^{-1} \begin{bmatrix} \mathbf{E}_{11} \\ \mathbf{E}_{21} \end{bmatrix} \{a_m^+\} \tag{4.40}$$

and

$$\begin{aligned}
\{c_m^+\} &= \left(\mathbf{E}_{12}\right)^{-1} \left(\mathbf{J}_{12} + \mathbf{K}_{12}\mathbf{R}_b\right) \{b_m^+\} \\
\{b_m^-\} &= \mathbf{R}_b \{b_m^+\}
\end{aligned} \tag{4.41}$$

where

$$\mathbf{R}_b = \left(-\left(\mathbf{E}_{22}\right)^{-1}\mathbf{K}_{22} - \left(\mathbf{E}_{12}\right)^{-1}\mathbf{K}_{12}\right)^{-1}\left(\left(\mathbf{E}_{12}\right)^{-1}\mathbf{J}_{12} - \left(\mathbf{E}_{22}\right)^{-1}\mathbf{J}_{22}\right) \tag{4.42}$$

and

$$\begin{aligned}
\mathbf{J}_{11} &= \mathbf{A}_{11} + \mathbf{C}_{11}\beta_1 + \mathbf{D}_{11}\beta_3 & \mathbf{K}_{11} &= \mathbf{B}_{11} + \mathbf{C}_{11}\beta_2 + \mathbf{D}_{11}\beta_4 \\
\mathbf{J}_{21} &= \mathbf{A}_{21} + \mathbf{C}_{21}\beta_1 - \mathbf{D}_{21}\beta_3 & \mathbf{K}_{21} &= \mathbf{B}_{21} - \mathbf{C}_{21}\beta_2 + \mathbf{D}_{21}\beta_4 \\
\mathbf{J}_{12} &= \mathbf{A}_{12} + \mathbf{C}_{12}\beta_1 + \mathbf{D}_{12}\beta_3 & \mathbf{K}_{12} &= \mathbf{B}_{12} + \mathbf{C}_{12}\beta_2 + \mathbf{D}_{12}\beta_4 \\
\mathbf{J}_{22} &= \mathbf{A}_{22} + \mathbf{C}_{22}\beta_1 - \mathbf{D}_{22}\beta_3 & \mathbf{K}_{22} &= \mathbf{B}_{22} - \mathbf{C}_{22}\beta_2 + \mathbf{D}_{22}\beta_4
\end{aligned} \tag{4.43}$$

4.2 Number of modes required in solution

For numerical solution the infinite series that forms the sound field must be truncated after a certain number of modes. A sufficiently large number of modes are required to give an accurate estimation of the modal pressure coefficients, but this must not be too large in order to avoid excessive computational effort or ill-conditioning. Cummings [62] states that the value of M should equal the number of propagating modes at the particular frequency, plus nine additional modes. McAlpine [80] in his work included 20 cut-off modes to improve the modelling of the near field in the vicinity of each matching plane.

In this section, a numerical study is conducted to find a suitable number of modes to be included for the mode-matching technique. This number can be found for example by simply keeping a check on the convergence of the modal amplitudes [96]. In addition to the cut-on modes, N_c cut-off modes are added gradually until the modal amplitudes in each duct section converge.

In Chapters 2 and 3, the wave modes have been ordered according to their transverse order which corresponds to the mode order in a rigid duct. However as frequency varies the wave modes can change nature, for example between the surface wave and airway mode in a duct with a locally reacting lining, or between the lining mode and the airway mode in a duct with a bulk-reacting lining, as discussed in section 3.3. Since the order for wavenumber solutions from Müller's method for each mode is kept constant, a reordering of the wavenumbers with frequency is required so that modes are ordered properly.

The modes to be added are ordered in accordance with their cut-on ratio [66] as given in equation (3.25). Since the quantity of interest is the duct transmission loss which is obtained from the transmitted wave amplitudes, in this study the number of modes to be included in the mode-matching process is determined based on the rate of convergence of the transmitted wave

amplitudes. Here an assumption of plane wave incidence is made, as is common in the literature [104]. A consequence of this assumption is that odd modes will not be excited and can be excluded from the calculations. Later (see chapter 5, section 5.8) other types of incident wave are considered, i.e. multi-mode incidence.

For a duct height of h = 0.3 m, for example, the cut-on frequencies are listed in Table 4.1. Studies are carried out at eight different frequencies each with a different number of cut-on modes. Figure 4.2 shows the rate of convergence of the transmitted modal wave amplitudes for the cut-on modes. The convergence of the transmitted wave amplitudes, Δc_p , is defined by:

$$\Delta c_p = \frac{\left| c_{p,N} - c_{p,R} \right|}{\left| c_{p,R} \right|} \tag{4.44}$$

where $c_{p,N}$ is the wave amplitude obtained from matching N modes, and $c_{p,R}$ is the 'true' amplitude. The 'exact' value $c_{p,R}$ is the amplitudes obtained by including a very large number of modes in calculating the wave amplitudes in equations (4.40) and (4.41). In this case the number of modes included, N, is 200. Although a large number of evanescent modes are included in the calculation of $c_{p,R}$, the problem of ill-conditioned matrices has not been encountered in this work.

Table 4.1: Cut-on frequencies for higher order even modes for a duct with an airway height of 0.3 m

Mode	Cut-on frequency (Hz)
2	1130
4	2270
6	3400
8	4530
10	5670
12	6800
14	7930

4.2.1 Number of modes required for a duct with a locally reacting lining

From the plots in Figure 4.2, as more modes are cut on, more cut-off modes are also required for the wave amplitudes to converge particularly for the higher order cut-on modes. The rule used by McAlpine [80] states that when there are five or fewer cut-on modes, an additional 20 cut-off modes are sufficient. With the inclusion of 20 cut-off modes, the calculated wave amplitudes at 500, 1500 and 2500Hz are within about 0.1% of the actual value.

Figure 4.3 shows the pressure and normalized axial particle velocity at the two junctions at 5000 Hz, obtained from a total of 25 modal contributions (5 cut-on modes and 20 cut-off modes). Junction 1 is the inlet junction at $x = 0$ and junction 2 is the outlet junction at $x = L_s$. The pressure is normalized to the pressure at wall and the axial particle velocity is normalized by $\rho_0 c_0$. The pressure and axial particle velocity at the right and left side of the two junctions match very well. Therefore, an agreementof within 0.1% of the cut-on wave amplitudes to the actual amplitudes is sufficient to give a proper match of pressure and velocity at the junction.

However, considering the results at 8500 Hz where 8 modes are cut-on, a convergence of 0.1% in all wave amplitudes requires the inclusion of 60 cut-off modes. Reducing this to 24 cut-off modes still gives a good match at the junction as shown in Figure 4.4. Figure 4.5 shows the pressure and axial particle velocity at 9800 Hz where 9 modes are cut on. 24 cut-off modes are included for mode-matching and this shows that this is sufficient to give a good match of pressure and velocity at the two junctions as well. In Figure 4.2, at 8500 Hz with 24 cut-off modes included, the first five modes have converged to 0.1% of their 'true' value. The lowest order mode, mode 0, is within 0.005% of its 'true' value but the percentage for the highest cut-on mode 8 is 0.5%. Clearly the lower order modes are fitted best. From these results it can be concluded that if the number of cut-on modes is more than five, for each additional cut-on mode, three or four additional cut-off modes should be included to ensure a good matching while avoiding an excessively large number of modes. In terms of computation time, the time taken to obtain all wave amplitudes in the duct sections with 33 modes included, for a frequency range of 10 Hz to 10 kHz with 10000 frequency steps, is 5 minutes. The simulation was carried out using MATLAB version (R2011a) on a university provided desktop with Intel Xeon quad core processor.

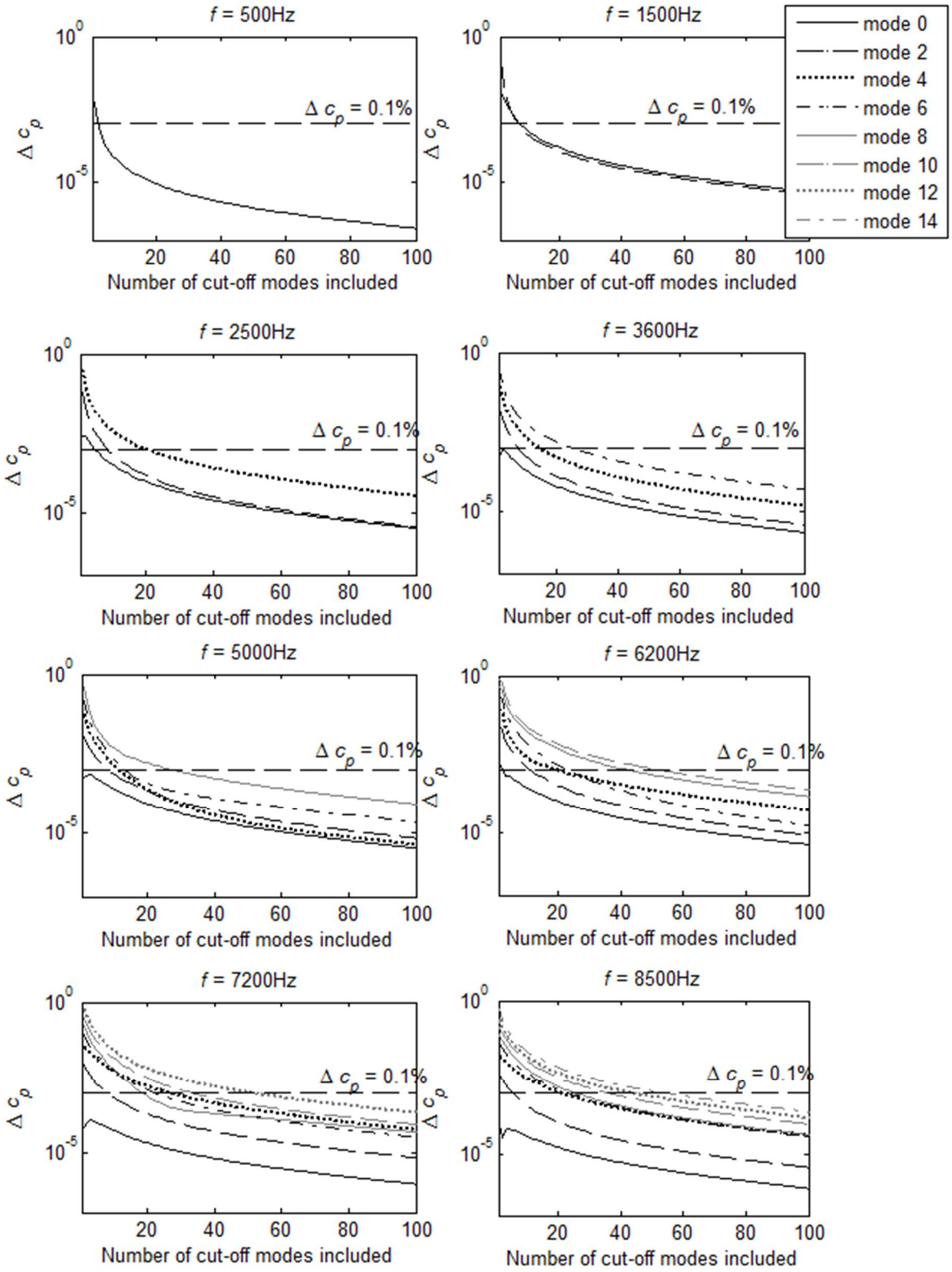

Figure 4.2: Convergence rate of modal wave amplitudes for the cut-on modes at eight different frequencies for a duct with a locally reacting lining

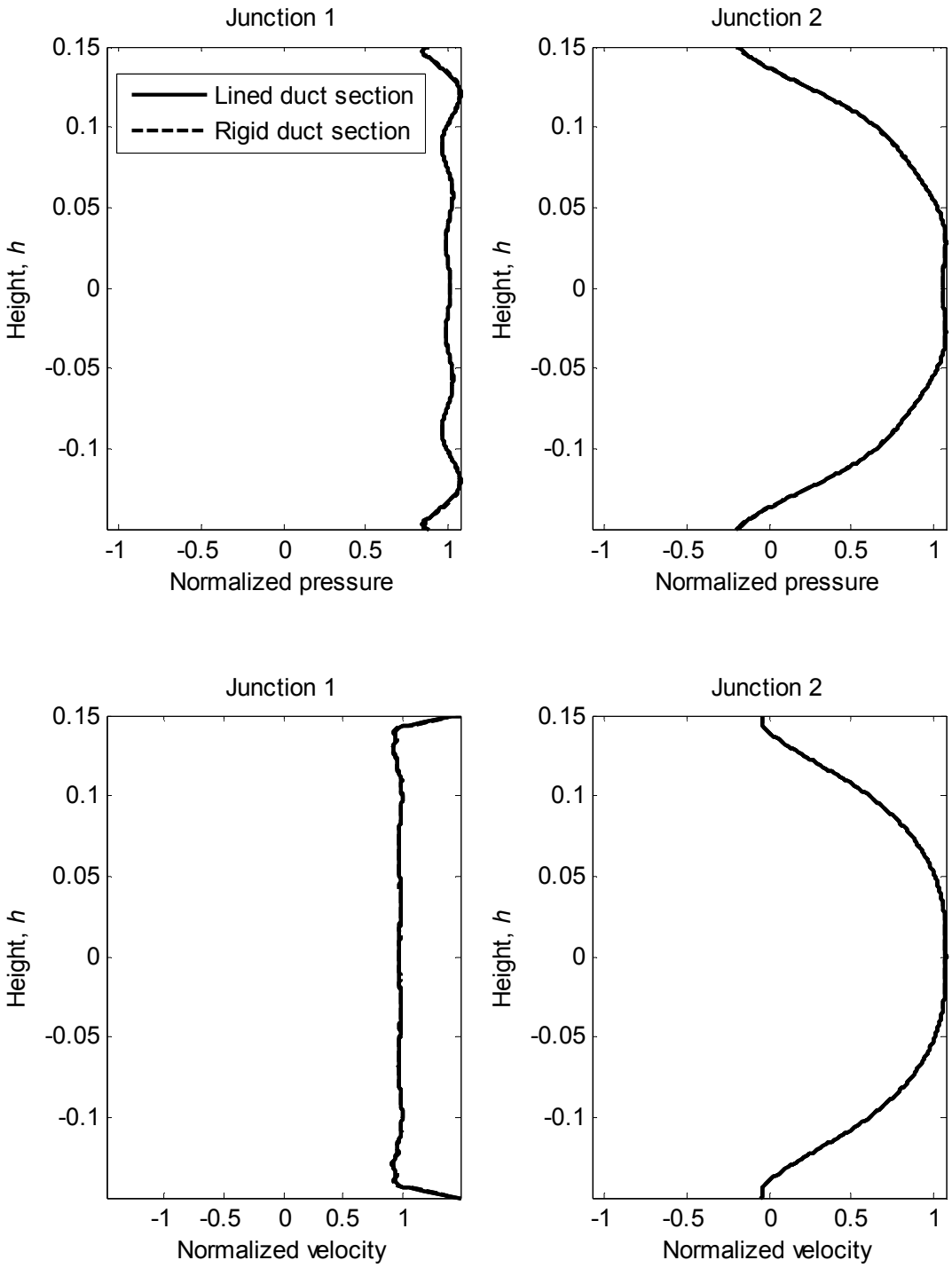

Figure 4.3: The pressure and axial particle velocity at the entrance junction, $x = 0$, and exit junction, $x = L_s$, obtained from the summation of 25 modal contributions, at 5000 Hz. Duct with a locally reacting lining

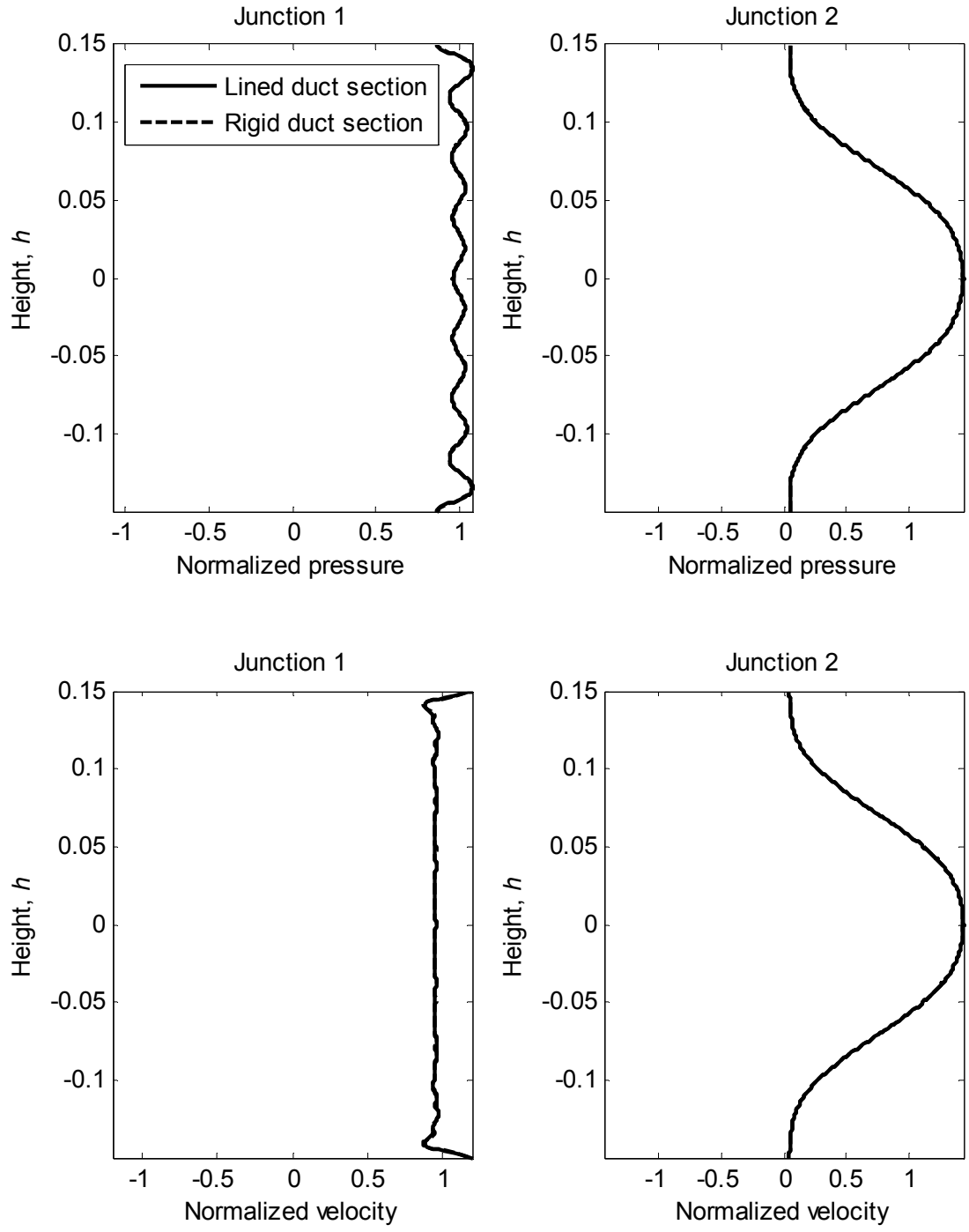

Figure 4.4: The pressure and axial particle velocity at the inlet junction, junction 1, and the outlet junction, junction 2, obtained from the summation of 32 modal contributions, at 8500 Hz. Duct with a locally reacting lining

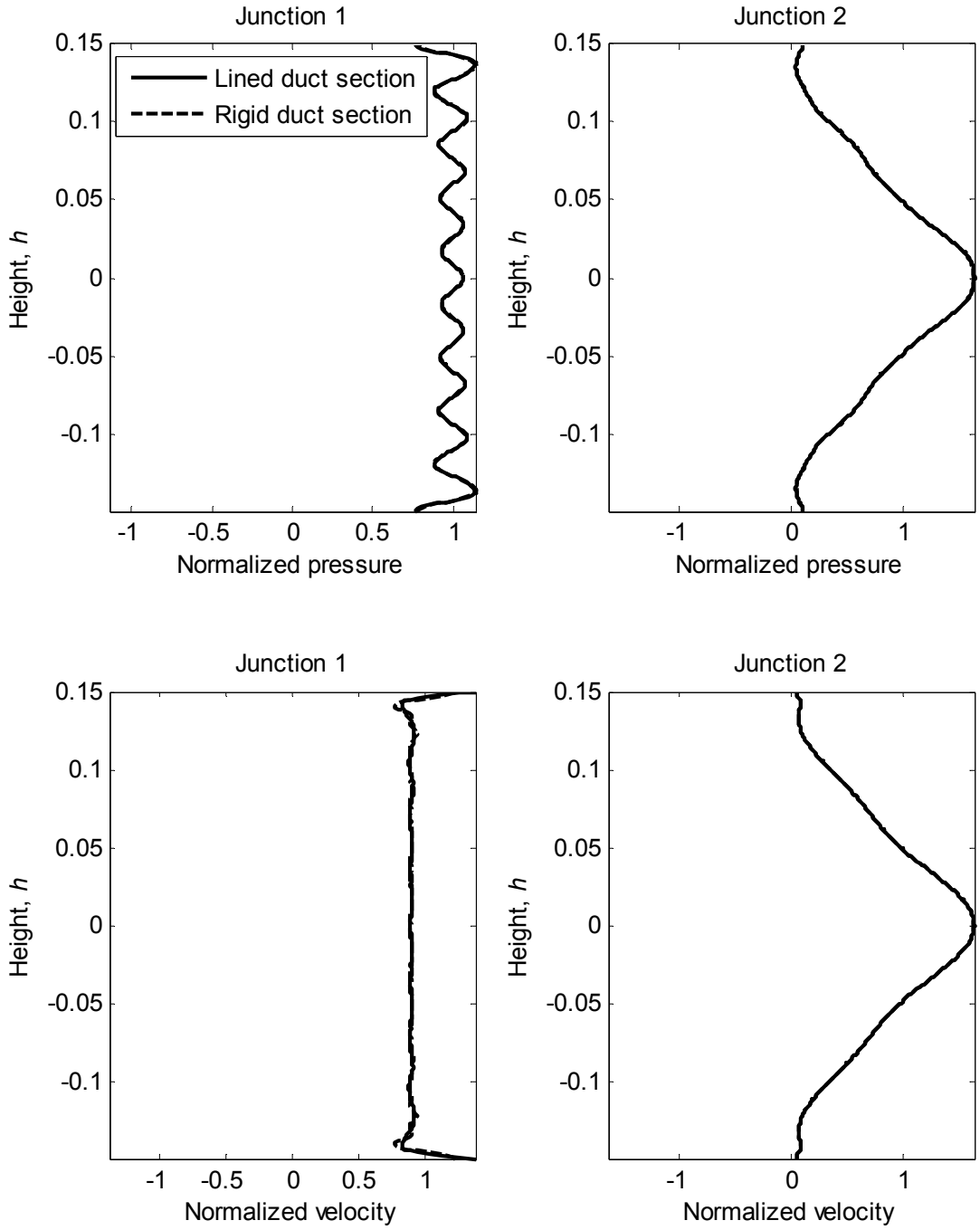

Figure 4.5 The pressure and axial particle velocity at the inlet junction, junction 1, and the outlet junction, junction 2, obtained from the summation of 33 modal contributions, at 9800 Hz. Duct with a locally reacting lining

4.2.2 Number of modes required for a duct with a bulk-reacting lining

The numerical study is repeated for the bulk-reacting lining. Here the number of additional cut-off modes is expected to be higher than for the locally reacting lining due to the existence of lining modes. The wave modes are first re-ordered as described in section 3.3 since the choice of which modes to be included may vary at different frequencies for reasons that have been explained in that section.

Figure 4.6 shows the convergence Δc_p of the transmitted wave amplitudes. As expected the wave amplitudes converge more slowly than for the locally reacting case. With five cut-on modes in the rigid walled duct at 5000 Hz, the transmitted wave amplitudes in Figure 4.6 only reach about 5% of their 'true' value when 30 cut-off modes in the rigid walled duct are included in the mode-matching process. For the lined duct section, there are 44 additional modes including the lining modes. However, this is sufficient to give a good match of the pressure and axial particle velocity at both sides of the two junctions as shown in Figure 4.7. At 8500 Hz, with 8 modes cut-on in the rigid walled duct, a total of 50 modes in the rigid walled duct and 88 in the lined duct is required to give a good match at the junctions as shown in Figure 4.8. Therefore, for a duct with bulk-reacting lining, when five or fewer modes have cut on, at least 30 cut-off modes should be included in the rigid walled duct in the mode matching process. More modes are required for the lined section due to the lining modes. With larger number of modes included in the computation, the simulation, with the same frequency range and frequency steps as in locally reacting case, took around 15 minutes to obtain all wave amplitudes in each duct section.

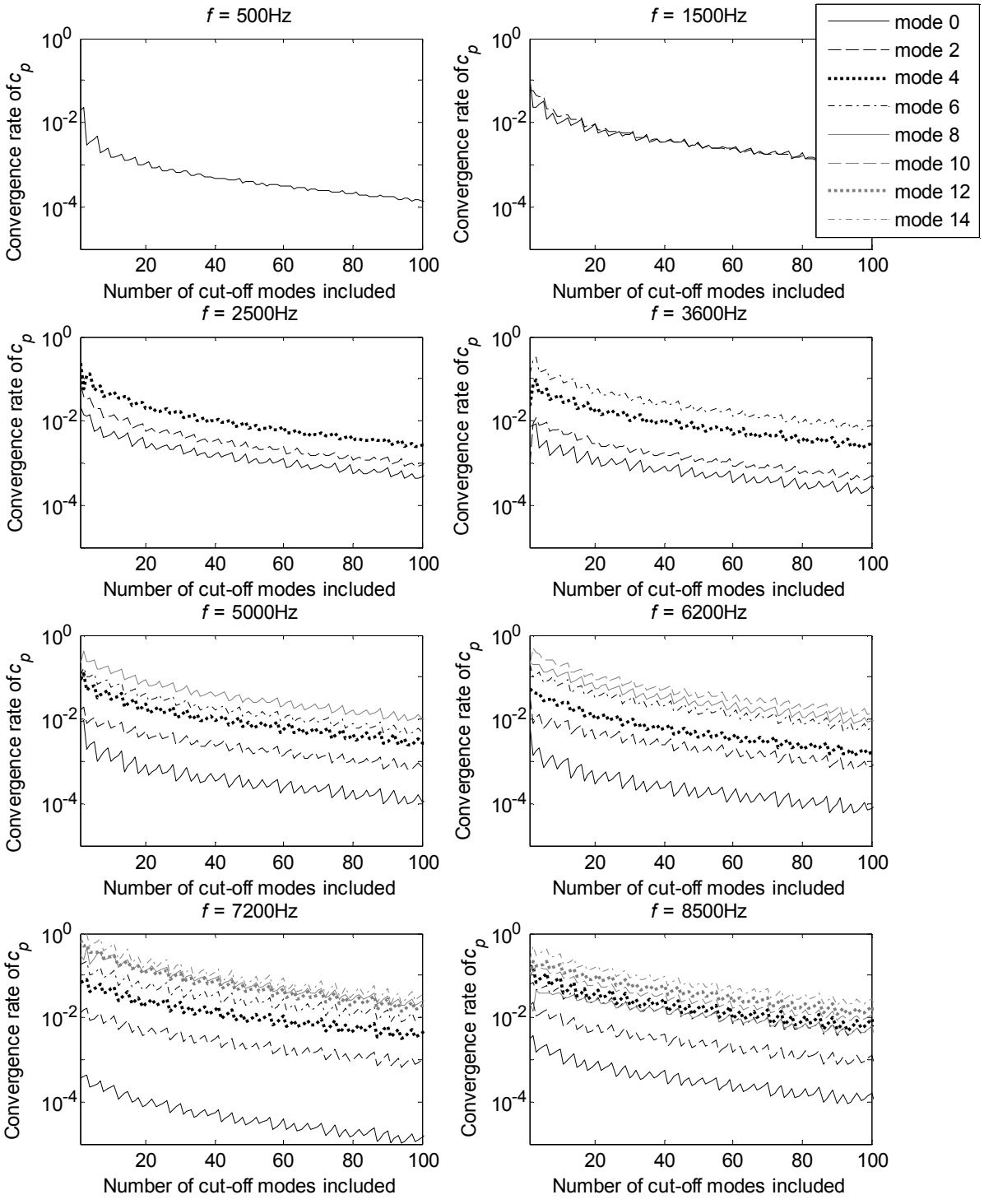

Figure 4.6: Convergence of modal wave amplitudes for the cut-on modes at eight different frequencies for a duct with a bulk-reacting lining

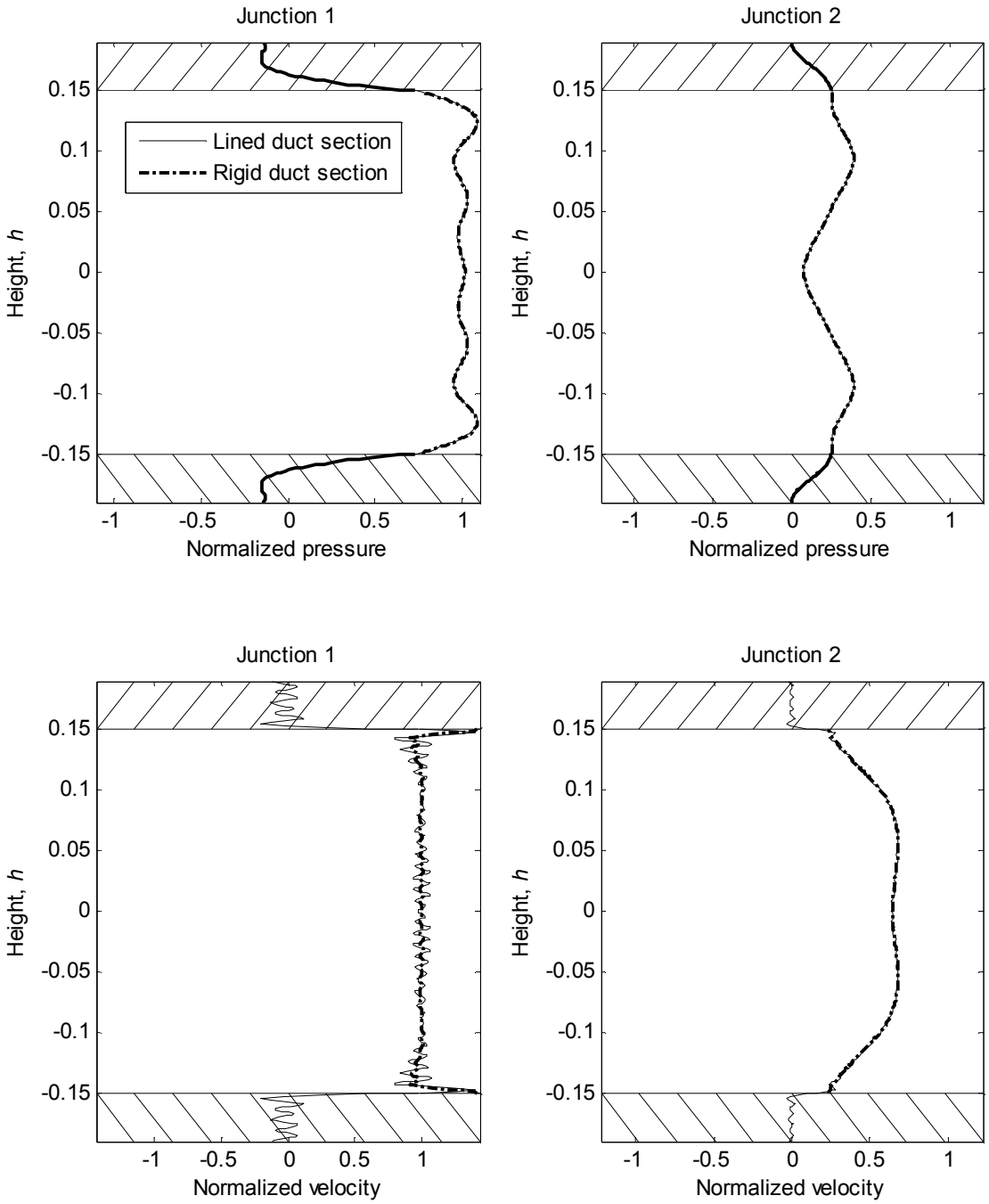

Figure 4.7: The pressure and axial particle velocity at 5000 Hz at the inlet junction, junction 1, and the outlet junction, junction 2, obtained from the summation of 35 modal contributions in the rigid duct and 50 modal contributions in the lined section with a bulk-reacting lining

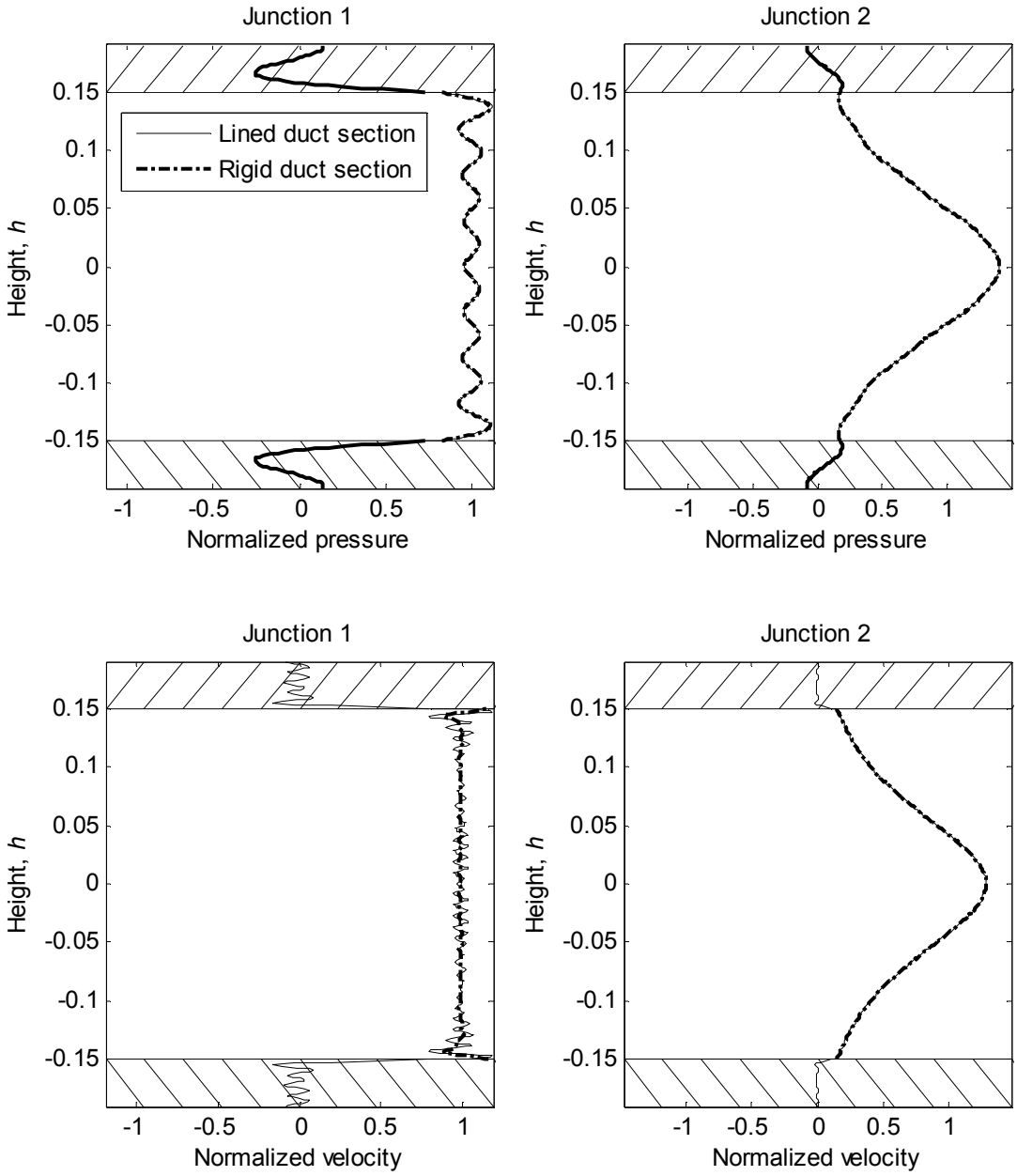

Figure 4.8 The pressure and axial particle velocity at 8500 Hz at the inlet junction, junction 1, and the outlet junction, junction 2, obtained from the summation of 50 modal contributions in the rigid duct and 88 modal contributions in the lined section with a bulk-reacting lining

4.3 Analysis on effect of design parameters on duct attenuation

The performance of a lined duct depends mainly on three parameters, the airway height *h*, the flow resistivity of the porous material used, *r*, and the porous lining thickness, *d*. The effects of these three parameters on lined duct performance are studied separately here using the locally reacting model due to its simplicity. Furthermore, a smaller number of modes are required at high frequency compared to the bulk-reacting model. For the material properties, typical values representative of Melamine foam are selected: $s = 1.0053$, $\varepsilon = 0.993$ and $r = 13000$ rayls/m [105]. Plane wave incidence is assumed throughout.

4.3.1 Effect of length of lined section on duct attenuation

As the length of the lined section increases, more sound energy is attenuated since more absorbing material is available. The effect of varying the length of lined section is studied and it is investigated whether the attenuation increases proportionally to the length of lined section. To generalize the study, the length of lined section is taken as a multiple of the duct height, *h*.

Figure 4.9 shows the transmission loss for a duct with a 300 mm airway height and 100 mm lining thickness but with various lengths of lined section. The transmission loss normalized to a length *h* is plotted against frequency. The upper figure shows the transmission loss across the lined section for lengths less than the duct height. For these short lined sections, there are troughs in the transmission loss at each cut-on frequency of higher order modes. These troughs become less prominent as the length of the lined section increases. The bottom figure shows the normalized transmission loss for $L_s > h$. No trough is found for the longer lined section and the transmission loss is proportional with the length of lined section, i.e. if the length of lined section is doubled, the duct transmission loss is doubled as well. Therefore for a lined section with a length equal to or larger than the duct height, the resulting normalized transmission loss can be expected to be independent of lined section length.

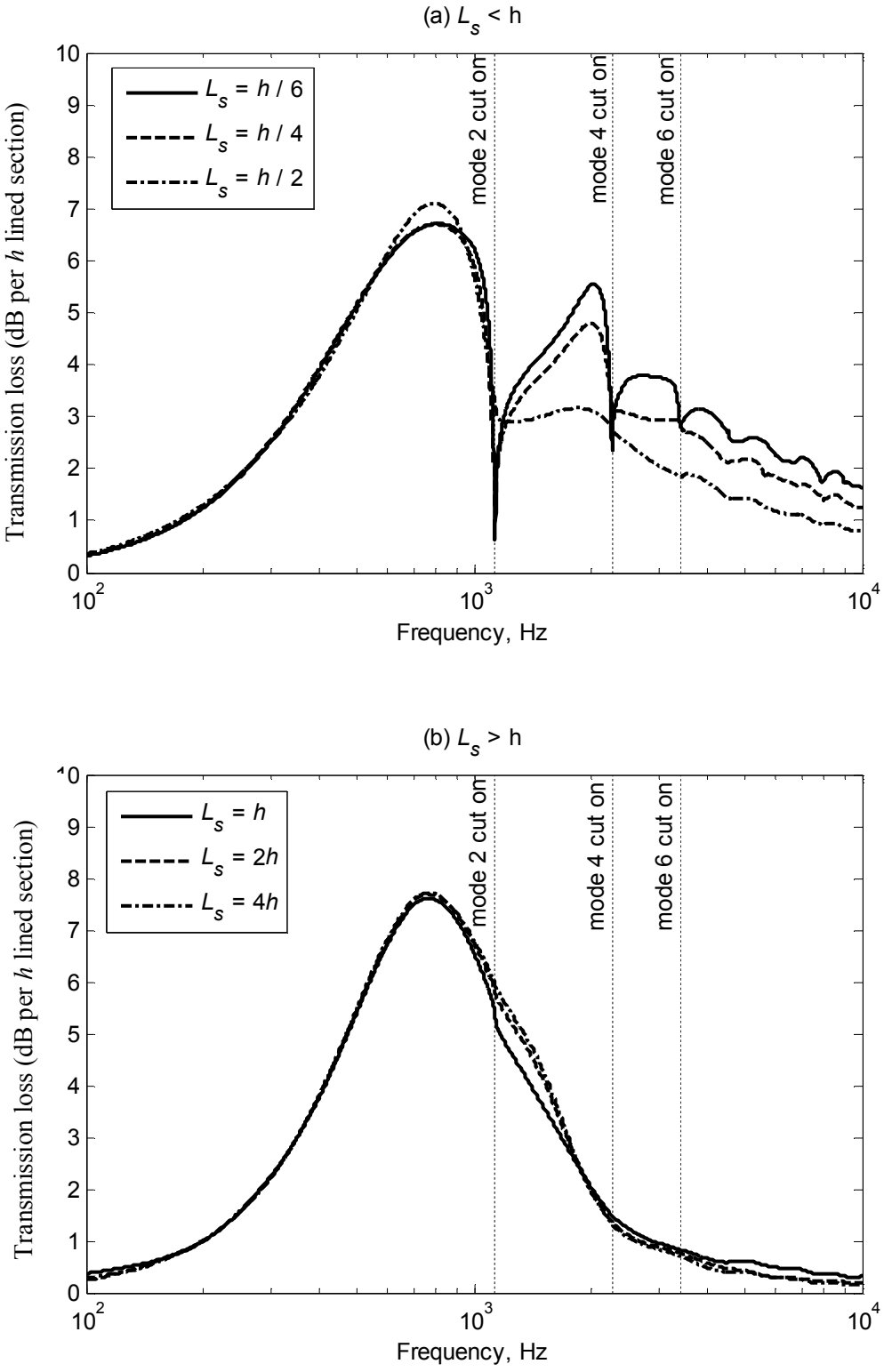

Figure 4.9: Transmission loss for different lengths of lined duct normalized to a length h. h = 300 mm, d = 100 mm and r = 13000 rayls/m

4.3.2 Effect of airway height on duct attenuation

The effect of duct airway height is studied here by keeping other duct parameters constant. The upper and lower walls are lined with 100 mm thick lining. Four different airway heights are considered here: h = 50, 150, 300 and 800 mm which constitute around 20%, 40%, 60% and 80% of the total corresponding area respectively. The transmission loss for a lined section of h is given in Figure 4.10 (a). The vertical dotted lines indicate the first cut-on frequency for each airway height. For all four cases, the maximum attenuation is achieved below the corresponding cut-on frequency.

At very low frequency the transverse wavenumber is close to zero as shown in Figure 4.10 (b), equivalent to the wavenumber in a hard-walled duct. The wall is stiffness-controlled and the wall impedance is very large such that the transverse particle velocity at the duct wall is almost zero and the wave travels as a plane wave. As frequency increases the duct wall softens and the sound attenuation starts to increase. The transverse particle velocity is non-zero and the spatial wave form changes and is no longer a plane wave. As the transverse wavenumber increases, the maximum attenuation is obtained when the real part of the normalized transverse wavenumber $k_y h$ is below 3.

At high enough frequency the acoustic waves in the airway see the wall lining as a pressure release boundary and the acoustic pressure close to the wall is zero. The transverse wavenumbers therefore approach the equivalent wavenumbers in a duct with a pressure release boundary. Consequently the acoustic energy is concentrated at the mid-section of the airway and there is little attenuation due to the lining. Referring to plots of $k_y h$ against $k_0 h$ in Figure 2.5 for example, bigger h means the switch to pressure release boundary occurs at lower k_0. Therefore the attenuation for a duct with a larger airway height is very poor at high frequency, even though the absorption coefficient of the lining is close to 1 at high frequency as shown in Figure 4.10 (c). By reducing the duct height, the pressure release approximation does not apply until a higher frequency and attenuation occurs over a wide frequency region.

In this particular case, the absorption coefficient is shown to oscillate at high frequency and this is reflected in the transmission loss of a duct with the smallest airway height as shown in Figure 4.9 (a). This oscillation is due to the resonances of the transverse waves propagating inside the lining which can occur in a lining with low flow resistivity or sufficiently thin lining thickness. These two factors will be investigated in the following section. Figure 4.11 shows the plot of the surface normal wall impedance. At these high frequencies, the impedance is mostly resistive with small reactance part. The real part of the normalized surface normal impedance Z_n' is oscillating around a value of 1. The incoming transverse acoustic waves have little restriction in

moving from the airway into the wall lining and the acoustic energy is then readily attenuated within the lining.

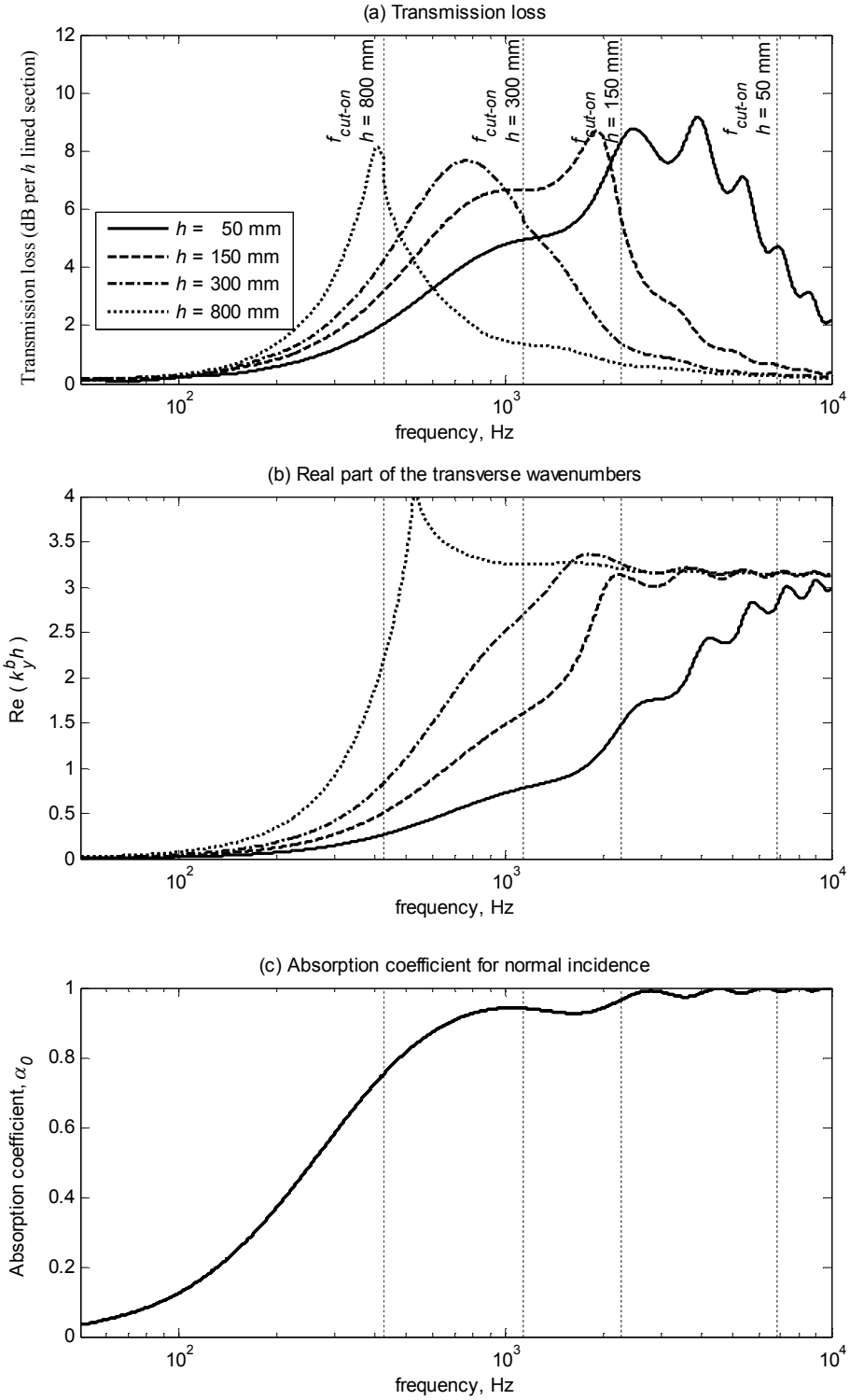

Figure 4.10: (a) Transmission loss normalized to a length h for ducts with four different heights (b) The real part of $k_y h$ for the fundamental mode and (c) The absorption coefficient for 100 mm thick porous material with normal wave incidence

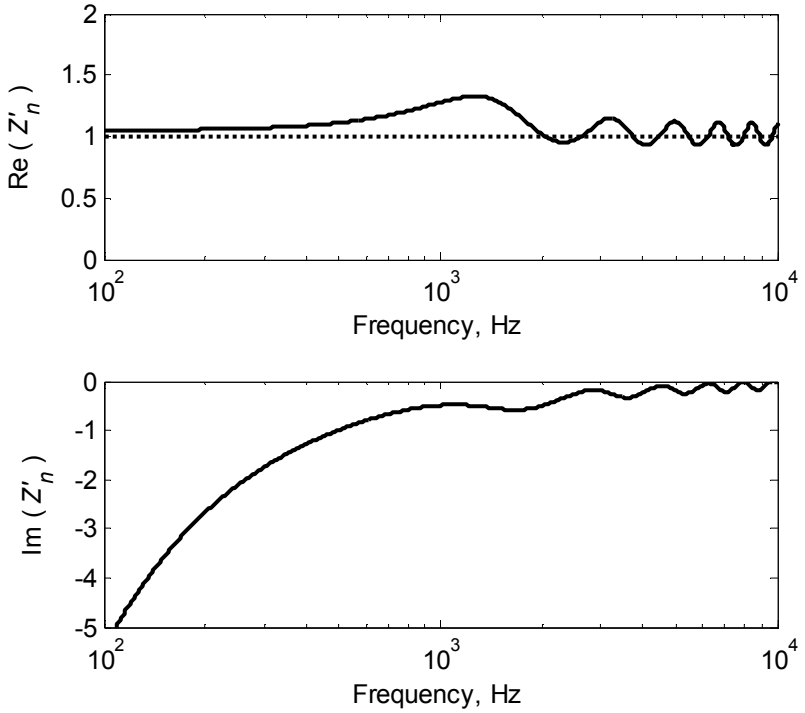

Figure 4.11: Plot of normalized surface normal impedance, Z'_n with s = 1.0053, ε = 0.993 and r = 13000 rayls/m

4.3.3 Effect of flow resistivity on duct attenuation

The flow resistivity is a characteristic of the material. At very low frequency, the imaginary part of the surface normal impedance is independent of flow resistivity and is controlled by the air stiffness inside the material while the real part of the non-dimensional impedance can be given approximately by $R/3$ [26] where R is the normalized flow resistivity given in equation (3.26). At high frequency, the surface normal impedance is mostly resistive and approaches the characteristic impedance of air. An in-depth discussion on the influence of flow resistivity can be found in [106, 107] and a design chart has been provided by Bies and Hansen [107] where they suggest that optimum attenuation in a duct with an airway height of h is achieved when the duct height parameter h/λ lies between 0.2 and 1.6 depending upon the percentage of airway area in the duct and the flow resistivity of the lining material.

In this section, the airway height and the lining thickness are held constant at h = 300 mm and d = 100 mm, so that the airway area is 60% of the total corresponding area. The normalized flow resistivity R is varied by varying only the flow resistivity r. Three values of r are used: r = 4200, 13000 and 21000 rayls/m, that correspond to R = 1, 3 and 5. The calculations are repeated for a narrower duct with h = 150 mm for the same value of d that gives a percentage airway area of

40%. The transmission loss for a duct length h is shown in Figure 4.12 for the two different values of h . The real and imaginary parts of the wall surface normal impedance are shown in Figure 4.13 (a) and (b) respectively and (c) shows the normal incidence absorption coefficient for all three values of r. At low frequency, the wall impedance is dominated by air stiffness and Z'_n has a large imaginary component. At high frequency, $Z'_n \to 1$ indicating that the wall impedance tends to the impedance of air. However for a lining with a low flow resistivity, especially r = 4200 rayls/m, resonances occur in the lining at high frequency and the impedance value oscillates.

The peaks in the oscillation occur when the liner thickness is close to an odd number of quarter wavelengths. The resonance effect can also be seen in the plotted transmission loss where there are peaks in the transmission loss for a lining with a low flow resistivity with a particularly strong peak at 600-800 Hz. However, a low flow resistivity gives a lower attenuation at low frequency. Higher flow resistivity tends to improve the attenuation of a lined duct at medium to high frequency, as also found in [92]. Furthermore, the frequency band where the liner is effective is narrower for low flow resistivity even though the peak attenuation is high.

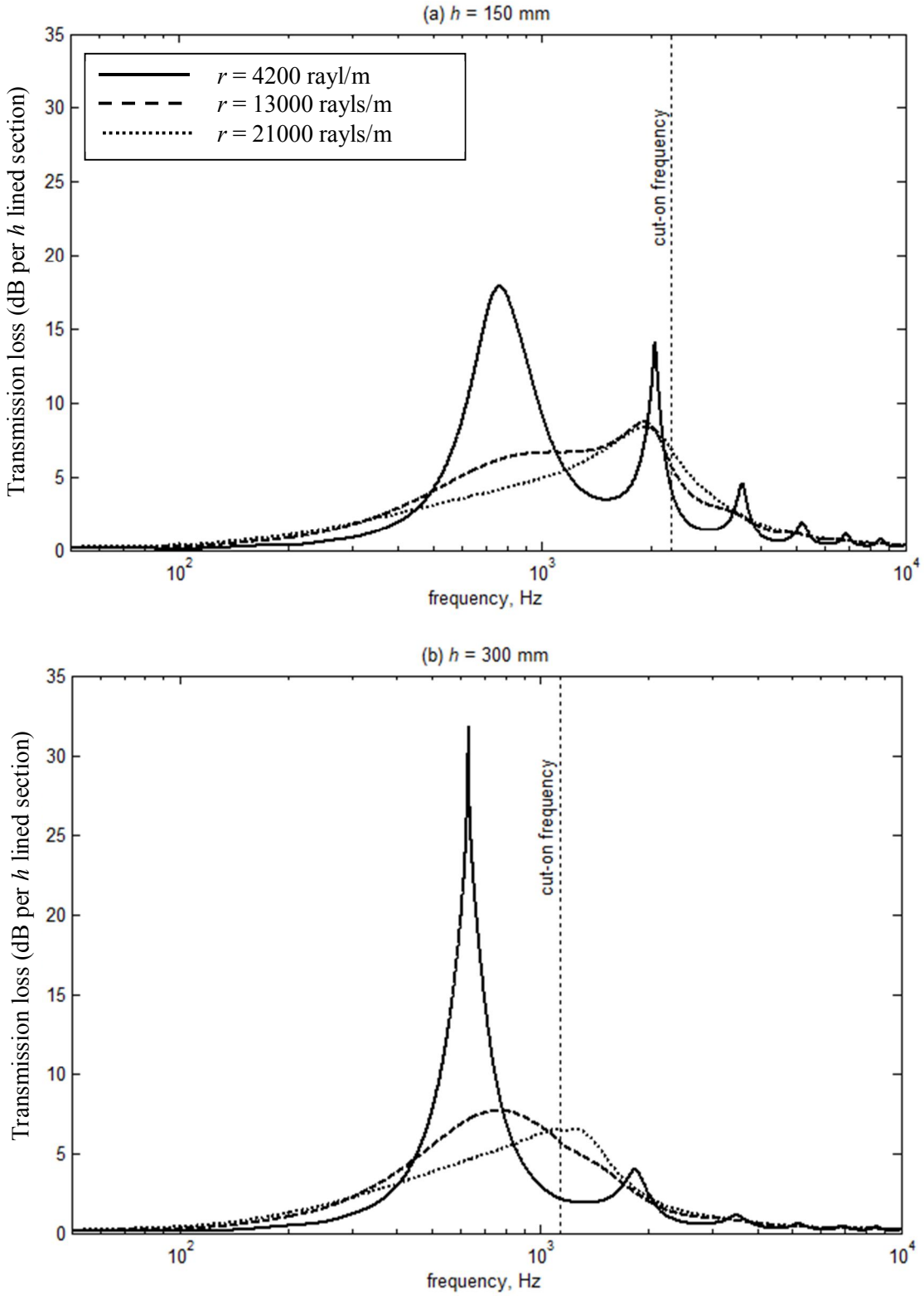

Figure 4.12: The transmission loss normalized to a length h for different values of flow resistivity for (a) h = 150 mm and (b) h = 300 mm

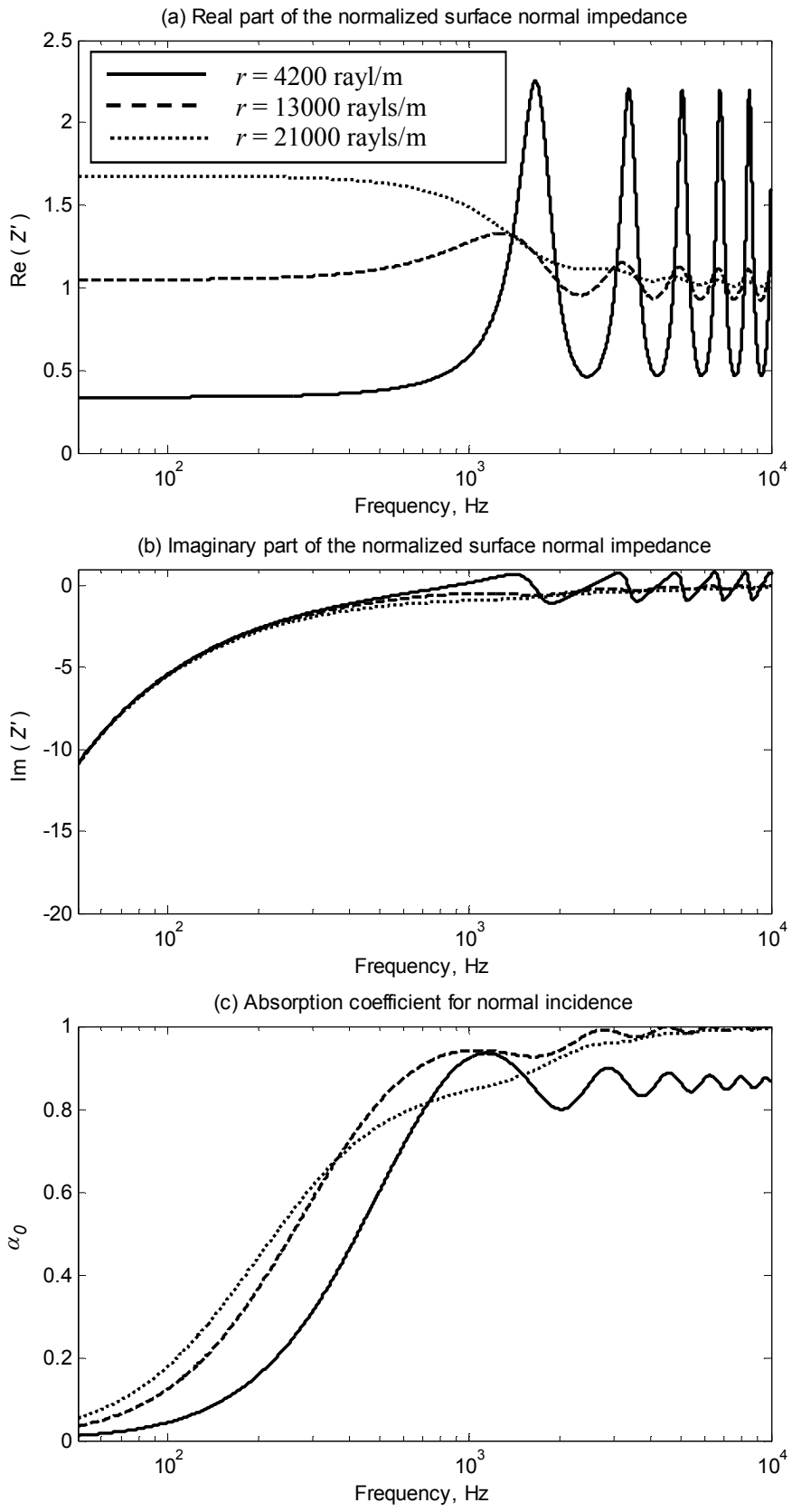

Figure 4.13: The surface normal impedance and the absorption coefficient for three different values of r with lining thickness d = 100 mm

4.3.4 Effect of lining thickness on duct attenuation

When the porous material is backed by a rigid wall, a wave travelling within the material is reflected at the wall and travels back towards the outer surface. To ensure that the reflected waves return to the surface with negligible amplitude it is necessary to have a sufficiently thick liner. However an incident sound wave in effect can penetrate into the material only to a certain depth which is called the penetration depth. This penetration depth depends on wavelength and flow resistance and to some extent on the angle of incidence. Beyond the penetration depth, the absorption of a porous layer does not change noticeably with added thickness.

The penetration depth, d_p is given by [26]:

$$d_p = \frac{1}{\mathrm{Im}\left(\tilde{k}_y\right)}$$

where $\tilde{k}_y = \tilde{k}\sin\phi$, ϕ is the incident angle, and $\tilde{k}$ is the wavenumber in the lining. After a wave travels this distance at the respective frequency, the sound pressure amplitude is reduced by a factor of 1/*e*. Figure 4.14 shows the penetration depth against a normalized frequency, Ω where $\Omega = \omega\rho_0 s/r\varepsilon$ and the depth is normalized by the acoustic wavelength in the free field.

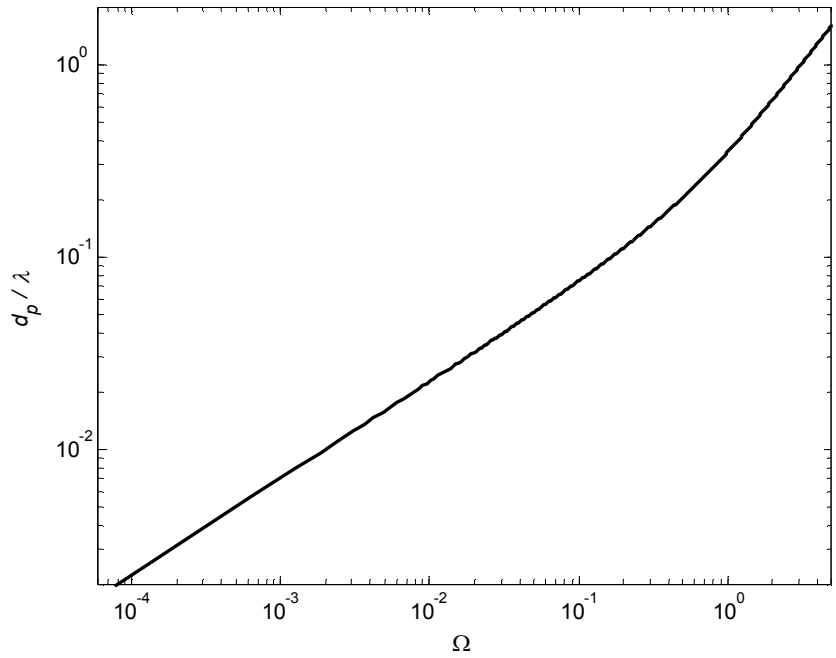

Figure 4.14: Penetration depth of a sound wave at normal incidence into a porous material.

Figure 4.15 (a) shows the absorption coefficient of a porous material with three different thicknesses and the flow resistivity r = 13000 rayls/m. The normalized flow resistivities, as introduced in section 3.4 where $R = rd/\rho_0 c_0$, for thicknesses d = 30, 100 and 160 mm, $R \simeq 1, 3$ and 5 respectively. The normalized frequency given in Figure 4.14 is around 0.6 at around 1 kHz. The penetration depth is then about 0.23 wavelengths which is approximately 78 mm. At the highest frequency in Figure 4.15, 10 kHz, the normalized frequency $\Omega \approx 5.95$ and the corresponding d_p is 1.9λ (i.e. 64.7 mm). This explains why the absorption coefficient in Figure 4.15 (a) for a 30 mm thick lining is lower than for the 100 mm and 160 mm thick liners at all frequencies.

At frequencies above 1 kHz, the absorption coefficients for the 100 mm and 160 mm thick liners do not differ much since the lining thickness for both exceeds the penetration depth. Apart from providing sufficient thickness for the liner to absorb the sound waves propagating inside the material, increasing the liner thickness reduces the lining resonance frequencies. Furthermore, at low frequency the absorption limitation due to the stiffness reactance of air in the material is reduced. This can be seen in the plot as the absorption of the thicker liner is much better at low frequency.

Figure 4.15 (b) shows the absorption coefficient for a porous material with a higher flow resistivity r = 21000 rayls/m for the same lining thicknesses. Comparing these two figures, the resonance frequencies are at similar frequencies but at high frequency the resonance effect is more pronounced for the lower flow resistivity. At 1 kHz $(\Omega = 0.37)$ the penetration depth is about 56 mm and at the highest frequency it is 40 mm. From Figure 4.15 (b) it can be seen that above 1 kHz the absorption coefficients for d = 100 and 160 mm are similar but again it is lower for the 30 mm thick lining, which is thinner than the penetration depth.

Figure 4.16 shows the transmission loss for the considered duct configuration. For both values of r considered, the 30 mm thick liner has the narrowest band of high attenuation. A very poor attenuation is achieved in the low frequency region. The large stiffness reactance of the air inside the material is dominating the wall impedance in this frequency region and the sound waves are mostly reflected back at the wall surface.

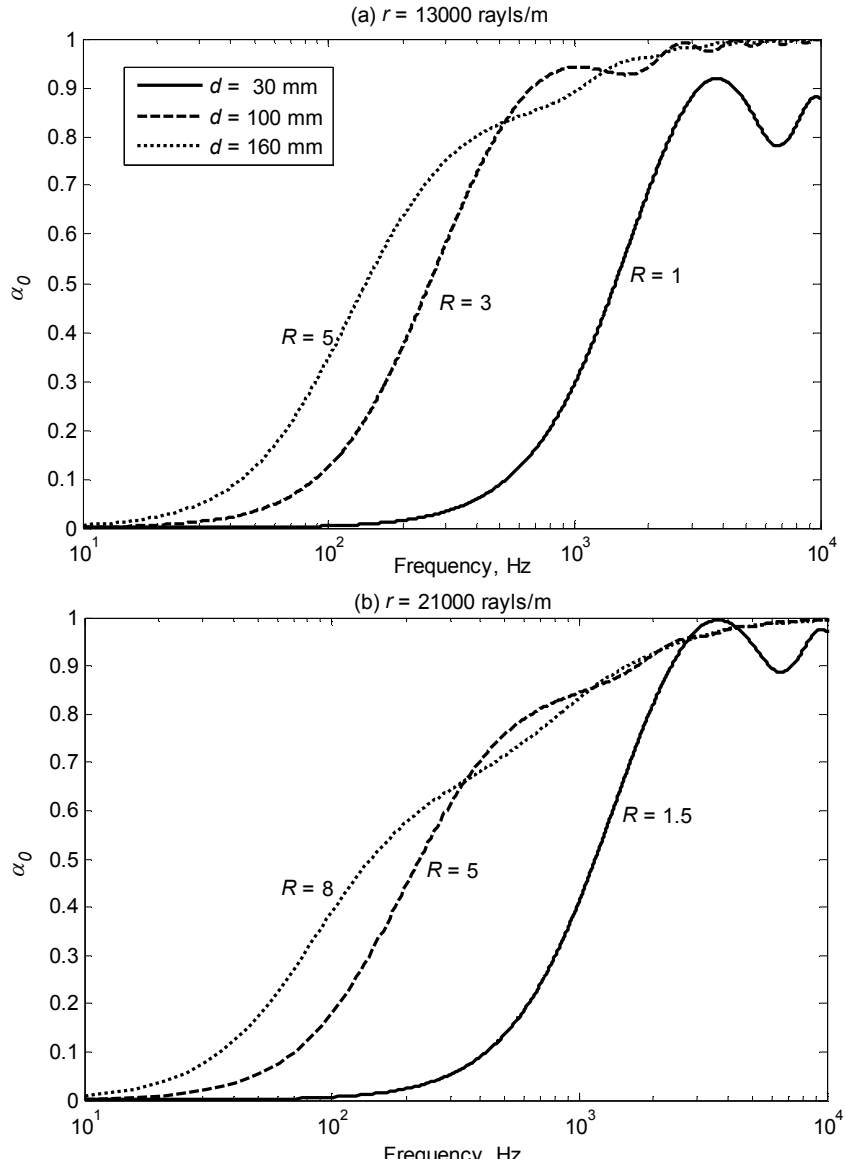

Figure 4.15: Absorption coefficient for normal wave incidence for a porous material with (a) r = 13000 rayls/m and (b) r = 21000 rayls/m with three different lining thickness.

At lower frequency where the attenuation is due to the fundamental mode, the region where the wall lining attenuates sound energy correspond to fundamental mode transverse wavenumbers between $0 < k_y^b h < 3$ as mentioned in section 4.3.2. The bandwidth of the attenuation peak for the 30 mm thick liner in Figure 4.16 is narrow since at low frequency the absorption coefficient is small. The frequency at which peak attenuation occurs is determined by the airway height but the attenuation rate depends on the effectiveness of the lining as indicated by the absorption coefficient value. At high frequency, the transverse wavenumber shown in Figure 4.17 is approaching that expected from a pressure release boundary at almost the same frequency for all three lining thicknesses. The attenuation rate deteriorates and the transmission loss for the 30 mm thick liner is smaller since the thickness is less than the penetration depth.

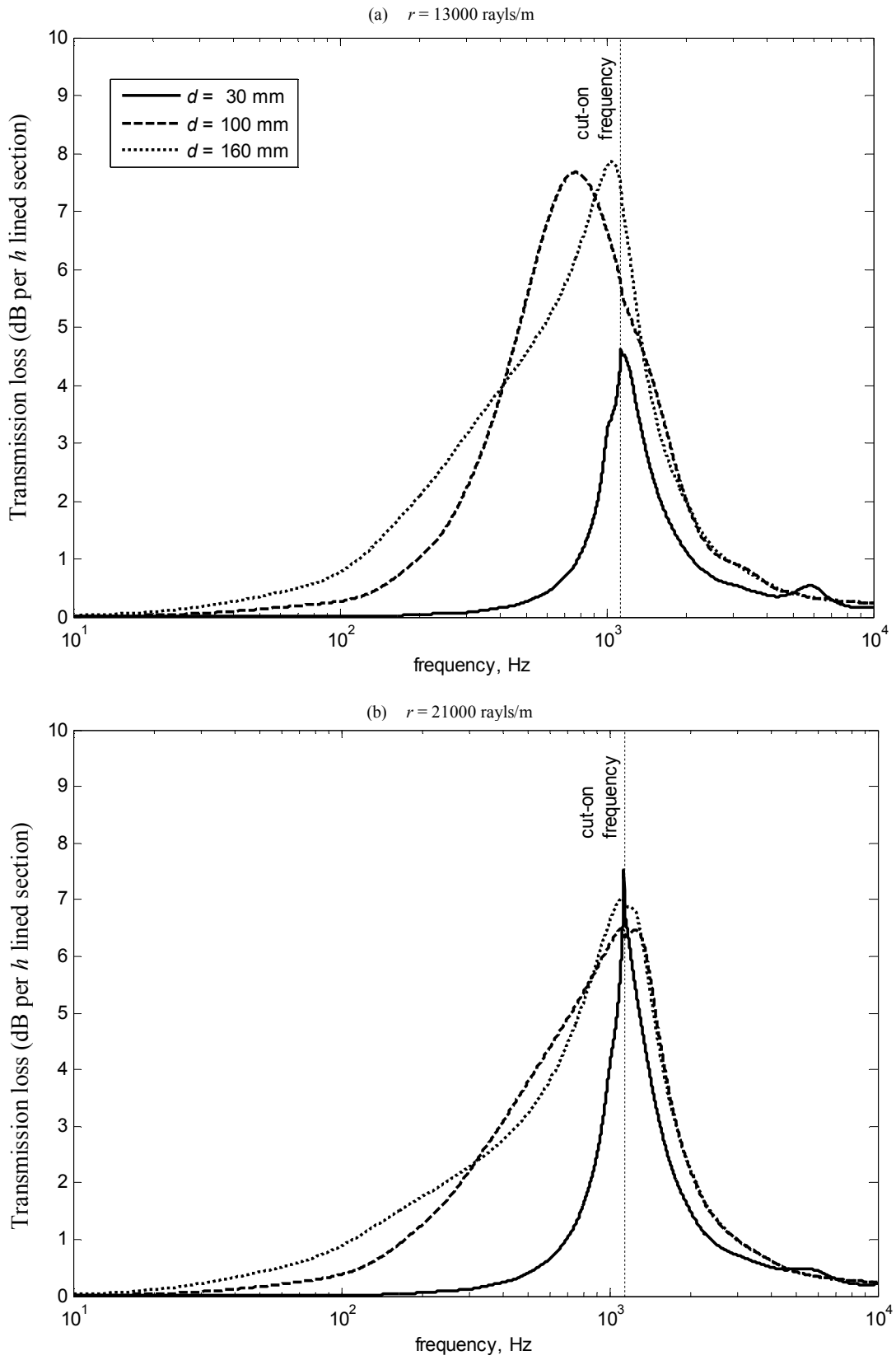

Figure 4.16: Transmission loss normalized to a length h for two values of flow resistivity with three different lining thicknesses. h = 300 mm.

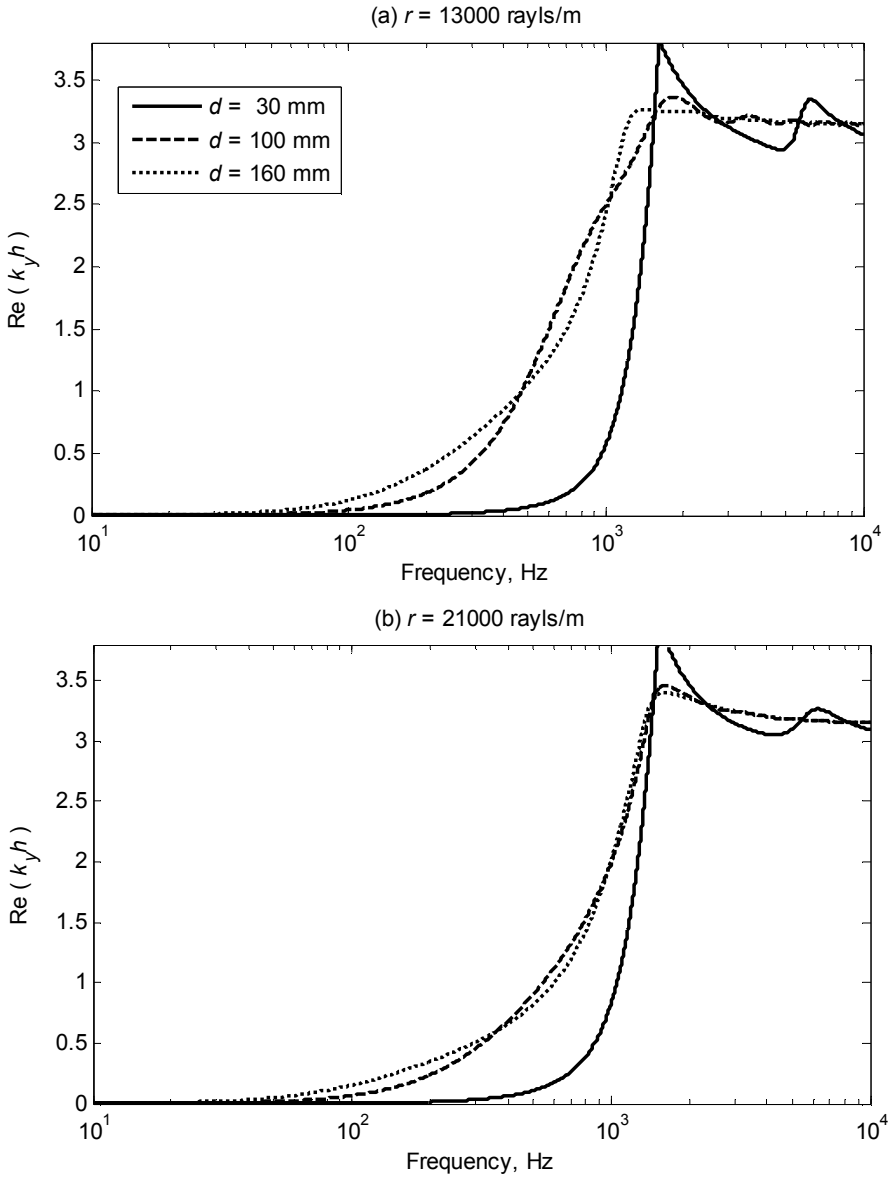

Figure 4.17: The real part of the transverse wavenumbers for the same airway height but different lining thicknesses.

4.4 Comparison of the predicted lined duct performance between locally reacting and bulk-reacting models

Figure 4.18 shows a comparison of the transmission loss predicted with locally reacting theory and bulk-reacting theory. The peak attenuation for the bulk-reacting material is lower than for the locally reacting material and it occurs at a higher frequency. The dotted line represents the cut-on frequency of the second mode. For both cases, peak attenuation is achieved below this frequency and the attenuation continues to drop beyond this frequency.

For the locally reacting lining, the surface normal impedance does not depend on the angle of incidence. This is due to the nature of local reaction where the particle velocity generated by the incident sound at any point on the surface of an absorbing material is linearly related to the local sound pressure. For a bulk-reacting material, the surface normal impedance depends not only on local pressure but its value elsewhere. Thus a proper model of bulk-reacting surface impedance requires information on the entire wave field inside the medium.

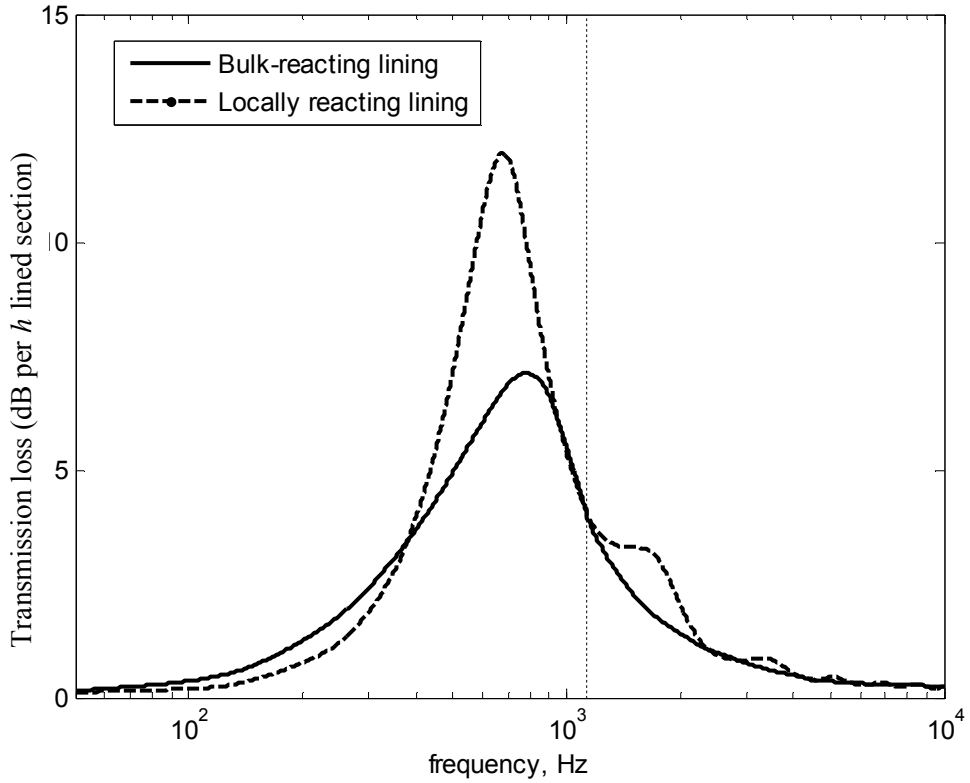

Figure 4.18: Transmission loss for locally and bulk-reacting lining with liner thickness of 50 mm and duct height is 200 mm. The flow resistivity r = 13000 rayls/m.

Figure 4.19 shows the surface normal impedance for a rigidly backed absorbent with a thickness of 50 mm for oblique sound incidence. The surface normal impedance for normal wave incidence is represented by the red lines and that for grazing wave incidence by the blue lines. The flow resistivity is 13000 rayls/m corresponding to R = 1.5. Consider the one-dimensional wave propagation discussed in section 3.1. The wavenumber equation given by equation (3.15) can be manipulated into a recognized form of surface impedance [30]:

$$Z_n^{'} = -iZ_c^{'}\frac{\tilde{k}}{\tilde{k}_y}\cot\left(\tilde{k}_y d\right) \tag{4.45}$$

From the wavenumber relationship, $\tilde{k}_y = \sqrt{\tilde{k}^2 - \tilde{k}_x}$ and $\tilde{k}_x = k_x$, $\tilde{k}_y$ in (4.45) can be replaced with $k_x = k_0 \sin\phi$ to give:

$$Z_n^{'} = -iZ_c^{'} \frac{\tilde{k}}{\sqrt{\tilde{k}^2 - {k_0}^2 \sin\phi}} \cot\left(\left(\sqrt{\tilde{k}^2 - {k_0}^2 \sin\phi}\right) d\right) \tag{4.46}$$

At low frequency, incident angle has little effect on the surface impedance. The air stiffness reactance inside the medium dominates the impedance as shown in the lower plot of Figure 4.19. From mid to higher frequency the surface normal impedance depends more strongly on the incident angle. For small incident angle, $\phi \leq 20°$, the surface impedance is close to the normal incidence surface impedance.

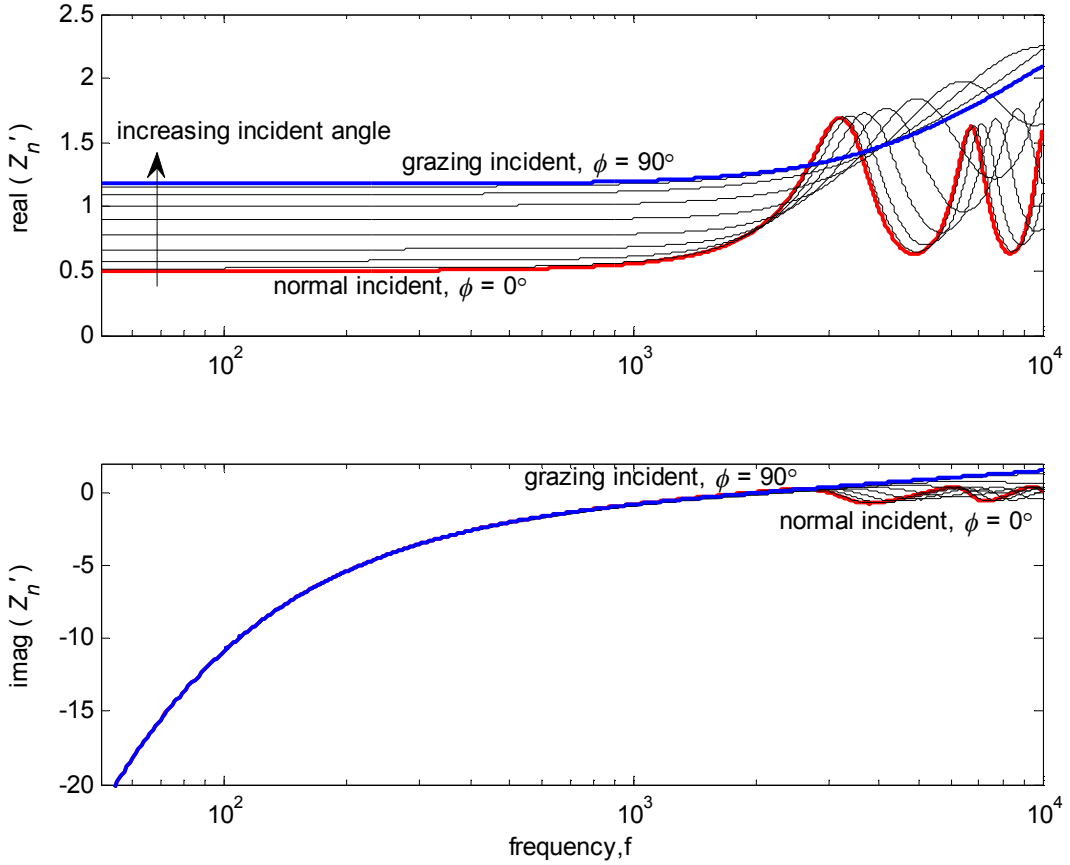

Figure 4.19: Surface normal impedance for bulk-reacting material of thickness 50 mm and r = 13000 rayls/m for oblique wave incidence.

This dependence on angle of incidence means that the surface impedance encountered by the sound wave in the bulk-reacting model is different from the surface impedance used in the

locally reacting theory. This affects the absorption coefficient of the lining material even though the same material properties are used to define the absorptive material at the beginning of the analysis.

The comparison of attenuation between a duct with a bulk-reacting lining and a locally reacting lining is repeated for a thinner lining thickness of 15 mm, and the result is shown in Figure 4.20. For this case of duct lining thickness, the predicted attenuation from the locally reacting model is lower than that predicted with the bulk-reacting model at all frequencies. The same observation is shown for a different duct airway height, h = 500 mm, in Figure 4.21. Therefore, in these cases of a duct with a thinner duct lining relative to the airway height, the predicted attenuation from the locally reacting model is lower than the prediction from the bulk-reacting model. Since the bulk-reacting model takes into account the wave propagation in the lining, it is more accurate to describe the wave propagation in a lined duct and the predicted attenuation should be closer to the actual duct performance, which will be quantified in experimental work presented in Chapter 6.

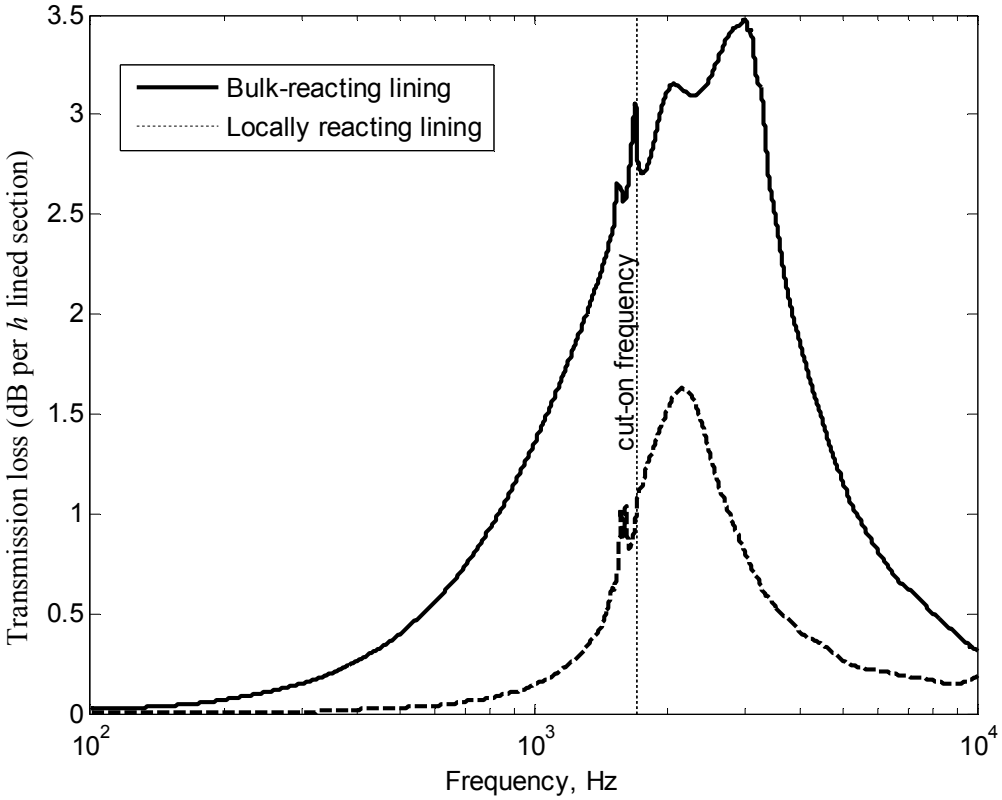

Figure 4.20: Transmission loss for locally and bulk-reacting lining with liner thickness of 15 mm and duct height is 200 mm. The flow resistivity $r \approx 13000$ rayls/m.

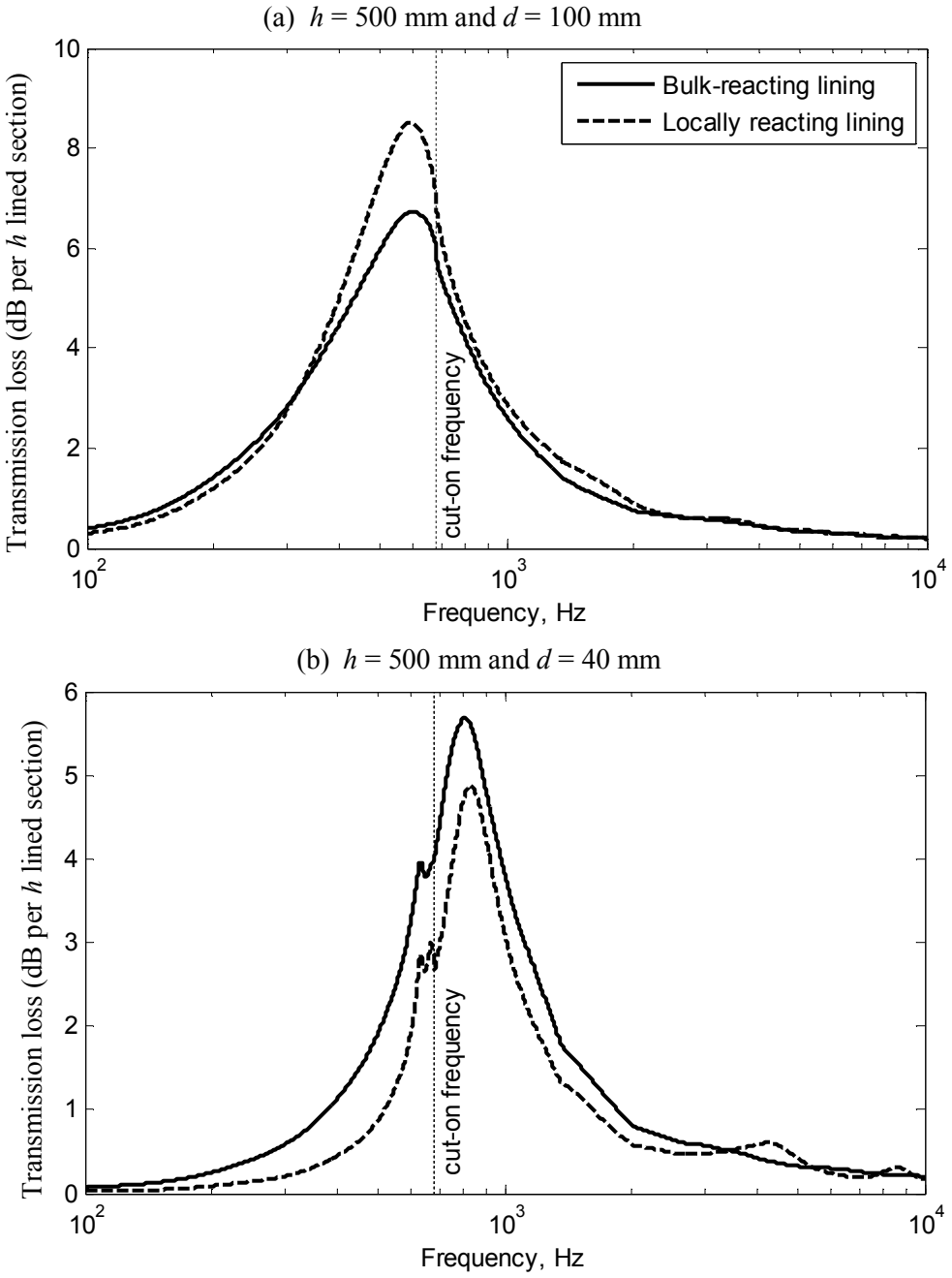

Figure 4.21: Comparison of predicted attenuation with the locally reacting and bulk-reacting model for a duct height of 500 mm and lining thickness of (a) 100 mm and (b) 40 mm. The flow resistivity $r \approx 13000$ rayls/m.

4.5 Conclusions

In this chapter, an analytical model for wave propagation in an infinite duct with a finite lined insert has been presented. The analytical model was derived from a mode-matching technique that matches the pressure and axial particle velocity at each cross-section with an impedance discontinuity. The model has been derived for both locally reacting and bulk-reacting materials.

Both flow resistivity and lining thickness affect the absorption of the lining. The influence of lining thickness is limited by the penetration depth, beyond which the absorption coefficient for the material will be approximately the same with added thickness. The ideal thickness should be sufficient to attenuate most of the reflected wave at the rigid backing before it reaches the outer surface again. A thicker liner will have resonance effects at a much lower frequency compared to a thinner one. Furthermore, the attenuation of a thicker liner at low frequency is better since the stiffness reactance of the air inside the porous medium can be reduced. The resonance in the lining is more pronounced when the lining flow resistivity is low. However a lining with low flow resistivity is poor at low frequency. The peak attenuation is high for low flow resistivity but narrow in frequency band.

A locally reacting model restricts the wave propagation in the lining to the direction perpendicular to the duct axis. Thus the surface impedance only relies on the local pressure and is not affected by the angle of sound incidence. This is not the case in a bulk-reacting model where the surface impedance changes with incident angle. The surface normal impedance used to obtain the properties of sound waves in the locally reacting duct may not be the same as the surface normal impedance in a bulk-reacting duct even though the same material properties are used to define the material. Thus the transmission loss predicted for an acoustic duct for the same duct geometry and same lining properties will be different for locally reacting and bulk-reacting models. Furthermore wave transmission within the lining is permitted in bulk-reacting model that further contribute to duct attenuation.

From the comparison of the duct attenuation between a duct with a bulk-reacting lining and with a locally reacting lining, the locally reacting lining overestimates the peak attenuation when the lining thickness is thick relative to the duct airway height, but this is not always the case at other frequencies. However, when the lining is thin relative to the airway height, the prediction based on a locally reacting lining is lower than that with a bulk-reacting lining at almost all frequencies. Since the bulk-reacting model takes into account the wave propagation in the lining and the differences in the impedance, it is expected that the bulk-reacting model is more accurate to model the sound propagation in a duct with a bulk-reacting lining.

5. Wave propagation through a periodically lined duct

In this chapter, following the mode-matching technique introduced in Chapter 4, the developed analytical model is extended to accommodate a multi-segmented liner, for both locally reacting and bulk-reacting linings. It is advantageous for the design of silencers to have a procedure that allows description of the sound field in ducts, with sections of different cross section and/or acoustic impedance on its internal surface. This can make the study of a multi-segmented duct (or periodically lined duct) accessible and the possibility of improving duct performance through this design can be explored. A duct with varying cross-section and/or acoustic impedance of its internal surface can be represented by a series of small duct sections. By solving the eigenvalue problems in each individual duct section a set of orthogonal modes is obtained. The amplitudes corresponding to each mode can then be obtained from the boundary conditions in terms of pressure and velocity at each junction using the mode matching technique.

Previous studies of multi-segmented lined ducts were motivated by the necessity to produce a fairly broad-band attenuation spectrum with a lined duct in a turbofan engine. The analytical approach was first presented by Lansing and Zorumski [25] for an axially segmented circular duct where the result indicated that multi-section liners have a potential for increased noise reduction. The transmission loss can be expected to increase as a result of multiple reflections and as the wall impedance in two lined sections become more dissimilar. However, an optimization study of an axially segmented liner conducted by Law *et al.* shows that an axially segmented design could only provide a small improvement over an optimised uniform liner [108]. Other studies on liner impedance discontinuities [109-111] state that the advantage of having an axially segmented liner to obtain extra bandwidth of attenuation is mainly due to the beneficial modal energy redistribution at the wall discontinuities. Apart from the axially segmented liner, other multi-segmented liner designs that have been considered are circumferentially segmented liners and checkerboard liners [112]. A checkerboard liner offers the best means of increasing the attenuation over and above that of a uniform lined duct [113] and a problem formulation and solution methodology for a periodic checkerboard liner is presented by Robinson and Watson [84].

The periodic liner arrangement has also been proposed for ventilation ducts [12] where the liner is separated into several sections by a short unlined duct section. All the studies on multi-segmented liners in the field of turbofan engines assume a locally reacting lining whereas in

ventilation ducts, this can no longer be assumed and a bulk-reacting lining should be considered. An analytical model for a multi-segmented bulk-reacting lining is yet to be found in the literature and this is addressed in this chapter. In the present work each segment is treated as identical so that the resulting system is periodic although the method is not limited to this case. The effect of periodicity on the attenuation with a locally-reacting lining and a bulk-reacting lining is compared. Further investigation is carried out to study the effect of other parameters on duct attenuation such as the number of liner segments, the length of unlined and lined duct segments, and the liner thickness.

5.1 Mode-matching model

Consider a periodically lined duct as shown in Figure 5.1. The arrangement is built up of N_s identical single sections as in Figure 4.1. The length of each lined section is L_s and the distance between adjacent lined sections is L_h, with this section having rigid walls. The inlet and outlet ducts are assumed to have rigid walls that extend to $-\infty$ and $+\infty$ with anechoic terminations. The wall linings in each section are of the same material with the same thicknesses. The wave propagation in any section N is shown in Figure 5.2. Note that $a^{\pm}_{m,N+1} = c^{\pm}_{m,N}$.

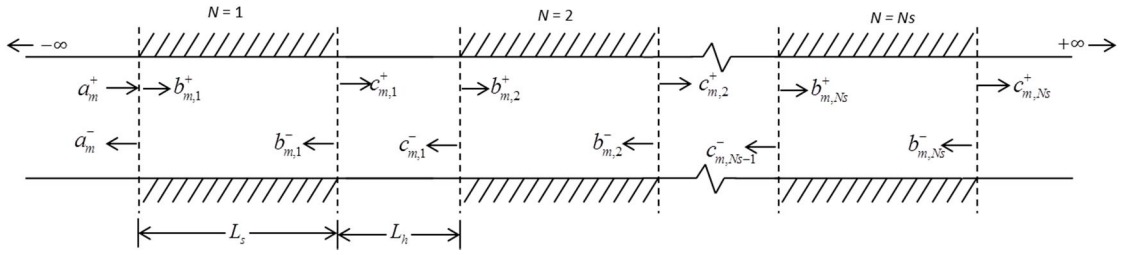

Figure 5.1: A periodically lined duct with N_s inserts

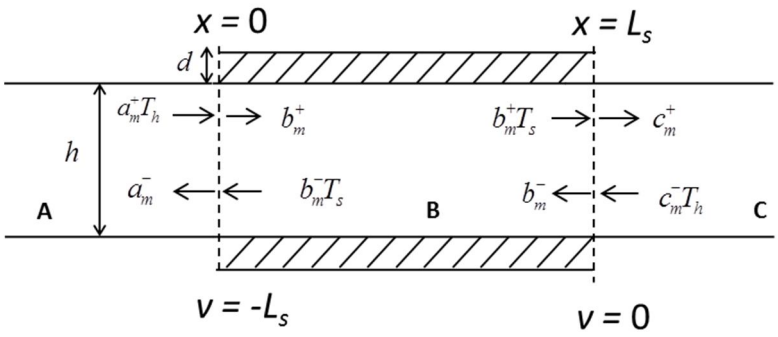

Figure 5.2: The N^{th} single unit insert

5.1.1 Locally reacting liner

For a locally reacting liner, the pressure and axial particle velocity in regions *A* and *B* are as given by equations (4.1) and (4.2). In region *C*, a negative coming wave c^- is the result of the reflection from c^+ at the neighbouring junction. The pressure and axial particle velocity in region *C* are given by:

$$\begin{aligned} p^c &= \sum_{m=0}^{M} \Phi_m^c \left(c_m^+ e^{-ik_{x,m}^c v} + c_m^- e^{ik_{x,m}^c v} \right) \\ u^c &= \frac{1}{\omega \rho_0} \left[\sum_{m=0}^{M} \Phi_m^c k_{x,m}^c \left(c_m^+ e^{-ik_{x,m}^c v} - c_m^- e^{ik_{x,m}^c v} \right) \right] \end{aligned} \tag{5.1}$$

With the same mode matching approach as given in section 4.1.1, the following matrices are obtained, with the same matrix components as defined previously:

$$\mathbf{A}_{11} \begin{Bmatrix} b_m^{+r} \\ b_m^{+i} \end{Bmatrix} + \mathbf{B}_{11} \begin{Bmatrix} b_m^{-r} \\ b_m^{-i} \end{Bmatrix} = \mathbf{E}_{11} \begin{Bmatrix} a_m^{+r} \\ a_m^{+i} \end{Bmatrix} + \mathbf{F}_{11} \begin{Bmatrix} a_m^{-r} \\ a_m^{-i} \end{Bmatrix} \tag{5.2}$$

$$\mathbf{A}_{21} \begin{Bmatrix} b_m^{+r} \\ b_m^{+i} \end{Bmatrix} - \mathbf{B}_{21} \begin{Bmatrix} b_m^{-r} \\ b_m^{-i} \end{Bmatrix} = \mathbf{E}_{21} \begin{Bmatrix} a_m^{+r} \\ a_m^{+i} \end{Bmatrix} - \mathbf{F}_{21} \begin{Bmatrix} a_m^{-r} \\ a_m^{-i} \end{Bmatrix} \tag{5.3}$$

$$\mathbf{A}_{12} \begin{Bmatrix} b_m^{+r} \\ b_m^{+i} \end{Bmatrix} + \mathbf{B}_{12} \begin{Bmatrix} b_m^{-r} \\ b_m^{-i} \end{Bmatrix} = \mathbf{E}_{12} \begin{Bmatrix} c_m^{+r} \\ c_m^{+i} \end{Bmatrix} + \mathbf{F}_{12} \begin{Bmatrix} c_m^{-r} \\ c_m^{-i} \end{Bmatrix} \tag{5.4}$$

$$\mathbf{A}_{22} \begin{Bmatrix} b_m^{+r} \\ b_m^{+i} \end{Bmatrix} - \mathbf{B}_{22} \begin{Bmatrix} b_m^{-r} \\ b_m^{-i} \end{Bmatrix} = \mathbf{E}_{22} \begin{Bmatrix} c_m^{+r} \\ c_m^{+i} \end{Bmatrix} - \mathbf{F}_{22} \begin{Bmatrix} c_m^{-r} \\ c_m^{-i} \end{Bmatrix} \tag{5.5}$$

where

$$\mathbf{F}_{12} = \begin{bmatrix} \Lambda_{mn}^{ab*} T_h^{\,r} & -\Lambda_{mn}^{ab*} T_h^{\,i} \\ \Lambda_{mn}^{ab*} T_h^{\,i} & \Lambda_{mn}^{ab*} T_h^{\,r} \end{bmatrix}$$

and

$$\mathbf{F}_{22} = \begin{bmatrix} K_{mn}^{ab*} \Lambda_{mn}^{ab*} T_h^{\,r} & -K_{mn}^{ab*} \Lambda_{mn}^{ab*} T_h^{\,i} \\ K_{mn}^{ab*} \Lambda_{mn}^{ab*} T_h^{\,i} & K_{mn}^{ab*} \Lambda_{mn}^{ab*} T_h^{\,r} \end{bmatrix} \tag{5.6}$$

5.1.2 Bulk-reacting liner

For a bulk-reacting liner, the pressure and axial particle velocity in regions *A* and *B* are as given by equations (4.1) and (4.25). For region *C*, the right hand side term in equations (4.32) and (4.33) are as given above in equations (5.4) and (5.5). Thus the solutions in the airway region for a bulk-reacting lining are given by:

$$\mathbf{A}_{11}\begin{Bmatrix} b_m^{+r} \\ b_m^{+i} \end{Bmatrix} + \mathbf{B}_{11}\begin{Bmatrix} b_m^{-r} \\ b_m^{-i} \end{Bmatrix} + \mathbf{C}_{11}\begin{Bmatrix} b_{m_e}^{+r} \\ b_{m_e}^{+i} \end{Bmatrix} + \mathbf{D}_{11}\begin{Bmatrix} b_{m_e}^{-r} \\ b_{m_e}^{-i} \end{Bmatrix} = \mathbf{E}_{11}\begin{Bmatrix} a_m^{+r} \\ a_m^{+i} \end{Bmatrix} + \mathbf{F}_{11}\begin{Bmatrix} a_m^{-r} \\ a_m^{-i} \end{Bmatrix} \tag{5.7}$$

$$\mathbf{A}_{21}\begin{Bmatrix} b_m^{+r} \\ b_m^{+i} \end{Bmatrix} - \mathbf{B}_{21}\begin{Bmatrix} b_m^{-r} \\ b_m^{-i} \end{Bmatrix} + \mathbf{C}_{21}\begin{Bmatrix} b_{m_e}^{+r} \\ b_{m_e}^{+i} \end{Bmatrix} - \mathbf{D}_{21}\begin{Bmatrix} b_{m_e}^{-r} \\ b_{m_e}^{-i} \end{Bmatrix} = \mathbf{E}_{21}\begin{Bmatrix} a_m^{+r} \\ a_m^{+i} \end{Bmatrix} - \mathbf{F}_{21}\begin{Bmatrix} a_m^{-r} \\ a_m^{-i} \end{Bmatrix} \tag{5.8}$$

$$\mathbf{A}_{12}\begin{Bmatrix} b_m^{+r} \\ b_m^{+i} \end{Bmatrix} + \mathbf{B}_{12}\begin{Bmatrix} b_m^{-r} \\ b_m^{-i} \end{Bmatrix} + \mathbf{C}_{12}\begin{Bmatrix} b_{m_e}^{+r} \\ b_{m_e}^{+i} \end{Bmatrix} + \mathbf{D}_{12}\begin{Bmatrix} b_{m_e}^{-r} \\ b_{m_e}^{-i} \end{Bmatrix} = \mathbf{E}_{12}\begin{Bmatrix} c_m^{+r} \\ c_m^{+i} \end{Bmatrix} + \mathbf{F}_{12}\begin{Bmatrix} c_m^{-r} \\ c_m^{-i} \end{Bmatrix} \tag{5.9}$$

$$\mathbf{A}_{22}\begin{Bmatrix} b_m^{+r} \\ b_m^{+i} \end{Bmatrix} - \mathbf{B}_{22}\begin{Bmatrix} b_m^{-r} \\ b_m^{-i} \end{Bmatrix} + \mathbf{C}_{22}\begin{Bmatrix} b_{m_e}^{+r} \\ b_{m_e}^{+i} \end{Bmatrix} - \mathbf{D}_{22}\begin{Bmatrix} b_{m_e}^{-r} \\ b_{m_e}^{-i} \end{Bmatrix} = \mathbf{E}_{22}\begin{Bmatrix} c_m^{+r} \\ c_m^{+i} \end{Bmatrix} - \mathbf{F}_{22}\begin{Bmatrix} c_m^{-r} \\ c_m^{-i} \end{Bmatrix} \tag{5.10}$$

where

$$\mathbf{C}_{11} = \begin{bmatrix} \Lambda_{m_e n}^{b_e b^* r} & -\Lambda_{m_e n}^{b_e b^* i} \\ \Lambda_{m_e n}^{b_e b^* i} & \Lambda_{m_e n}^{b_e b^* r} \end{bmatrix} \text{ and } \mathbf{D}_{11} = \begin{bmatrix} \Lambda_{m_e n}^{b_e b^*} T_s^{\,r} & -\Lambda_{m_e n}^{b_e b^*} T_s^{\,i} \\ \Lambda_{m_e n}^{b_e b^*} T_s^{\,i} & \Lambda_{m_e n}^{b b^*} T_s^{\,r} \end{bmatrix}$$

$$\mathbf{C}_{21} = \begin{bmatrix} K_{m_e n}^{b_e b^*} \Lambda_{m_e n}^{b_e b^* r} & -K_{m_e n}^{b_e b^*} \Lambda_{m_e n}^{b_e b^* i} \\ K_{m_e n}^{b_e b^*} \Lambda_{m_e n}^{b_e b^* i} & K_{m_e n}^{b_e b^*} \Lambda_{m_e n}^{b_e b^* r} \end{bmatrix} \text{ and } \mathbf{D}_{21} = \begin{bmatrix} K_{m_e n}^{b_e b^*} \Lambda_{m_e n}^{b_e b^*} T_s^{\,r} & -K_{m_e n}^{b_e b^*} \Lambda_{m_e n}^{b_e b^*} T_s^{\,i} \\ K_{m_e n}^{b_e b^*} \Lambda_{m_e n}^{b_e b^*} T_s^{\,i} & K_{m_e n}^{b_e b^*} \Lambda_{m_e n}^{b_e b^*} T_s^{\,r} \end{bmatrix}$$

$$\mathbf{C}_{12} = \begin{bmatrix} \Lambda_{m_e n}^{b_e b^*} T_s^{\,r} & -\Lambda_{m_e n}^{b_e b^*} T_s^{\,i} \\ \Lambda_{m_e n}^{b_e b^*} T_s^{\,i} & \Lambda_{m_e n}^{b_e b^*} T_s^{\,r} \end{bmatrix} \text{ and } \mathbf{D}_{12} = \begin{bmatrix} \Lambda_{m_e n}^{b_e b^* r} & -\Lambda_{m_e n}^{b_e b^* i} \\ \Lambda_{m_e n}^{b_e b^* i} & \Lambda_{m_e n}^{b_e b^* r} \end{bmatrix}$$

$$\mathbf{C}_{22} = \begin{bmatrix} K_{m_e n}^{b_e b^*} \Lambda_{m_e n}^{b_e b^*} T_s^{\,r} & -K_{m_e n}^{b_e b^*} \Lambda_{m_e n}^{b_e b^*} T_s^{\,i} \\ K_{m_e n}^{b_e b^*} \Lambda_{m_e n}^{b_e b^*} T_s^{\,i} & K_{m_e n}^{b_e b^*} \Lambda_{m_e n}^{b_e b^*} T_s^{\,r} \end{bmatrix} \text{ and } \mathbf{D}_{22} = \begin{bmatrix} K_{m_e n}^{b_e b^*} \Lambda_{m_e n}^{b_e b^* r} & -K_{m_e n}^{b_e b^*} \Lambda_{m_e n}^{b_e b^* i} \\ K_{m_e n}^{b_e b^*} \Lambda_{m_e n}^{b_e b^* i} & K_{m_e n}^{b_e b^*} \Lambda_{m_e n}^{b_e b^* r} \end{bmatrix}$$

The solution for the lining region is as given in equations (4.34) and (4.35). The relationship between airway modes and lining modes is as given in equation (4.39).

5.2 Evaluation of wave amplitude coefficients

The wave amplitudes in the first section, $N=1$, can be determined from a known incident wave profile. The negative going wave in equation (5.2) is replaced with $a_{m,1}^{-}=\mathbf{R_a}a_{m,1}^{+}$ and $b_{m,1}^{-}=\mathbf{R_b}b_{m,1}^{+}$ where $\mathbf{R_a}$ and $\mathbf{R_b}$ are to be determined. With $a_{m,1}^{+}$ as the input, the transmitted wave in the lined duct section, $b_{m,1}^{+}$ can be determined. Similarly, for the second junction, substituting the negative going wave amplitudes in equation (5.4) in terms of their reflection matrix coefficients, the transmitted wave amplitudes in the unlined section, $c_{m,1}^{+}$ is determined from $b_{m,1}^{+}$. The same process is repeated for the next section, $N=2$, where the previously determined transmitted wave amplitude $c_{m,1}^{+}$ is now used as the input i.e. $a_{m,N+1}^{+}=c_{m,N}^{+}e^{-ik_{x,m}^{c}L_h}$.

Therefore, to evaluate the unknown wave amplitudes, the reflection matrix coefficients at each junction, i.e. $\mathbf{R_a}$, $\mathbf{R_b}$ and $\mathbf{R_c}$, have to be obtained first. The reflection matrix coefficients in the last insert, $\mathbf{R_{a,Ns}}$ and $\mathbf{R_{b,Ns}}$ are obtained first by assuming that the end termination is anechoic such that $\mathbf{R_{c,Ns}}=0$. Next, $\mathbf{R_{a,Ns}}$ is used as $\mathbf{R_{c,Ns-1}}$ for the previous insert, $N=N_s$-1, and $\mathbf{R_{b,Ns-1}}$ and $\mathbf{R_{a,Ns-1}}$ are evaluated. This process is repeated until the first insert at the duct inlet is reached.

Once all the reflection matrix coefficients have been obtained, the wave amplitude coefficients can be determined from $a_{m,1}^{+}$. The matrices required for this can be obtained from equations (5.2)-(5.5) for the locally reacting liner, and from equations (5.7)-(5.10) for the bulk-reacting liner. This procedure is given in the following sections for locally reacting and bulk-reacting liners.

5.2.1 Locally reacting liner

From equations (5.4) and (5.5), replacing c_m^{-} with $\mathbf{R_c}c_m^{+}$, one can write:

$$\mathbf{R_b}=\left(-\left(\mathbf{H}_{22}\right)^{-1}\mathbf{B}_{22}-\left(\mathbf{H}_{12}\right)^{-1}\mathbf{B}_{12}\right)^{-1}\left(\left(\mathbf{H}_{12}\right)^{-1}\mathbf{A}_{12}-\left(\mathbf{H}_{22}\right)^{-1}\mathbf{A}_{22}\right) \tag{5.11}$$

where

$$\mathbf{H}_{12}=\mathbf{E}_{12}+\mathbf{F}_{12}\mathbf{R_c}$$
$$\mathbf{H}_{22}=\mathbf{E}_{22}-\mathbf{F}_{22}\mathbf{R_c}$$

and for the last segment $\mathbf{H}_{12} = \mathbf{E}_{12}$ and $\mathbf{H}_{22} = \mathbf{E}_{22}$ where $\mathbf{R}_\mathbf{c} = 0$.

Substituting equation (5.11) into equations (5.2) and (5.3) and rearranging it, one can write

$$\mathbf{R}_\mathbf{a} = \left(-\left(\mathbf{H}_{21}\right)^{-1}\mathbf{F}_{21} - \left(\mathbf{H}_{11}\right)^{-1}\mathbf{F}_{11}\right)^{-1}\left(\left(\mathbf{H}_{11}\right)^{-1}\mathbf{E}_{11} - \left(\mathbf{H}_{21}\right)^{-1}\mathbf{E}_{21}\right) \tag{5.12}$$

where

$$\mathbf{H}_{11} = \mathbf{A}_{11} + \mathbf{B}_{11}\mathbf{R}_\mathbf{b}$$
$$\mathbf{H}_{21} = \mathbf{A}_{21} - \mathbf{B}_{21}\mathbf{R}_\mathbf{b}$$

With the known reflection matrix coefficients, the wave amplitudes in each section can be calculated where

$$\begin{aligned} a_m^- &= \mathbf{R}_\mathbf{a} a_m^+ \\ b_m^+ &= \left(\mathbf{H}_{11}\right)^{-1}\left(\mathbf{E}_{11} + \mathbf{F}_{11}\mathbf{R}_\mathbf{a}\right)a_m^+ \\ b_m^- &= \mathbf{R}_\mathbf{b} b_m^+ \\ c_m^+ &= \left(\mathbf{H}_{12}\right)^{-1}\left(\mathbf{A}_{12} + \mathbf{B}_{12}\mathbf{R}_\mathbf{b}\right)b_m^+ \\ c_m^- &= \mathbf{R}_\mathbf{c} c_m^+ \end{aligned} \tag{5.13}$$

Having obtained $\mathbf{R}_\mathbf{a}$, this is used as $\mathbf{R}_\mathbf{c}$ for the next segment and the process is repeated.

5.2.2 Bulk-reacting liner

For the bulk-reacting liner, the relationship between lining modes and airway modes is obtained by solving the boundary conditions at $h/2 \le |y| \le (h/2 + d)$ at each end of the lined section. The lining modes can be written in terms of airway modes as in equation (4.39). Substituting equation (4.39) into equations (5.7)-(5.10) and following the steps in section 5.2.1, the reflection matrix coefficients are given by:

$$\mathbf{R}_\mathbf{b} = \left(-\left(\mathbf{H}_{22}\right)^{-1}\mathbf{K}_{22} - \left(\mathbf{H}_{12}\right)^{-1}\mathbf{K}_{12}\right)^{-1}\left(\left(\mathbf{H}_{12}\right)^{-1}\mathbf{J}_{12} - \left(\mathbf{H}_{22}\right)^{-1}\mathbf{J}_{22}\right) \tag{5.14}$$

and

$$\mathbf{R}_\mathbf{a} = \left(-\left(\mathbf{H}_{21}\right)^{-1}\mathbf{F}_{21} - \left(\mathbf{H}_{11}\right)^{-1}\mathbf{F}_{11}\right)^{-1}\left(\left(\mathbf{H}_{11}\right)^{-1}\mathbf{E}_{11} - \left(\mathbf{H}_{21}\right)^{-1}\mathbf{E}_{21}\right) \tag{5.15}$$

Here $\mathbf{H}_{12}$ and $\mathbf{H}_{22}$ are the same as in the locally reacting case, but $\mathbf{H}_{11}$ and $\mathbf{H}_{21}$ are given by:

$$\mathbf{H}_{11} = \mathbf{J}_{11} + \mathbf{K}_{11}\mathbf{R}_{\mathbf{b}}$$
$$\mathbf{H}_{21} = \mathbf{J}_{21} - \mathbf{K}_{21}\mathbf{R}_{\mathbf{b}}$$

with the **J** and **K** matrices as defined in equation (4.42). The wave amplitudes are then given by:

$$\begin{aligned}
a_m^- &= \mathbf{R}_{\mathbf{a}} a_m^+ \\
b_m^+ &= \left(\mathbf{H}_{11}\right)^{-1}\left(\mathbf{E}_{11} + \mathbf{F}_{11}\mathbf{R}_{\mathbf{a}}\right)a_m^+ \\
b_m^- &= \mathbf{R}_{\mathbf{b}} b_m^+ \\
b_{me}^+ &= \beta_1 b_m^+ + \beta_2 b_m^- \\
b_{me}^- &= \beta_3 b_m^+ + \beta_4 b_m^- \\
c_m^+ &= \left(\mathbf{H}_{12}\right)^{-1}\left(\mathbf{J}_{12} + \mathbf{K}_{12}\mathbf{R}_{\mathbf{b}}\right)b_m^+ \\
c_m^- &= \mathbf{R}_{\mathbf{c}} c_m^+
\end{aligned} \tag{5.16}$$

5.3 Effects of periodicity on a duct with a locally reacting liner

With the analytical model of sound propagation through a periodic lining duct developed above, simulations are carried out to investigate the effect of periodicity on duct attenuation. A plane wave incidence is considered for all the following cases of a simple duct configuration. Due to the symmetrical duct arrangement, an even incident wave will not excite odd modes. Therefore only even modes are included in the following analysis.

The effect of periodicity is first studied for a duct with a locally reacting liner. The continuous lining is sectioned into two and then four inserts, separated by an unlined section with a length of 10% of the length of lined section. Each insert has the same lining thickness, material properties and airway height. The flow resistivity is set to 13000 rayls/m and the airway height, h is 300 mm. With 300 mm airway height, at 10 kHz, 8 even modes are cut on. Therefore a total of 32 modes are included in the simulation in accordance with the considerations in section 4.2.

The total length of the lined duct section is kept at 1 m. The transmission loss for the 1 m long lined duct is shown in Figure 5.3 where figure (a) is for a thin lining with d = 40 mm and figure (b) is for a thicker lining with d = 100 mm. For both lining thicknesses, the peak attenuation is achieved below the cut-on frequency. The continuously lined duct has 1 m of lining material. For the duct lined with two inserts, each insert length, L_s is 476 mm and these are separated by an unlined section of length L_h = 48 mm. For the duct with four inserts, L_s = 233 mm and L_h = 23 mm. For the latter two cases, the lining material is reduced by approximately 5% for two inserts and 7% for four inserts, compared to the continuously lined duct.

For the thinner lining in Figure 5.3 (a), the attenuation of a continuously lined duct is almost the same as for two inserts. However, the peak attenuation increases when the lining is divided into four sections. For the thicker lining the peak attenuation is reduced slightly with two or four inserts as shown in Figure 5.3 (b). For both considered thicknesses, the duct attenuation at high frequency, above the cut-on frequency of the first even mode in the hard-walled duct, is slightly improved by the multi-segmented duct linings. This may be due to the scattering of wave energy carried by the fundamental mode into higher order propagating modes that are more readily attenuated.

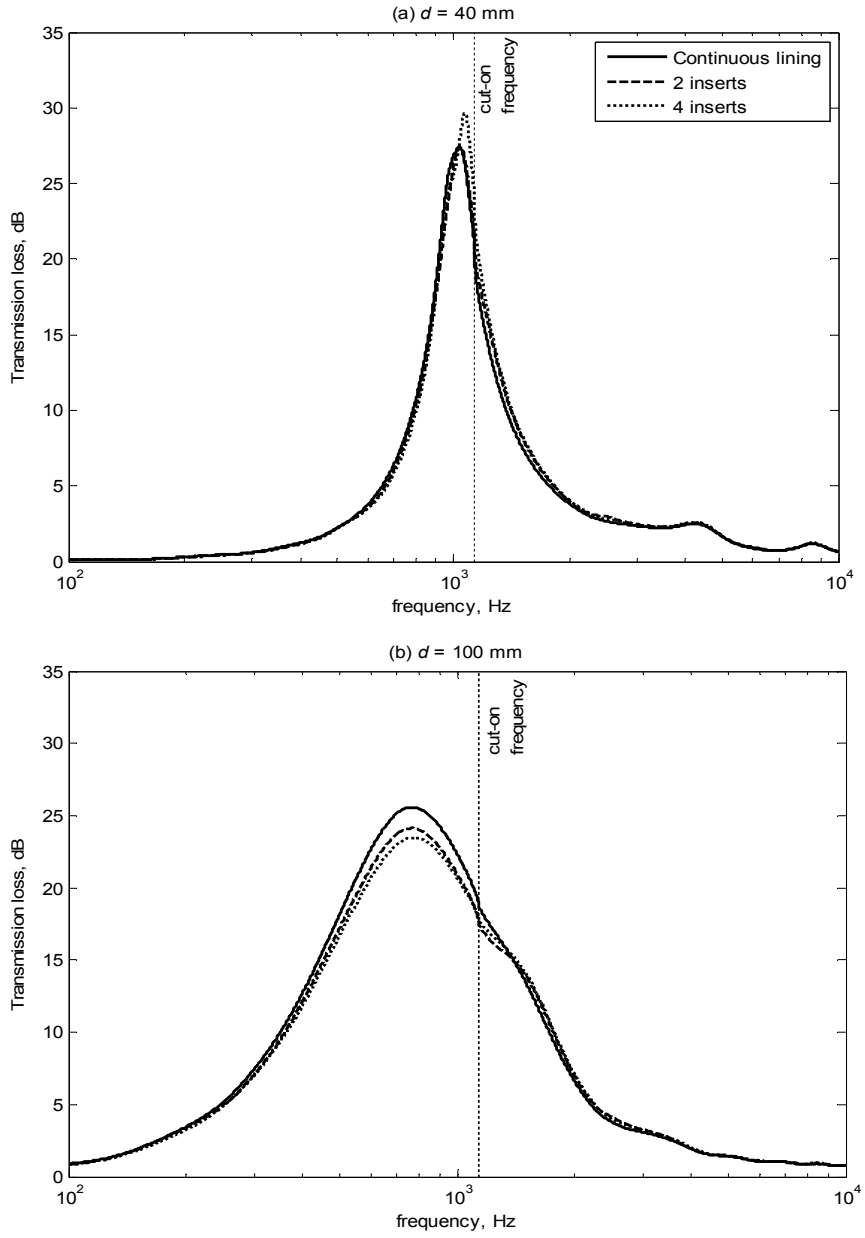

Figure 5.3: Transmission loss for a duct with continuous lining, two and four inserts. Locally reacting lining, h = 300 mm with (a) d = 40 mm and (b) d = 100 mm thick lining.

5.4 Effects of periodicity on a bulk-reacting lined duct

The previous simulation is repeated for a bulk-reacting lining model with the same duct height and lining properties and thickness. The total length of porous material is maintained at 1 m as before. Figure 5.4 shows the attenuation of a duct with a continuous lining, two inserts and four inserts, for both thicknesses, d = 40 and 100 mm. 34 airway modes are included for mode-matching with an additional 9 lining modes for the 40 mm thick lining and 22 lining modes for the 100 mm thick lining. The same effect of periodicity is observed in a duct with a bulk-reacting lining as for the locally reacting case. For the thinner lining of 40 mm, a duct with four inserts shows an improvement in the peak attenuation while for the thicker lining of 100 mm the peak attenuation is lower than for the continuously lined duct. For the duct with two inserts, no improvement in duct attenuation is found compared to the continuously lined duct. However, with 40 mm lining, there are two peaks in attenuation. The first peak occurs below the cut-on frequency and is due to the fundamental mode, and the second peak occurs at a higher frequency. This second peak does not appear in the case of a locally reacting lining considered above, or for the 100 mm thick bulk-reacting lining.

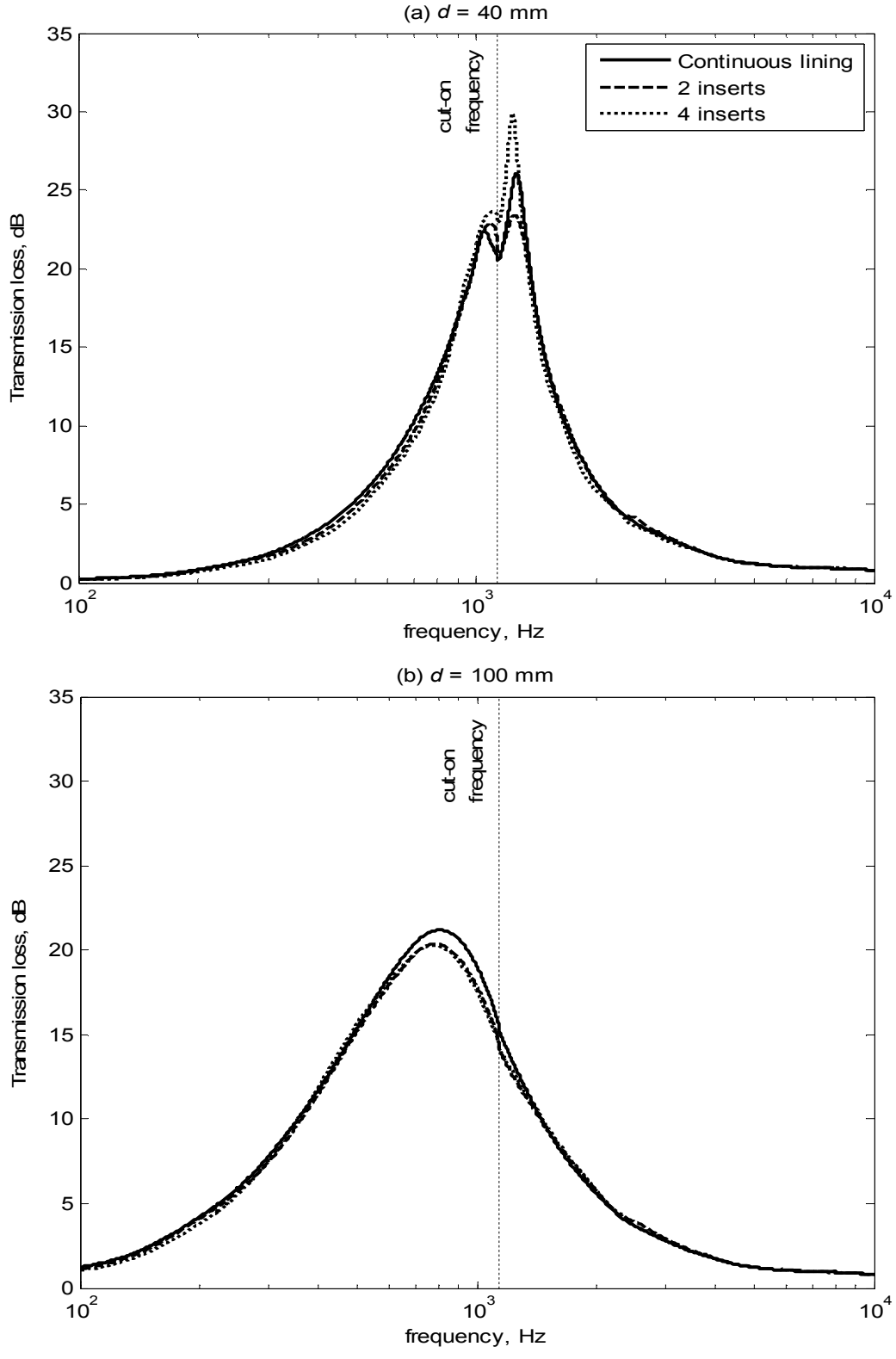

Figure 5.4: Transmission loss for a duct with continuous lining, two and four inserts. Bulk-reacting lining, h = 300 mm with (a) d = 40 mm and (b) d = 100 mm thick lining

5.5 Influence of number of sections on duct attenuation

Studies on the previously considered duct, with locally reacting and bulk-reacting linings, are repeated but the number of inserts is increased to 5, 10, 15 and 20. The length of each unlined section remains at 10% of the length of each lined section. Table 5.1 lists the length of each lined and unlined section of the 1 m long duct with different numbers of inserts. Figure 5.5 shows the transmission loss for the same duct with a locally reacting lining as in Figure 5.3 but with 5, 10, 15 and 20 inserts. For both thicknesses, 40 mm and 100 mm, increasing the number of inserts does not have any significant effect on the attenuation, and the transmission loss in these four cases is the same as that obtained with four inserts.

However, for a duct with a bulk-reacting lining, for both lining thicknesses noticeable changes are found with increasing number of inserts as shown in Figure 5.6, especially for the 40 mm thick liner. The peak frequencies for both thicknesses are slightly shifted to lower frequency and moved towards the peak frequency of a duct with a locally reacting lining. In the case of a 40 mm thick liner, the second peak found in Figure 5.4 (a) does not appear with 10 or more inserts. Increasing the number of periodic elements in a duct with a bulk-reacting lining gives a calculated transmission loss which is more similar to the transmission loss of a duct with a locally reacting lining. In a continuously lined duct with a bulk-reacting material, axial waves can travel in the lining along the axial direction. By partitioning the liner, axial wave propagation in the lining is restricted hence rendering the lining behaviour more similar to the locally reacting case. Therefore, the predicted transmission loss for a duct with a bulk-reacting lining with a larger number of periodic elements will be close to the predicted transmission loss for a duct with a continuous locally-reacting lining. With increasing number of periodic element, the computation time increases as well. For a bulk-reacting lining with up to 56 modes included in the simulation, with 10 or less inserts the computation time is less than 1 hour. 2 hours computation time is required to simulate a duct with 20 inserts.

Table 5.1: Length of lined and unlined sections for a 1m duct with different number of inserts

Number of inserts	Length of lined section, L_s (mm)	Length of unlined section, L_h (mm)	Total length of lining material (mm)
2	476	47.6	952
4	233	23.3	930
5	185	18.5	925
10	92	9.2	920
15	61	6.1	915
20	46	4.6	913

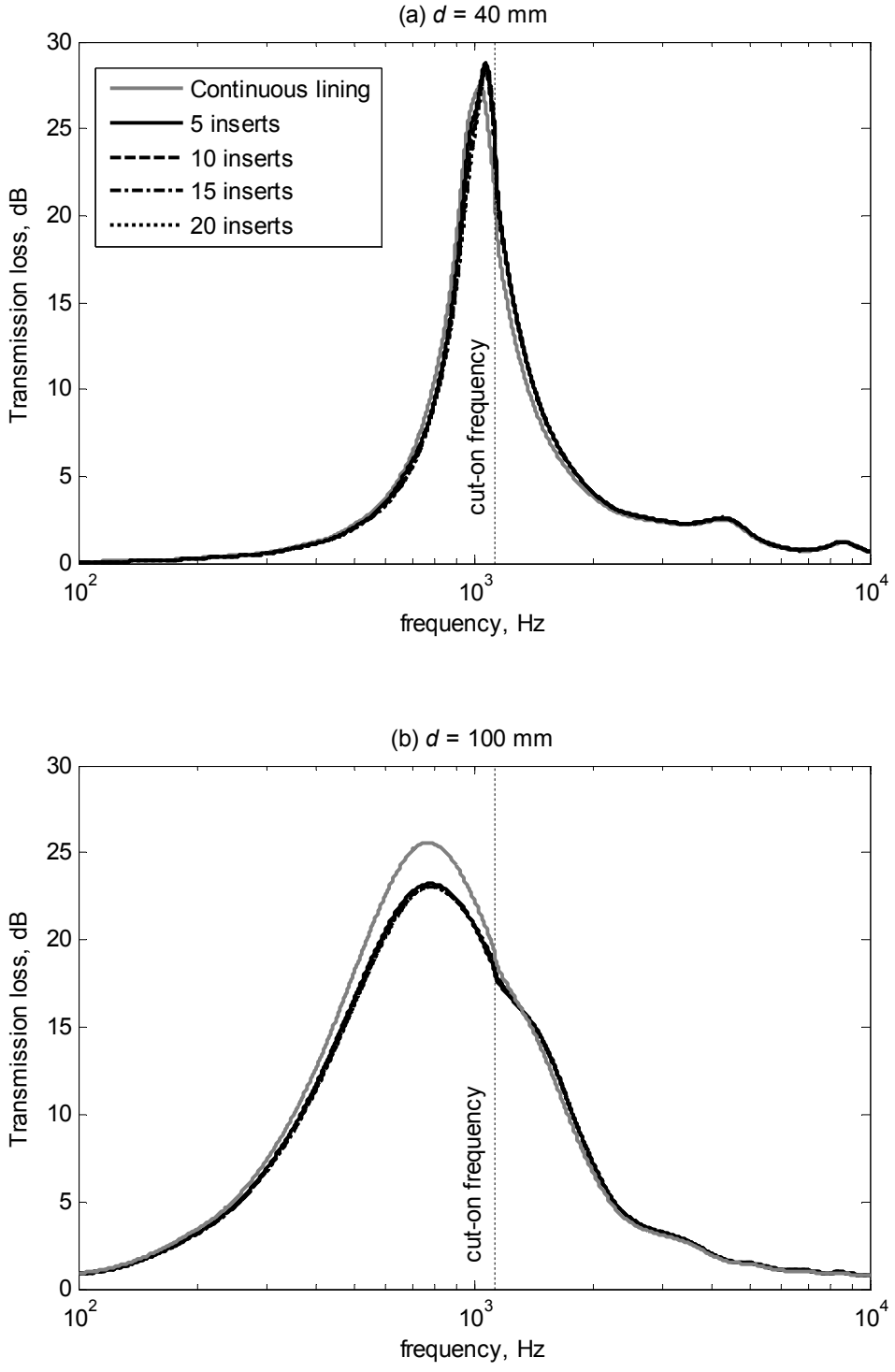

Figure 5.5: Transmission loss for a periodically lined duct with h = 300 mm and r = 13000 rayls/m and the lining thickness of (a) 40 mm and (b) 100 mm. The duct is lined with a locally reacting material.

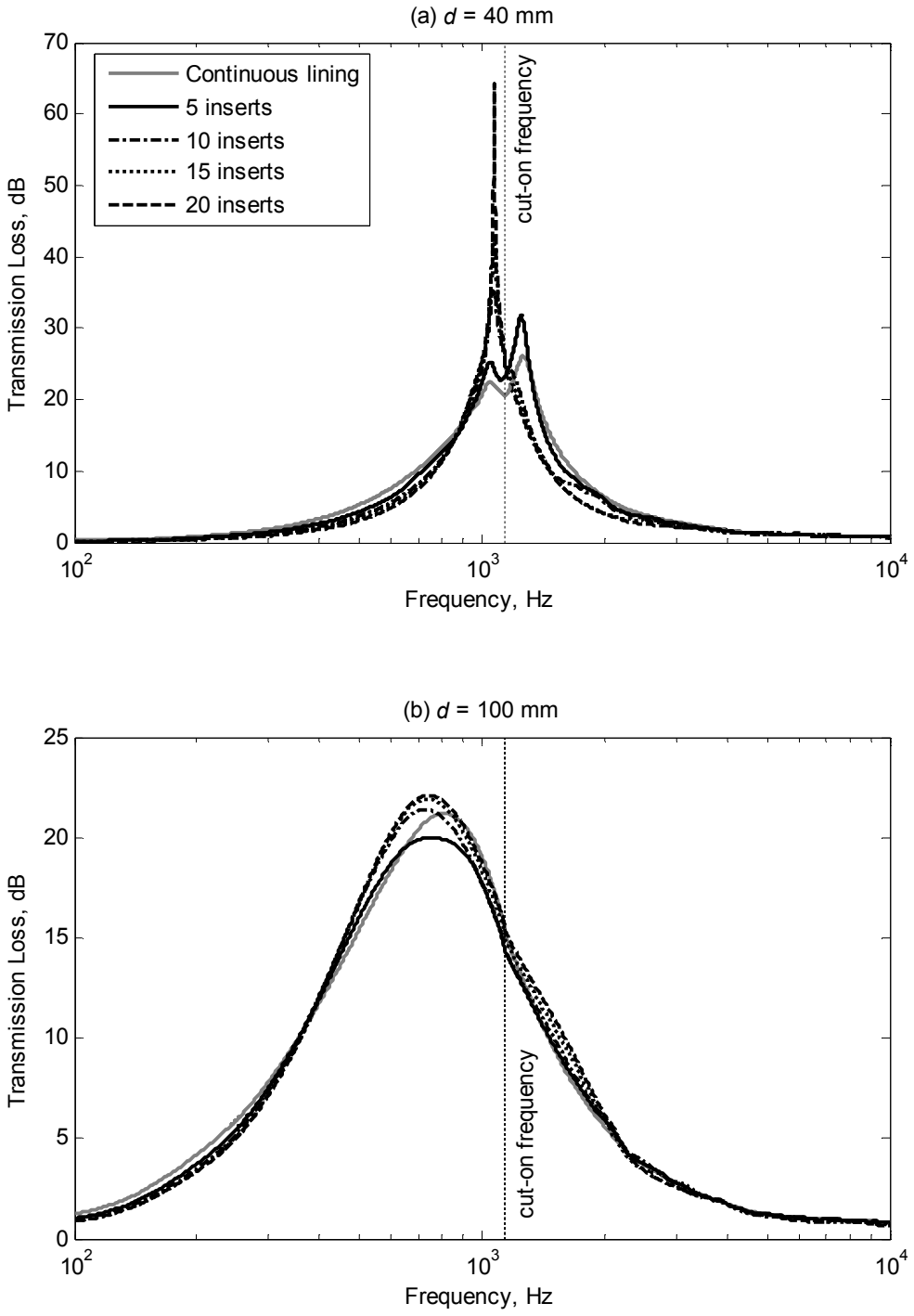

Figure 5.6: Transmission loss for a periodically lined duct with h = 300 mm and r = 13000 rayls/ m and the lining thickness of (a) 40 mm and (b) 100 mm. The duct is lined with a bulk-reacting material.

Since partitioning the bulk-reacting lining has a bigger effect on duct attenuation than for a locally reacting lining, the simulation is repeated for a different flow resistivity and two different airway heights. The results are shown in Figure 5.7 and Figure 5.8. The lining thicknesses in all three cases are maintained at 40 mm. In Figure 5.7 with a lower flow resistivity, the same effect of periodicity is found as in Figure 5.6 (a). The second peak in the attenuation does not appear with 10 inserts, making the results more similar to a continuously lined duct with a locally reacting lining. With 5 and 10 inserts, the duct attenuation at the peak is improved but at other frequencies it deteriorates.

In Figure 5.8(a), the second peak is not as prominent as in the previous case for a continuously lined duct and it disappears when the duct lining is partitioned. The peak attenuation continues to improve with increasing number of inserts, but in a taller duct where h = 500 mm in Figure 5.8(b), little effect of periodicity is found in the duct attenuation.

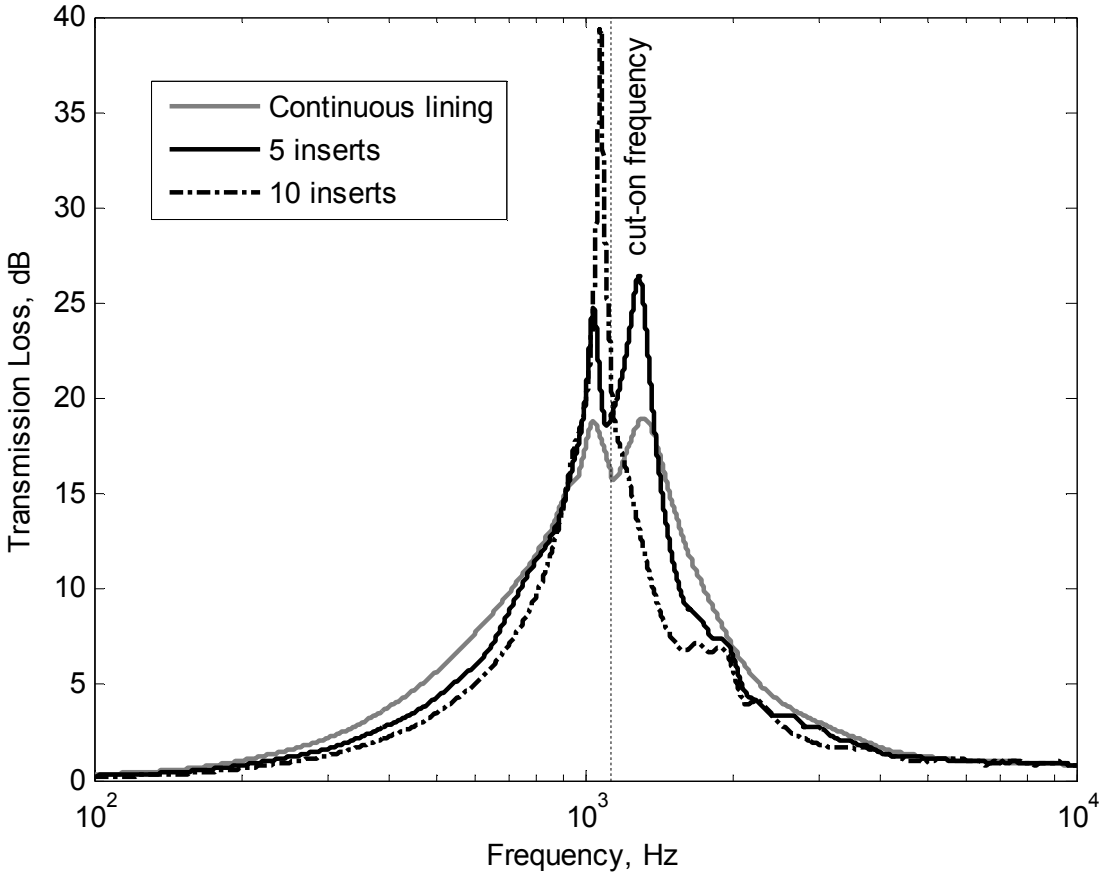

Figure 5.7: Transmission loss for a duct with a lower flow resistivity, r = 8500 rayls/m. The airway height is 300 mm and lining thickness is 40 mm. The duct lining is bulk-reacting

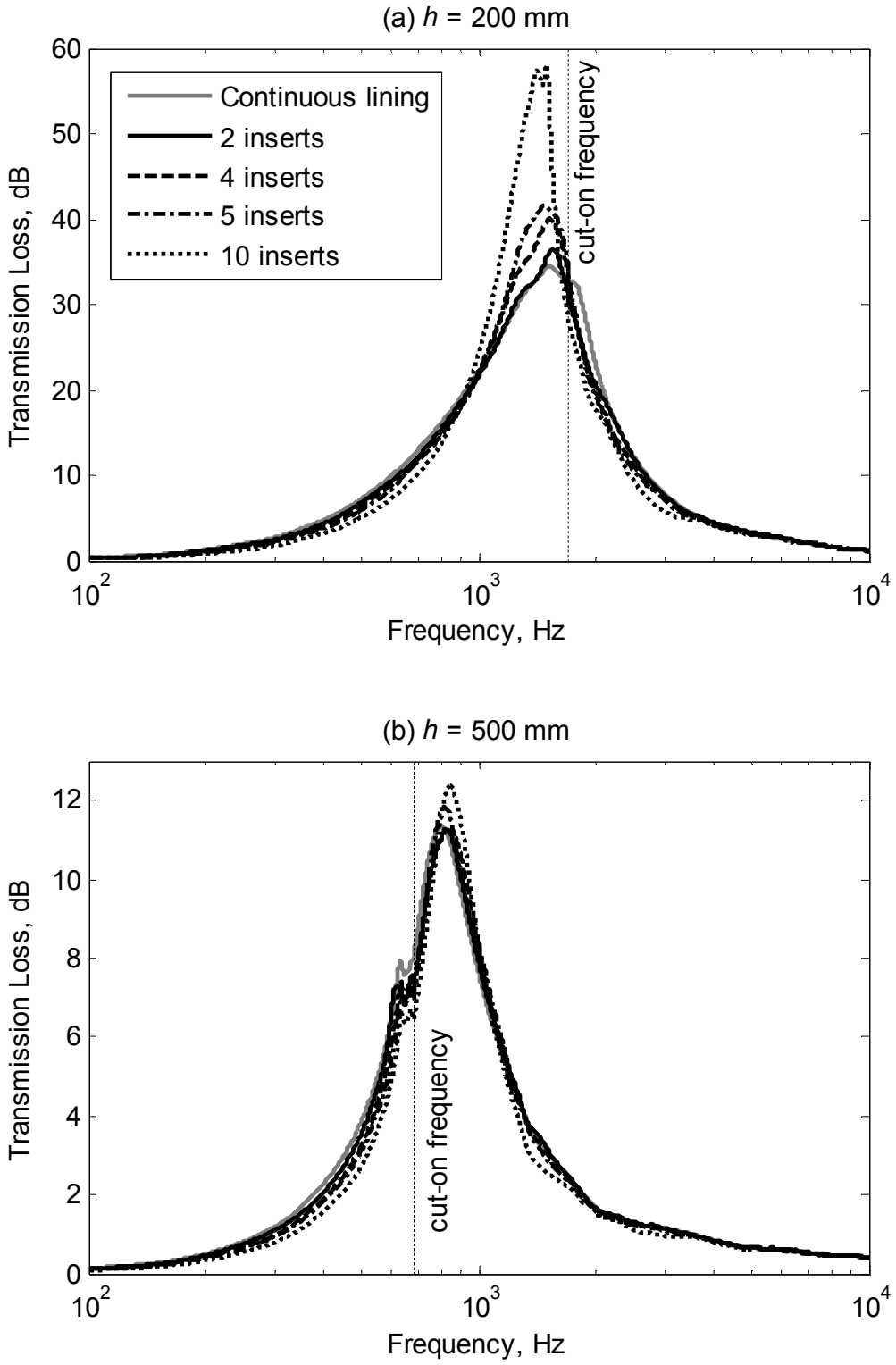

Figure 5.8: Transmission loss for a duct with an airway height of (a) 200 mm and (b) 500 mm, lined with 40 mm thick lining and r = 13000 rayls/m. The duct lining is locally reacting.

5.6 Influence of liner thickness on duct attenuation

In the previous example, the effect of periodicity for a thicker duct lining is less pronounced than for a thinner duct lining. More values of duct lining thickness are considered here and the attenuation of a continuously lined duct and two periodically lined ducts, with five and ten inserts respectively, are compared. The results are shown in Figure 5.9 and Figure 5.10 for ducts with a locally reacting lining with different flow resistivity, 8500 rayls/m and 13000 rayls/m respectively. For thinner duct linings, 20 mm and 40 mm, periodicity with five inserts slightly improves the peak attenuation. However, for d = 65 and 100 mm, periodicity reduces the attenuation at the peak and does not have a strong effect elsewhere. However, for a bulk-reacting lining, periodicity increases the peak attenuation for all the considered lining thicknesses as shown in Figure 5.11 and Figure 5.12. This is due to the effect of periodicity that renders the bulk-reacting lining behaviour more similar to the locally reacting lining, which generally gives higher peak attenuation.

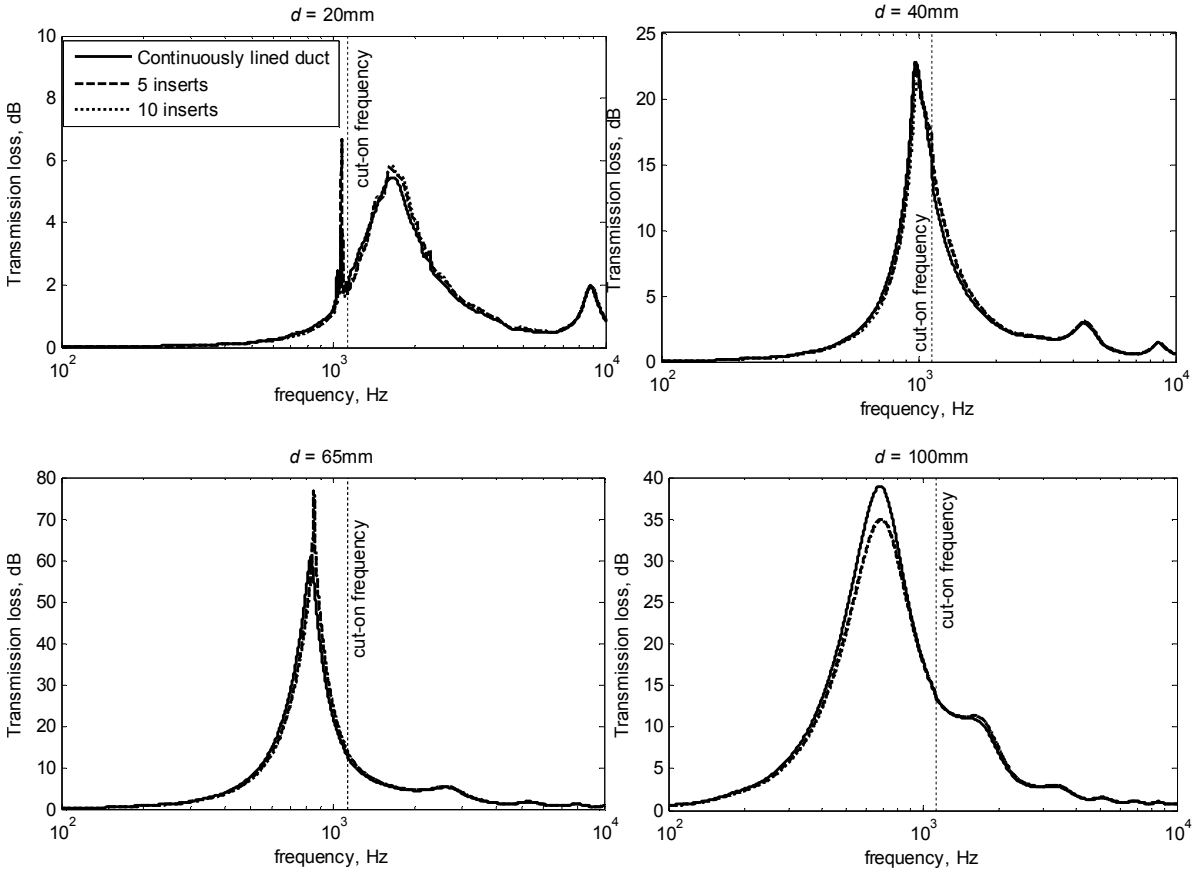

Figure 5.9: Transmission loss for a duct with continuous lining, five and ten inserts. h = 300 mm and r = 8500 rayls/m. The duct is lined with a locally reacting lining.

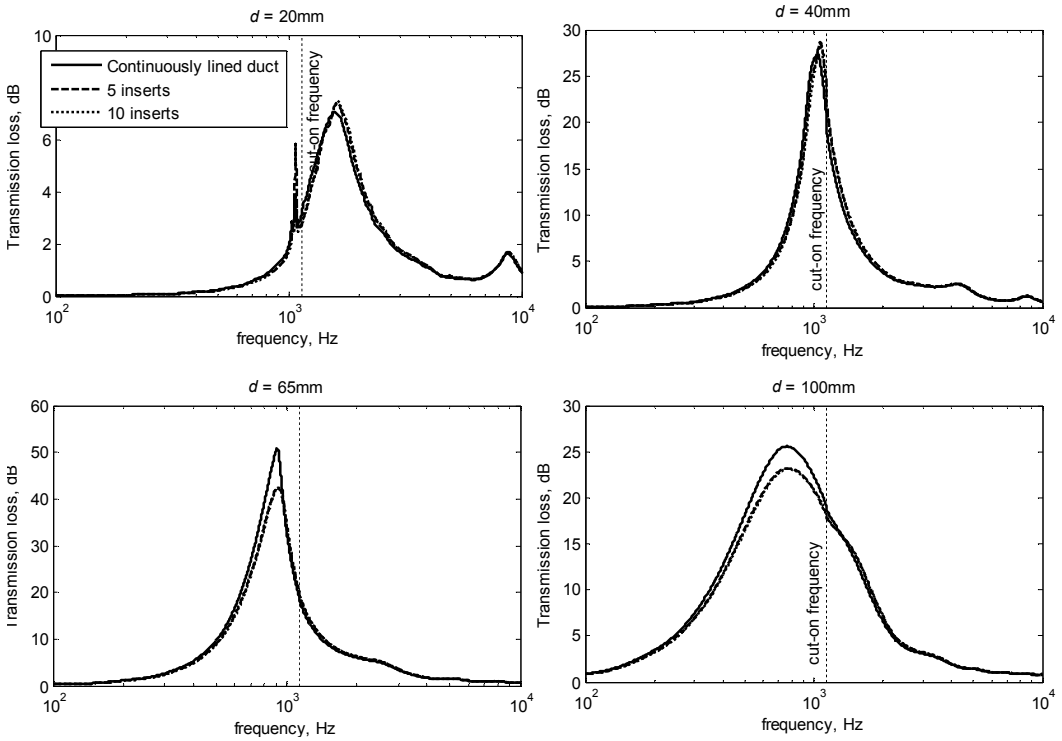

Figure 5.10: Transmission loss for a duct with continuous lining, five and ten inserts. h = 300 mm and r = 13000 rayls/m. The duct is lined with a locally reacting lining.

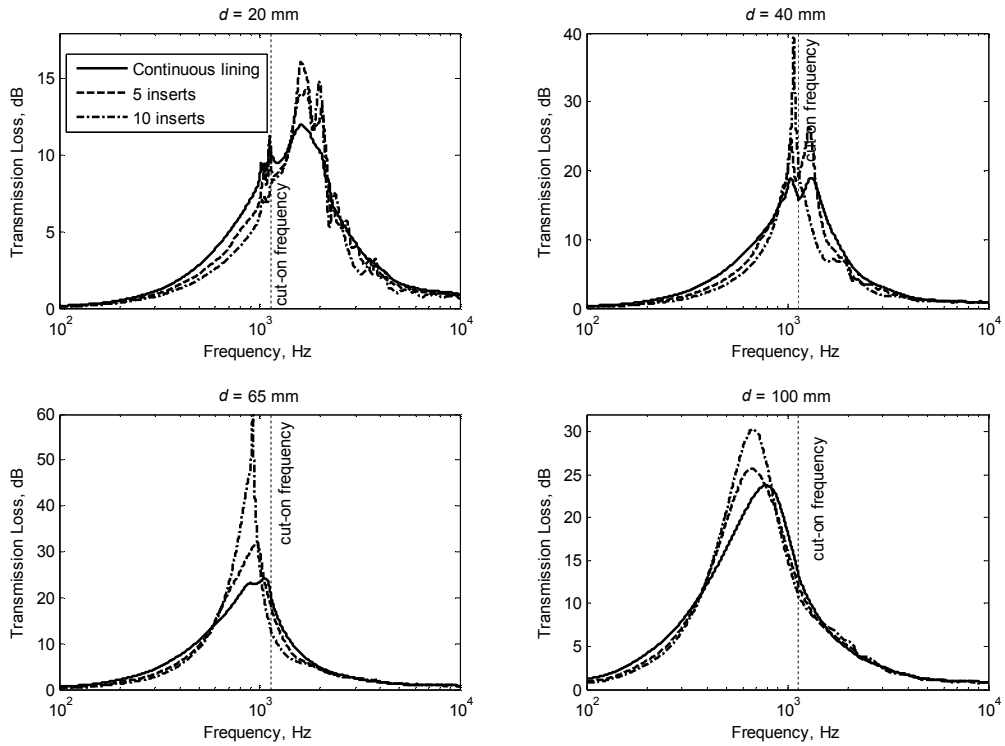

Figure 5.11: Transmission loss for a duct with continuous lining, five and ten inserts. h = 300 mm and r = 8500 rayls/m. The duct is lined with a bulk-reacting lining.

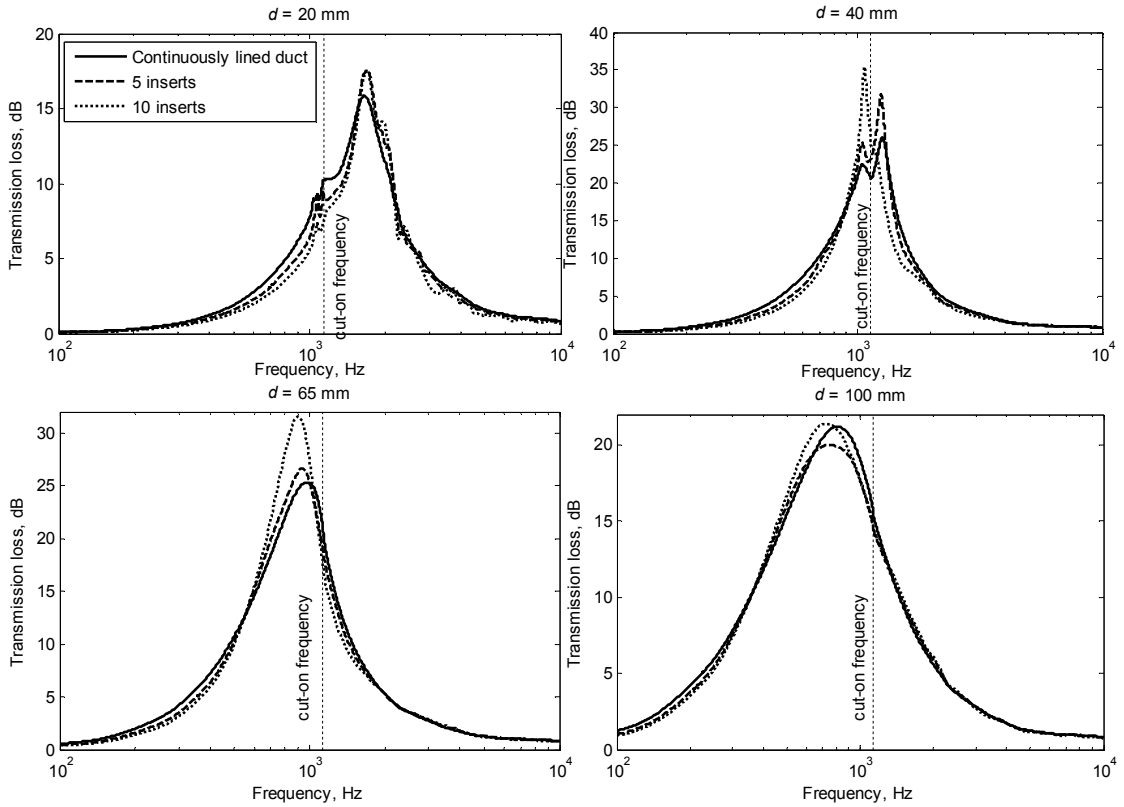

Figure 5.12: Transmission loss for a duct with continuous lining, five and ten inserts. h = 300 mm and r = 13000 rayls/m. The duct is lined with a bulk-reacting lining.

5.7 Influence of length of lined/unlined section on duct attenuation

The effect on the duct attenuation of varying the length of the unlined section while maintaining a total duct length of 1 m is studied. The length ratio is varied according to Table 5.2 and the lined section is periodic with five inserts in each case. Figure 5.13 (a) and (b) shows the transmission loss for ducts with the same airway height and lining flow resistivity, but with lining thicknesses of 40 mm and 100 mm respectively. The length of the unlined section is varied to be 1/100, 1/2, 1 and 2 times the length of the lined section.

Table 5.2: Length of lined and unlined section for various ratios of L_h/L_s

Number of inserts	L_h/L_s	L_h (mm)	L_s (mm)	Total length of lining material (mm)
5	0.01	2	198.4	992
	0.50	71.4	142.9	714
	1	111	111	556
	2	154	77	385

For both 40 mm and 100 mm lining thickness, the attenuation below the first cut-on frequency reduces with increasing ratio of L_h/L_s but this is compensated with increased attenuation at high frequency, hence broadening the effective frequency range. Increasing the length of the unlined sections L_h improves the attenuation at high frequency where a significant improvement is obtained for a duct with a thinner lining, d = 40 mm. When the length of lined section is less than half the airway height, there are dips in the transmission loss at frequencies where higher order modes cut on. The same behaviour was found in Figure 4.9 where the dips were found to be deeper with shorter L_s and at frequencies where the first two higher order modes cut-on.

The simulation is repeated for a duct with a bulk-reacting lining and the results are shown in Figure 5.14. The same effect as in the duct with a locally reacting lining is observed except that the improvement at high frequency is not as great and for 100 mm thick lining very little improvement is achieved above the second cut-on frequency.

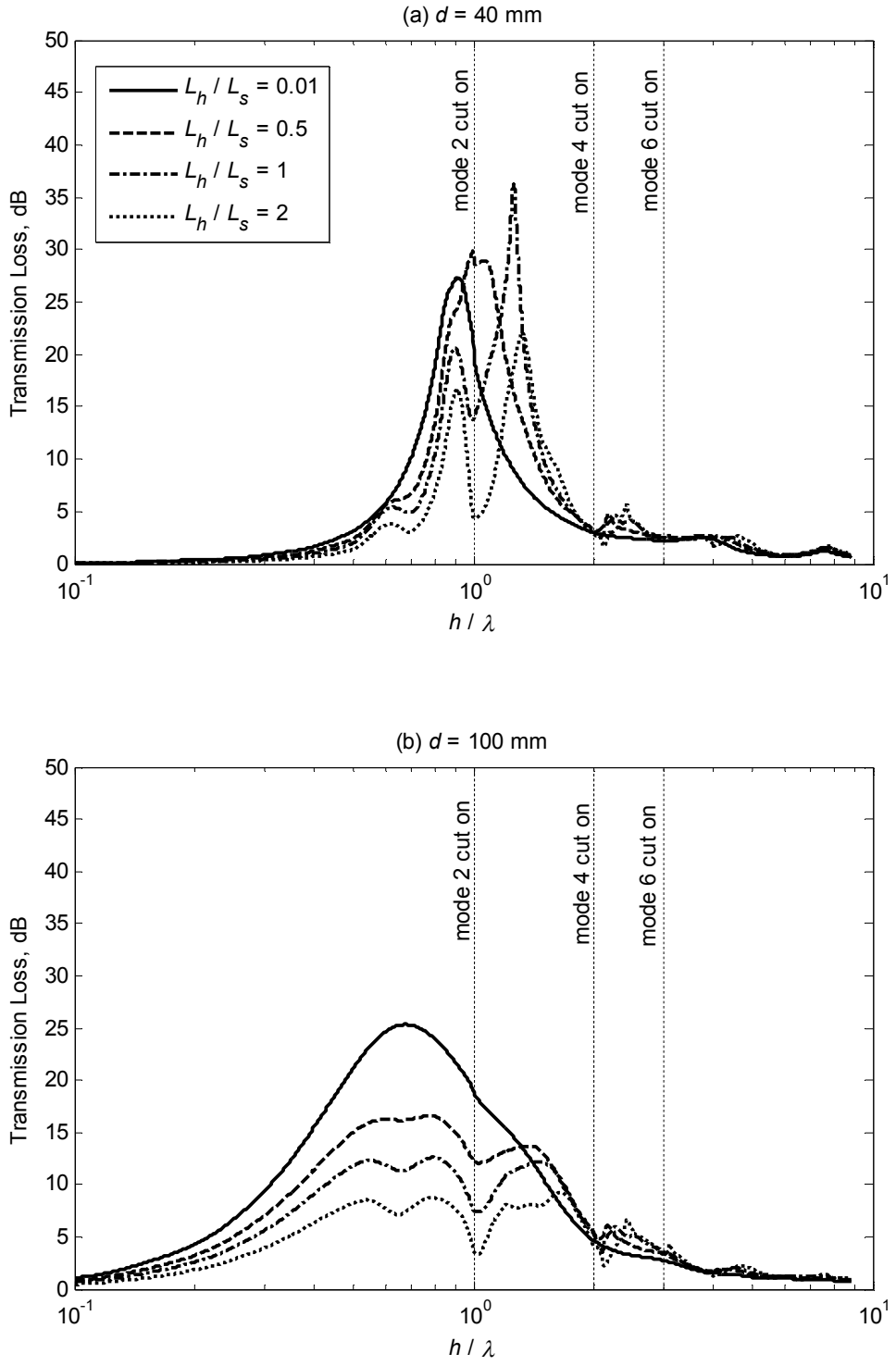

Figure 5.13: Transmission loss for a duct with a locally reacting lining with 5 inserts and varying length ratio of unlined section to lined section (a) d = 40 mm and (b) d = 100 mm. h = 300 mm and r = 13000 rayls/m

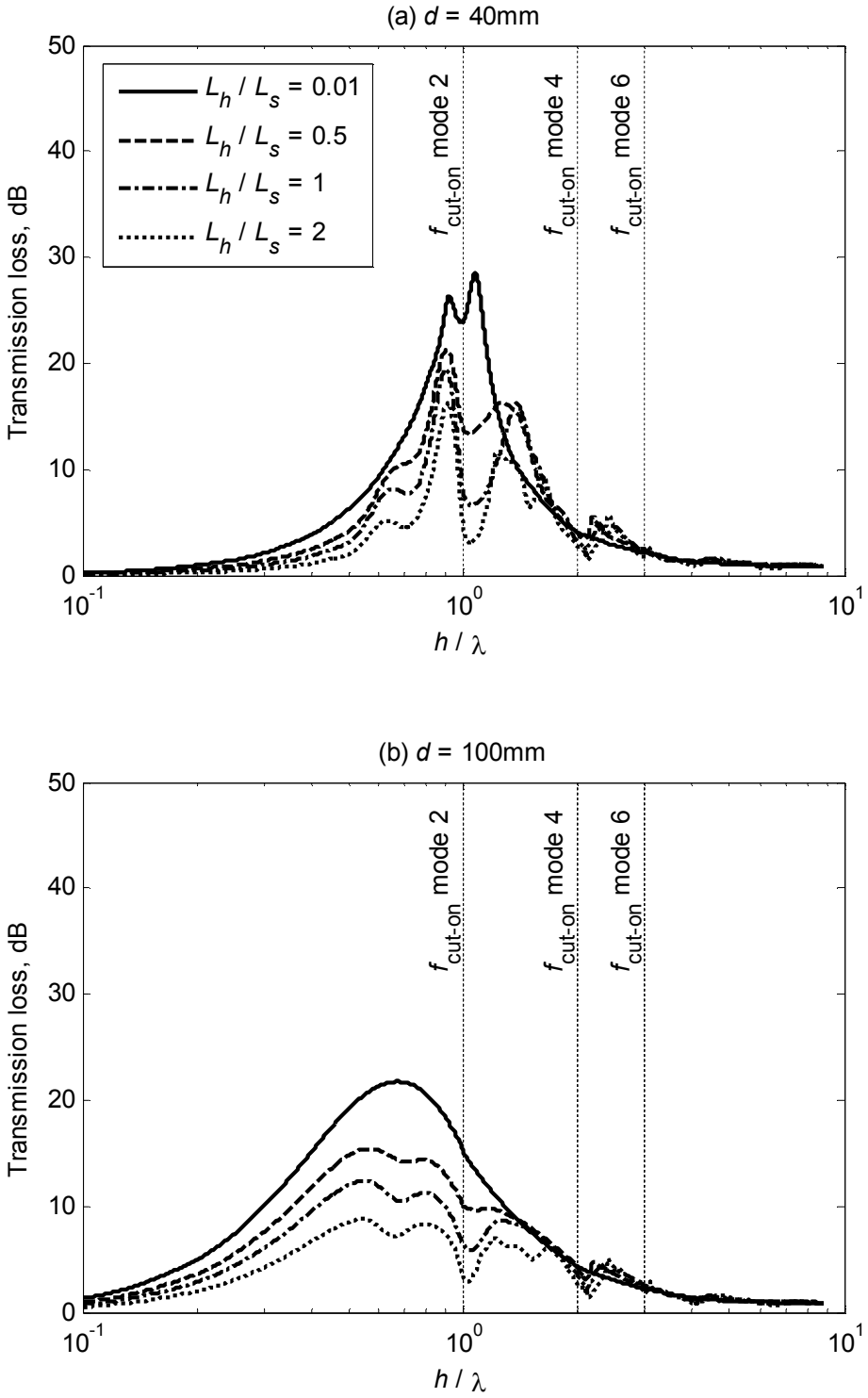

Figure 5.14: Transmission loss for a duct with a bulk-reacting lining with 5 inserts and varying length ratio of unlined section to lined section (a) d = 40 mm and (b) d = 100 mm. h = 300 mm and r = 13000 rayls/m

5.8 Duct attenuation for multi-modal incident wave

In all the preceding results, plane wave incidence is assumed where, due to the symmetrical duct geometry, no anti-symmetrical duct modes are excited. To consider a case of multi-modal incidence equal energy density is assumed in each cut-on mode. This gives a wave amplitude [67]:

$$a_m^+ = \left(a_m^{ref} \Big/ \sqrt{\Lambda_n} \right) e^{-ik_{x,m}^a x_s} \tag{5.17}$$

where a_m^{ref} is the reference sound pressure amplitude of the m^{th} incident mode, set equal to unity. Λ_n is the integration of the squared mode shape, $\int_{-h/2}^{h/2} \Phi_m^{a\,2} dy$, and x_s is the distance of the sound source to the first junction, $x = 0$, taken to be $x_s = 0.1$ m.

With this two-dimensional assumption, many of the incident modes are missing in the multi-modal incident wave model. Thus, this will only give approximation to the attenuation above the cut-on frequency for the multi-modal incidence case. Figure 5.15 shows a comparison of duct transmission loss between plane wave incidence and equal incident modal energy. The duct is lined with a 40 mm thick bulk-reacting lining and has an airway height of 300 mm. Three lining insert arrangements are considered: continuous, two and five inserts. For all these numbers of inserts, the transmission losses are the same for the two cases of incident waves until mode 2 cuts on although the transmission loss in the multi-modal case is slightly higher after mode 1 cuts on due to the inclusion of attenuation of the odd mode. At high frequency, the attenuation for multi-modal incidence is much higher than for plane wave incidence since the energy in higher order incident modes is more readily attenuated. Another example is shown in Figure 5.16 for the same duct but with a larger airway height, 500 mm. The same observation can be made that the transmission loss above the cut-on frequency is higher in the case of multi-mode incidence.

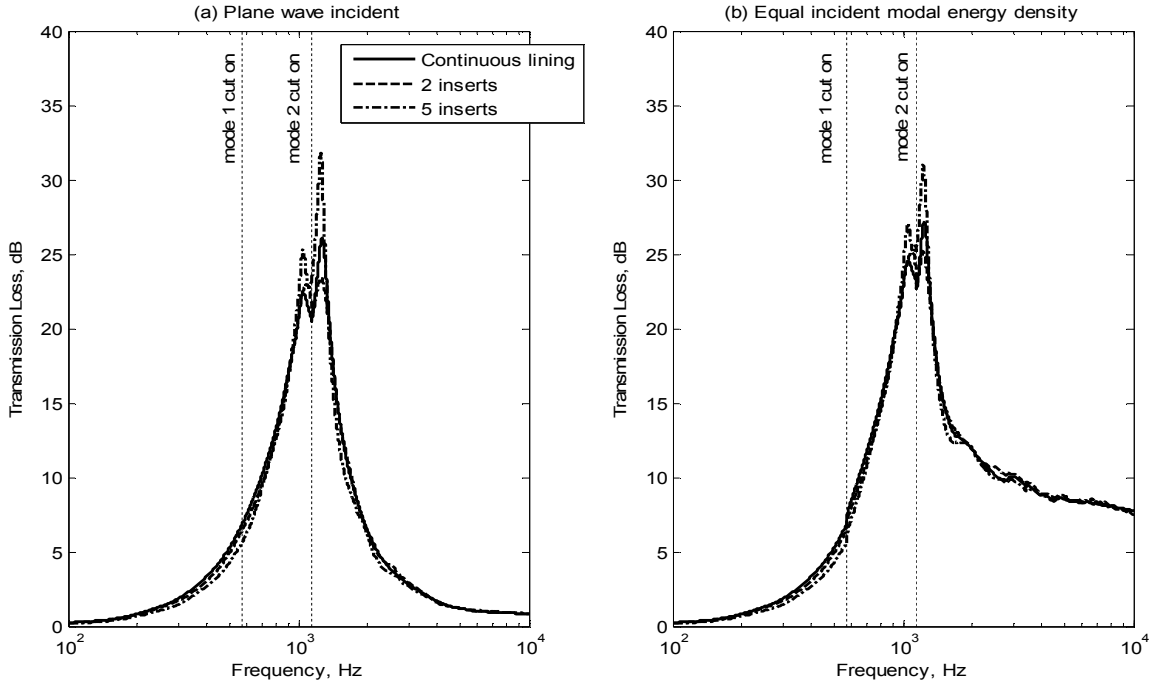

Figure 5.15: Comparison of transmission loss for a duct with a bulk-reacting lining, h = 300 mm, d = 40 mm and r = 13000 rayls/m between (a) plane wave incidence and (b) multi-mode incidence

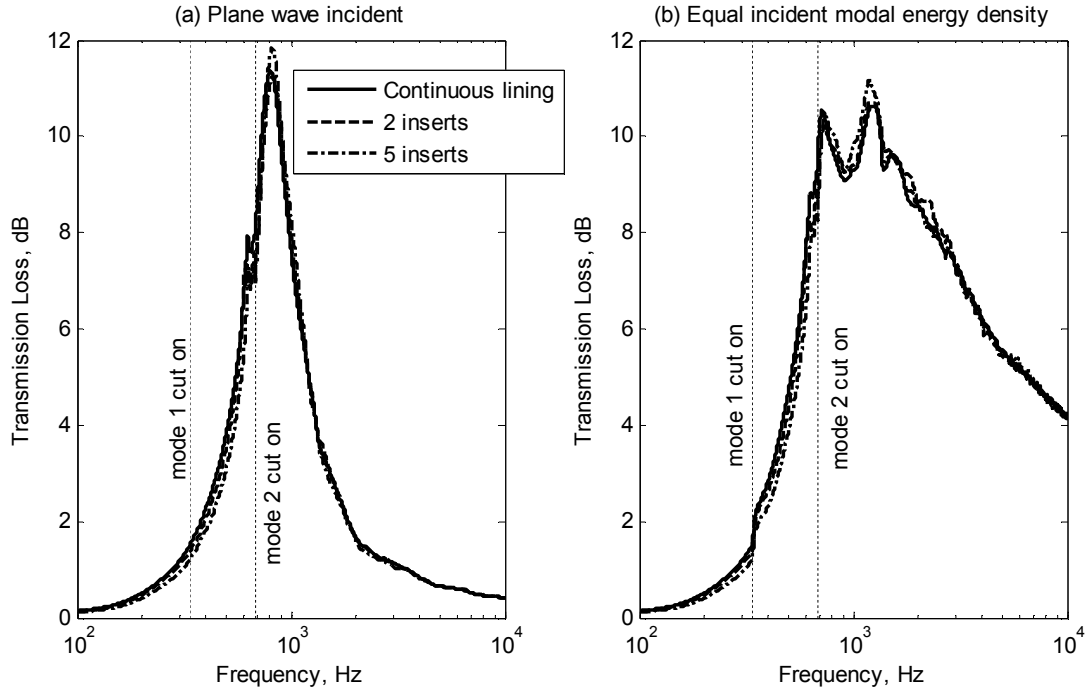

Figure 5.16: Comparison of transmission loss for a duct with a bulk-reacting lining, h = 500 mm, d = 40 mm and r = 13000 rayls/m between (a) plane wave incidence and (b) multi-mode incidence

5.9 Conclusions

In this chapter, an analytical model for sound propagation through a multi-segmented lined duct with either a locally reacting lining or bulk-reacting lining was developed. The analytical model is an extension from the analytical model of sound propagation through a finite length duct presented in the previous chapter. The calculation of wave mode amplitudes involves two steps; the backward step where the reflection matrices at each impedance mismatch junction are obtained, and the forward step, where from these reflection matrices, with known incident wave profile, the wave amplitudes in each duct section can be evaluated. Therefore, the wave amplitudes in each duct sections can be found in a direct manner such that no iteration is needed.

From the simulated results with a plane wave incidence, periodicity has little effect for a duct with a locally reacting lining. For a duct with a 40 mm thick lining, having four inserts of equal length increases the peak attenuation. For other cases considered of a duct with a locally reacting lining, periodicity reduces the peak attenuation while having very little effect on attenuation at other frequencies. Some improvements in attenuation are observed at high frequency if the length of lined section is less than half the airway height with a relatively longer unlined section. However, a dip in transmission loss occurs when higher order modes cut-on and this can give a reduction of 20 dB in peak attenuation compared to a continuously lined duct.

On the other hand, for ducts with a bulk-reacting lining with certain values of duct parameters, dividing the lining up into segments has quite a significant effect especially at the peak of duct transmission loss. This is shown in Figure 5.7, 5.11 and 5.12. This restricts axial waves travelling inside the lining and renders the bulk-reacting lining more similar to a locally reacting behaviour which generally has higher peak attenuation. From the simulation, it is found that a periodic arrangement improves the attenuation of a duct lined with a bulk-reacting lining at certain frequencies but reduces the performance at other frequencies. Therefore sectioning a bulk reacting lining in a periodic manner will not give a consistent improvement for a broadband application, but may be beneficial in applications when further attenuation is required at a prescribed frequency.

By considering multi-modal incidence with equal modal energy density in each wave, the transmission loss at high frequency is expected to be higher than for plane wave incidence. This is due to the presence of higher order modes in the incident field which are more readily attenuated compared to the fundamental mode.

6. Measurements of the insertion loss of a lined duct

The experimental measurement of a lined ventilation duct in an environment close to actual practice is important to support the validity and practicality of the developed theoretical model. This experimental work is divided into two parts. The first part is to determine the properties of the melamine foam based on the measured surface normal impedance using a standard impedance tube test. The second part is the measurement of the sound attenuation through a lined duct between the two reverberation chambers. From the material properties obtained in the first part, predictions of the transmission loss from the analytical model are obtained and compared with the measured insertion loss.

In the lined duct construction, melamine foam is used as the wall lining. Melamine foam has an open cell structure and is an isotropic material. It is one of the widely used materials for sound absorbing purposes due to its light weight and good sound absorbing properties. To get comparable numerical results for the duct performance, the acoustical properties of the melamine foam are required. These are and can be obtained by carrying out a standard impedance tube measurement.

6.1 Measurement of material properties of melamine foam

The semi-analytical impedance model in Appendix 1 requires three material properties, namely porosity, tortuosity and flow resistivity. Each of these parameters can be measured individually, for example using techniques introduced by Beranek [114], Champoux *et al*. [115] or Leonard [116] to measure porosity, electrical measurement [117] or ultrasonic measurement of transmitted waves [118, 119] to measure tortuosity, and direct [107], [120] or comparative methods [121] or acoustic transmissivity method [122] to measure flow resistivity. However a simpler way of estimating all these microstructure parameters is through curve fitting to measure the surface normal impedance. The semi-analytical impedance model is used to determine parameter values the unknown parameters that give the best fit curve to the measurements.

From a study on three different melamine foams by Kino and Ueno [105], the properties of the melamine samples given in Table 6.1 show that the values of tortuosity and porosity do not vary significantly between the three samples. Therefore the average values for these two properties are assumed to be $\varepsilon = 0.993$ and $s = 1.0056$. Then, the only parameter that is required is the flow resistivity, r. The value of r can be inferred by comparing a prediction and measurement of the surface normal impedance.

Table 6.1: Melamine foam properties [105]

	Foam 1	Foam 2	Foam 3
Density, ρ, kgm^{-3}	8.6	10.3	13.27
Flow resistivity, *r*, rayls/m	10500	13100	17500
Tortuosity, *s*	1.0059	1.0053	1.0055
Porosity, ε	0.995	0.993	0.992

The surface normal impedance of a melamine foam sample can be measured by using the standard impedance tube test. Samples of melamine foam have been obtained with thicknesses of 30, 37 and 50 mm. The surface normal impedance is measured according to the standard ISO 10534-2:2001 [123] and the detailed technique is given in Appendix 3. The measured results are shown in Figure 6.1.

Using the assumed values of ε , *s* and *r*, a plot of surface normal impedance $Z_n^{'}$ can be obtained from equation , and . The value of flow resistivity that best fits all three plots is found to be *r* = 25000 rayls/m.

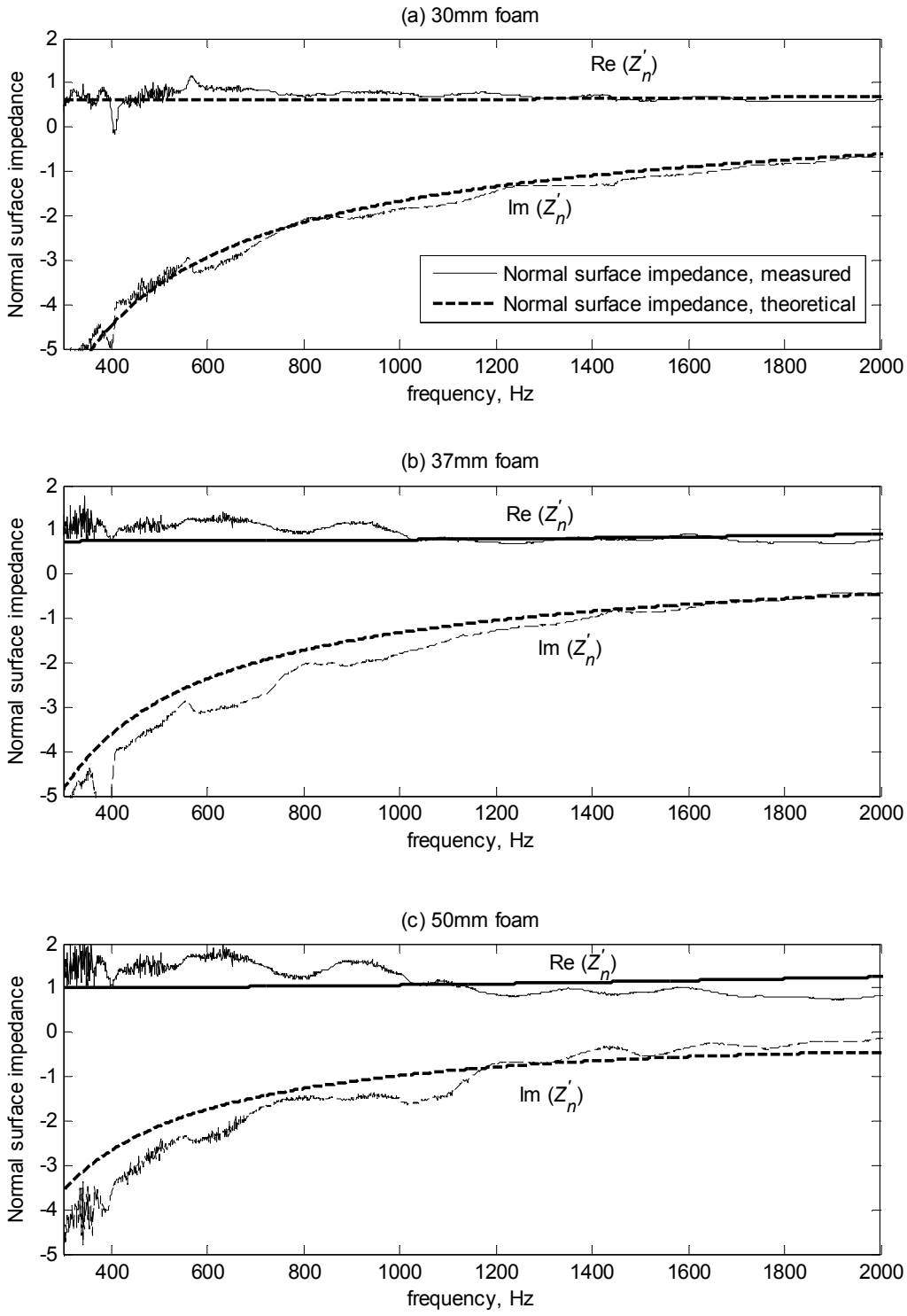

Figure 6.1: Measured and estimated non-dimensional surface normal impedance for three different thicknesses of melamine foam

6.2 Measurement of insertion loss of a lined duct

The main part of the experimental work is the measurement of insertion loss of a lined duct. The experimental work was carried out in two adjacent small reverberation chambers between which a 1.2 m long rectangular test duct was fitted. The rooms are located off room 4061 in the Tizard building at the University of Southampton and have dimensions of 2.5 x 2.4 x 2.6 m and 2.5 x 2.1 x 2.6 m. The bigger room is used as the source room and the other room as the receiving room. The standard procedure for measuring the insertion loss of lined duct is detailed in the standard ISO 7235:2009 [14]. However the reverberation rooms used in this work do not meet the requirements of this international standard [124] due to their smaller size. Therefore, the following measurements are not strictly according to the standard.

A sound field is generated in the source room by means of a loudspeaker. The sound is transmitted to the receiving room through the acoustic duct. The average sound pressure levels were measured within both reverberation rooms and are used to calculate duct insertion loss. The insertion loss is the decrease in the sound pressure level in the receiving room when a lined duct is installed in the connecting duct compared with an unlined duct of the same size and length. Insertion loss is measured instead of a transmission loss since it is easier to measure where, as well as the attenuation of the lined duct itself, the effects of the incident field and duct termination impedance would have to be taken into account. By using insertion loss these effects are minimised as much as possible by including the measurement of an unlined duct for the same excitation and duct termination conditions.

Before the measurement was carried out, the background noise of the two rooms was measured to ensure low noise level. Then the sound pressure level difference between the two rooms for an unlined duct was acquired and used as the reference value. Next, the unlined duct was replaced with a lined duct with various configurations. The sound pressure level difference between the two rooms was recorded for the various lining configurations. From the material properties determined in section 6.1, the predicted attenuation through the lined duct can be simulated using the analytical model and compared with the measured insertion loss. All measurements were performed in one-third octave bands.

6.2.1 Background noise and Schroeder frequency of reverberation rooms

Figure 6.2 shows the background noise measured at two positions in each room. The sound pressure amplitude was measured as a narrow frequency band spectrum and was then converted into one-third octave bands. When the measurements for the acoustic duct are carried out, the

test signal should be at least 15 dB greater than the background noise so that no background noise corrections are required on the measured data.

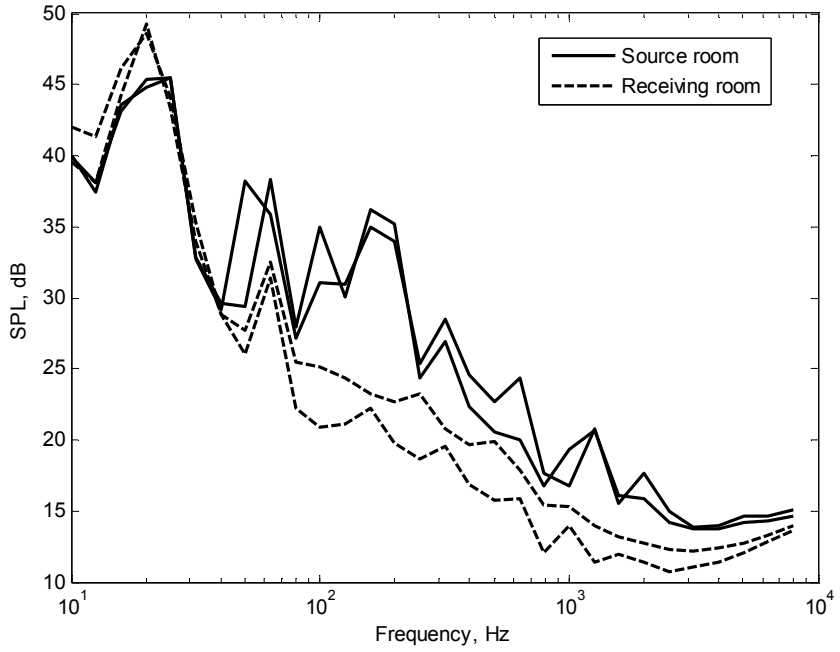

Figure 6.2: Background noise measured at two positions in source room and receiving room

The Schroeder frequency is an estimate of the boundary between the frequency region where individual room modes dominate the response, and the region where the sound field can be considered to be diffused. It can be estimated from the following formula [125]:

$$f_s = 2000\sqrt{\frac{T_{60}}{V}} \tag{6.1}$$

where V is the room volume and T_{60} is the reverberation time. The reverberation time of the source room can be estimated using the Sabine formula. The room walls are made up of painted concrete with an average absorption coefficient, $\bar{\alpha}$, of 0.03 [30]. The Sabine formula states that reverberation time is given by:

$$T_{60} = 55.3\frac{V}{c_0 A} \tag{6.2}$$

with $A = S\bar{\alpha}$ is the total absorption of all room surfaces. From the room's dimensions, the approximate valueof T_{60} for both rooms is 2 s which gives $f_s \simeq 700$ Hz.

6.2.2 Experimental setup

A rectangular duct was constructed using plywood with cross-sectional dimensions of 598 x 580 mm and with a length of 1.2 m. The outer rigid duct main frame has a thickness of 24 mm as shown in Figure 6.3 (a). Inside the main duct frame, four internal walls can be inserted and these walls form the different lining configurations required for testing. Two different duct airway widths are tested, (i) h = 430 mm as shown in Figure 6.3 (b) where sliding walls are placed on all four duct sides, and (ii) h = 155 mm where in addition to the four sides, another two walls are placed in the middle of the duct as shown in Figure 6.3 (c), hence dividing the duct into two smaller units.

The different lining configurations and wall arrangements tested are listed in Table 6.2 for ducts with an airway width of 430 mm and Table 6.3 for ducts with an airway width of 155 mm. Walls I, II and III refer to the arrangement shown in Figure 6.3 (b) and (c). Two different lining thicknesses were used in these experiments, 17 mm and 50 mm. Referring to Table 6.2, the first configuration is the unlined duct used as the reference duct. Ducts 2-4 have two opposite walls continuously lined with the melamine foam. An example of a continuously lined wall is shown in Figure 6.4. The lined section is 1 m in length, leaving 10 cm of unlined section at the duct entrance and exit. The foam is backed with a 10 mm thick plywood panel in each case within the 24 mm thick main frame.

The following configurations, ducts 5 and 6, have all of their four walls continuously lined with melamine foam. As well as these continuously lined ducts several periodically lined ducts are considered. Ducts 7-10 are similar to ducts 3-6 respectively, but with periodically lined walls. For these periodic linings, the foam is partitioned into 10 equal width sections with 10 mm thick plywood panels between them, as shown in Figure 6.5.

Ducts 11-16 in Table 6.3 have an airway width of 155 mm (Figure 6.3(c)). These ducts are lined only on the side walls, II and III. The side walls for ducts 11-13 are continuously lined while for ducts 14-16, the walls are periodically lined. Detailed drawings for all these wall configurations are given in Appendix 4.

The outer frame of the duct was inserted in the aperture between the two reverberation rooms as shown in Figure 6.6 and Figure 6.7. A wooden panel is used to seal any gap between the wall aperture and the duct outer frame. A schematic diagram of the experimental setup is shown in Figure 6.8. The sound pressure in each room was measured with four PCB microphones, with two microphones located in each room. These were located in turn at different positions giving a total of eight positions in each room. A Data Physics SignalCalc Dynamic Signal Analyzer was

used to acquire and process the measured signals from the microphones. A small loudspeaker driven from the output channel of the analyser was placed in the source room in the lower corner facing the wall away from the duct.

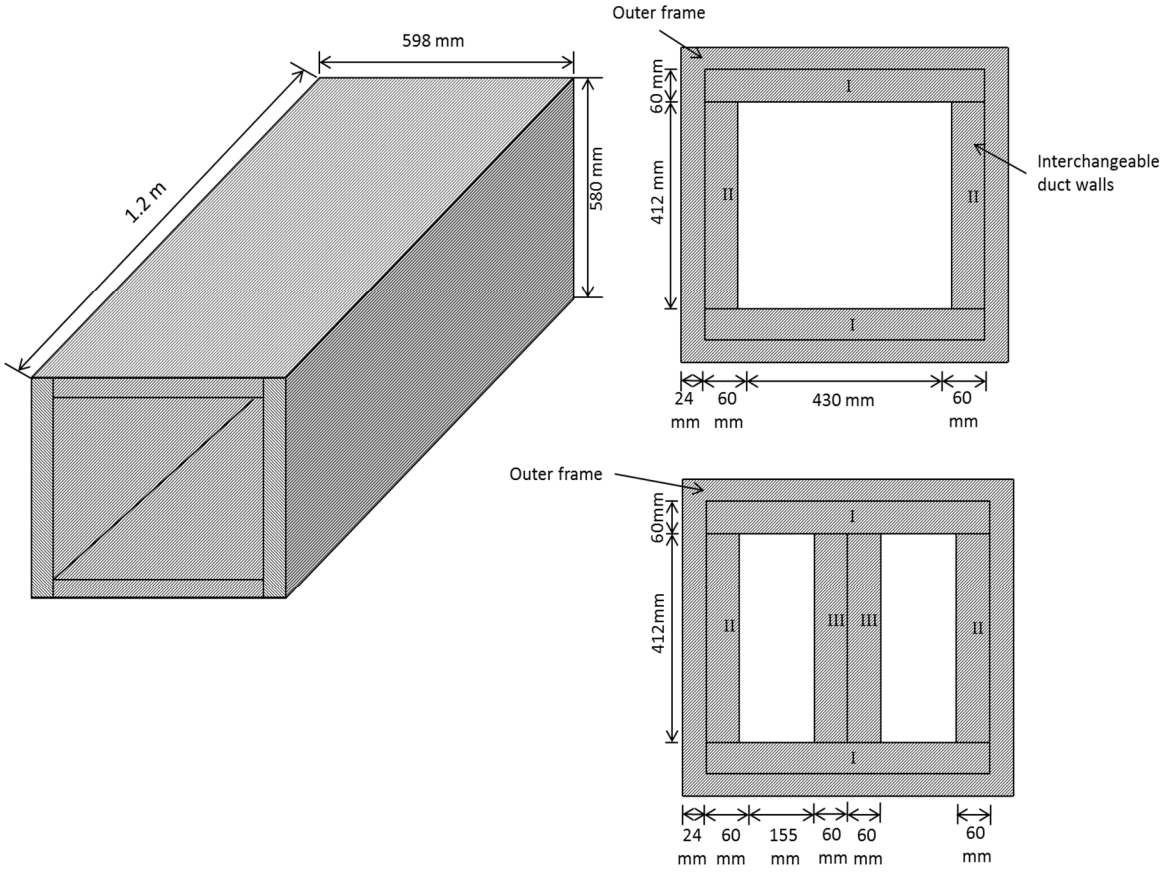

Figure 6.3: The constructed rectangular acoustic duct

Table 6.2: List of lined wall configurations for a duct with an airway width of 430 mm

		Lining thickness (mm)	
	Type of lining	Upper and lower walls (I)	Side walls (II)
1	Unlined	Rigid	Rigid
2	2 sided continuous lining	50	Rigid
3	2 sided continuous lining	Rigid	50
4	2 sided continuous lining	Rigid	17
5	4 sided continuous lining	50	50
6	4 sided continuous lining	50	17
7	2 sided periodic lining	Rigid	50
8	2 sided periodic lining	Rigid	17
9	4 sided periodic lining	50	50
10	4 sided periodic lining	50	17

Table 6.3: List of lined wall configurations for a duct with an airway width of 155 mm

		Lining thickness (mm)		
	Type of lining	Upper and lower walls (I)	Side walls (II)	Middle walls (III)
11	Continuous	Rigid	50	50
12	Continuous	Rigid	17	50
13	Continuous	Rigid	17	17
14	Periodic	Rigid	50	50
15	Periodic	Rigid	17	50
16	Periodic	Rigid	17	17

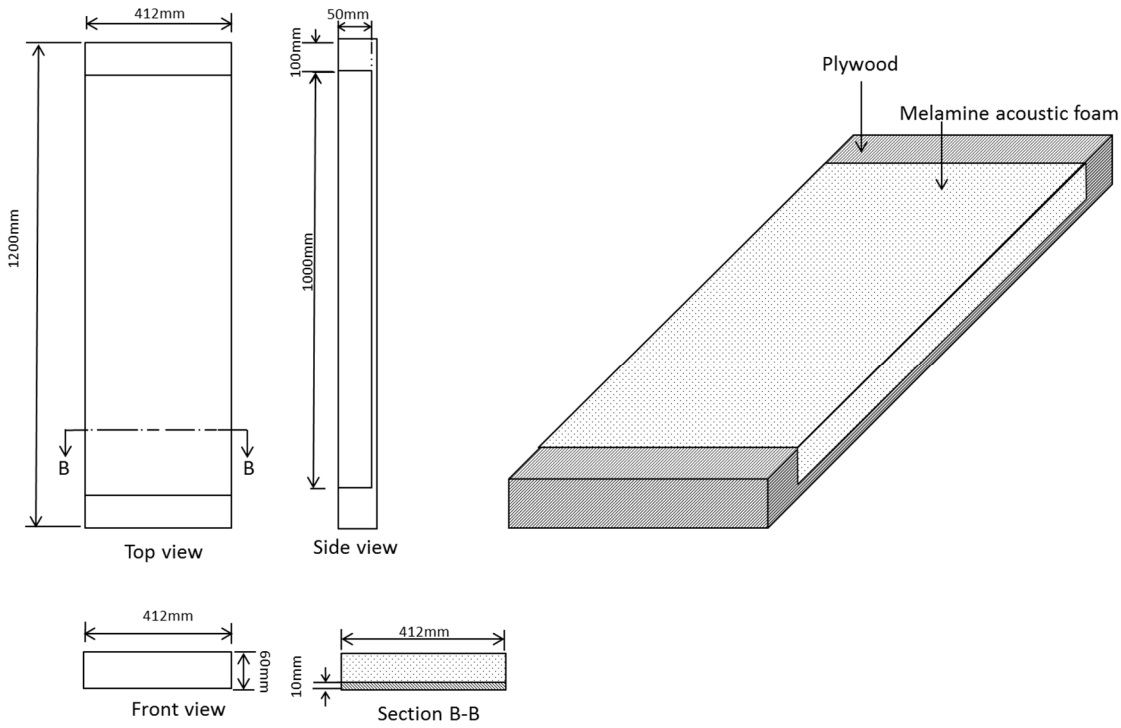

Figure 6.4: Configuration of the lined side walls

Figure 6.5: Periodically lined wall, side wall on the left and upper wall on the right

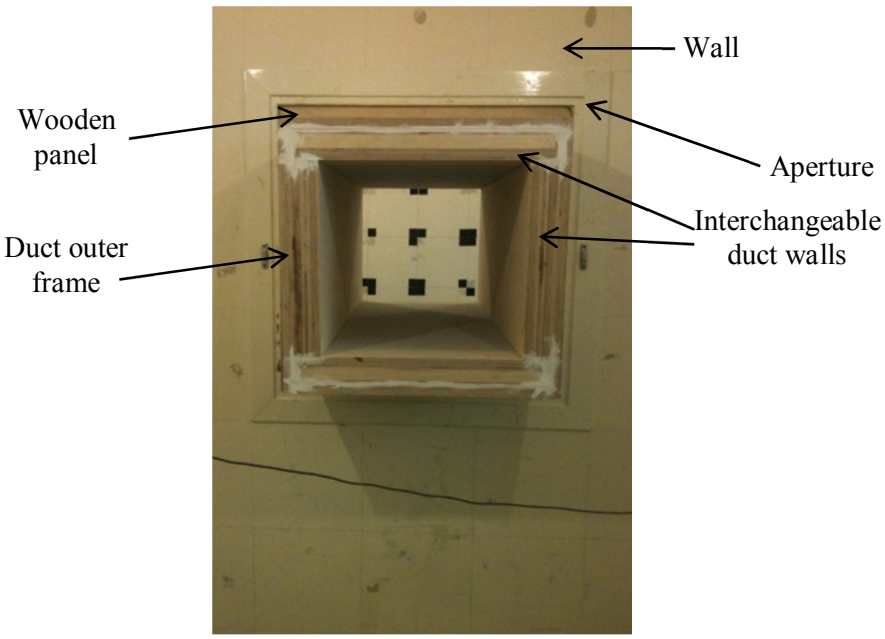

Figure 6.6: A test duct fit in the wall aperture

(a) Source room

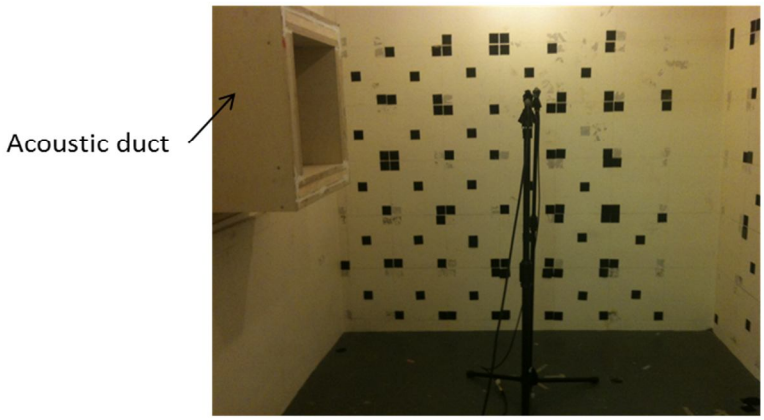

(b) Receiving room

Figure 6.7: Test rig in small reverberation rooms

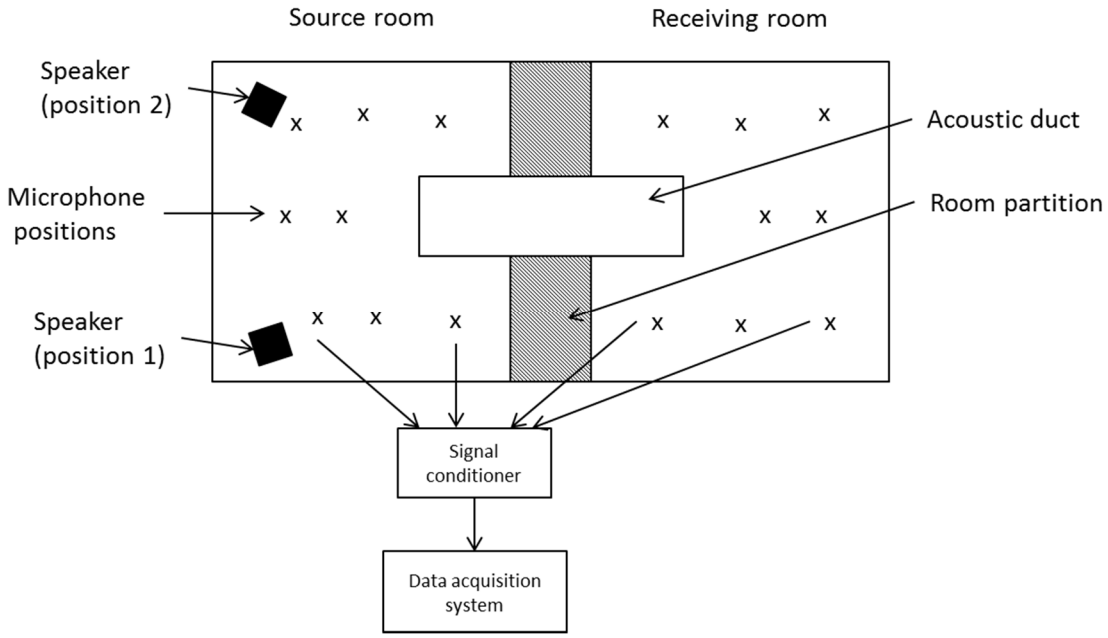

Figure 6.8: Schematic diagram of the reverberation room setup

6.2.3 Measurement of transmission loss of an unlined duct

Measurements were first carried out on an unlined duct where walls I and II in Figure 6.3 (b) are rigid. A pseudo-random signal was use to drive the loudspeaker in the source room. The sound pressures at the eight different positions were acquired twice, with two different positions of the loudspeaker as shown Figure 6.8, giving a total of 16 recorded sound pressures in each room. The acquisition time for each measurement is 5 minutes. The average one-third octave SPL in each room is given by:

$$L = 10\log_{10}\left(\frac{p_1^2 + p_2^2 + \ldots + p_n^2}{n\left(20\times10^{-6}\right)^2}\right)\text{dB} \tag{6.3}$$

where $n = 16$ is the number of microphone positions used, times the number of source positions. $p_1^2, p_2^2, \ldots, p_n^2$ are the one-third octave mean square sound pressures at each position. The level difference for the hard-walled duct is then given by:

$$\mathrm{D_{hw}} = L_s - L_r, \quad \text{dB} \tag{6.4}$$

where L_s is the average SPL in the source room and L_r is the average SPL in the receiving room. This measurement is used as the reference value. It includes the reflection at the duct entrance (and exit) which should be the same for the lined ducts.

6.2.4 Measurement of insertion loss of a lined duct

The rigid walls I and II were next replaced with lined walls as listed in Table 6.2. The procedure in section 6.2.3 was repeated to obtain the average level difference for a lined duct. The insertion loss, IL, is defined as the difference in D between a given duct configuration and the reference duct, in this case the unlined duct:

$$\mathrm{IL} = \mathrm{D_{ld}} - \mathrm{D_{hw}}, \mathrm{dB} \tag{6.5}$$

The procedure was repeated each configuration including the smaller airway widths where wall (III) was inserted in the middle of the duct as shown in Figure 6.3 (c) and measurements on all configurations listed in Table 6.3 were carried out.

6.3 Experimental results

Figure 6.9 shows the individual measured SPL in one-third octave bands in the source room, L_s, and the transmitted SPL in the receiving room, L_r through a fully lined duct (configuration 5). From the figure, above 600 Hz there is little variation between the different microphone positions implying that both source room and receiving room have a diffuse sound field. This can be compared with the estimated Schroeder frequency from equation (6.1) of 700 Hz. Below 600 Hz and particularly below 300 Hz there are differences between individual measured SPL due to the effects of room modes. The measured SPL in both rooms are well above the background noise (more than 10 dB) therefore background noise correction is not required for the measured data.

From the average SPL in both rooms, the level difference is calculated according to equation (6.4) and plotted in Figure 6.10. The transmission loss through the fully lined duct, where all duct sides are lined with 50 mm thick melamine foam, is compared with the transmission loss through an unlined duct. The difference between these two gives the insertion loss of the lined duct.

Figure 6.11 shows the measured insertion loss for three different duct configurations. The first is the fully lined duct discussed above, while the other two configurations are ducts lined only on two opposite sides, the left and right, and the upper and lower sides. The four dotted vertical lines indicate the frequencies at which higher order modes are predicted to cut on. The blue dotted lines refer to the cut-on frequency for modes across the duct width, and the red dotted lines refer to the cut-on frequency for modes across the duct height. From the airway width of 430 mm, mode 1 and mode 2 cut on at 396 Hz and 791 Hz, respectively, whereas from the

airway height of 412 mm, and mode 1 and mode 2 in the duct height cut on at 413 Hz and 826 Hz, respectively.

The insertion loss for the duct lined on all four sides is found to be almost double those of the duct lined on two sides at most high frequencies but less at the peak and lower frequencies. The peak attenuation of the duct lined on all four sides occurs at the same frequency as the duct lined on two sides, at the 630 Hz band. This finding agrees with the numerical result shown by Kakoty and Roy [61]. The peaks for the insertion loss of the two configurations lined on two sides occur at the same frequency. This is because the height of the duct is almost the same as its width. The peaks are well below the cut-on frequency of mode 2. These results agree broadly with the predicted transmission loss discussed in section 4.3.2.

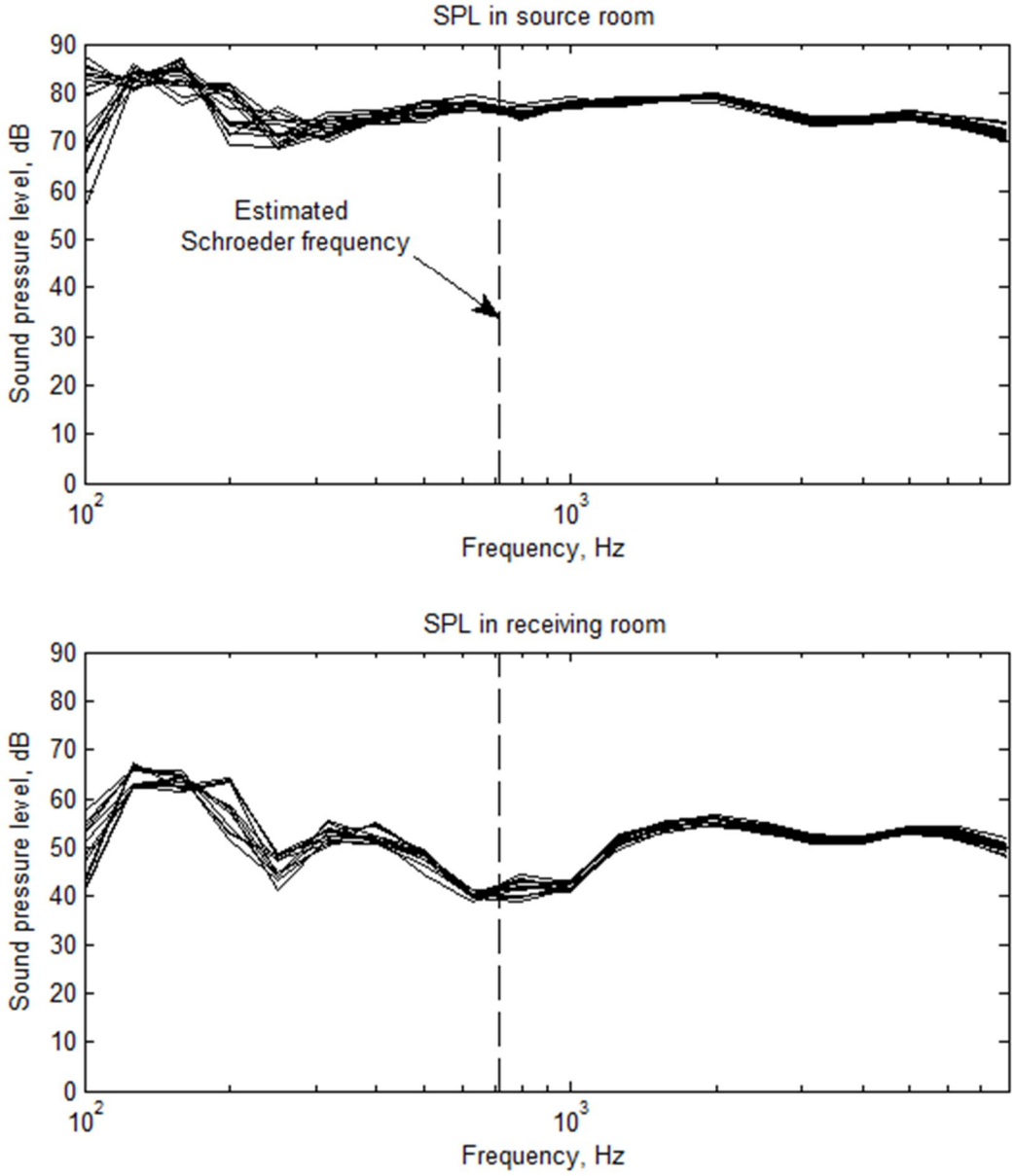

Figure 6.9: (a) SPL measured at eight different positions with two different loudspeaker locations in source room and (b) the measured SPL in receiving room due to transmitted sound through a fully lined duct (Duct 5 in Table 6.2)

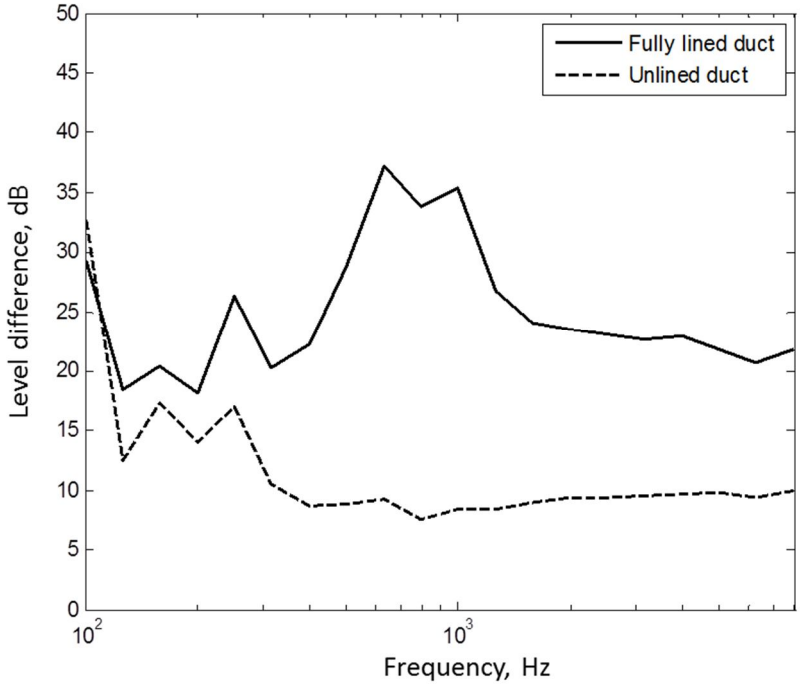

Figure 6.10: Transmission loss through a fully lined duct and an unlined duct

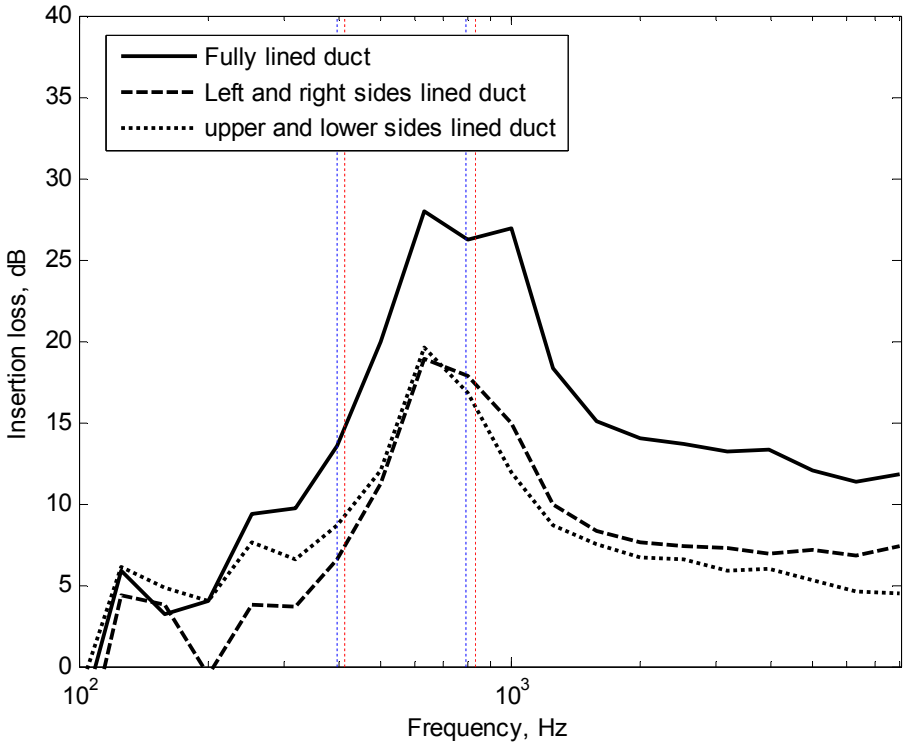

Figure 6.11: Insertion loss of a fully lined duct, and two sides lined ducts. Dotted lines indicate predicted cut-on frequencies of mode 1 and 2 across the width (blue) and across the height (red)

6.3.1 Vertical position of the microphone in test room

Most of the wall configurations considered were tested with the microphone height level at the centre of the duct vertical axis, at different room positions as shown in Figure 6.8. Since the centre of the duct vertical axis coincides with the room centre axis, this raise a question of how much the room modes in the vertical direction affect the accuracy of the measurement below the Schroeder frequency. Some additional measurements were taken to check whether these microphone positions give representative results. In these additional measurements the SPL was measured at various room positions and heights.

Figure 6.12 shows an example of the average measured SPL in the source room and the receiving room. The grey shaded region represents the confidence interval of the average measured SPL. The confidence interval indicates the reliability of the sample measurements and it is given by $CI = L \pm \Delta L$ where the 95% upper and lower limit, ΔL is given by $1.96\left(\sigma/\sqrt{n}\right)$. σ is the standard deviation of the 16 measured SPL, with $n = 16$. The dashed line is the average SPL from the set of measurements at the height of the duct centre. It shows that the average SPL from this second set lies well within the confidence interval of the other set at most frequencies, but below the Schroeder frequency some small systematic differences occur.

Figure 6.13 shows the calculated insertion loss obtained from the two sets of measurements for three example wall configurations for a duct with an airway height of 430 mm. Figure 6.14 shows the same result but for two configurations with an airway height of 155 mm. From these two figures, it is seen that the result obtained from the SPL measured at the height of the duct centre mostly lies within the confidence interval, especially at the peak frequency. However at frequencies with low attenuation, the calculated IL is below the shaded region, and below the Schroeder frequency there are systematic differences between the two results of up to 2 dB. However at this low frequency, the SPL is very much dominated by individual room modes and so less attention is given to this low frequency region. Above 500 Hz both sets of results give consistent results so the use of the central microphone height is acceptable and will be used in the remainder of this chapter.

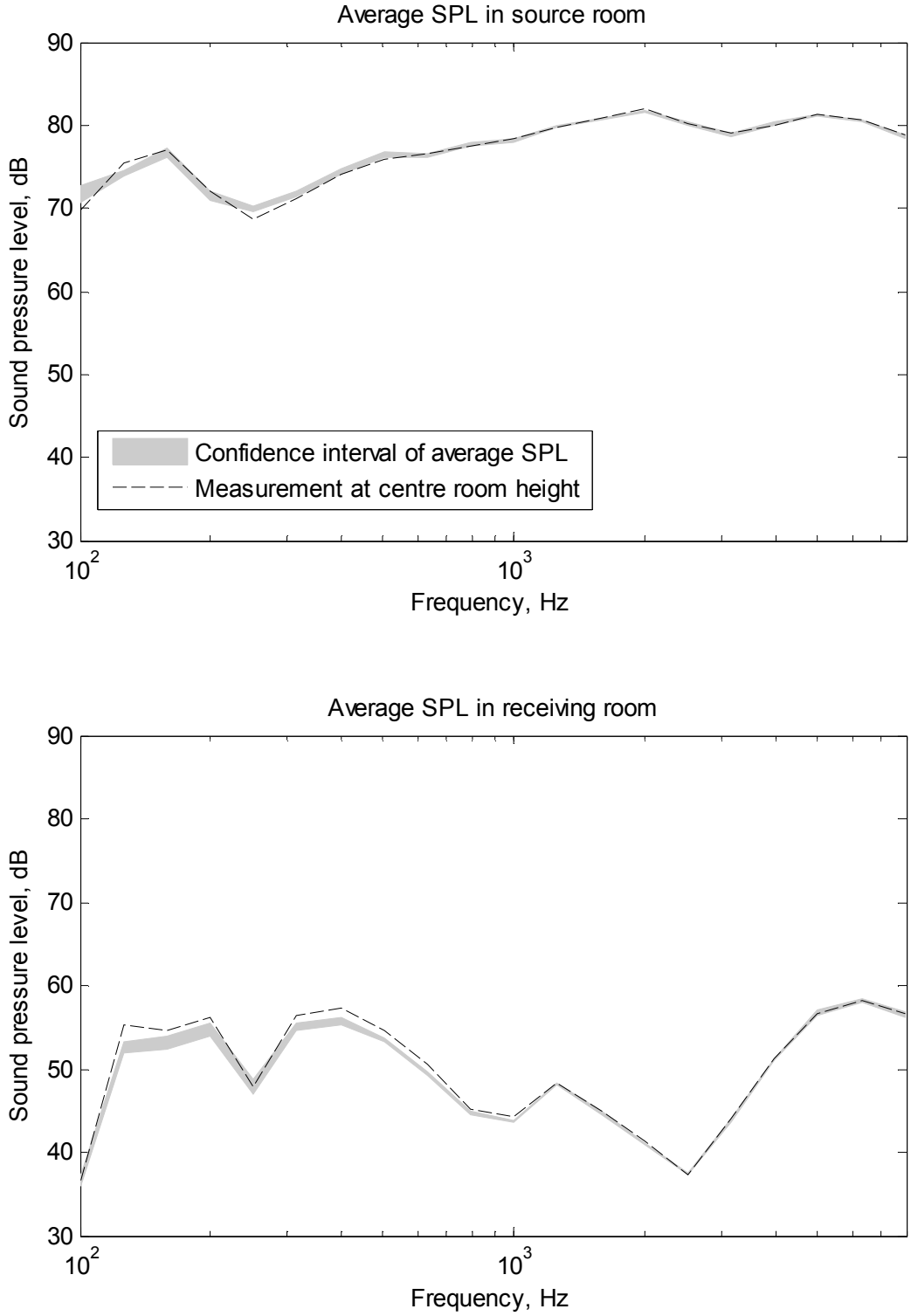

Figure 6.12: Average SPL obtained at various room height locations compared with the average SPL obtained at the centre room height. Measurement for Duct 12 in Table 6.3.

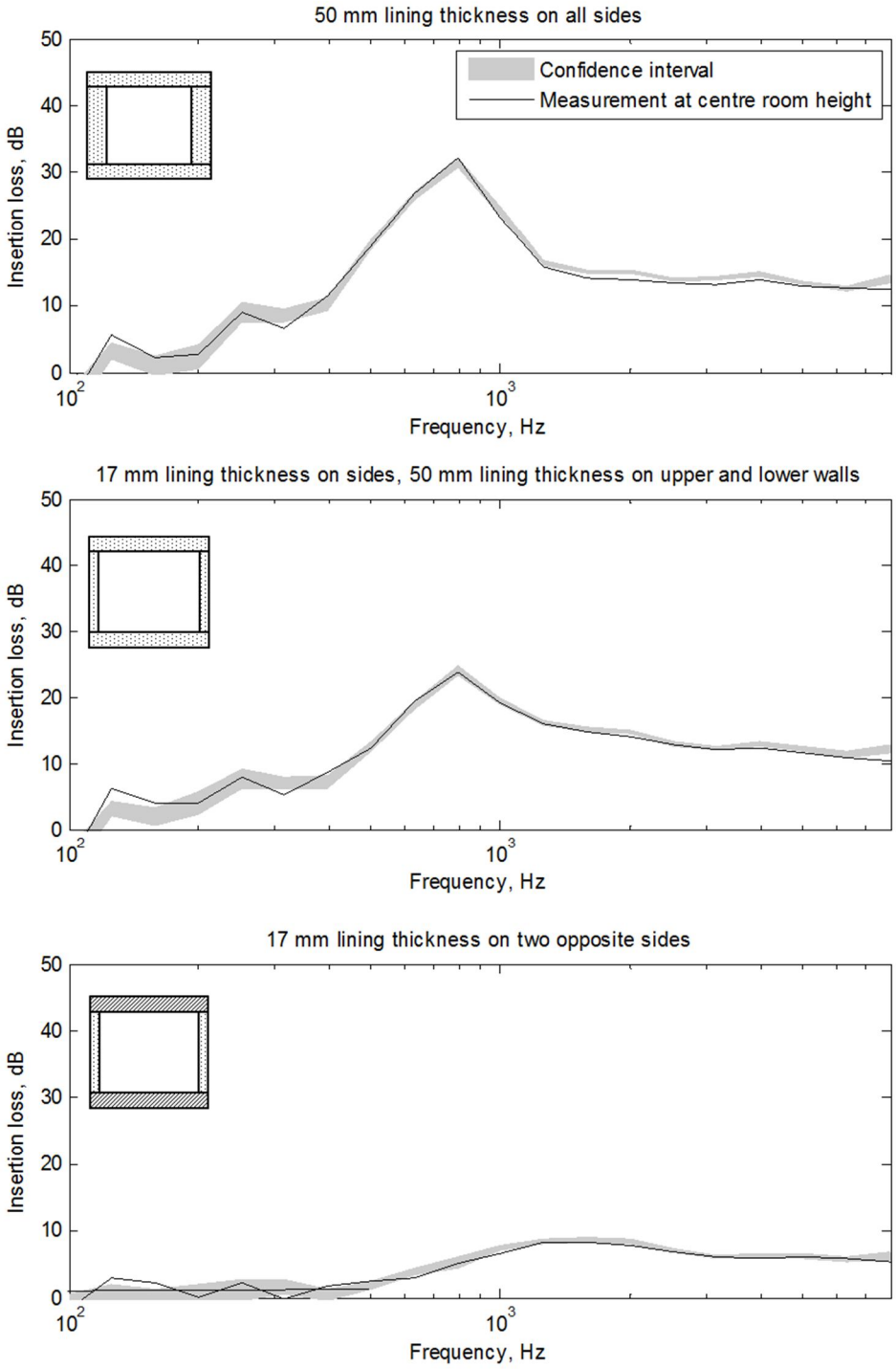

Figure 6.13: Comparison of insertion loss for a duct with an airway height of 430 mm, calculated from SPL from the two sets of measurement. Shaded region: confidence interval for measurement at different heights, solid line: average result for microphones at height of duct centre.

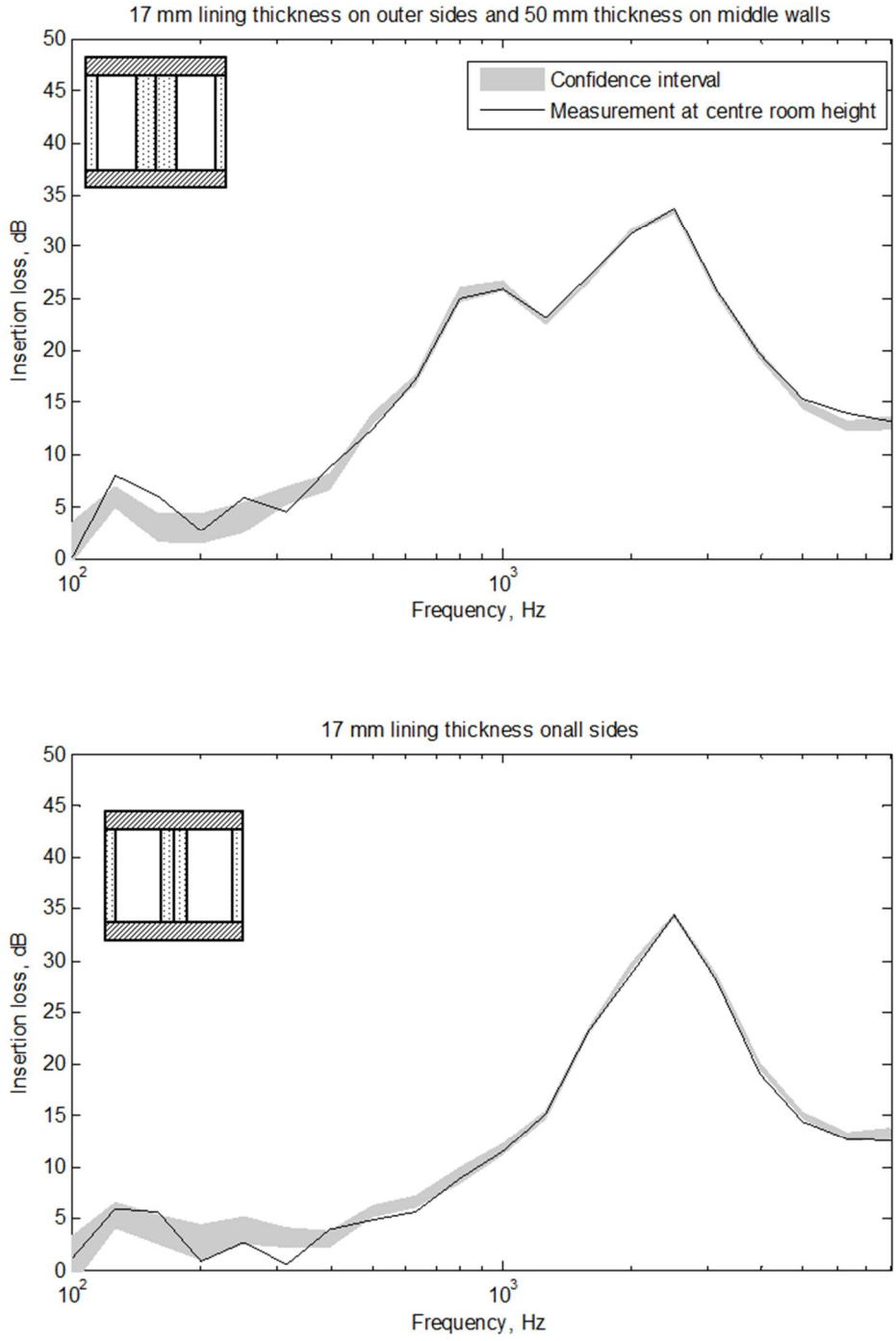

Figure 6.14: Comparison of insertion loss for a duct with an airway height of 155 mm, calculated from SPL from the two sets of measurement. Shaded region: confidence interval for measurement at different heights, solid line: average result for microphones at height of duct centre.

6.3.2 Comparison between measurement and theoretical prediction

The analytical model developed in Chapters 4 and 5 is based on two assumptions which are not reflected in the measurements: sound propagates as a two-dimensional field, and the inlet and outlet of the lined duct are connected to two semi-infinite unlined ducts. In practice sound propagates in three dimensions in the duct and the unlined sections at the duct inlet and outlet are open to the source and receiver rooms introducing reflection of sound at this boundary. The latter effect is compensated by the use of insertion loss.

Figure 6.15 shows comparisons between the measured insertion loss and the predicted transmission loss obtained from the derived analytical model in Chapter 4. The duct walls are lined with continuous lining and the comparison is given for four different duct configurations. The actual profile of the incident wave in the experiment is unknown, therefore the analytical model is used with two possible conditions: the incident wave carries only plane waves, or multi-modal incident waves are assumed with equal energy density according to equation (5.17) . Although in practice the latter condition is unlikely to occur, it is the most commonly used assumption in analysing sound transmission through a duct with multi-modal incidence [16].

From the figure it can be seen that the analytical model predicts the peak frequency quite well. Above the cut-on frequency, simulation results with equal energy density of multi-modal incident waves give a closer prediction to the measured insertion loss. This suggests that above the cut-on frequency, the incident field contains not only the plane wave, but higher order modes as well. The differences between the measured and simulated results are not surprising given the simplifications in the analytical model mentioned above.

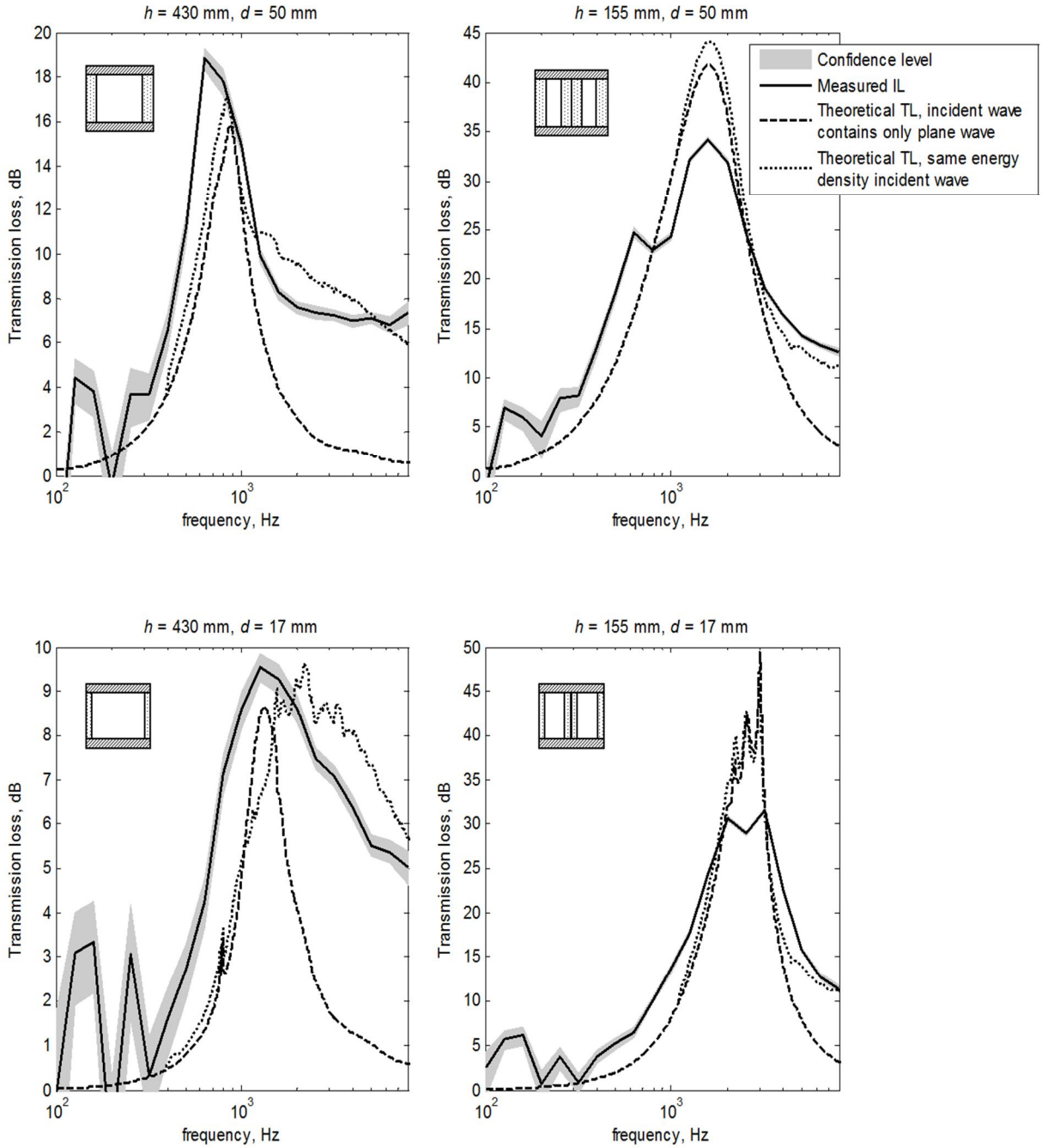

Figure 6.15: Comparison between measured insertion loss and the predicted transmission loss from the analytical model for ducts with continuous lining

6.3.3 Effect of periodicity: measurement and theoretical results

The continuous duct linings for the configurations shown in Figure 6.15 are now replaced with a periodic lining, as shown in Figure 6.5. From the results discussed in Chapter 5, periodicity is not expected to give significant improvement in the duct transmission loss. This is also shown in the predicted results when multi-modal incident waves with equal energy density are assumed as shown in Figure 6.16 and Figure 6.17.

Figure 6.16 (a) shows the comparison between the measured results and the theoretical results for a duct with an airway height of 430 mm. For a 50 mm thick liner the measurement shows that the periodic lining improves the attenuation at the peak frequency by up to 5 dB. However this improvement does not occur for the duct with the same airway height but with the thinner liner, d = 17 mm in Figure 6.16 (b). Figure 6.17 for the narrower airway exhibits an improvement in attenuation at the peak frequency due to periodicity for both lining thicknesses. None these improvements are found by the theoretical model. Although at low attenuations, the predicted results are close to the measured results, the differences at the peak frequency may be due to the actual incident wave profile which is not known and the inlet and outlet conditions of the duct in the experiment, which are not included in the theoretical model. It is widely agreed that the performance of segmented liners are sensitive to the incident modal content [96, 111].

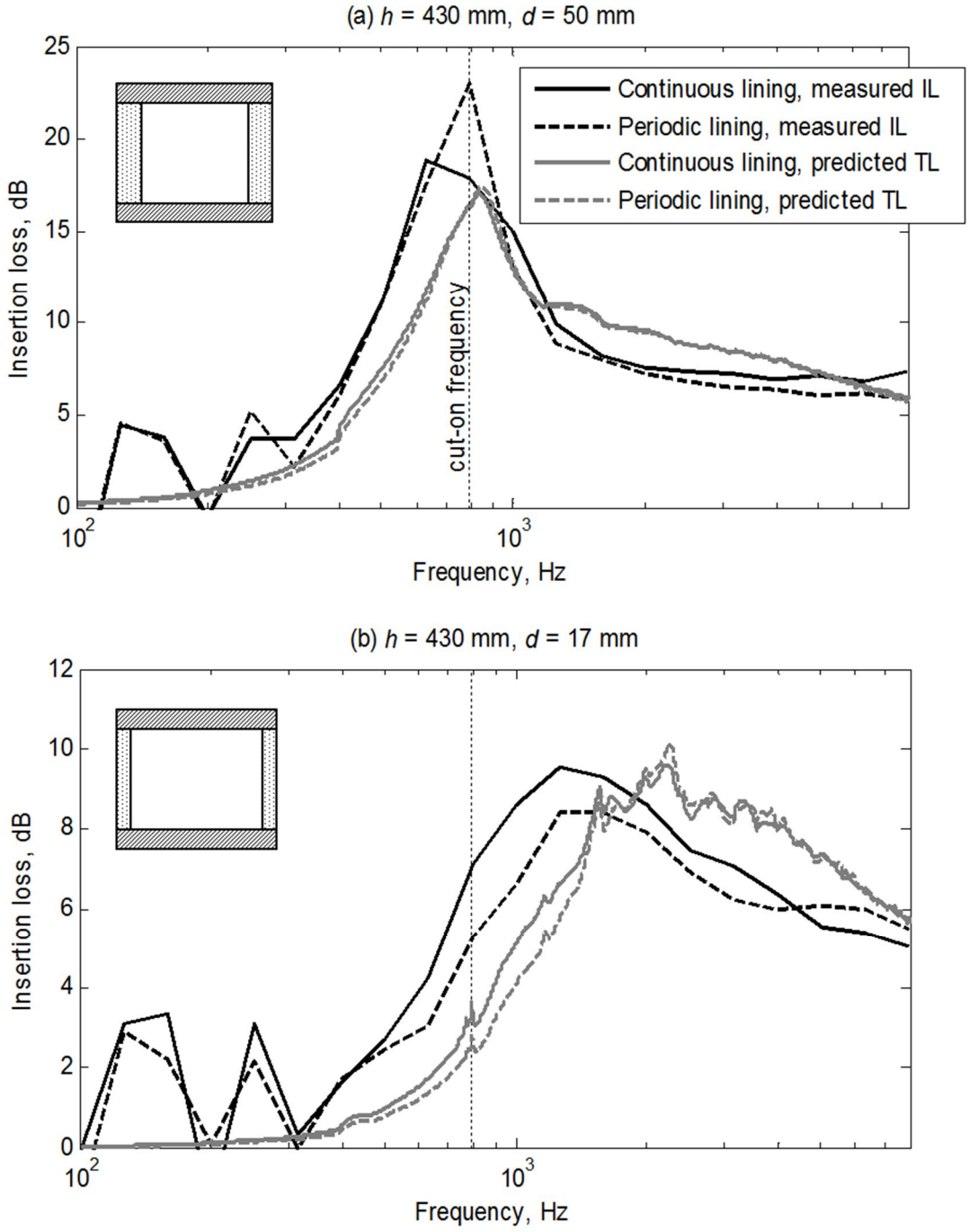

Figure 6.16: Effect of periodicity, measurement results (left) compared to theoretical prediction (right) for a duct with an airway height of 430 mm

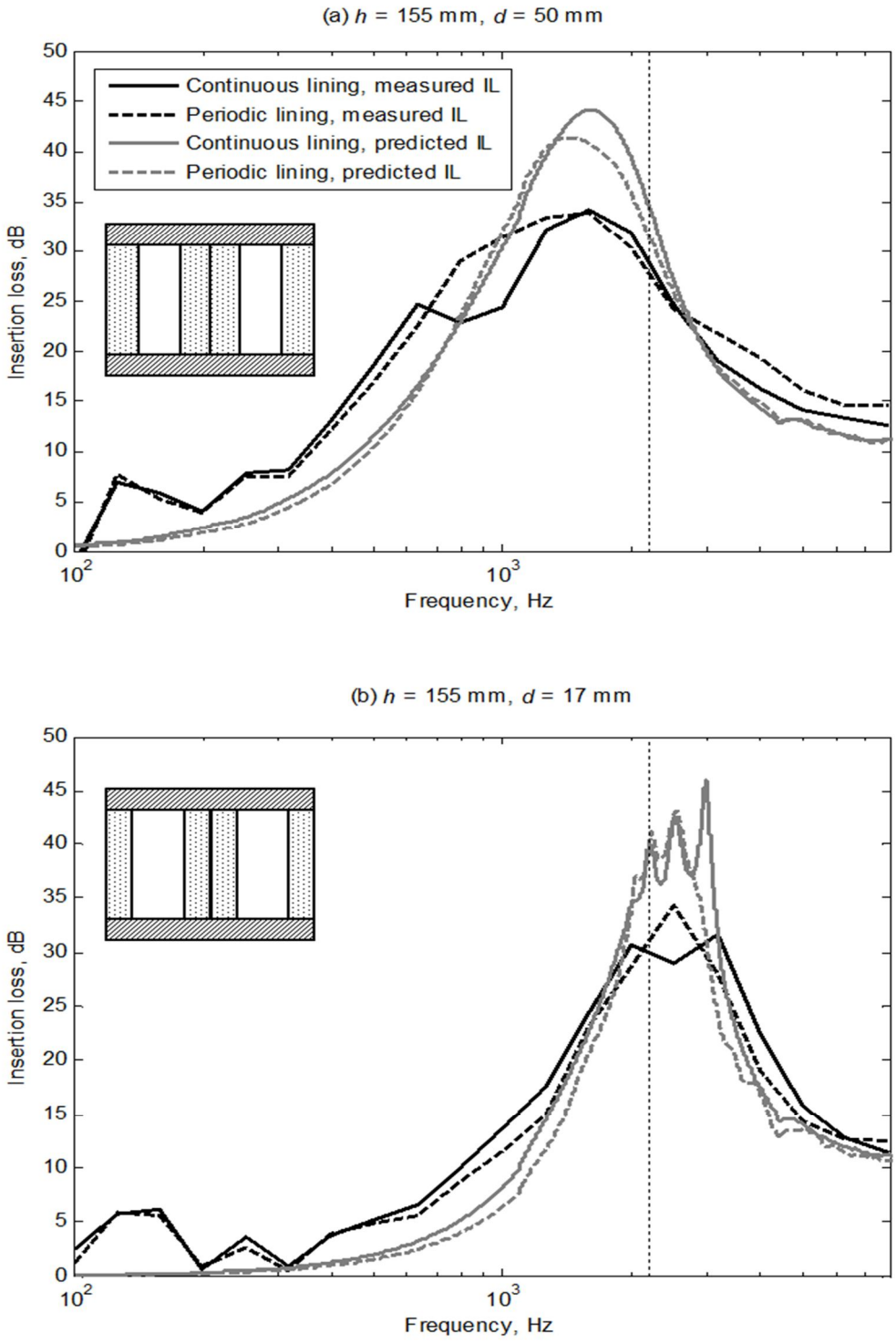

Figure 6.17: Effect of periodicity, measurement results compared to theoretical prediction for a duct with an airway height of 155 mm

6.3.4 Performance of a lined duct with different lining thickness on opposite sides

A duct with a thicker lining has a better attenuation at low frequency but at high frequency a better attenuation can be achieved by having a thin liner (see Figure 4.16). At low frequency, if the lining thickness is small compared with the wavelength, the amount of absorptive material available is not sufficient to dissipate a large amount of sound energy, hence the poor attenuation at low frequency. It is desirable in practice to have a good attenuation over a broader frequency range. The feasibility of having a combination of two different lining thicknesses is investigated here. The insertion loss of a duct lined with two different thicknesses on its two opposite walls is measured. The side walls are lined with 17 mm thick lining and the middle walls are lined with 50 mm thick lining as shown in the figure insert in Figure 6.18. The upper and lower walls are unlined and rigid.

The upper figure in Figure 6.18 shows the measured insertion loss for a duct with continuous linings and the lower plot is for a duct with periodic lining. The solid lines are the measured insertion loss when the duct is lined with both 17 mm and 50 mm thick lining. These results are compared with the measured insertion loss for a duct lined with 50 mm thick lining (dashed line) and the insertion loss for a duct lined with 17 mm thick lining (dotted line). From the results it can be seen that for both continuous and periodic lining, a combination of lining thicknesses combines the benefit of both lining thicknesses at low and high frequency, and hence broadens the frequency range of attenuation. Thus although the attenuation of a duct with different lining thicknesses lies in between the two reference cases, the effective frequency range is wider. The effectiveness of lining an acoustic duct with different lining thicknesses and/ or different material types can be explored further and from this initial result it shows a promising benefit.

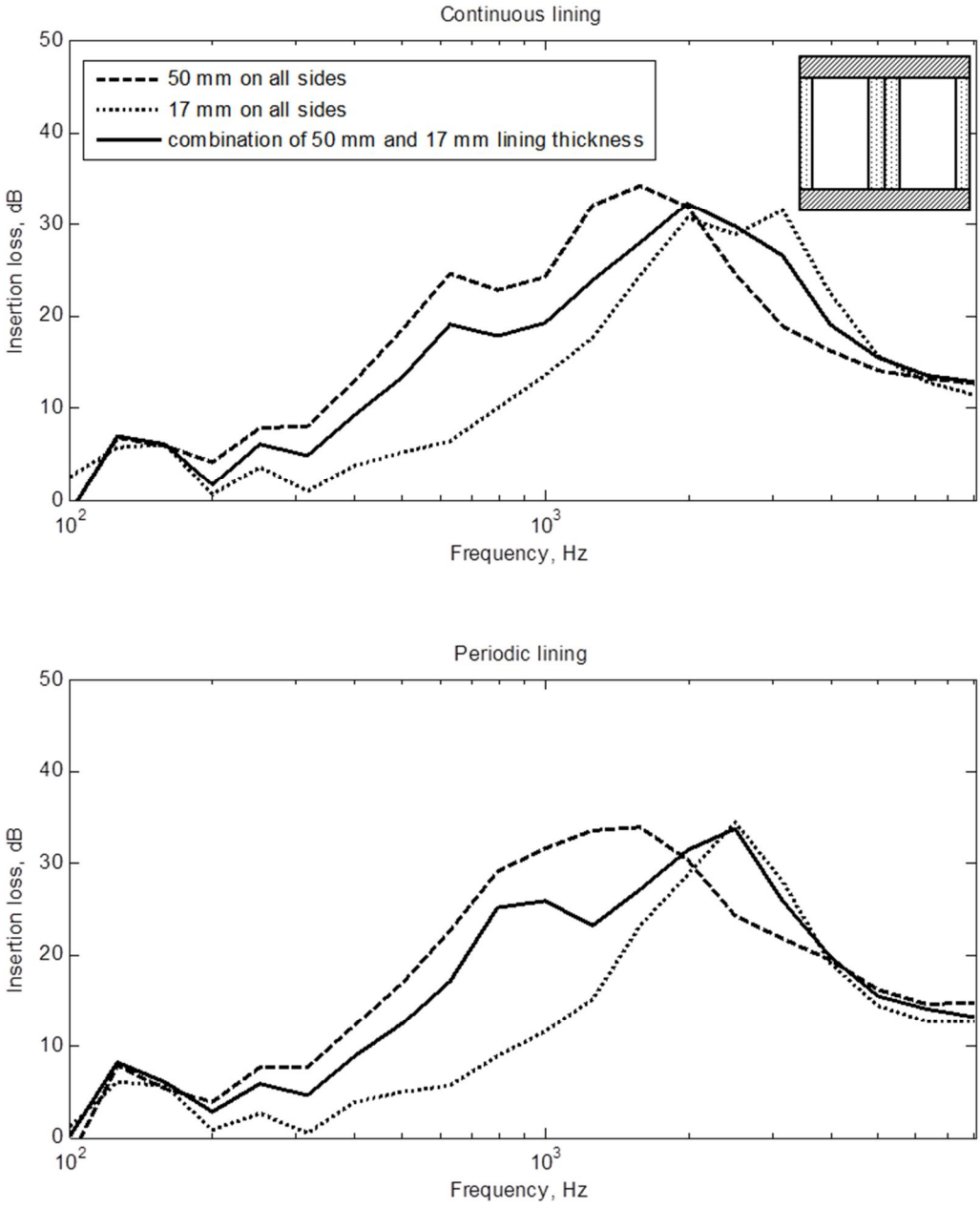

Figure 6.18: Comparison of insertion loss of a duct with the same lining thickness on its walls, and a duct with a combination of two different thicknesses on the opposite walls

6.4 Conclusions

In this chapter, initially the surface normal impedance of melamine foam was measured using the standard impedance tube. Values of porosity, and tortuosity, were assumed from the literature and the value of flow resistivity was inferred from the measured surface normal impedance. It was found that a value of r = 25000 rayls/m matches the experimental results well.

The main part of the experimental work involves the measurement of the insertion loss of a lined duct. Sixteen different wall configurations have been tested including both continuous lining and periodic lining. At low frequency, especially below 300 Hz, the measured results are very much influenced by room modes but in any case the attenuation is low. Above this frequency, the measured data appears to be reliable and can be used for comparison with the theoretical predictions.

A comparison is made between the measured insertion loss and the predicted theoretical results. The theoretical results are derived from a two-dimensional model, and do not fully represent the actual application when the duct is lined on all four sides. The provision of lining on four sides instead of two leads to a doubling of the attenuation. Three-dimensional effects are expected to be the primary source of discrepancy between theoretical results and measured results. However the main features of the behaviour of a lined duct can be shown by the theoretical approximation. The results show that the predicted peak frequency is quite close to that obtained from the measurement.

A simulated result with a multi-modal incident wave field with equal energy density in each mode shows a good agreement with the measurements at high frequency. This suggests that the incident wave field at the duct entrance contains higher order modes as would be expected for a source room with a diffuse field. The remaining differences between the measured and theoretical results may be due to the unknown actual incident wave profile. Furthermore the condition of the inlet and outlet termination in the theoretical model is assumed to be anechoic, which is different from the actual termination in the experimental setup. Although the use of an insertion loss based on a reference hard-walled duct mostly eliminates this effect, there may be remaining some differences caused by this.

While the theoretical prediction does not reveal any significant improvement in attenuation due to periodic lining, the measured insertion loss shows a noticeable improvement at the peak frequency of up to 5 dB. The fact that this is not predicted may be related to the aforementioned factors.

A combination of different lining thicknesses in a lined duct can give the benefits that both thicknesses can offer. This broadens the frequency range over which the duct can attenuate sound effectively, although it gives lower attenuations than were found at the original peak frequencies.

7. Conclusions and future work

7.1 Overall conclusions

The initial motivation for this work was the requirement to predict the performance of a duct with a section/s lined with a bulk-reacting lining as applied in ventilation ducts commonly used in naturally ventilated buildings. Such predictions are required so that the performance of a duct with different lining design parameters can be assessed easily. Furthermore the feasibility of lining a duct section in a periodic manner can also be studied. The predictions on duct attenuation with a locally reacting model and a bulk-reacting model are compared and analysed.

In this thesis, two-dimensional analytical models of sound propagation in a duct with a finite length lined section/s have been developed. Two types of lining behaviour have been considered: a locally reacting lining and a bulk-reacting lining. The mode-matching technique is used as the analytical tool in developing the model. This requires a complete set of wavenumbers, the process of acquiring which is addressed in Chapters 2 and 3. The technique itself is introduced in Chapter 4 where sound propagation through a finite lined duct system is modelled. The analytical model then is extended in a straight forward manner to include a multi-segmented lined duct and is presented in Chapter 5. Experimental work was carried out to validate theoretical predictions on duct attenuations and is presented in Chapter 6.

In a duct with a bulk-reacting lining, there exist additional modes termed the lining modes that depend on the lining thickness. These modes do not appear in a duct with a locally reacting lining or rigid-walled duct. The lining modes are found using Müller's method by working from low to high frequency with a frequency step of 1 Hz, provided that the solutions at the starting frequency are found by the argument principle method. At low frequency, these lining modes have a significant pressure distribution in the airway as well as in the lining, and their behaviour is similar to a typical duct mode. At high frequencies, these modes become localized in the lining. However, although the lining modes propagate in the lining they are well attenuated in the axial direction.

The lining modes in a duct with a bulk-reacting lining require additional equations for the mode matching technique. These additional equations are obtained by solving the boundary condition in the lining section at the junctions of the impedance discontinuity. The number of modes required to be included in the matching process depends on frequency and the number of modes that have cut on. For frequencies up to 10 kHz, 24 cut-off modes are shown to be sufficient in the case of a typical duct with a locally reacting lining. For a duct with a bulk-reacting lining, a

larger number of modes are required where in the study 50 airway modes are to be included in addition to all the lining modes whose transverse wavenumbers are less than the highest order cut-off airway mode.

For a liner that is thick relative to the airway height (duct with less than 80% airway opening), the peak attenuation occurs at a frequency below the cut-on frequency. The predicted attenuation from a locally reacting model will overestimate the peak attenuation compared to the predicted duct attenuation with a bulk-reacting model. However, for a duct with a thin liner, the duct attenuation predicted from a locally reacting model is lower at most frequencies compared to predictions with a bulk-reacting model.

Segmenting the wall lining into several sections in a periodic manner causes a bulk-reacting lining to behave in a locally reacting manner and this, in general, can improve the duct attenuation at the peak. However, for the case of a duct with a locally reacting lining, the effect of segmenting the wall lining is not significant and very little change in attenuation is caused by periodicity.

As well as excitation by a plane wave, a multi-modal incident field is also considered. The developed analytical model handles the two incident field assumptions well and gives a computational time of less than 15 minutes for a continuously lined duct with a locally reacting lining or a bulk-reacting lining. For a multi-segmented duct with for example 10 inserts, for a case with a bulk-reacting lining, the computation can take up to half an hour. However this computation time depends on frequency resolution, frequency range and the number of modes included in the calculation.

Based on the study with two incidence wave profiles, plane wave and multi-modal incident field, the results from segmenting the lined duct do not give significant improvement in the duct transmission loss. This finding does not support the reported performance of Soundscoop [12]. However, the other two factors, the position of the lined duct with respect to the plane of source and receiver, and the optimised duct cross section, have not been explored in this work.

It has been demonstrated in this thesis that the mode-matching model of sound propagation in a single insert lined duct can be extended to a multi-segmented duct in a straightforward manner. This includes the model for a duct with a bulk-reacting lining, which has yet to receive attention in the literature. The advantage of the mode matching technique is the ability to assess the impact of discontinuities in the wall impedance on the duct attenuation. Since the methods directly calculate the modal amplitudes, in-depth analysis of the scattering problem is made possible. Furthermore the approach to the mode matching technique used in this thesis enables

direct evaluation of wave amplitudes from known incident field such that no iteration is needed (in contrast to the method used in [67]).

Although the nature of the wavenumber solution for a rectangular lined duct with zero mean flow has been studied and it has been identified that two wave mode types exist in the case of bulk-reacting lining, the search for the initial guess for the lining mode is still deemed problematic. Problems in locating them at low frequency and for any value of d that could result in $m2d = Mh$, are due to the location of zeros and poles of the wavenumber function which are very close to each other. For these values of d it is difficult to identify the location of zeros for the lining modes at low frequency since they lie close to the solution for the airway mode.

While the analytical methods are based upon idealised geometry, they have been shown to provide a good approximation to experimental results for a broadband noise source. The predicted attenuation for a periodically lined duct shows only a small improvement compared to a continuously lined duct, while the experimental results show an improvement of up to 5 dB at the peak due to the segmented lining. One of the possible reasons is the unknown actual incident wave profile which according to the literature can have a great influence on the performance of a multi-segmented duct.

Furthermore, results from the experiment show that the two-dimensional analytical model gives a good approximation to the behaviour of a three-dimensional system. Considerable simplifications have been made and the complexity of the problem has been reduced to a great extent. This results in a short computation time, even when a large number of sections of lined duct is involved. However, the two-dimensional model cannot be used if the duct does not have a uniform cross-section across the width.

The same approach could in principle be used to handle changes in cross-section. Change of cross-section could be dealt with in a similar way to the bulk-reacting case where additional boundary conditions are required. However, in the presence of mean flow, this approach can be applied only to ducts with uniform cross-section in the axial direction [56].

A clear guideline for finding the roots to the eigenfunctions has been presented in chapters 2 and 3. However some difficulties are still encountered when dealing with a duct with certain ratios of duct height to lining thickness, as mentioned in 3.2.1. It would be interesting to extend this work to a three-dimensional model where the limitations of the two-dimensional model can be overcome. This applies to the high frequency region, especially for a multi-modal incident wave profile. A numerical approach is very viable and is a popular choice among researchers when dealing with three-dimensional ducts and with complicated duct geometry or multi-segmented

ones. However, it is more difficult to gain insight into physical understanding with such an approach. Although the analytical method appears to be more complicated compared with a numerical method, and is still limited to basic duct geometry such as cylindrical or rectangular, it can serve to validate the reults from numerical studies. Furthermore, it is important that the model should be able to cope well with the corner conditions, which could be challenging to apply in an analytical model of a three-dimensional duct.

7.2 Future work

This section outlines research areas and applications in which the work undertaken in the current study can be usefully extended by further investigation.

- Mean flow can be incorporated in the model developed here which would make it applicable to mufflers or turbo fan aero-engines.
- The two-dimensional model can be expanded into three-dimensions which is more of representative of the actual duct used in practice. Further attention may be required in modelling the sound field at the four duct corners. Computation time would also become an issue.
- It has been shown in this thesis that the modal contents of the incident field have an influence on the performance of a duct. Modal analysis can be carried out to identify the incident wave profile that can best bring out the potential of a periodic lining.
- It is possible that the position of the lined duct with respect to the plane of source and receiver, and the optimised duct cross section may actually improve the lined duct performance, and this is recommended for future work. Furthermore, the developed analytical model is two-dimensional and the inclusion of three-dimensional effects on the duct attenuation is another possible area to be explored.
- The analytical model can be modified to include expansion/ contraction lined segments. The peak attenuation is very much controlled by the duct airway height so this has a potential to broaden the effective attenuation bandwidth.
- Further experiments could be carried out where the wave modes are identified in the various segments, either in the laboratory or in situ

List of References

[1] WHO. (2013, 25 July 2013). *Global Health Observatory (GHO)*. Available: http://www.who.int/gho/urban_health/en/index.html

[2] C. Ghiaus and F. Allard, *Natural Ventilation in the Urban Environment: Assessment and Design* London: James & James, 2005.

[3] F. Allard, *Natural Ventilation in Buildings: A Design Handbook*. London: James & James, 1998.

[4] M. J. Mendell, W. J. Fisk, J. A. Deddens, W. G. Seavey, A. H. Smith, D. F. Smith*, et al.*, "Elevated sympton prevalence associated with ventilation type in office buildings," *Epidemiology,* vol. 7, pp. 583-589, 1996.

[5] K. J. Lomas, "Architectural design of an advanced naturally ventilated building form," *Energy and Buildings,* vol. 39, pp. 166-181, 2007.

[6] T. Kleiven, "Natural Ventilation in Buildings: Architectural Concepts, Consequences and Possibilities," Doktor Ingeniør Department of Architectural Design, History and Technology, Norwegian University of Science and Technology, Norway, 2003.

[7] D. J. Oldham, M. H. d. Salis, and S. Sharples, "Reducing the ingress of urban noise through natural ventilation openings," *Indoor Air,* vol. 14, pp. 118-126, 2004.

[8] HM. Government, *Approved Document F - Means of ventilation 2010 Edition*, H M Government, 2010.

[9] S. J. Emmerich, W. S. Dols, and J. W. Axley, "Natural ventilation review and plan for design and analysis tools," National Institute of Standards and Technology, Colorado2001.

[10] D. P. D. Hamlyn, J. D. Cash, C. J. Biggs, and S. D. Fitzgerald, "Whole building ventilation strategy selection - A toolkit," presented at the CIBSE Technical Symposium, De Montfort University, Leicester, UK 2011.

[11] M. H. F. De Salis, D. J. Oldham, and S. Sharples, "Noise control strategies for naturally ventilated buildings," *Building and Environment,* vol. 37, pp. 471-484, 2002.

[12] Passivent. (2011, 02/10/2012). *SoundScoop: Acoustic air transfer unit*. Available: http://www.passivent.com/soundscoop.html

[13] Z. Nunes and A. Rickard. (2011) An assessment of cross talk attenuation in line with natural ventilation. *Acoustics Bulletin* 32-38.

[14] BS EN ISO. 7235:2009, *Acoustics. Laboratory measurement procedures for ducted silencers and air-terminal units. Insertion loss, flow noise and total pressure loss*, British Standard Institution(2009).

[15] R. Kirby, "Predicting the acoustic performance of HVAC splitter silencers," *Noise & Vibration Worldwide,* vol. 38, pp. 20-24, 2007.

[16] R. Ramakrishnan and W. R. Watson, "Design curves for rectangular splitter silencers," *Applied Acoustics,* vol. 35, pp. 1-24, 1992.

[17] A. H. Nayfeh, J. Sun, and D. P. Telionis, "Effect of bulk-reacting liners on wave propagation in ducts," *AIAA Journal,* vol. 12, pp. 838-843, 1974.

[18] M. E. Aly and M. T. S. Badawy, "Sound propagation attenuation in lined annular-variable area ducts using bulk-reacting liners " *Applied acoustics,* vol. 62, pp. 769-778, 2001.

[19] T. Elnady, "Modelling and Characterization of Perforates in Lined Ducts and Mufflers (Paper III)," Ph.D, The Royal Institute of Technology (KTH), Stockholm, Sweeden, 2004.

[20] L. J. Sivian, "Sound propagation in ducts lined with absorbing materials," *Journal of the Acoustical Society of America,* vol. 9, pp. 135-140, 1937.

[21] P. M. Morse, "The transmission of sound inside pipes," *Journal of the Acoustical Society of America,* vol. 11, pp. 205-210, 1939.

[22] H. J. Sabine, "The absorption of noise in ventilating ducts," *Journal of the Acoustical Society of America,* vol. 12, pp. 53-57, 1940.

[23] R. Rogers, "The attenuation of sound in tubes," *The Journal of the Acoustical Society of America,* vol. 11, pp. 480-484, 1940.

[24] J. Kaiser, B. Shaker, and A. Nayfeh, "Influence of liner thickness on wave propagation in ducts," *Journal of Sound and Vibration,* vol. 37, pp. 169-183, 1974.

[25] D. L. Lansing and W. E. Zorumski, "Effects of wall admittance changes on duct transmission and radiation of sound," *Journal of Sound and Vibration,* vol. 27, pp. 85-100, 1973.

[26] K. U. Ingard, *Notes on sound absorption technology*. Poughkeepsie, NY, 1994.

[27] L. Rayleigh, *The theory of sound* vol. 2: Macmillan, 1896.

[28] R. A. Scott, "The absorption of sound in a homogeneous porous medium," *Proceedings of the Physical Society,* vol. 58, pp. 165-183, 1946.

[29] M. Delany and E. Bazley, "Acoustical properties of fibrous absorbent materials," *Applied acoustics,* vol. 3, pp. 105-116, 1970.

[30] T. Cox, *Acoustic absorbers and diffusers: theory, design and application*: Taylor & Francis, 2009.

[31] F. P. Mechel, *Formulas of acoustics* vol. 2: Springer, 2004.

[32] F. J. Fahy, *Foundations of engineering acoustics*. London: Academic Press, 2001.

[33] D. L. Johnson, J. Koplik, and R. Dashen, "Teory of dynamic permeability and tortuosity in fluid-saturated porous media," *Journal of Fluid Mechanics,* vol. 176, pp. 379-402, 1987.

[34] J. F. Allard and N. Atalla, *Propagation of Sound in Porous Media: Modelling Sound Absorbing Materials*, Second edition ed.: Wiley, 2009.

[35] Y. Champoux and J. F. Allard, "Dynamic tortuosity and bulk modulus in airsaturated porous media," *Journal of Applied Physics,* vol. 70, pp. 1975-1979, 1991.

[36] D. K. Wilson, "Simple, relaxational models for the acoustical properties of porous media," *Applied Acoustics,* vol. 50, pp. 171-188, 1997.

[37] L. L. Beranek, "Sound absorption in rectangular ducts," *Journal of the Acoustical Society of America,* vol. 12, pp. 228-231, 1940.

[38] R. A. Scott, "The propagation of sound between walls of porous material," *Proceedings of the Physical Society,* vol. 58, pp. 358-368, 1946.

[39] T. W. Wu and P. Zhang, "Boundary element analysis of mufflers with an improved method for deriving the four pole parameters," *Journal of Sound and Vibration,* vol. 217, pp. 767-779, 1998.

[40] D. W. Herrin, T. W. Wu, and A. F. Seybert, "Boundary element modelling," in *Handbook of Noise and Vibration Control*, M. J. Crocker, Ed., ed New York: Wiley, 2007, pp. 116-127.

[41] K. S. Peat and K. L. Rathi, "A finite element analysis of the convected acoustic wave motion in dissipative silencers," *Journal of Sound and Vibration,* vol. 184, pp. 529-545, 1995.

[42] R. J. Astley and A. Cummings, "A finite element scheme for attenuation in ducts lined with porous material: Comparison with experiment," *Journal of Sound and Vibration,* vol. 116, pp. 239-263, 1987.

[43] R. Astley, A. Cummings, and N. Sormaz, "A finite element scheme for acoustic propagation in flexible-walled ducts with bulk-reacting liners, and comparison with experiment," *Journal of sound and vibration,* vol. 150, pp. 119-138, 1991.

[44] D. W. Herrin, T. W. Wu, and A. F. Seybert, "Practical issues regarding the use of the finite and boundary element methods for acoustics," *Building Acoustics,* vol. 10, pp. 257-279, 2003.

[45] R. Kirby, "A comparison between analytic and numerical methods for modelling automotive dissipative silencers with mean flow," *Journal of Sound and Vibration,* vol. 325, pp. 565-582, 2009.

[46] W. Eversman, "Theoretical models for duct acoustic propagation and radiation," 1991.

[47] B. Nennig, E. Perrey-Debain, and M. Ben Tahar, "A mode matching method for modeling dissipative silencers lined with poroelastic materials and containing mean flow," *The Journal of the Acoustical Society of America,* vol. 128, pp. 3308-3320, 2010.

[48] P. M. Morse, "Some aspects of the theory of room acoustics," *The Journal of the Acoustical Society of America,* vol. 11, pp. 56-66, 1939.

[49] F. P. Mechel, "Modal Solutions in Rectangular Ducts Lined with Locally Reacting Absorbers," *Acta Acustica united with Acustica,* vol. 73, pp. 223-239, 1991.

[50] C. T. Molloy and E. Honigman, "Attenuation of Sound in Lined Circular Ducts," *The Journal of the Acoustical Society of America,* vol. 16, pp. 267-272, 1945.

[51] L. Cremer, "Theory regarding the attenuation of sound transmitted by air in a rectangular duct with an absorbing wall, and the maximum attenuation constant produced during this process," *Acustica,* vol. 3, pp. 249-263, 1953.

[52] S. W. Rienstra, *Hydrodynamic instabilities and surface waves in a flow over an impedance wall*: Nationaal Lucht-en Ruimtevaartlaboratorium, 1986.

[53] S. W. Rienstra, "A classification of duct modes based on surface waves," *Wave Motion* vol. 37, pp. 119-135, 2003.

[54] D. A. Bies and C. H. Hansen, *Engineering noise control*: Spon Press/Taylor & Francis, 2009.

[55] J. B. Lawrie and R. Kirby, "Mode-matching without root-finding: application to a dissipative silencer," *The Journal of the Acoustical Society of America,* vol. 119, p. 2050, 2006.

[56] R. Doolittle, H. Überall, and P. Uginčius, "Sound scattering by elastic cylinders," *The Journal of the Acoustical Society of America,* vol. 43, p. 1, 1968.

[57] F. Mechel, "Modal solutions in circular and annular ducts with locally or bulk reacting lining," *Acta Acustica united with Acustica,* vol. 84, pp. 201-222, 1998.

[58] W. Eversman, "Computation of axial and transverse wave numbers for uniform two-dimensional ducts with flow using a numerical integration scheme," *Journal of Sound Vibration,* vol. 41, pp. 252-255, 1975.

[59] W. Eversman, "Initial values for the integration scheme to compute the eigenvalues for propagation in ducts," *Journal of Sound and Vibration,* vol. 50, pp. 159-162, 1977.

[60] M. L. Munjal, "Analysis and design of pod silencers," *Journal of Sound and Vibration,* vol. 262, pp. 497-507, 2003.

[61] S. Kakoty and V. Roy, "Bulk reaction modeling of ducts with and without mean flow," *The Journal of the Acoustical Society of America,* vol. 112, pp. 75-83, 2002.

[62] A. Cummings and N. Somaz, "Acoustic attenuation in dissipative splitter silencers containing mean fluid flow," *Journal of Sound and Vibration,* vol. 168, pp. 209-227, 1993.

[63] W. Koch and W. Möhring, "Eigensolutions for liners in uniform mean flow ducts," *AIAA Journal,* vol. 21, pp. 200-213, 1983.

[64] S. W. Rienstra and N. Peake, "Modal scattering at an impedance transition in a lined flow duct," presented at the 11th AIAA/CEAS Aeroacoustics Conference (26th AIAA Aeroacoustics Conference), Monterey, California, 2005.

[65] W. Koch, "Attenuation of sound in multi-element acoustically lined rectangular ducts in the absence of mean flow," *Journal of Sound and Vibration,* vol. 52, pp. 459-496, 1977.

[66] G. Gabard and R. Astley, "A computational mode-matching approach for sound propagation in three-dimensional ducts with flow," *Journal of Sound and vibration,* vol. 315, pp. 1103-1124, 2008.

[67] A. Cummings, "High frequency ray acoustics models for duct silencers," *Journal of Sound and Vibration,* vol. 221, pp. 681-708, 1999.

[68] R. Mittra and S.-W. Lee, *Analytical techniques in the theory of guided waves*. New York: Macmillan, 1971.

[69] J. Barros and M. Moser, "Acoustic effects of broadening and contracting transition between ducts of different cross-section. part i: Theoretical treatment," *Acta Acustica united with Acustica,* vol. 89, pp. 416-425, 2003.

[70] J. Barros and M. Moser, "Acoustic ffeects of broadening and contracting transition between ducts of different cross-section. Part ii: Numerical results and measurements," *Acta Acustica united with Acustica,* vol. 90, pp. 221-231, 2004.

[71] L. Huang, "A theoretical study of duct noise control by flexible panels," *The Journal of the Acoustical Society of America,* vol. 106, pp. 1801-1809, 1999.

[72] L. Huang, "Modal analysis of a drumlike silencer," *The Journal of the Acoustical Society of America,* vol. 112, pp. 2014-2025, 2002.

[73] R. Kirby, "Transmission loss predictions for dissipative silencers of arbitrary cross section in the presence of mean flow," *The Journal of the Acoustical Society of America,* vol. 114, pp. 200-209, 2003.

[74] R. Kirby and J. Lawrie, "A point collocation approach to modelling large dissipative silencers," *Journal of sound and vibration,* vol. 286, pp. 313-339, 2005.

[75] R. Mittra and S.-W. Lee, "Analytical techniques in the theory of guided waves," 1971.

[76] S. W. Rienstra and A. Hirschberg, *An Introduction to Acoustics*, 2010.

[77] J. F. Unruh, "Finite length tuning for low frequency lining design," *Journal of Sound and Vibration,* vol. 45, pp. 5-14, 1976.

[78] M. S. Tsai, "Mode scatterer design for fan noise suppression in two-dimensional ducts," *Journal of Sound and Vibration,* vol. 83, pp. 501-512, 1982.

[79] L. Lafronza, A. McAlpine, A. Keane, and R. Astley, "Computer-aided liner optimization for broadband noise," presented at the 10th AIAA/CEAS aeroacoustics conference, Manchester, United Kingdom, 2004.

[80] A. McAlpine, R. J. Astley, V. J. T. Hii, N. J. Baker, and A. J. Kempton, "Acoustic scattering by an axially-segmented turbofan inlet duct liner at supersonic fan speeds," *Journal of Sound and Vibration,* vol. 294, pp. 780-806, 2006.

[81] T. Law, A. Dowling, and R. Corral, "Optimisation of axially segmented liners for aeroengine broadband noise," *Journal of Sound and Vibration,* vol. 329, pp. 4367-4379, 2010.

[82] D. Christie, "Theoretical attenuation of sound in a lined duct: some computer calculations," *Journal of Sound and Vibration,* vol. 17, pp. 283-286, 1971.

[83] R. Kirby, "The influence of baffle fairings on the acoustic performance of rectangular splitter silencers," *The Journal of the Acoustical Society of America,* vol. 118, pp. 2302-2312, 2005.

[84] J. Robinson and W. Watson, "Performance of a checkerboard liner with uncertain impedances," in *11th AIAA/CEAS Aeroacoustics Conference, Monterey, CA*, 2005, pp. 23-25.

[85] M. L. Munjal, *Acoustics of ducts and mufflers with application to exhaust and ventilation system design*: Wiley New York (NY) et al., 1987.

[86] C. Gerald and P. Wheatley, *Applied Numerical Analysis*: Addison-Wesley, USA, 2004.

[87] C. F. Gerald and P. O. Wheatley, *Applied Numerical Analysis, 7th ed., International ed.* Boston, MA: Pearson/Addison-Wesley, 2004.

[88] F. T. G. Berginc, "A numerical study of TM-type surface waves on a grounded dielectric slab covered by a doubly periodic array of metallic patches," *Progress In Electromagnetics Research,* vol. 43, pp. 75-100, 2003.

[89] J. M. Restrepo. (8th April 2011). Available: http://www.physics.arizona.edu/~restrepo/475A/Notes/sourcea-/node25.html

[90] I. L. Vér, "Acoustical design of parallel baffle mufflers," in *Proc.-Int. Conf. Noise Control Eng.;(United States)*, 1982.

[91] A. Cummings, "Sound attenuation in ducts lined on two opposite walls with porous material, with some applications to splitters," *Journal of Sound and Vibration,* vol. 49, pp. 9-35, 1976.

[92] A. Selamet, M. Xu, I. J. Lee, and N. Huff, "Analytical approach for sound attenuation in perforated dissipative silencers," *Acoustical Society of America Journal,* vol. 115, pp. 2091-2099, 2004.

[93] M. A. Biot, "Theory of Propagation of Elastic Waves in a Fluid-Saturated Porous Solid. I. Low-Frequency Range," *The Journal of the Acoustical Society of America,* vol. 28, pp. 168-178, 1956.

[94] M. A. Biot, "Theory of Propagation of Elastic Waves in a Fluid-Saturated Porous Solid. II. Higher Frequency Range," *The Journal of the Acoustical Society of America,* vol. 28, pp. 179-191, 1956.

[95] X. Sagartzazu, L. Hervella-Nieto, and J. Pagalday, "Review in sound absorbing materials," *Archives of Computational Methods in Engineering,* vol. 15, pp. 311-342, 2008.

[96] C. J. Brooks, "Prediction and control of sound propagation in turbofan engine bypass ducts," University of Southampton, 2007.

[97] B. R. Mace and E. Manconi, "Wave motion and dispersion phenomena: Veering, locking and strong coupling effects," *Journal of Acoustical Society of America,* vol. 131, pp. 1015-1028, 2012.

[98] N. C. Perkins and C. D. M. Jr., "Comments on curve veering in eigenvalue problems," *Journal of Sound and Vibration,* vol. 106, pp. 451-463, 1986.

[99] ASTM Standard E477, *Standard method of testing duct liner materials and prefabricated silencers for acoustical and airflow performance*, ASTM International, (1984).

[100] A. Cummings and I. J. Chang, "Sound attenuation of a finite length dissipative flow duct silencer with internal mean flow in the absorbent," *Journal of Sound and Vibration,* vol. 127, pp. 1-17, 1988.

[101] K. S. Peat, "A transfer matrix for an absorption silencer element," *Journal of sound and vibration,* vol. 146, pp. 353-360, 1991.

[102] R. Kirby, "Simplified techniques for predicting the transmission loss of a circular dissipative silencer," *Journal of Sound and Vibration,* vol. 243, pp. 403-426, 6/7/ 2001.

[103] R. Glav, "The transfer matrix for a dissipative silencer of arbitrary cross-section," *Journal of Sound and Vibration,* vol. 236, pp. 575-594, 2000.

[104] F. Mechel, "Numerical results to the theory of baffle-type silencers," *Acta Acustica united with Acustica,* vol. 72, pp. 7-20, 1990.

[105] N. Kino and T. Ueno, "Comparisons between characteristic lengths and fibre equivalent diameters in glass fibre and melamine foam materials of similar flow resistivity," *Applied Acoustics,* vol. 69, pp. 325-331, 2008.

[106] I. L. Vér and L. L. Beranek, *Noise and Vibration Control*: McGraw-Hill, 1971.

[107] D. Bies and C. H. Hansen, "Flow resistance information for acoustical design," *Applied Acoustics,* vol. 13, pp. 357-391, 1980.

[108] T. R. Law, A. P. Dowling, and R. Corral, "Optimisation of axially segmented liners for aeroengine broadband noise," *Journal of Sound and Vibration,* vol. 329, pp. 4367-4379, 2010.

[109] K. J. Baumeister, "Generalized wave envelope analysis of sound propagation in ducts with stepped noise source profiles and variable axial impedance," in *Presented at 2d Aeron. Specialists Conf., Hampton, Va., 24-26 Mar. 1975; sponsored by AIAA*, 1975, pp. 24-26.

[110] D. T. Sawdy, R. Beckemeyer, and J. D. Patterson, "Analytical and experimental studies of an optimum multisegment phased liner noise suppression concept," *Final Report Boeing Co., Wichita, KS.,* vol. 1, 1976.

[111] K. J. Baumeister, "Evaluation of optimized multisectioned acoustic liners," *AIAA Journal,* vol. 17, pp. 1185-1192, 1979.

[112] R. Mani, "Acoustic duct with peripherally segmented acoustic treatment," ed: Google Patents, 1976.

[113] M. Howe, "The attenuation of sound in a randomly lined duct," *Journal of Sound and Vibration,* vol. 87, pp. 83-103, 1983.

[114] L. L. Beranek, "Acoustic impedance of porous materials," *The Journal of the Acoustical Society of America,* vol. 13, p. 248, 1942.

[115] Y. Champoux, M. R. Stinson, and G. A. Daigle, "Air-based system for the measurement of porosity," *The Journal of the Acoustical Society of America,* vol. 89, pp. 910-916, 1991.

[116] R. Leonard, "Simplified porosity measurements," *The Journal of the Acoustical Society of America,* vol. 20, p. 39, 1948.

[117] D. L. Johnson, T. Plona, C. Scala, F. Pasierb, and H. Kojima, "Tortuosity and acoustic slow waves," *Physical Review Letters,* vol. 49, pp. 1840-1844, 1982.

[118] C. W. Kosten and C. Zwikker, *Sound Absorbing Materials*: Elsevier, 1949.

[119] Z. E. A. Fellah, M. Fellah, W. Lauriks, and C. Depollier, "Direct and inverse scattering of transient acoustic waves by a slab of rigid porous material," *The Journal of the Acoustical Society of America,* vol. 113, pp. 61-72, 2003.

[120] L. B. Richard and H. B. Richard, "The Measurement of Flow Resistance of Porous Acoustic Materials," *The Journal of the Acoustical Society of America,* vol. 13, pp. 337-344, 1942.

[121] R. S. Michael and A. D. Gilles, "Electronic system for the measurement of flow resistance," *The Journal of the Acoustical Society of America,* vol. 83, pp. 2422-2428, 1988.

[122] Z. E. A. Fellah, M. Fellah, N. Sebaa, W. Lauriks, and C. Depollier, "Measuring flow resistivity of porous materials at low frequencies range via acoustic transmitted waves," *The Journal of the Acoustical Society of America,* vol. 119, pp. 1926-1928, 2006.

[123] BS EN ISO 10534-2:2001, *Acoustics-Determination of sound absorption coefficient and impedance in impedance tubes-Part 2: Transfer-function method*. British Standard Institution (2001).

[124] BS EN ISO 3741:2010, *Acoustics - Determination of sound power levels and sound energy levels of noise sources using sound pressure - Precision methods for reverberation test rooms*, British Standard Institution (2010).

[125] M. R. Schroeder, "The "Schroeder frequency" revisited," *Journal of Acoustical Society of America,* vol. 99, pp. 3240-3241, 1996.

[126] E. T. Copson, *An introduction to the theory of functions of a complex variable*: Clarendon Press Oxford, 1935.

[127] P. Brazier-Smith and J. Scott, "On the determination of the roots of dispersion equations by use of winding number integrals," *Journal of sound and vibration,* vol. 145, pp. 503-510, 1991.

Appendix 1

Semi-analytical material model

To model the sound propagation within an absorptive material a semi-analytical approach is used. A simple semi-analytical model provided by Fahy [32] use the conservation of mass and momentum to come with a modified linearized wave equation that took into account the effects of porosity, ε, tortuosity, s, and flow resistivity, r . In one dimensional form this is given by:

$$\frac{\partial^2 p}{\partial x^2} = \frac{s}{c_0^2}\frac{\partial^2 p}{\partial t^2} + \frac{r\varepsilon}{\rho_0 c_0^2}\frac{\partial p}{\partial t} \tag{A1.1}$$

where p is the acoustic pressure, ρ_0 is the density of air, c_0 is the speed of sound in air, x is the spatial coordinate, and t is time. For harmonic motion at circular frequency ω, substituting wave type solutions of the form $p(x,t) = Ae^{i(\omega t - \tilde{k}x)}$ into the above equation gives the non-dimensional wavenumber, k':

$$k' = \frac{\tilde{k}}{k_0} = s^{1/2}\left(1 - \frac{i}{\Omega}\right)^{1/2} \tag{A1.2}$$

where $\tilde{k}$ is the complex wavenumber in the porous material, $k_0 = \omega/c_0$ is the wavenumber in air, and $\Omega = \omega\rho_0 s/r\varepsilon$ is a non-dimensional frequency. The ratio of the characteristic specific acoustic impedance to that of air is given by:

$$Z_c' = \frac{Z_c}{\rho_0 c_0} = \frac{k'}{\varepsilon} \tag{A1.3}$$

and from , the non-dimensional characteristic specific acoustic impedance can be written as:

$$Z_c' = \frac{s^{1/2}}{\varepsilon}\left(1 - \frac{i}{\Omega}\right)^{1/2} \tag{A1.4}$$

Since $Z = \tilde{\rho}\tilde{c}$ and $\tilde{k} = \omega/\tilde{c}$, the complex density of the bulk material can be written as:

$$\tilde{\rho} = s\frac{\rho_0}{\varepsilon} - i\frac{r}{\omega} \tag{A1.5}$$

Appendix 1

For a finite depth layer of sound-absorbent material of thickness *d* mounted on a rigid backing, the non-dimensional surface normal impedance is given by:

$$Z_n' = -iZ'_c \cot \tilde{k}d \tag{A1.6}$$

Figure shows the plot of Z'_c and Z'_n for typical parameters as listed in Table 3.1.

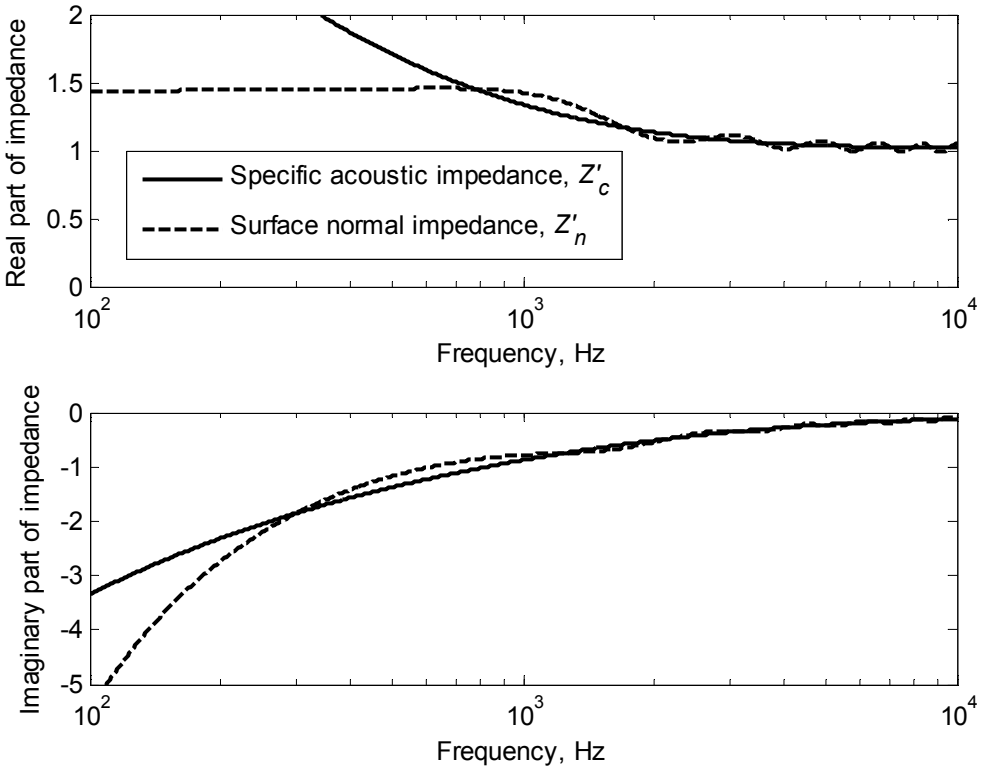

Figure A1.1: The plot of non-dimensional specific acoustic impedance and non-dimensional surface normal impedance for a typical material parameters listed in Table 3.1.

Appendix 2

Use of the argument principle method to find transverse wavenumbers

Consider a function $F(z)$ to be analytic over a region in the complex z-plane except for n_p simple poles. Moreover it is assumed that the function also contains n_z zeros. From Cauchy's theorem of residues [126],

$$\frac{1}{2\pi i}\oint_C \frac{F'}{F}dz = n_z - n_p \tag{A2.1}$$

where the winding number is defined as the difference between the number of zeros and poles, $n_z - n_p$, of the function F, and C is an anti-clockwise path enclosing the region. A rectangular search area is used where the overall search region is divided into smaller grids. Care has to be taken to ensure that the contour path does not lie on any of the function's poles.

Suppose for example, a region contains only one zero. The winding number N then is 1. If N = 0, it is possible that there is no zero or pole in the region, or that there is one zero and one pole in the region, or indeed more than one. These cases can be distinguished by taking higher moments of the winding number integral [127]. This is done by weighting the integrand in equation by z^n:

$$I_n = \frac{1}{2\pi i}\oint_C z^n \frac{F'}{F}dz = \sum_i \left(z_z^i\right)^n - \sum_i \left(z_p^i\right)^n \tag{A2.2}$$

where z_z^i is the location of the i^{th} zero and z_p^i is the location of the i^{th} pole. Thus, if there is a zero and a pole at different locations z, although the winding number is zero, the first moment integral is not. For a single pole and zero, the first moment defines the distance between the location of the zero and the pole:

$$I_1 = z_z - z_p \tag{A2.3}$$

By taking the second moment

$$I_2 = \left(z_z\right)^2 - \left(z_p\right)^2 \tag{A2.4}$$

the location of the zero and pole may easily be established as

$$z_z = \frac{1}{2}\left\{\frac{I_2}{I_1} + I_1\right\}, \qquad z_p = \frac{1}{2}\left\{\frac{I_2}{I_1} - I_1\right\} \tag{A2.5}$$

In this case, the function F is the function of non-dimensional wavenumber $k_y h$ given in equations (2.16) and (2.17) for a duct with a locally reacting lining, and equations (3.19) and (3.20) for a duct with a bulk-reacting lining. For the case of a duct with a locally reacting lining, from the wavenumber functions in equation (2.16) and (2.17), it is required to find the zeros in terms of the non-dimensional wavenumber $k_y h$. It is easy to identify the poles of the function since they lie on the real axis of the complex plane i.e. the poles of $\tan\left(k_y h/2\right)$ or $\cot\left(k_y h/2\right)$.

If the search areas are defined sufficiently above the real axis, all poles can be excluded and the winding number then gives only the number of zeros in the search region. The location for each zero can be obtained if the search grid is small enough that only one zero occurs in one cell of the grid. Equation indicates whether any zero exists in a search grid, and if it does, the location is given by the first moment, i.e. $z_z = I_1$.

The size of the search grid is selected such that at most only one pole and one zero will exist in a grid cell. This is chosen as the highest moment integral used is of order 2. Although the evaluation of higher moment integrals is possible, it is possible that the higher order equations do not yield solutions in closed form [127]. Table A2.1 summarises the possible number of zeros and poles in a search grid and the outcome of the winding number and the corresponding moment integrals.

The argument principle algorithm is carried out with an assumption that at most there exists only one pole and one zero in a search grid. A condition check is done for each search grid according to Table A2.1 and if any of the last two conditions are met, the search grid is refined into a smaller grid and the search process is repeated.

To illustrate the use of the argument principle method for a locally reacting lining, consider a duct with an airway height h of 300 mm and lining thickness d of 40 mm. The complex z-plane is searched where $0 \le \mathrm{Re}(z) \le 50$ and $0.05 \le \mathrm{Im}(z) \le 1$. Here the unknown z is the sought wavenumbers, $k_y h$ which are the zeros of equations (2.16) and (2.17). For this example the material properties of the lining are s = 1.0056, ε = 0.993 and r = 18000 rayls/m. The search for the even mode wavenumbers and odd mode wavenumbers are carried out separately at 1 kHz.

Table A2.1: Possible location of zeros and poles and the resulting winding number, moment integrals and the calculated location of zeros and poles from argument principle method

Zero	Pole	N	Conditions on moment integrals, I_1 and I_2 and location of pole and zero
0	0	0	I_1 is zero
1	0	1	$Z_z = I_1$
0	1	-1	$Z_p = -I_1$ $Z_z = 0$
1	1	0	$I_1 \neq 0$ and the location of zero and pole is given by Z_z and Z_p
1	2	-1	$Z_p \neq -I_1$ $Z_z \neq 0$
2	1	1	$Z_z \neq I_1$

Figure A2.1 shows the wavenumbers for even and odd modes obtained from the argument principle method described above. The results are compared with the wavenumbers found by using Müller's method. The search area for the argument principle algorithm is defined sufficiently above the real axis to avoid the location of the poles. Thus, with only zeros in the search area, the winding number gives exactly the number of zeros and by reducing the search area into smaller grids as shown in the figure, the location of the zeros can be found from the first moment integral.

Although the case of a locally reacting lining is quite simple and straight forward, the case of a bulk-reacting lining proves to be more difficult and the search grid must be carefully selected and defined. Unlike the locally reacting case where all the transverse wave modes decay away from the wall, some transverse wave modes in a duct with a bulk-reacting lining grow exponentially towards the centre of the duct, i.e. negative Im($k_y h$). Therefore it is impossible to exclude the poles on the real axis of the complex z-plane in the search area. Furthermore, it is found that some complex poles exist on the z-plane away from the real axis as well.

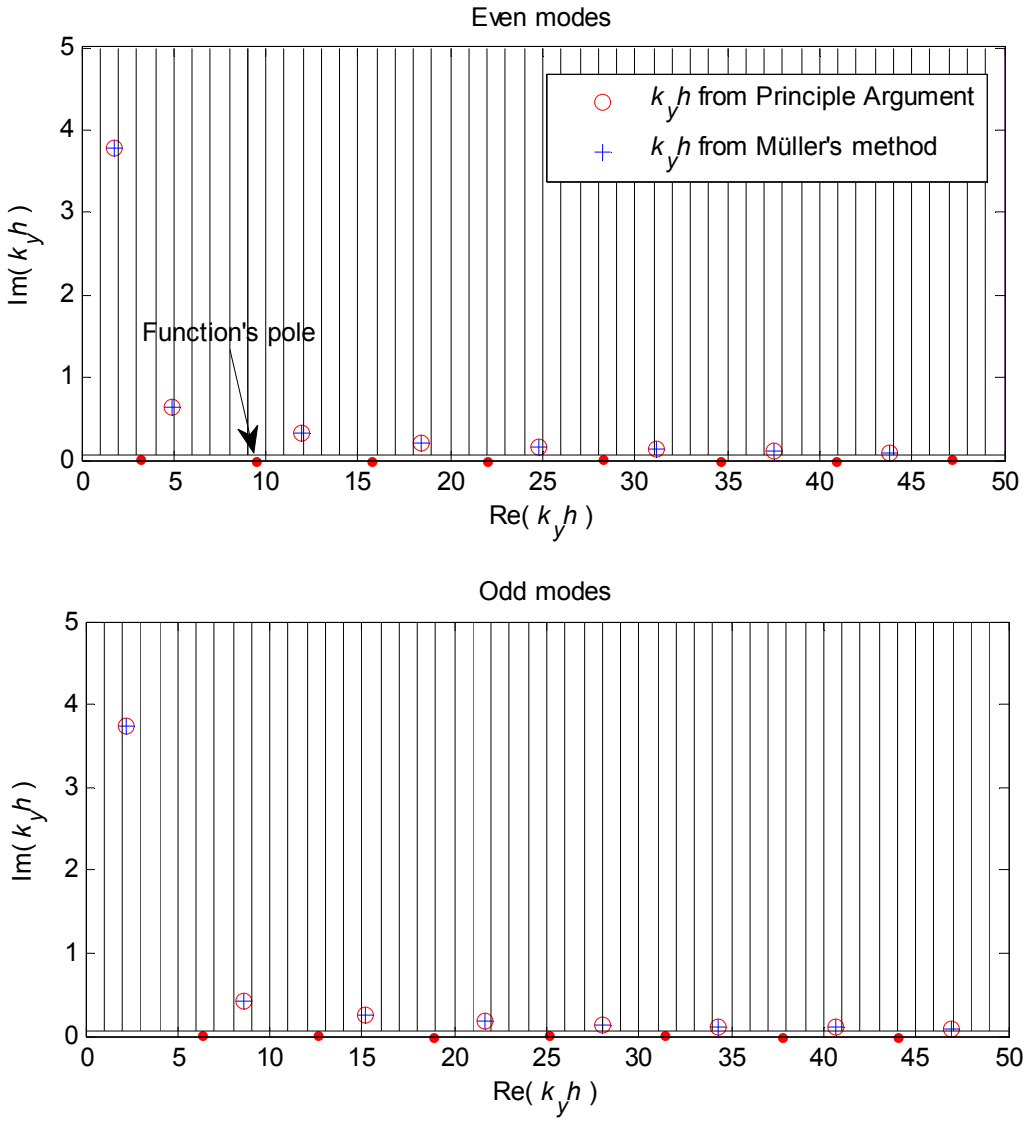

Figure A2.1: The transverse wavenumbers for a duct with a locally reacting lining at 1 kHz

The functions for bulk-reacting wavenumbers are given by equations (3.19) and (3.20). Apart from the poles due to $\cot\left(k_y h/2\right)$ (or $\tan\left(k_y h/2\right)$ for odd modes), there are other poles associated with $\tan\left(\sqrt{\tilde{k}^2 - k_0^2 + k_y h}\; d\right)$ which are in a very close neighbourhood of a corresponding zero. This zero is the wavenumber that belongs to the lining modes and it is no surprise that many numerical techniques have missed this root, especially at low frequency.

The search for roots in a closed area of the complex z-plane using the argument principle approach is repeated for the case of a bulk-reacting lining. The same material properties are used and the wavenumbers are searched at a frequency of 1 kHz as before. The area is searched

in the region of $0 \le \mathrm{Re}(z) \le 50$ and $-1.2 \le \mathrm{Im}(z) \le 4.8$ but with a finer search grid as shown in Figure A2.2.

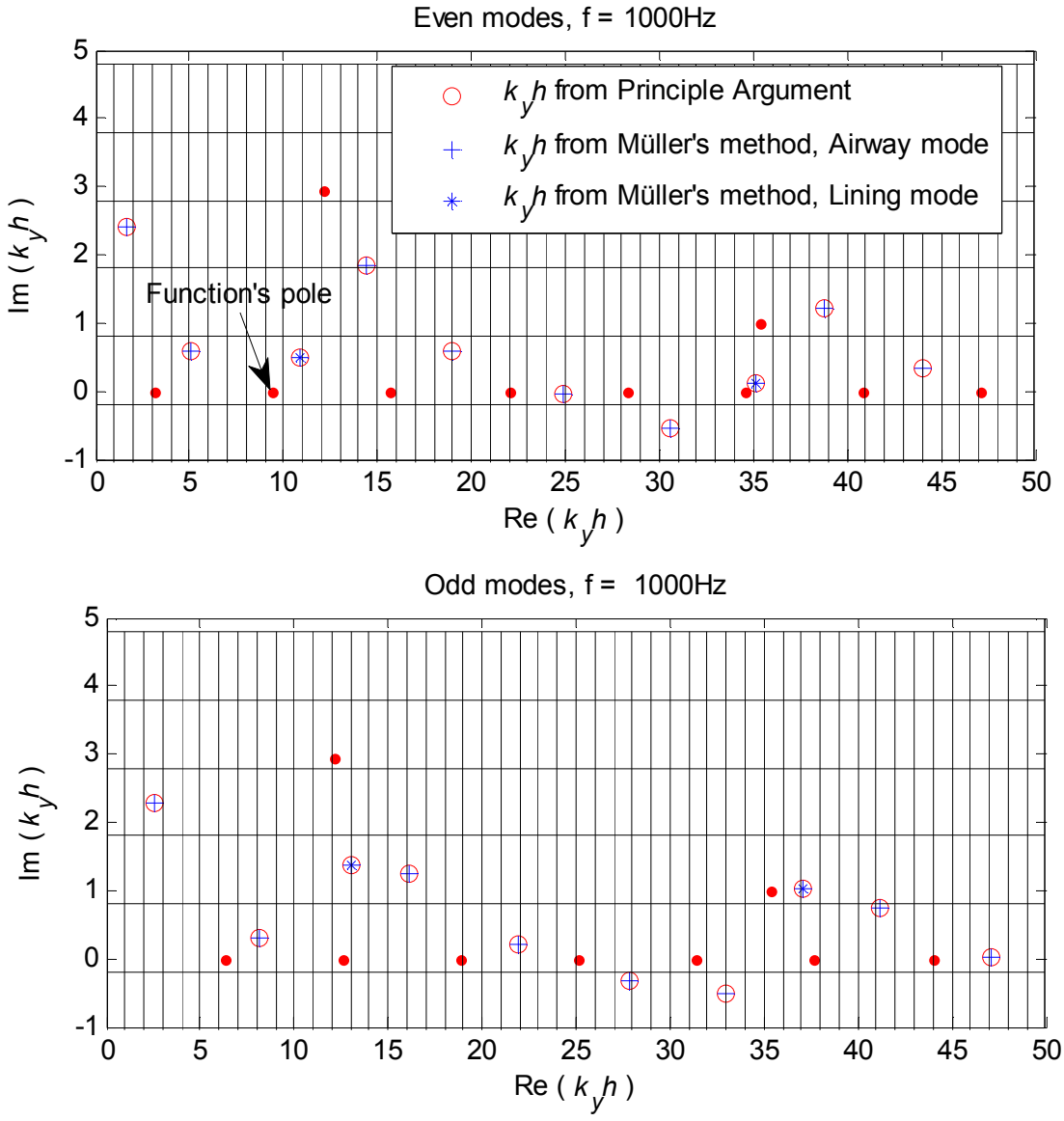

Figure A2.2: The transverse wavenumbers for a duct with a bulk-reacting lining at 1 kHz

Figure A2.3 and Figure A2.4 show the wavenumbers for even modes and odd modes respectively, obtained from the argument principle method and Müller's method at six different frequencies. The argument principle search is carried out to demonstrate that there is no mode missed by the Müller's method that has been used extensively in this thesis. Since in a bulk-reacting case, the search grid defined is very small to limit the number of poles and zeros in each cell, the algorithm has to be repeated numerous times to cover the large search area. The time taken to compute the location of zeros at a single frequency as presented in the figures

using the argument principle method is much longer than the time taken using Müller's method to obtain the same number of modes' wavenumbers for the whole range of frequency with 10000 equally spaced frequency points. The comparison was conducted using MATLAB on the same platform. The only drawback of Müller's method is the requirement of the three initial guesses which in this case can be assisted by the use of the argument principle method.

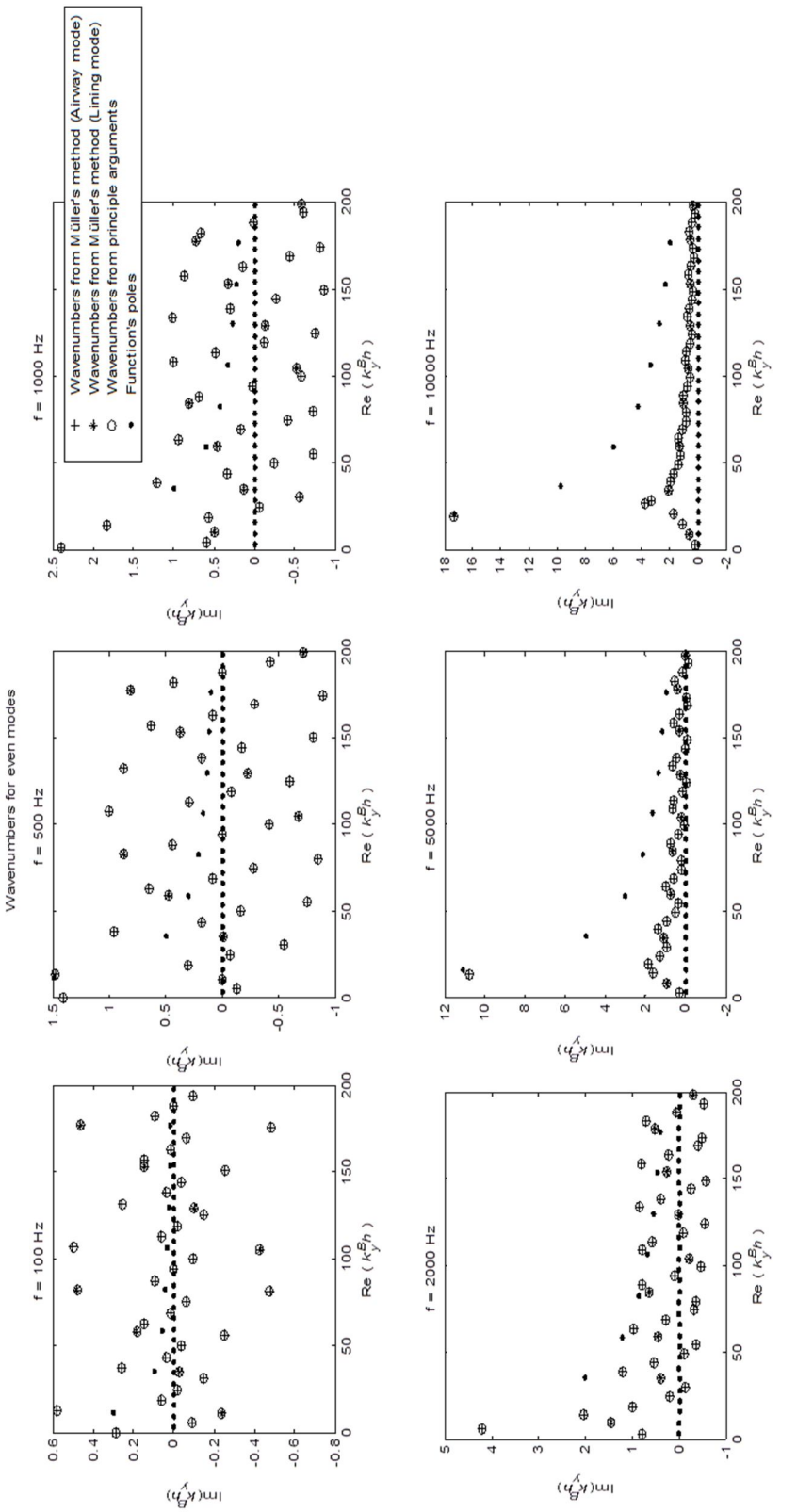

Figure A2.3: Wavenumbers found from both Müller's method and argument principle method for even modes at different frequencies

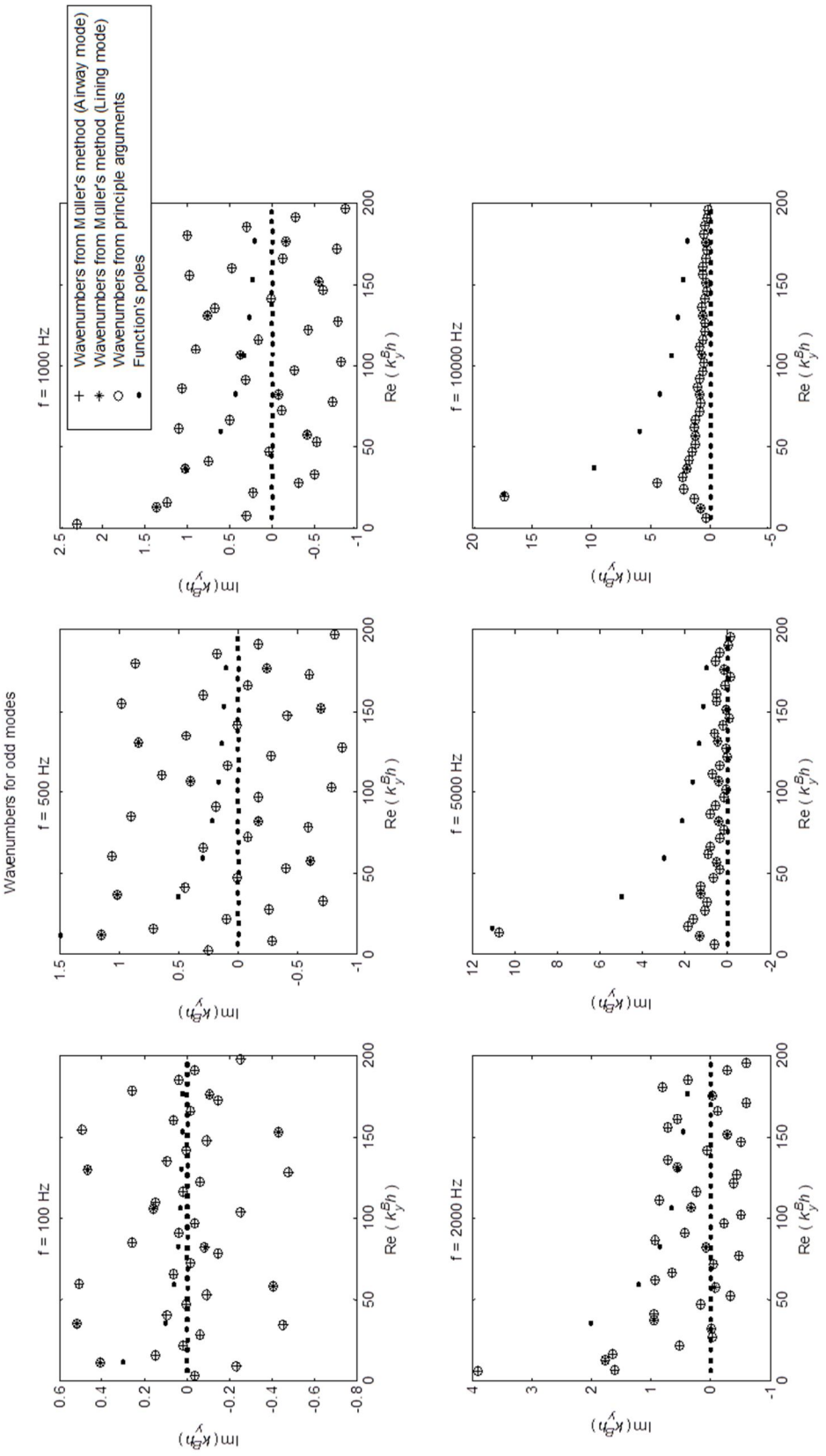

Figure A2.4: Wavenumbers found from both Müller's method and argument principle method for odd modes at different frequencies

Appendix 3

Determination of sound absorption coefficient and impedance in impedance tubes: Transfer-function method

The standard impedance tube rig is shown in Figure A3.1. The tube has a circular cross-section with a diameter of 10 cm and a length of 1m. The tube is straight with uniform cross section and the wall is rigid and smooth. A small sample of melamine material with a diameter of 10cm is placed at one end of the rigid test tube. A loudspeaker at the other end is driven by pseudo random signal and a microphone probe is arranged to traverse the length of the test tube and measure the sound pressure at two different positions. The surface impedance is obtained from the transfer function H_{12} measured between the two microphone positions, according to the standard ISO 10534-2:2001.

The working frequency range depends on the cross section of the tube and its length. The lower limit of the frequency range is determined by the requirement for the tube length to accommodate 3/4 of the wavelength. Furthermore the loudspeaker will generally produce higher order modes besides plane waves that eventually die out at a length of about three tube diameters. Therefore the lower frequency limit is determined by $l \geq \frac{3}{4}\frac{c_0}{f_{lower}} + 3D$. This gives a lower limit of 350 Hz.

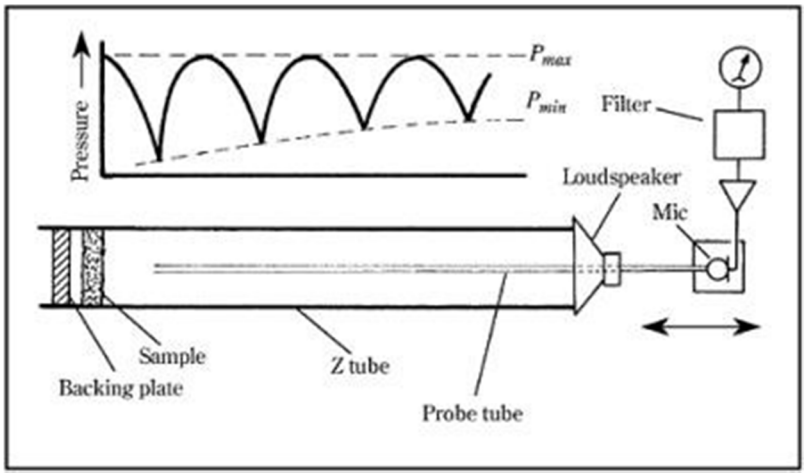

Figure A3.1: The impedance tube method of measuring the absorption coefficient of absorbing materials at normal incidence

The upper limit is determined by the requirement that only plane waves can propagate along the tube. For a tube of diameter *D*, the upper frequency limit is given by $f_{upper} = 1.84c_0/\pi D$. The minimum spacing between microphone positions, Δ, should satisfy $f_{upper}\Delta < 0.45c_0$ but also exceed 5% of the wavelength corresponding to the lowest frequency. Therefore f_{upper} is 2000 Hz in this case and the microphone spacing should satisfy 0.049 m < Δ < 0.077 m.

Following the method described in ISO 10534-2:2001, the measurement method is based on the fact that the sound reflection factor at normal incidence can be determined from the measured transfer function between two microphone positions in front of the tested material. In the test tube, there are two travelling waves propagating in opposite directions from each other: an incident wave that travels away from the loudspeaker towards the sample surface, and a reflected wave due to reflection at sample surface at normal incidence. The sound pressure of the incident wave is given by:

$$p_I = \hat{p}_I e^{ik_0 x} \qquad \text{A3.1}$$

and the sound pressure of the reflected wave is:

$$p_R = \hat{p}_R e^{-ik_0 x} \qquad \text{A3.2}$$

where $\hat{p}_I$ and $\hat{p}_R$ are the magnitudes of p_I and p_R at the sample front surface which is taken as the reference plane, $x = 0$.

The sound pressures at two microphone positions x_1 and x_2 can then be written as:

$$\begin{aligned} p_1 &= \hat{p}_{1I}\left(e^{ik_0x_1} + Re^{-ik_0x_1}\right) \\ p_2 &= \hat{p}_{2I}\left(e^{ik_0x_2} + Re^{-ik_0x_2}\right) \end{aligned} \qquad \text{A3.3}$$

where $R = \hat{p}_R / \hat{p}_I$. The transfer function between the two pressures due to the incident wave alone is:

$$H_I = \frac{p_{2I}}{p_{1I}} = e^{-ik_0(x_1 - x_2)} = e^{-ik_0\Delta} \qquad \text{A3.4}$$

and similarly the transfer function between the two pressures due to the reflected wave alone is:

$$H_R = \frac{p_{2R}}{p_{1R}} = e^{ik_0(x_1 - x_2)} = e^{ik_0\Delta} \qquad \text{A3.5}$$

Defining H_{12} as the transfer function between the total sound pressure at the two microphone positions, from equation (A3.3), we can write:

$$H_{12} = \frac{p_2}{p_1} = \frac{e^{ik_0x_2} + Re^{-ik_0x_2}}{e^{ik_0x_1} + Re^{-ik_0x_1}} \qquad \text{A3.6}$$

Rearranging equation (A3.6) and using equations (A3.4) and (A3.5), the reflection factor R can be written as:

$$R = \frac{H_{12} - H_I}{H_R - H_{12}} e^{2ik_0x_1} \qquad \text{A3.7}$$

and the normalized surface normal impedance is:

$$Z_n^{'} = \frac{1 + R}{1 - R} \qquad \text{A3.8}$$

Appendix 4

Designs for wall lining

Unlined wall (I)

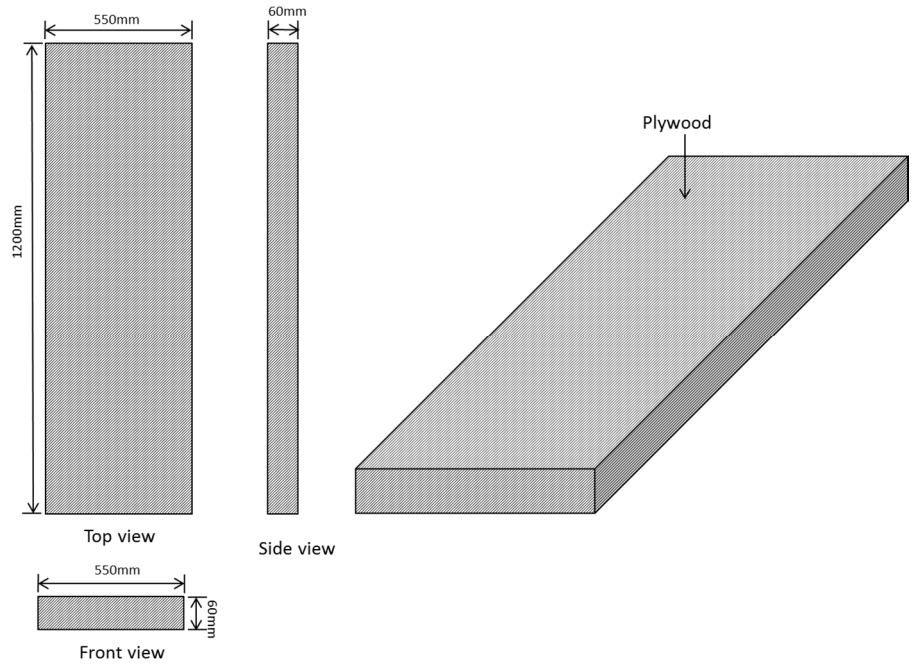

Unlined wall (II)

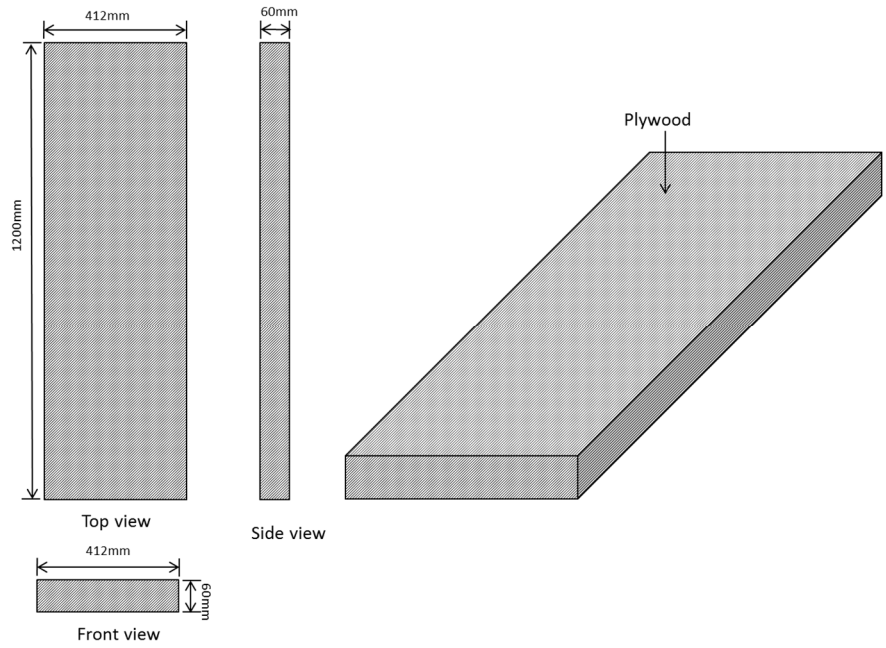

Appendix 4

Continuous lining wall (I)

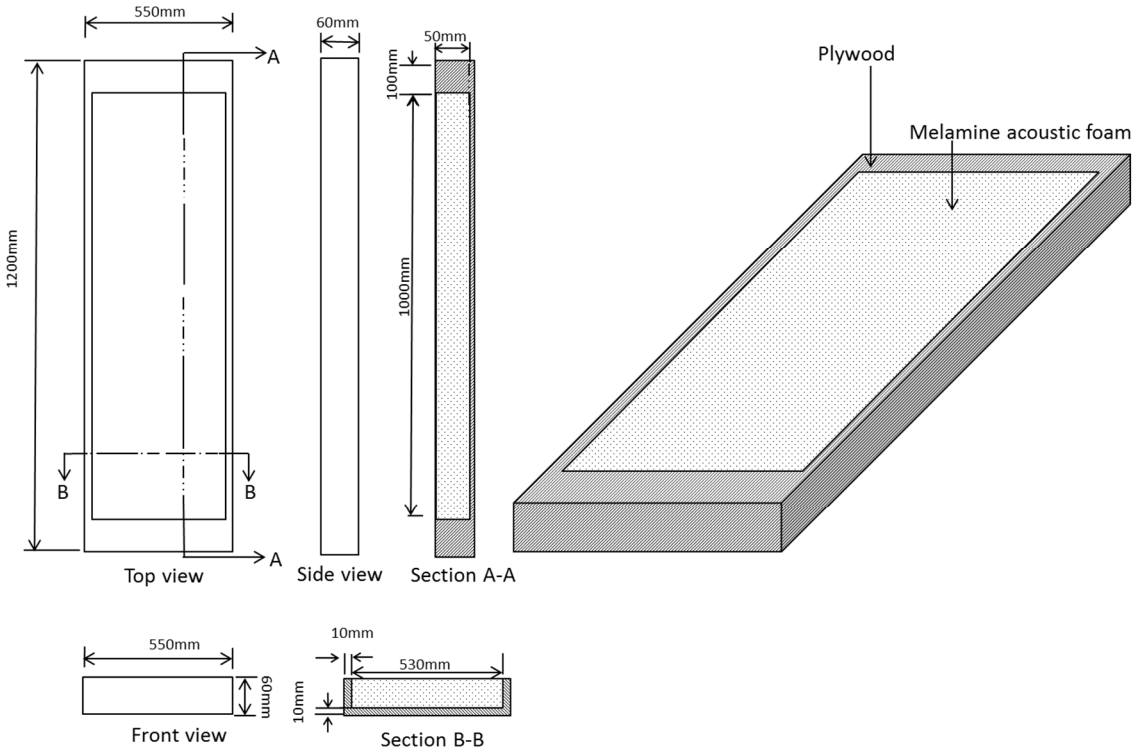

Periodic lining wall (I)

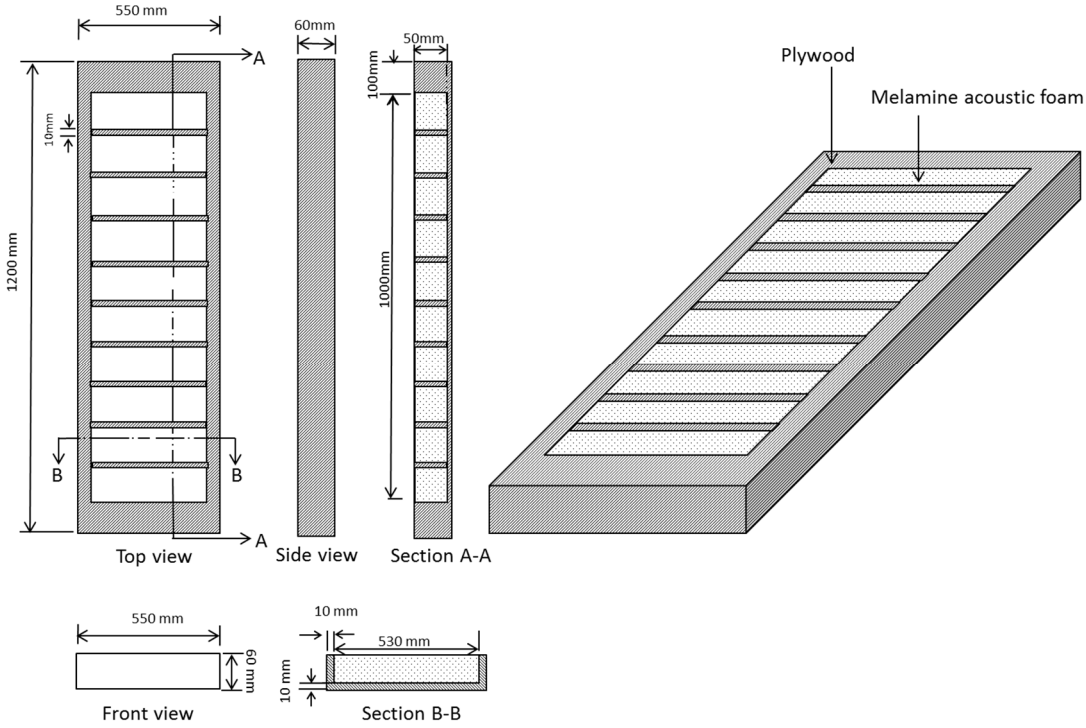

Continuous lining wall (II) and (III)

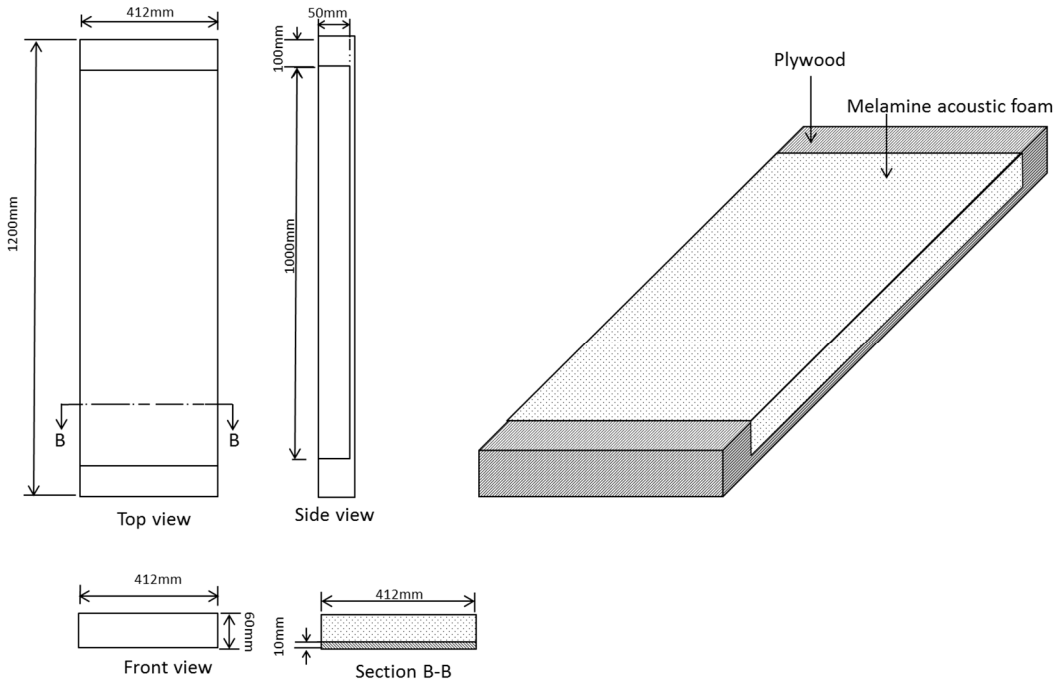

Periodic lining wall (II) and (III)